A peroxisomal sub-family of Arabidopsis NDR1 homologs: Molecular characterization of a novel targeting pathway and the proteins' functions in plant immunity

Dissertation with the aim of achieving a doctoral degree at the Faculty of Mathematics, Informatics and Natural Sciences

Department of Biology

Universität Hamburg

Submitted by

Binh Anh Thu Nguyen

May 2021 in Hamburg, Germany

TABLE OF CONTENTS

LIST OF ABBREVIATIONS

3-AT	3-amino-1,2,4-triazole
ABA	Abscisic acid
ABI	ABA insensitive
ABRC	Arabidopsis biological resource center
AD	Activation domain
APX	Ascorbate peroxidase
ATP	Adenosine triphosphate
AGI	*AvrRpt2-induced gene 1*
BD	Binding domain
Bar	BASTA resistance
bp	Base pair
BSA	Bovine serum albumin
bZIP	Basic leucine zipper
CaMV	Cauliflower mosaic virus
CBB	Coomassie brilliant blue
CC	Coiled-coil
CCD	Charge-coupled device
cDNA	Complementary DNA
CFP	Cyan fluorescent protein
CFU	Colony forming unit
CMV	Cucumber mosaic virus
Conc.	Concentration
COPI/II	Coat protein complex I/II
c-myc	Cellular myelocytomatosis
CSM	Complete supplement mixture
DEG15	Degradation of periplasmic proteins 15
DLP/DRP	Dynamin-like/related protein
DMSO	Dimethyl sulfoxide
dNTP	Deoxynucleotide triphosphate
dpc	Days post co-cultivation

dpi	Days post infection
EDS1	Enhanced disease susceptibility 1
EFR	EF-Tu receptor
elf	elongation factor
ER	Endoplasmic reticulum
ERES	ER exit site
ETI	Effector-triggered immunity
EYFP	Enhanced yellow fluorescent protein
Exp	Experiment
FIS	Fission
flg22	Flagellin 22
FLS2	Flagellin insensitive 2
gDNA	Genomic DNA
Get	Guided entry of TA protein
GOI	Gene of interest
H_2O_2	Hydrogen peroxide
HA	Hemagglutinin
HIN1	Harpin-induced 1
hpi	Hours post infection
hpt	Hours post transformation
HR	Hypersensitive response
IAN	Immune associated nucleotide binding
JA	Jasmonic acid
KO	Knockout
LB	Luria-Bertani
LEA	Late embryogenesis abundant
LRR	Leucine-rich repeat
MAMP	Microbe-associated molecular pattern
MAP	Mitogen-activated protein
MAPK	Mitogen-activated protein kinase
MBP	Maltose-binding protein

mCerulean	Monomeric Cerulean
MCS	Multicloning sites
MIF1	Macrophage migration inhibitory factor 1
mRNA	Messenger RNA
MS	Murashige and Skoog
MSB	Microtubule stabilizing buffer
mVenus	Monomeric Venus
NaOCl	Sodium hypochlorite
NBS	Nucleotide-binding site
NDR1	Non-race specific disease resistance 1
NHL	NDR1/HIN1-like
NO	Nitric oxide
OE	Overexpressor
PAMP	Pathogen-associated molecular pattern
PBS	Phosphate-buffered saline
PCR	Polymerase chain reaction
Pex	Peroxin
PMP	Peroxisomal membrane protein
PR1	Pathogenesis-related gene 1
PRR	Pattern recognition receptor
Psm	*Pseudomonas syringae* pv. *maculicola*
Pst	*Pseudomonas syringae* pv. *tomato*
PTI	Pattern-triggered immunity
PTS1	Peroxisomal targeting signal type 1
PTS2	Peroxisomal targeting signal type 2
qRT-PCR	Quantitative reverse transcription PCR
R	Resistance
RLK	Receptor-like kinase
RLP	Receptor-like protein
ROS	Reactive oxygen species
RPM	Resistance to *Pseudomonas syringae* pv. *maculicola*

RPP	Resistance to *Peronospora parasitica*
RPS	Resistance to *Pseudomonas syringae*
RT	Room temperature
SA	Salicylic acid
SAR	Systemic acquired resistance mechanism
sCMOS	Scientific Complementary Metal–oxide–semiconductor
SD	Synthetic defined
SDM	Site directed mutagenesis
SDS-PAGE	Sodium dodecyl sulphate–polyacrylamide gel electrophoresis
SNF1	Sucrose non-fermenting 1
SnRK2	(SNF1)-related protein kinase 2
SPSS 16	Statistical Package for the Social Sciences 16
TA	Tail-anchored
TAIR	The Arabidopsis information resource
TEM	Transmission electron microscopy
TF	Transcription factor
TIR	Toll/interleukin-1 receptor
TMD	Transmembrane domain
TPR	Tetratricopeptide repeat
TRC40	TMD recognition complex 40
VP1	Viviparous 1
Vsp1p	Vacuolar protein sorting 1
WT	Wild-type
X-Gal	5-bromo-4-chloro-3-indolyl-β-D-galactopyranoside
X-Gluc	5-bromo-4-chloro-3-indolyl glucuronide
Xcc	*Xanthomonas campestris* pv. *campestris*
Y2H	Yeast two-hybrid
YNB	Yeast nitrogen base
YPDA	Yeast peptone dextrose adenine hemi-sulfate

LIST OF TABLES

LIST OF FIGURES

ABSTRACT

Arabidopsis NDR1 plays an important role in plant innate immunity and represents the best characterized member of the NDR1/HIN1-like (NHL) protein family. Of the 45 NHL proteins identified in Arabidopsis, none had been proven to act in peroxisomes. Three members of one subclade (NHL4, NHL6, and NHL25) are single-pass membrane proteins with the novel feature of carrying a predicted peroxisomal targeting signal type 1 (PTS1), even though this was presumably specific to soluble matrix proteins. Preliminary data of former group members had shown that the three proteins were primarily targeted to small puncta and were possibly further directed to peroxisomes, as observed (occasionally) in Arabidopsis and tobacco mesophyll protoplasts (Kataya, 2011; Crappe, 2016).

To verify peroxisome targeting of the three NHL proteins and characterize their postulated vesicular targeting pathway, a new transient expression system of entire Arabidopsis seedlings of very high biogenetic activity was established in the group. Only very specific fluorophore combinations (EYFP or mVenus with mCer) were found to prevent weak fluorophore heterodimerization and unspecific import of cytosolic proteins into peroxisomes by the so-called piggy-back mechanism and were concluded to be suitable for *in vivo* peroxisome targeting analyses, as published jointly in Falter et al. (2019). Not only NHL4 terminating with the canonical PTS1, AKL>, but also NHL6 (LRL>) and NHL25 (FRL>) with their non-canonical PTS1 tripeptides were shown to carry functional PTS1 domains that were sufficient to direct EYFP to peroxisomes. The PTS1 domain of NHL4 also interacted with the tetratricopeptide repeat (TPR) domain of the receptor of soluble PTS1 proteins, AtPex5, in yeast two-hybrid (Y2H) analyses. Peroxisome targeting of the three full-length NHL proteins remained difficult to reveal and required longer expression times but was reproducibly detected in a considerable number of transformed cells in Arabidopsis seedlings. Representatively for NHL4, peroxisome targeting was confirmed in stable transgenic Arabidopsis lines upon expression from its endogenous promoter. By a comprehensive set of additional methods, including confocal microscopy of fluorophore-tagged full-length, mutated, and deletion constructs and also transmission electron microscopy, the complex trafficking pathway of the NHL proteins was described in detail. Accordingly, it starts at the ER and continues *via* vesicle-like cargo structures to so-called "docking structures" between mature peroxisomes and attached vesicles and ends at peroxisomes as the NHL proteins' final destination and site of physiological activity. The results allowed the deduction of a model for

this novel PTS1-dependent, multi-step vesicular trafficking pathway of these signal-anchor proteins to plant peroxisomes.

To reveal the proteins' physiological functions, gene expression analyses using publicly available microarray data were verified by qRT-PCR and demonstrated that *NHL4* was strongly induced by abscisic acid (ABA), while *NHL6* and *NHL25* were highly expressed upon infection by virulent *Pseudomonas syringae* pv. *tomato* DC3000 (*Pst*) and two avirulent *Pst* strains expressing the effector proteins, AvrRpm1 and AvrRpt2. As revealed by transgenic Arabidopsis *GUS* reporter lines, the promoters of *NHL4, NHL6,* and *NHL25* were constitutively active specifically in tissue related to defense, including hydathodes and vascular tissue, as well as in stomata and trichomes (for *NHL6*), which further strengthened the indicated protein functions in pathogen defense. To characterize their functions in innate immunity, single, double, and triple *nhl* knockout (KO) mutants were infected with the above-mentioned avirulent bacteria. However, bacterial proliferation was not significantly different between the *nhl* mutants and wild-type plants (WT). In-depth kinetic analyses of electrolyte leakage in KO mutants were carried out to investigate a potential regulatory role of the NHL proteins in the hypersensitive response, as reported for NDR1. Upon infection with *Pst* expressing *avrRpt2*, the three single *nhl* KO mutants showed a higher relative electrolyte leakage compared to WT, and this effect was not additive in the double and triple mutants, indicating that each NHL has an important non-redundant function in restricting the hypersensitive response locally.

To study the hypothesized functions of the NHL proteins in ABA-dependent plant responses, the inhibitory effect of ABA on seed germination was investigated. Compared to WT seeds, germination of the single KO mutants, *nhl4-1* and *nhl6-1*, was significantly less inhibited by ABA, indicating that NHL4 and NHL6 might play a role in ABA-mediated inhibition of seed germination and possibly also in ABA-transduced abiotic stress responses. Bacterial growth analyses of *E. coli* transformants producing soluble NHL4 further confirmed that the protein has typical properties of LEA proteins that are able to confer hypertonic stress resistance in *E. coli*, most likely by protecting specifically sensitive proteins from osmotic damage. This result implied a similar stress-protective chaperone function of NHL4 *in planta*. Based on the characterized properties of these three NHLs, their physiological roles in ABA-mediated responses (for NHL4) and plant defense (for NHL6 and NHL25) are proposed.

ZUSAMMENFASSUNG

Arabidopsis NDR1 spielt eine wichtige Rolle in der angeborenen Immunität von Pflanzen und stellt das am besten charakterisierte Mitglied der NHL (NDR1/HIN1-like) Proteinfamilie dar. Vor Beginn der Arbeit war noch für keines der in Arabidopsis identifizierten 45 NHL-Proteine eine Lokalisation in Peroxisomen nachgewiesen worden. Zudem wurde angenommen, dass das peroxisomale Zielsteuerungssignal des Typs 1 (PTS1) spezifisch für lösliche Matrixproteine ist und nicht in die Zielsteuerung von peroxisomalen Membranproteinen involviert ist. Drei Mitglieder einer phylogenetischen Untergruppe (NHL4, NHL6 und NHL25) sind Membranproteine mit einer N-terminalen transmembranen Domäne und einem vorhergesagten PTS1. Vorläufige mikroskopische Untersuchungen ehemaliger Gruppenmitglieder an Protoplasten aus Arabidopsis- und Tabakblättern hatten gezeigt, dass die drei Proteine primär in kleinen vesikelartigen Strukturen lokalisiert waren und möglicherweise über diese Vesikel zu Peroxisomen transportiert wurden (Kataya, 2011; Crappe, 2016).

Um die peroxisomale Zielsteuerung der drei NHL-Proteine nachzuweisen und ihren postulierten vesikulären Transportweg zu charakterisieren, wurde in der Arbeitsgruppe ein neues transientes Expressionssystem von Arabidopsis-Keimlingen mit sehr hoher biogenetischer Aktivität etabliert. In diesem Expressionssystem konnten jedoch nur sehr spezifische Fluorophor-Kombinationen (EYFP oder mVenus mit mCer) eingesetzt werden, um eine schwache Fluorophor-Dimerisierung und einen Ko-Import zytosolischer Proteine in Peroxisomen über den sog. „Huckepack-Mechanismus" zu unterbinden. Diese Ergebnisse wurden gemeinsam in Falter et al. (2019) veröffentlicht. Es konnte gezeigt werden, dass tatsächlich sowohl das kanonische PTS1-Tripeptid von NHL4 (AKL>) als auch die nicht-kanonischen PTS1-Domänen von NHL6 (LRL>) und NHL25 (FRL>) das Reporterprotein EYFP zu Peroxisomen dirigieren konnten, womit ihre Funktionalität als peroxisomale Zielsteuerungssignale bestätigt wurde. Die PTS1-Domäne von NHL4 interagierte zudem mit der PTS1-Bindungsdomäne des Rezeptors AtPex5 in Zwei-Hybrid-Analysen in Hefen. Die peroxisomale Zielsteuerung der Volllängen-NHL-Proteine war schwierig nachzuweisen und erforderte längere Expressionszeiten, wurde aber reproduzierbar in einer signifikanten Anzahl von transformierten Zellen in Arabidopsis-Keimlingen nachgewiesen. Repräsentativ für NHL4 wurde die peroxisomale Zielsteuerung in stabilen transgenen Arabidopsis-Linien nach Expression des Gens unter Kontrolle seines endogenen Promotors verifiziert. Mit Hilfe eines umfassenden Methodenspektrums, welches die konfokale Mikroskopie Fluorophor-markierter Volllängen-, mutierter

und Deletionskonstrukte sowie die Transmissionselektronenmikroskopie umfasste, wurde der komplexe Transportweg der NHL-Proteine detailliert beschrieben. Demzufolge beginnt er am ER, setzt sich über vesikelartige Strukturen fort und führt weiter zu sogenannten "Docking-Strukturen" zwischen Vesikeln und Peroxisomen bis hin zum Bestimmungsort der Peroxiso-menmembran und Ort der physiologischen Aktivität. Die Ergebnisse bildeten die Basis für die Ableitung eines Modells für diesen neuartigen, mehrstufigen vesikulären Transportweg dieser Signalanker-Proteine zu pflanzlichen Peroxisomen.

Um die physiologische Funktion der Proteine aufzudecken, wurden Genexpressions-analysen unter Verwendung öffentlich zugänglicher Microarray-Daten durchgeführt und durch eigene qRT-PCR-Analysen verifiziert. Die Expression von *NHL4* wurde stark durch Abscisinsäure (ABA) induziert, während die Transkription von *NHL6* und *NHL25* überaus intensiv durch Infektion mit Pseudomonas hochreguliert wurde, und zwar sowohl durch den virulenten Stamm von *Pseudomonas syringae* pv. *tomato* DC3000 (*Pst*) als auch durch zwei avirulente *Pst*-Stämme, die die Effektorproteine AvrRpm1 und AvrRpt2 exprimierten. Über die Herstellung und Untersuchung transgener GUS-Reporterlinien von Arabidopsis konnte gezeigt werden, dass die Promotoren von *NHL4*, *NHL6* und *NHL25* konstitutiv und spezifisch in Hydathoden und vaskulärem Gewebe aktiv sind sowie der NHL6 Promotor zusätzlich in Spaltöffnungen und Trichomen. Diese *NHL*-Expression in Blattzellen und -gewebe, die als „Eintrittspforten" für diverse Pathogene fungieren, erhärtete weiter ihre postulierte Proteinfunktion in der Patho-genabwehr. Um ihre Funktion in der pflanzlichen Immunität zu charakterisieren, wurden die Einzel-, Doppel- und Dreifach-Knockout (KO) Mutanten mit den zwei oben genannten avirulenten Bakterienstämmen infiziert. Die bakterielle Vermehrung unterschied sich jedoch nicht signifikant vom Wildtyp. Um die regulatorische Rolle der NHL-Proteine bei der hyper-sensitiven Reaktion zu untersuchen, wurden eingehende kinetische Analysen der Elektrolyt-freisetzung in KO-Mutanten durchgeführt. Nach einer Infektion mit dem *Pst*-Stamm, der *avrRpt2* exprimierte, zeigten die drei einzelnen *nhl*-KO Mutanten eine höhere relative Elektrolytfreisetzung im Vergleich zum Wildtyp, und dieser Effekt war bei den Doppel- und Dreifachmutanten nicht additiv, was auf eine nicht-redundante Funktion der drei NHLs bei der negativen Regulation der hypersensitiven Reaktion hindeutete.

Im Zuge der Untersuchungen der möglichen Funktion der drei NHL-Proteine in der Pflanzenantwort auf ABA war die Samenkeimung der einzelnen KO-Mutanten von *nhl4-1* und *nhl6-1* im Vergleich zum Wildtyp signifikant schwächer durch ABA inhibiert, was darauf

hinwies, dass NHL4 und NHL6 eine Rolle bei der ABA-vermittelten Hemmung der Samen-keimung und möglicherweise auch bei abiotischen Stressreaktionen spielen könnten. Bakteri-elle Wachstumsanalysen von *E. coli*-Transformanten, die eine lösliche NHL4-Version unter osmotischen Stressbedingungen produzierten, bestätigten außerdem, dass NHL4 tatsächlich die typischen Eigenschaften von LEA-Proteinen aufweist. Diese sind in der Lage, die Stress-resistenz von *E. coli* zu erhöhen, höchstwahrscheinlich durch den Schutz spezifischer empfind-licher Proteine vor osmotischer Schädigung. Dieses Ergebnis in *E. coli* deutet auf eine ähnliche Funktion der NHL-Proteine *in planta* hin. Basierend auf den Charakteristika dieser drei NHLs wird ihre physiologische Rolle in ABA-vermittelten Reaktionen (primär für NHL4) und in der Pathogenabwehr (für NHL6 und NHL25) vorgeschlagen.

1 INTRODUCTION

1.1 Peroxisomes

1.1.1 General structure and functions

Peroxisomes were first identified as single membrane-bound organelles in 1954 by electron microscopy and were termed microbodies (Rhodin, 1954). Due to their high content of oxidases and catalase that produce and degrade hydrogen peroxide (H_2O_2), respectively (De Duve and Baudhuin, 1966), the cell organelles were called "peroxisomes", referring to their peroxidases that degrade peroxides. Peroxisomes are found in most eukaryotic cells and generally have a spherical shape of 0.1 – 2.0 µm in diameter, but may also be elongated or even associated with each other up to 2.5 µm in size and may form a reticulum in mammalian cells (Yamamoto and Fahimi, 1987; Schrader et al., 1994; Schrader et al., 2000).

Morphology and functions of peroxisomes have been intensively studied in yeast and mammals as model organisms and to lesser extent in plants. Hence, several metabolic enzymes, transport proteins, regulatory proteins, chaperones, and peroxins (Pex) involved in peroxisome biogenesis have been identified in *S. cerevisiae* (Kiel et al., 2006), mammals (Schrader and Fahimi, 2008), and plants (Nito et al., 2007; Cross et al., 2016). Noticeably, unlike mitochondria and plastids, peroxisomes are devoid of DNA and ribosomes. Thus, all peroxisomal proteins are nuclear-encoded and require distinct pathways and Pex proteins to be imported (1.1.3 and 1.1.4).

A number of metabolic pathways are compartmentalized in peroxisomes and are important for growth and development, such as fatty acid β-oxidation, detoxification of reactive oxygen species (ROS) and nitrogen species, synthesis of ether phospholipids (in mammals), photorespiration, phytohormone biosynthesis (both in plants), and the glyoxylate cycle (in plants and fungi) (Van den Bosch et al., 1992; Del Río et al., 2003). The metabolic enzymes of peroxisomes vary greatly between organismal groups. For instance, plant peroxisomes contain a unique set of enzymes that are involved in the biosynthesis of phylloquinone, and phytohormones, including jasmonic acid (JA) and indole-3-acetic acid (Reumann and Bartel, 2016). A widespread function of peroxisomes across organisms is fatty acid β-oxidation, generating H_2O_2 by acyl-CoA oxidase. To degrade different ROS, peroxisomes produce scavenging enzymes such as catalase, superoxide dismutase, peroxidases, and enzymes involved in the ascorbate-glutathione cycle. Peroxisomal deficiencies in biogenesis

and functions cause genetic diseases in human, for instance, the so-called Zellweger syndrome (Goldfischer et al., 1973; Brown et al., 1982; Wanders, 2014).

Within a single organism, the enzymes of peroxisomes vary depending on cell and tissue types and growth conditions. In order to utilize different carbon sources (e.g., ethanol, acetate or oleate), yeasts induce the corresponding peroxisomal enzymes for fatty acid β-oxidation and alter the size and number of peroxisomes (Veenhuis et al., 1987; Gurvitz and Rottensteiner, 2006). Peroxisomes are characterized by a high metabolic plasticity that enables organisms to be more adaptive to external cues. Peroxisome biogenesis and degradation (pexophagy) regulate the number of peroxisomes of organisms in responses to environmental stimuli (Schrader et al., 2016). Moreover, to fulfill their metabolic functions, peroxisomes can physically interact and exchange molecules *via* tethering sites with other organelles, such as the endoplasmic reticulum (ER), mitochondria, lipid droplets, chloroplasts, and lysosomes (Shai et al., 2016).

Peroxisome biogenesis includes two different levels, (i) biogenesis of peroxisomal matrix and membrane proteins (PMPs) including Pex proteins and (ii) growth and division of peroxisomes from pre-existing peroxisomes and peroxisome proliferation (Hu et al., 2012). In the following sections, these processes are described in detail (1.1.2, 1.1.3, and 1.1.4). Moreover, functions of peroxisomes with respect to plant health are also presented (0).

1.1.2 Growth and division of peroxisomes

Peroxisomes can either arise and proliferate from pre-existing peroxisomes or be synthesized *de novo* from the ER (Cross et al., 2016). Peroxisome proliferation by growth and division is believed to be the predominant route, while the *de novo* biogenesis primarily happens when (mutant) cells lack peroxisomes. Peroxisome division consists of three stages, including elongation, constriction, and scission (Hu et al., 2012). Although constriction remains poorly understood, core proteins of this process, which are functionally conserved across fungi, mammals, and plants, have been identified (Aung et al., 2010).

Regarding the elongation step, Pex11p was first identified in yeast as a PMP that is required for early peroxisomal proliferation (Erdmann and Blobel, 1995; Marshall et al., 1995). *S. cerevisiae* lacking Pex11p had giant peroxisomes but fewer in number compared to the wild-type (WT) when growing on oleic acid. The C-termini of Pex25p and Pex27p share high sequence similarity with Pex11p, and their functions are partially redundant with Pex11p (Smith et al., 2002; Rottensteiner et al., 2003; Tam et al., 2003). Several functional homologs of

Pex11p were found in mammals (Pex11α, β, γ) and Arabidopsis (Pex11a-e) (Lingard and Trelease, 2006; Nito et al., 2007; Orth et al., 2007). They are known to regulate peroxisome proliferation (the number and size) in responses to various degrees of environmental cues.

Peroxisome fission requires an additional group of the large superfamily of GTPases, which consists of dynamin-like/related proteins (DLPs/DRPs) acting as a key factor in this process. DRPs that function in peroxisome division have been identified in yeast (vacuolar protein sorting 1 (Vsp1p); Hoepfner et al., 2001) and in mammals (DLP1; Koch et al., 2003). In Arabidopsis, the two orthologs DRP3A and DRP3B display conserved functions with mammalian DLP1 and yeast Vsp1p in peroxisomal fission. DRP3B functions redundantly with DRP3A in mitochondria fission, and it plays a minor role in peroxisome division compared to DRP3A which might predominantly function in this process (Mano et al., 2004; Fujimoto et al., 2009; Zhang and Hu, 2009). The loss-of-function *DRP3A* mutant showed impaired plant growth and aberrant peroxisome morphology (Mano et al., 2004). Another Arabidopsis paralog of DRP3s, DRP5B, found only in plants and algae, has been reported as a chloroplast and peroxisome division protein, and it could cooperate in a complex with other DRP3s, with FISSION1A (FIS1A), and with other Pex11 isoforms (Gao et al., 2003; Zhang and Hu, 2010).

The protein Fis1 involved in mitochondrial fission has also been revealed to be essential for peroxisome division in yeast and mammals (Koch et al., 2005; Kobayashi et al., 2007). Studies in Arabidopsis identified two Fis1 orthologs (FIS1A and FIS1B) that display conserved functions (Scott et al., 2006; Zhang and Hu, 2008; Zhang and Hu, 2009). The data show that peroxisomes commonly share components of the division machinery with other cellular organelles including mitochondria and chloroplasts.

1.1.3 Peroxisomal matrix protein import

In addition to reverse and forward genetics, proteomic analyses of peroxisomes and subsequently validations by *in vivo* subcellular localization have identified numerous peroxisomal proteins (Reumann et al., 2007; Arai et al., 2008; Eubel et al., 2008; Reumann et al., 2009). The import mechanism of peroxisomal matrix and membrane proteins has been characterized relatively well. Most matrix proteins contain either a C-terminal PTS1 or a cleavable N-terminal PTS2, both of which are recognized and bound by two specific cytosolic receptors, Pex5 and Pex7, respectively (Figure 1.1). The PTS1 proteins, which are most numerous, were originally defined by the C-terminal tripeptide SKL> or a conserved motif, i.e. (S/A/C)-(K/R/H)-(L) (Gould et al., 1987; Gould et al., 1989). High-abundance PTS1 proteins

often carry a canonical PTS1. This motif is generally conserved in most of eukaryotes, and canonical PTS1 tripeptides are sufficient to target proteins to peroxisomes. Canonical PTS1s could be identified solely based on the C-termini end or by prediction tools available for different species (Emanuelsson et al., 2003; Neuberger et al., 2003a, b; Reumann, 2004; Reumann et al., 2004; Hawkins et al., 2007; Lingner et al., 2011). However, some differences and diversity in the PTS1 were observed across kingdoms (Elgersma et al., 1996b; Hayashi et al., 1997; Amery et al., 1998; Reumann, 2004; Reumann et al., 2016).

In proteome analyses of plant peroxisomes, non-canonical PTS1s that are weak peroxisomal signals and present in low-abundance proteins have been identified (Reumann et al., 2007; Eubel et al., 2008; Reumann et al., 2009). The identification of novel PTS1s has been further expanded using bioinformatics (Lingner et al., 2011). Also, several studies demonstrated that residues upstream the C-terminal tripeptide influence the peroxisomal targeting efficiency of PTS1s *via* the recognition of Pex5 (Mullen et al., 1997; Neuberger et al., 2003a; Brocard and Hartig, 2006; Lingner et al., 2011; Skoulding et al., 2015).

The PTS2 motif is normally located within the N-terminal 20 – 40 residues. The PTS2 nonapeptide motif consists of four conserved residues that are spaced by five rather variable ones, i.e. $(R/K)-(L/V/I)-X_5-(H/Q)-(L/A)$ (Osumi et al., 1991; Swinkels et al., 1991; De Hoop and Ab, 1992; Kato et al., 1996; Flynn et al., 1998). The prediction of plant PTS1 and PTS2 proteins has been comprehensively reviewed (Reumann and Chowdhary, 2018).

Many components of the peroxisomal matrix import machinery are already known. Apart from Pex5 and Pex7, the import system involves the importomer that comprises the docking complex, including Pex13 (Elgersma et al., 1996a; Gould et al., 1996), Pex14 (Komori et al., 1996; Hayashi et al., 2000), and Pex17 (only found in yeast) (Huhse et al., 1998) and the RING-finger complex (Pex2, Pex10, and Pex12). PTS1 cargo is bound by the C-terminal domain of Pex5 containing numerous tetratricopeptide repeats (TPRs), as revealed by structural analyses of yeast and human Pex5 (Gatto et al., 2000; Stanley et al., 2006; Hagen et al., 2015). The conserved functional TPR domain has also been found in plant orthologs (Kragler et al., 1998; Bonsegna et al., 2005; Khan and Zolman, 2010). Pex5 binds to Pex13 and Pex14 (Elgersma et al., 1996a; Albertini et al., 1997; Girzalsky et al., 1999; Otera et al., 2002). The N-terminus of Arabidopsis Pex5 (AtPex5) contains nine WxxxF/Y repeats that are responsible for interaction with the N-terminus of AtPex14 (Nito et al., 2002). The physical interaction between AtPex5 and AtPex13 needs to be further clarified.
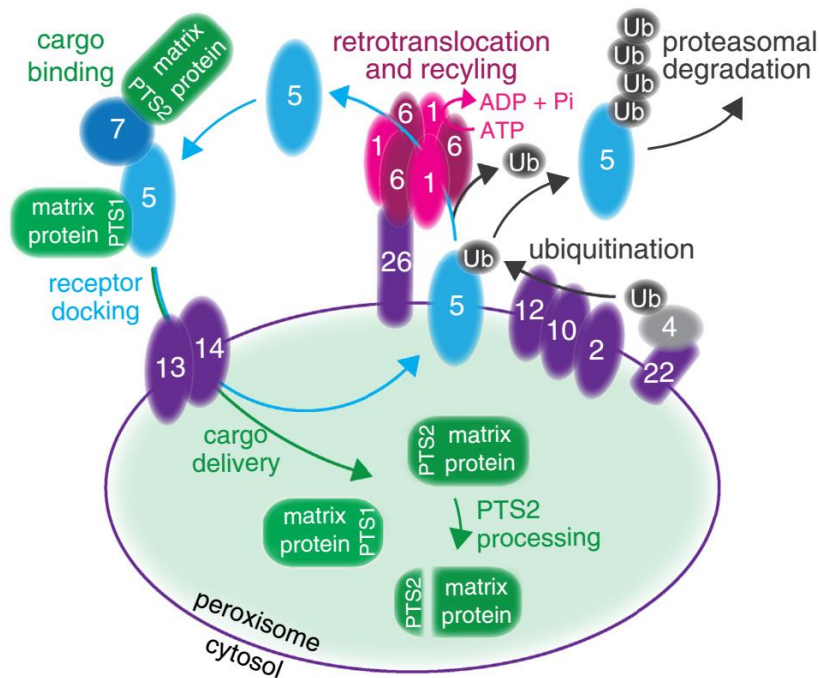
Figure 1.1: Import pathways of peroxisomal matrix proteins in plants

The two cytosolic receptors, Pex5 and Pex7, recognize and bind to PTS1 and PTS2 cargos, respectively. Cargo proteins are translocated into the matrix while the receptors interact with the docking complex residing on the peroxisomal membrane, including Pex13 and Pex14. The N-terminal PTS2 domain is cleaved after cargo delivery and the receptor Pex5 is either mono- or polyubiquitinated, presumably by the assistance of the RING-finger complex (Pex2, Pex10, and Pex12) and a ubiquitin-conjugating enzyme Pex4, anchored in the membrane by Pex22. Monoubiquitinated Pex5 is further recycled back to the cytosol by Pex1 and Pex6 tethered to the peroxisomal membrane by Pex26/APEM9, while polyubiquitinated Pex5 is degraded by the proteasome. The image was fully reproduced from Reumann and Bartel (2016) with permission of use from Elsevier.

After docking and cargo release, the fate of Pex5 is regulated by other Pex proteins (Figure 1.1). In detail, Pex5 is either mono- or polyubiquitinated, presumably by the assistance of the membrane associated RING-finger complex (Pex2, Pex10, and Pex12) and an ubiquitin-conjugating enzyme Pex4, which is anchored to the peroxisomal membrane by Pex22 (Koller et al., 1999; Platta et al., 2007; Williams et al., 2008). After transport back to the cytosol, polyubiquitinated Pex5 is degraded by the proteasome, while monoubiquitinated Pex5 is recruited for further rounds of import by the heterohexameric complex of two AAA ATPases (Pex1 and Pex6) (Platta et al., 2005). The respective Arabidopsis orthologs have been functionally characterized (Hayashi et al., 2000; Zolman and Bartel, 2004; Zolman et al., 2005; Nito et al., 2007; Burkhart et al., 2014).

5

Interestingly, an additional PTS1 receptor, referred to as Pex9p, a paralog of Pex5, has been recently found in *S. cerevisiae* (Effelsberg et al., 2016). Moreover, for PTS1 protein import in yeast, the interaction of Pex5p with the intraperoxisomal protein, Pex8p, is required, which is an additional component of the importomer complex (Rehling et al., 2000; Ma et al., 2009). However, orthologs of Pex8p and Pex9p have not been found yet in plants and animals.

Regarding the import of PTS2 cargos Pex7 recognizes and binds the cargo *via* multiple WD40 repeats (Marzioch et al., 1994; Zhang and Lazarow, 1995). After translocation, cargos are processed in the matrix to remove their PTS2 by a protease, degradation of periplasmic proteins 15 (DEG15 or TYSND1 in mammals) (Helm et al., 2007; Kurochkin et al., 2007; Schuhmann et al., 2008). Such a process is absent in yeasts. The C-terminal domain of AtPex7 was shown to associate with AtPex5, suggesting that AtPex5 might play a role in PTS2 protein import (Nito et al., 2002). Similar to mammals but unlike yeast, the PTS2 cargo import in plants requires the association of Pex7 with Pex5, proving the interdependence of this process on the PTS1 import pathway (Woodward and Bartel, 2005). In yeasts, two additional PTS2 receptors of redundant function have been identified, namely Pex18p and Pex21p (*S. cerevisiae*)/Pex20p (designated orthologs of Pex21p in other fungi) (Edward Purdue et al., 1998; Titorenko et al., 1998; Otzen et al., 2005). However, orthologs of these auxiliary PTS2 coreceptors have not been found yet in plants and mammals. Like yeast and human Pex7, AtPex7 also binds to AtPex13 (Mano et al., 2006), but no evidence supports its interaction with AtPex14. Furthermore, the molecular basis and factors involved in the recycling mechanism of Pex7 are poorly understood.

Early studies in *S. cerevisiae* had shown that soluble proteins without a PTS can be co-imported into peroxisomes by association with another PTS protein *via* dimerization, demonstrating that peroxisomes are capable of importing oligomers (Glover et al., 1994; McNew and Goodman, 1994). This process is referred to as piggy-back import (Glover et al., 1994). The physiological relevance of this phenomenon remained long unclear because native proteins were unknown to be imported by this mechanism. However, in *S. cerevisiae* the nicotinamidase enzyme lacking any PTS was shown to be co-imported into peroxisomes under stress conditions by interacting with glycerol-phosphate dehydrogenase 1, which contains a PTS2 (Kumar et al., 2016). First evidence for piggy-back import of endogenous PTS-lacking proteins in mammals and plants has also been reported (Islinger et al., 2009; Kataya et al., 2015).

1.1.4 Peroxisomal membrane protein import

The proteins sorted to the peroxisomal membrane possess a membrane PTS. According to their import route, PMPs are classified into class I and class II PMPs and tail-anchored (TA) proteins (Kim and Hettema, 2015; Cross et al., 2016). The class I PMPs are inserted into the peroxisomal membrane directly by the cytosolic chaperone Pex19 and in a Pex3-dependent manner, while class II PMPs are sorted to the ER and reach peroxisomes indirectly *via* budding of so-called pre-peroxisomal vesicles from the ER, considered as the *de novo* biogenesis of peroxisomes. TA proteins have been also shown to traffic to peroxisomes directly *via* Pex19 (in mammals) or indirectly *via* the ER, i.e., are sorted to the ER by the guided entry of TA protein (Get) complex (in yeast and plants) (Mayerhofer, 2016). Several lines of evidence have shown that Pex3, Pex19, and Pex16 (absent in yeast) are essentially required for PMP import. Thus, the lack of any of them resulted in cells with impaired peroxisomal membrane synthesis (Höhfeld et al., 1991; Honsho et al., 1998; Hettema et al., 2000). These two import pathways of PMPs have been found not only in fungi and mammals but also in plants (Cross et al., 2016).

Most PMPs belong to class I and contain one or several mPTSs including at least one transmembrane domain (TMD). The analysis of mPTSs of yeast, human, and plant class I PMPs showed the presence of positively charged aa (mixed with hydrophobic residues) located within approx. 11 aa next to the TMD (Honsho and Fujiki, 2001; Murphy et al., 2003; Rottensteiner et al., 2004). The class I PMPs are stabilized by binding of Pex19, which is partially associated with the peroxisomal membrane by its C-terminal farnesyl anchor, to their mPTS (Figure 1.2A) (Götte et al., 1998; Sacksteder et al., 2000; Jones et al., 2004). A study in Arabidopsis revealed the two isoforms of Pex19 (Nito et al., 2007), and both are farnesylated and targeted to the cytosol as their yeast and mammalian orthologs (McDonnell et al., 2016). The two isoforms redundantly function as each single *pex19* mutant showed no defect in peroxisomal protein import but the double mutant lines were embryo lethal (McDonnell et al., 2016). In *in vitro* assays, Arabidopsis Pex19 isoforms were shown to bind Pex10 (AtPex19-1) (Hadden et al., 2006) and an ATP binding cassette transporter of the peroxisomal membrane (AtPex19-1 and AtPex19-2 isoforms) (Nyathi et al., 2012), suggesting their capability of binding PMPs *in vivo*. During PMP insertion into the peroxisomal membrane, the PMP-Pex19 complex binds to Pex3, thereby inserting the PMPs into the membrane before Pex19 shuttles back to the cytosol (Fang et al., 2004; Matsuzono and Fujiki, 2006).
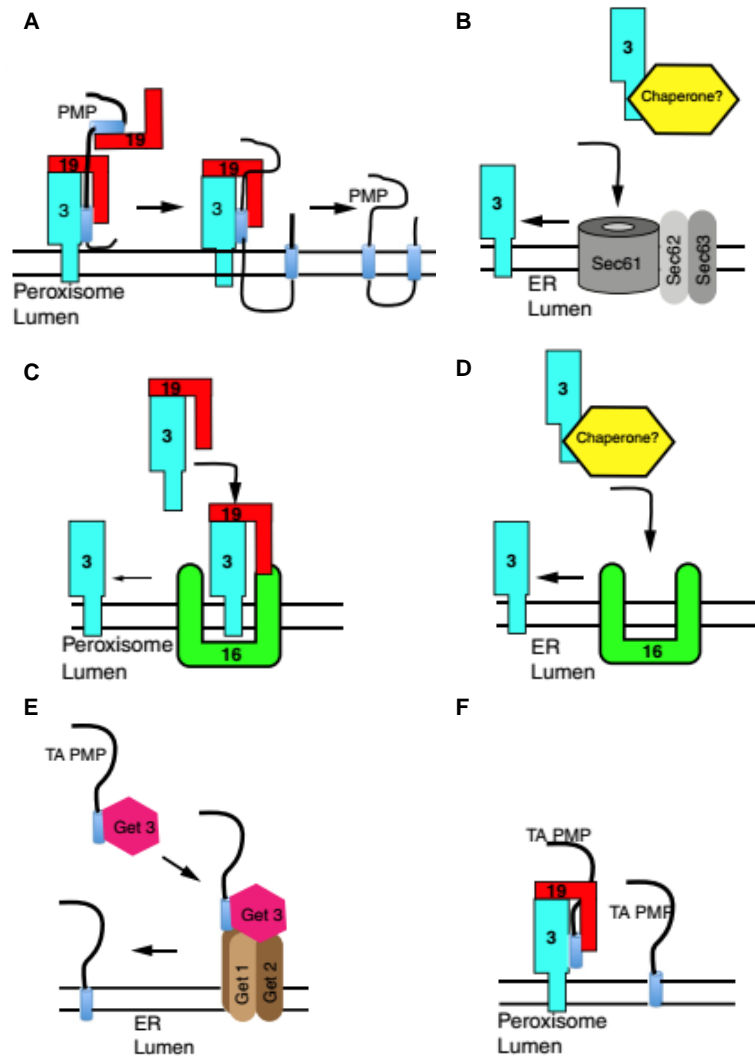
Figure 1.2: Schematic view of peroxisomal membrane import of PMPs including TA proteins

(A) Direct peroxisomal membrane insertion of class I PMPs by the Pex19 receptor. Class I PMPs possess an mPTS that is bound and chaperoned by Pex19 in the cytosol. The complex docks to Pex3 in order to translocate PMPs to the peroxisomal membrane. After translocation, the receptor is returned to the cytosol for the further rounds of import. (B) ER insertion of Pex3 and other class II PMPs by the ER-associated Sec translocon. The requirement of a cytosolic receptor for class II PMP import remain unknown, however, the involvement of Pex19 has been proven for the ER insertion of yeast Pex3p (Hoepfner et al., 2005). (C) Direct peroxisomal insertion of Pex3 by Pex19 in mammals. (D) Pex16-dependent ER insertion of in mammals. It is not known whether a cytosolic chaperone is involved in this process. (E) The peroxisome traffic of TA proteins indirectly *via* the ER by the Get machinery in yeast. (F) Unlike yeast, mammalian TA proteins follow the direct peroxisomal import by Pex19. The figure was modified from Kim and Hettema (2015). This article was distributed under the terms of the Creative Commons CC-BY license, which permits unrestricted use, distribution, and reproduction in any medium (https://creativecommons.org/licenses/by/4.0/).

Class II PMPs are targeted to the peroxisomal membrane by an ER-dependent pathway. Across yeast, mammals, and plants, our knowledge about the *de novo* synthesis of peroxisomes is primarily based on the intensive research on Pex3 as the best studied PMP of this group (Mayerhofer, 2016). Studies in *S. cerevisiae* showed that Pex3 is sorted first to the ER by a signal located in the N-terminal 46-aa domain, subsequently to a specific ER subdomain, and finally is targeted to pre-peroxisomal structures that bud off from the ER (Figure 1.2B) (Hoepfner et al., 2005; Kragt et al., 2005; Tam et al., 2005). The ER sorting and the budding process of yeast Pex3 were described to be dependent on the Sec61 translocon (Thoms et al., 2012) and Pex19 (Hoepfner et al., 2005). Mammalian Pex3 is either directly targeted to peroxisomes in a Pex19-dependent pathway (Figure 1.2C) (Matsuzaki and Fujiki, 2008) or indirectly *via* the ER, the pathway which recruits Pex16 (absent in yeast) (Figure 1.2D) (Kim et al., 2006; Hua et al., 2015). Arabidopsis Pex3 orthologs, e.g. one isoform of AtPex3, AtPex3-2 was not observed in the ER and was localized rapidly to the peroxisomal membrane (Hunt and Trelease, 2004). The only Arabidopsis class II PMP for which the ER-peroxisome traffic route is strongly confirmed is AtPex16, as it was observed in the cytosol, the ER, and non-peroxisomal structures at early expression time (2 – 4 h), before eventually being detected in peroxisomes in Arabidopsis and tobacco suspension cells (Karnik and Trelease, 2007). Thus, microscopic evidence has been provided that in plants at least one PMP, AtPex16, is first sorted to the ER. However, details of the ER-peroxisome trafficking route in plants, i.e., an ER budding event of pre-peroxisomal structures and/or their fusion with pre-existing per-oxisomes, have not been described.

A small subset of PMPs are TA proteins. They have a C-terminal TMD. Once this TMD emerges from the cytosolic ribosomes, TA proteins are recognized by cytosolic interacting proteins and are post-translationally targeted to the membrane of organelles, such as the ER, chloroplasts, and mitochondria by ER-associated and ATP-dependent machineries. The Get complex (Get1, 2, and 3) in yeast or the cytosolic TMD recognition complex in mammals (TRC40, a Get3 homolog) are involved in ER insertion of TA proteins (Stefanovic and Hegde, 2007; Schuldiner et al., 2008). Regarding peroxisomal membrane import of TA proteins *via* ER sorting, in yeast and plants, the Get machinery is involved, at least this was strongly demonstrated for yeast (Figure 1.2E) while in mammals Pex19 but not the TRC40 complex is required for the direct import mechanism of TA proteins, e.g. Pex26 (Figure 1.2F) (Yagita et al., 2013; Chen et al., 2014). In details, yeast Pex15p was proven to first be an ER-localized protein by the Get machinery prior to be sorted to the peroxisomal membrane. However, peroxisomal

import of Pex15p was not tightly regulated by the Get pathway (Schuldiner et al., 2008; van der Zand et al., 2010). Although the Get machinery-dependent pathway has been merely investigated for plant peroxisomal TA proteins, their peroxisome traffic *via* the ER was apparently observed, e.g. Arabidopsis ascorbate peroxidase isoform 3 (AtAPX3) and its orthologs in cottonseed and pumpkin (Mullen et al., 1999; Mullen and Trelease, 2000; Nito et al., 2001; Lisenbee et al., 2003). Therefore, across kingdoms both Pex19- and ER-dependent pathways are required for peroxisomal membrane insertion of TA proteins.

Recently, in human patient cells lacking peroxisomes, peroxisomal membrane assembly of class II PMPs, including Pex3 and Pex14, have been proposed to be *de novo* synthesized from both mitochondria- and the ER-derived pre-peroxisomal vesicles (Sugiura et al., 2017). The approach of live cell imaging by confocal microscopy showed the budding events as well as the fusion events of these vesicles before they became fully import competent peroxisomes. Thus, the *de novo* biogenesis of peroxisomes is described well for mammals, but much less for other organisms, especially for plants.

1.1.5 Function of peroxisomes in plant responses to abiotic and biotic stress

Beyond the obvious link between peroxisome functions and catabolic and anabolic metabolism, a growing body of evidence supports a central role for peroxisomes as defense organelles against biotic and abiotic stress. ROS are normally generated as byproducts of metabolism, however, ROS levels are rapidly increased and the molecules function as signal transducers in plant responses to biotic and abiotic stress (Apel and Hirt, 2004; Del Río and López-Huertas, 2016). In addition to mitochondria and chloroplasts, the peroxisome is a cellular compartment of ROS production with its own detoxifying system of a pool of antioxidants such as ascorbate and glutathione and ROS-scavenging enzymes (1.1.1). Thus, peroxisomes contribute to cell protection from oxidative damage. Higher activities of catalase, superoxide dismutase, and ascorbate peroxidase correlated with suppressed ROS production when plants were challenged with salt (Mittova et al., 2004), drought, and cold stress (Guo et al., 2006). A couple of studies documented the induction of peroxisome proliferation by oxidative stress and that was mediated by ROS (Morré et al., 1990; Palma et al., 1991). A similar proliferation of peroxisomes was also observed under salinity (Mitsuya et al., 2010) and cadmium stress (Rodríguez-Serrano et al., 2016). An up-regulation of *Pex* genes by ROS and environmental cues has been demonstrated, e.g. of *Pex1* upon wounding and pathogen attack (Lopez-Huertas et al., 2000) and of *Pex1*, *Pex10* (Charlton et al., 2005), and *Pex11e* (Mitsuya et

al., 2010) under salt stress. Recently, the formation of dynamic extension of peroxisomes before proliferation, named peroxules, was shown to require Pex11 in response to ROS produced by cadmium stress (Rodríguez-Serrano et al., 2016). Taken together, these studies suggest that an adequate number of peroxisomes are required to assist in maintaining the cellular redox balance.

Apart from ROS, nitric oxide (NO) generation is also part of plant responses to pathogens (Trapet et al., 2015) and abiotic stress (Corpas et al., 2011). Covalent binding of NO to proteins, the so-called S-nitrosylation, is a post-translational modification that has been found in Arabidopsis proteins during hypersensitive response (HR) (Moreau et al., 2012). A group of peroxisomal proteins, which are involved in β-oxidation, ROS detoxification, and photorespiration, has been shown to be S-nitrosylated under physiological conditions, and of these, the S-nitrosylated protein amount of catalase and glycolate oxidase was reduced and disappeared, respectively in plant responses to cadmium stress (Ortega-Galisteo et al., 2012). The same study also showed that the activity of these two enzymes was inhibited by NO donors. Thus, it was suggested that the reduction in the S-nitrosylated enzyme amounts under cadmium stress could be a way how NO regulates H_2O_2 level in peroxisomes through S-nitrosylation.

Peroxisomes catalyze the last phase of the synthesis of the defense hormone JA, upon transport of JA precursors from chloroplasts into peroxisomes. JA plays a role as a regulator in wound-activated and defense responses and functions antagonistically with salicylic acid (SA) in biotic stress (León, 2013). However, the involvement of peroxisomes in terms of mediating JA synthesis in response to wounding and defense remains unclear. Notably, diverse functions of peroxisomes in biotic stress defense have been proposed based on (i) the prediction of novel PTS1 proteins related to pathogen defense or homologous to known defense proteins (Sørhagen et al., 2013) or (ii) from revealed functions of some peroxisomal proteins, e.g. PENETRATION 2, a peripheral membrane enzyme which hydrolyzes indole glucosinolates, which are important for the resistance to fungal preinvasion (Lipka et al., 2005; Bednarek et al., 2009).

1.2   Plant immunity responses

Due to constant challenges by pathogens, plants continuously evolve diverse adaptation mechanisms at the level of physical barriers and at the cellular level of molecular mechanisms,

all of which are well-explored and involved in two layers of plant innate immunity, the so-called pattern- and effector-triggered immunity.

1.2.1 Pattern-triggered immunity (PTI)

PTI is triggered by the perception of pathogen-associated molecular patterns (PAMPs), e.g. bacterial flagellin and fungal chitin acting as elicitors, also preferentially termed microbe-associated molecular patterns (MAMPs). To recognize these factors, there are several well-characterized pattern recognition receptors (PRRs) that are localized in the plasma membrane and categorized as receptor-like kinases (RLKs) or receptor-like proteins (RLPs). For example, FLAGELLIN INSENSITIVE2 (FLS2) and the EF-Tu receptor (EFR) recognize the N-terminal domain of bacterial flagellin (e.g., flg22) and an 18-aa epitope from elongation factor (e.g., elf18), respectively (Zipfel et al., 2004; Zipfel et al., 2006).

Upon the perception of PAMPs or MAMPs, Ca^{2+} channels and pumps are activated, resulting in Ca^{2+} influx and a rapid increase in cytosolic Ca^{2+} concentration (Jeworutzki et al., 2010). The perception of elf18 and flg22 was shown to lead to an extracellular alkalinization due to an H^+ influx and anion efflux and a depolarization of the plasma membrane (Jeworutzki et al., 2010). Other cellular defense responses that are essential for plants to restrict pathogen infection include the accumulation of ROS, NO, and phosphatidic acid, the activation of a MAP kinase cascade, biosynthesis of phytohormones (ethylene, JA, and SA), callose deposition, as well as massive transcriptional activation of defense-related genes such as *PR1* (Bigeard et al., 2015).

1.2.2 Effector-triggered immunity (ETI)

In order to escape PTI and successfully infect the host, pathogenic bacteria secrete effector proteins into plant cells. The effector proteins can either interfere with PTI and/or inhibit this signal transduction pathway, referred to as effector-triggered susceptibility. If host cells are able to recognize these effectors, ETI is triggered, e.g. induction of HR to limit pathogen invasion as well as initiating SA-dependent local responses or systemic acquired resistance mechanism (SAR) (Jones and Dangl, 2006).

To trigger ETI, cells contain resistance (R) proteins that bind either directly or indirectly their respective effectors (encoded by the avirulence genes from the pathogen), activating downstream R-gene-mediated signaling pathways (Hammond-Kosack and Jones, 1997). Most R proteins belong to the largest class and carry a central nucleotide-binding site (NBS) and C-

terminal leucine-rich repeat (LRR) domains, the so-called NBS-LRR class. This class is subdivided depending of the presence of either an N-terminal coiled-coil (CC) or a TOLL/INTERLEUKIN-1 RECEPTOR (TIR) domain (Dangl and Jones, 2001). The domain structure of few other R-proteins are different, and one of them, Pto, a Ser/Thr kinase from tomato, is required for resistance against *Pseudomonas syringae* (*Ps*) carrying *avrPto* in addition to the NBS-LRR protein Prf (Salmeron et al., 1996; Tang et al., 1996). Several R proteins belonging to the NBS-LRR class have been functionally characterized, e.g. CC–NBS–LRR proteins including RESISTANCE TO *PSEUDOMONAS SYRINGAE* PV. *MACULICOLA* 1 (RPM1), RESISTANCE TO *PSEUDOMONAS SYRINGAE* 2 (RPS2), RESISTANCE TO *PERONOSPORA PARASITICA* 7 and 8 (RPP7 and RPP8). With respect to other R proteins (TIR–NBS–LRR proteins), e.g. RPP1 and RPP5, their functions in plant immunity have also been resolved. These R-proteins mediated different downstream signaling pathways (Glazebrook, 2001). In details, RPP1 and RPP5 regulate one specific signaling pathway that requires ENHANCED DISEASE SUSCEPTIBILITY 1 (EDS1), while RPM1 and RPS2 activate another signaling pathway that is dependent on NON-RACE SPECIFIC DISEASE RESISTANCE 1 (NDR1) (Aarts et al., 1998). Neither EDS1 nor NDR1 is required for the pathway mediated by two other CC–NBS–LRR type R-proteins, RPP7 and RPP8, defining a third signaling pathway of ETI (McDowell et al., 2000).

Among ETI responses, HR is a phenomenon of cell death (necrotic lesions) that are associated with plant resistance to pathogen infection. This response often occurs within a few hours after infection, and the time for developing the HR and the impact of the HR may vary depending on the lifestyle of pathogens (Morel and Dangl, 1997). The HR could be initiated not only by effector proteins, which are encoded by *avr* genes and secreted from pathogen, but also by elicitors (Eder and Cosio, 1994). Following the recognition and as a consequence of signal transduction, the activation of pathogen-inducible genes, also known as defense-related genes, is facilitated. Among these, there are structural proteins incorporated into the cell wall, pathogenesis related proteins, and enzymes involved in the synthesis of anti-microbial compounds (Bradley et al., 1992). Other than this, molecular events such as SA accumulation, elevated ROS production, MAPK activation cascade, and changes in intracellular calcium levels also involve in initiation of HR (Coll et al., 2011). To avoid destructive damage caused by uncontrolled cell death, plants also develop anti-cell death pathways consisting of proteins involved in detoxification of phenolic compounds, e.g. lethal leaf spot 1, known as a suppressor of cell death by scavenging SA (Gray et al., 1997; Morel and Dangl, 1997).

1.3 Abscisic acid (ABA), a master hormone in plant responses to abiotic stress

The phytohormone ABA plays many crucial roles in plant growth and development. ABA biosynthesis has been characterized in detail. This pathway begins in chloroplast with an oxidative cleavage of a carotenoid precursor (C_{40}) to synthesize the intermediate xanthoxin (C_{15}). The remaining reactions leading to ABA take place in the cytosol. Genetic studies on physiological processes mediated by ABA such seed germination and dormancy revealed the ABA-deficient (*aba*) mutants of Arabidopsis, allowing the identification of the enzymes involved in ABA biosynthesis, e.g. *ABA1 – 4* (Finkelstein, 2013).

Molecular analyses revealed several ABA-responsive transcription factors (TFs) and functional genes activated as downstream targets by the ABA signaling pathway (Leng et al., 2013). Signal transduction by ABA is well understood with a three-step signal relay: (i) ABA is perceived by the cytosolic receptors, REGULATORY COMPONENTS OF ABA RECEPTOR, PYRABACTIN RESISTANCE 1, or PYRABACTIN RESISTANCE 1-LIKE proteins, (ii) the ABA-receptor binding complex is stabilized which subsequently interacts with a protein phosphatase of type 2C, thereby blocking the inhibition activity of this phosphatase on SUCROSE NON-FERMENT-ING-1 (SNF1)-RELATED PROTEIN KINASE 2 (SnRK2), and (iii) ABA-responsive target genes such as TFs and membrane channels are activated by SnRK2 (Soon et al., 2012; Yoshida et al., 2019).

Although ABA is not the sole regulator of plant growth and development, it is known to initiate embryo maturation during seed development as well as seed dormancy (Nambara et al., 2010). During dehydration stress, a high accumulation of late embryogenesis abundant (LEA) proteins is induced by ABA resulting in the preservation of embryo vitality and dehydration tolerance (Xiong and Zhu, 2003). Under water deficit and higher CO_2, ABA regulates stomatal aperture by activating anion channels of guard cells, thereby, inducing stomatal closure (Sussmilch et al., 2017). The increase of ABA level correlates with plant responses to severe environmental conditions, such as dehydration, salt, and low temperature. Although ABA is better known for its regulation during abiotic stress responses, it is also involved in biotic stress responses. ABA suppressed the elevation of SA by inhibiting the signal transduction upstream and downstream of SA accumulation, suggesting that ABA functions antagonistically with SA during pathogen defense (Yasuda et al., 2008).

1.4 The NHL protein family

The tobacco *HARPIN-INDUCED 1* (*HIN1*) gene was first isolated due to its induced expression by harpin, a protein elicitor secreted from bacterial pathogens, and became a known HR

marker gene (Gopalan et al., 1996). Arabidopsis NDR1 is homologous to HIN1 and was identified as a signal modulator in ETI (1.4.1) against bacterial and fungal pathogens (Century et al., 1995; Century et al., 1997). The Arabidopsis family of NDR1/HIN1-like (NHL) proteins consists of at least 45 members (Dörmann et al., 2000; Zheng et al., 2004). They typically possess one or two predicted TMD and contain three conserved motifs, of which the second (NPNKRIGIYYD) and the third (PFYQGHKN) are highly conserved (Zheng et al., 2004). However, in the past two decades, apart from NDR1, the biological function of most NHLs has not yet been uncovered.

1.4.1 Role of NHLs in plant responses to biotic and abiotic stress

The role of NDR1 in pathogen defense has been studied comprehensively. The loss of NDR1 function (lacking a DNA fragment) rendered the WT highly susceptible to fungal and bacterial pathogens and revealed an important function of NDR1 in plant immunity (Century et al., 1995). Relative to WT, the *ndr1-1* mutant displayed enhanced susceptibility to virulent *Pseudomonas syringae* pv. *tomato* DC3000 (*Pst*) and avirulent *Pst* expressing any one of the four avirulence genes, *avrB*, *avrRpm1*, *avrRpt2,* and *avrPph3*. Thus, NDR1 is considered as a signal modulator that is essential for the stimulation of signaling pathways mediated by relevant R proteins, e.g. RPM1, RPS2, and RPS5, independently of EDS1 (see also 1.2.2; Century et al., 1995; Aarts et al., 1998). The inducible expression of NDR1 was observed upon infection by both virulent and avirulent *Pst* strains, implying its role in both PTI and ETI (Century et al., 1997). A role of NDR1 has been revealed in plant immunity responses, which are part of ETI, e.g. SAR and HR, as SA accumulation and SAR induction were abolished in the *ndr1-1* mutant upon the infection with *Pst*(*avrRpt2*) (Shapiro and Zhang, 2001). NDR1 was shown to be specifically involved in the HR induced by AvrRpt2 but not by other effector proteins including AvrB, AvrRpm1, and AvrRph3 (Century et al., 1995; Aarts et al., 1998). NDR1 self-associates and undergoes posttranslational modification by *N*-glycosylation and glycosylphosphatidyl-inositol anchoring at its C-terminus (Coppinger et al., 2004). NDR1 resides in the plasma membrane and act as a signal transducer. To activate the downstream components of the RPM1- and RPS2-mediated signaling pathways, RPM1-INTERACTING PROTEIN 4, a negative regulator of these pathways, is known to associate with NDR1, which is essential for downstream signal transduction (Day et al., 2006). Furthermore, NDR1 has been shown to be involved in maintaining the integrity of the cell wall and plasma membrane connection (Knepper et al., 2011a). Taken together, NDR1 displays important functions in signaling plant

defense responses to pathogen infection and in the regulation of cell wall adhesion (Knepper et al., 2011b).

Since computational description of the NHL protein family, several members were reported to be induced upon pathogen infection. Expression analysis of a subset of eight Arabidopsis *NHL* genes revealed that *NHL3* and *NHL25* were induced upon infection by *Pst* expressing any of the four avirulence genes (*avrRpm1*, *avrRpt2*, *avrB*, or *avrRps4*) and upon SA treatment (Varet et al., 2002). The *Pst*(*avrRpm1*)-dependent induction of *NHL25* (but not of *NHL3*) was suppressed in the Arabidopsis mutant expressing a bacterial salicylate hydroxylase (*nahG*), which therefore lacks endogenous SA, suggesting that NHL25 is specifically involved in SA-dependent immunity responses. Also, because the pathogen-inducible expression of both *NHL25* and *NHL3* was unaffected in mutants defective in signaling by ethylene (e.g., in the *etr1-3* and *ein2-1* mutants) and jasmonate (e.g., in the *coi1-1* mutant) as well as in pathogen susceptible mutants including *ndr1-1* and *pad4-1*, NHL25 and NHL3 are likely not involved in ethylene and jasmonate signaling pathways or in pathogen resistance regulated by NDR1 and PAD4 (Varet et al., 2002). In addition, *NHL3* expression (but not that of *NHL25*) was upregulated not only by avirulent but also by virulent *Pst* (Varet et al., 2002). By immunofluorescence and immunogold labeling, NHL3 was demonstrated to be localized in the plasma membrane and *N*-glycosylated in stable transgenic Arabidopsis plants expressing a tagged version of NHL3 from the dexamethasone-inducible promoter (Varet et al., 2003). Except for *ndr1, nhl6, nhl13,* and *nhl26* knockout (KO) mutants have not been characterized phenotypically. Interestingly, transgenic Arabidopsis plants overexpressing *NHL3* showed enhanced resistance to virulent *Pst*, and the degree of resistance correlated with the level of *NHL3* transcript (Varet et al., 2003).

The Arabidopsis ortholog of tobacco *HIN1*, *NHL10,* accumulated during HR triggered by the avirulent *Cucumber mosaic virus* (CMV) strain (Zheng et al., 2004). When expressed as C-terminal GFP fusion in *Vicia faba* guard cells, NHL10 as well as NHL2 were observed in chloroplasts. Experimental data allowed the conclusion that the CMV-induced expression of *NHL10* was mediated by an SA-dependent pathway (Zheng et al., 2004). NHL2 shares high sequence identity of 56% with HIN1 (Dörmann et al., 2000). Even though *NHL2* expression was unaffected by *Pst* and Arabidopsis NHL2 overexpressor (OE) lines were unaffected in *Pst* susceptibility, the expression of pathogenesis-related gene 1 (*PR1*) was increased and light-dependent 'speck disease-like' symptoms became visible in the leaves of the transgenic plants

(Dörmann et al., 2000). *NHL13* was found to be down-regulated by *Pst* if expressing two effector proteins, AvrE and HopM1, which function redundantly in Arabidopsis. The disruption of *NHL13* rendered the WT more susceptible to these strains, demonstrating that NHL13 is specifically required for this antibacterial immunity (Xin et al., 2015).

In on-going attempts to render crop plants more resistant to pathogen attack by heterologous overexpression of *NHL* genes in the long-run, *AtNHL1* and *AtNHL8* were overexpressed in soybean (*Glycine max*) and could enhance disease resistance to nematodes (Maldonado et al., 2014). Other studies documented that NHL homologs of potato and grape contributed to enhanced resistance to an oomycete (Chen et al., 2018), *Pst*, and *Botrytis cinerea* (Chong et al., 2008). By genome-wide analysis, 15 NHL homologs in pepper (*Capsicum annuum*) were identified, and three of them were highly induced by *Phytophthora capsici*, tobacco mosaic virus, and *P. syringae* (Liu et al., 2020). The function of CaNHL4 was revealed to be important for pepper resistance to these pathogens.

Apart from the roles of NHLs in plant pathogen defense, a couple of studies also revealed promising biological functions of NHLs in plant responses to abiotic stress. *NHL6* was found to be highly induced by ABA, and loss of function of *NHL6* rendered WT less sensitive to ABA at early developmental stages, including seed germination and post-germinative seedling growth. Transgenic plants overexpressing *NHL6* from the *Cauliflower Mosaic Virus* (*CaMV*) *35S* promoter became more sensitive to ABA, salt, and osmotic stress and displayed increased endogenous ABA concentrations under stress conditions (Bao et al., 2016). Thus, a possible role of NHL6 in ABA-dependent signaling pathway response to abiotic stress had been proposed. Some NHLs have also been shown to regulate plant growth and development. Overexpression of *NHL26*, encoding a phloem-specific protein localized to the ER and plasmodesmata membrane (in the interfaces between companion cells, sieve elements, and phloem parenchyma cells), resulted in an increased level of carbohydrates and higher shoot biomass in plants compared to WT (Vilaine et al., 2013). Further evidence in the same study demonstrated that increased *NHL26* was responsible for changing phloem export and sugar partitioning in Arabidopsis.

A change of subcellular localization in plant responses to abiotic stress was proposed for one NHL homolog of *Brassica napus*. This protein was primarily enriched in the ER of Arabidopsis protoplasts and translocated outside of the ER in response to NaCl and H_2O_2

treatments (Lee et al., 2006). However, the final localization of this protein in the cytosol or other membrane compartments was unable to be concluded.

1.4.2 NHL proteins as a sub-group of late embryogenesis abundant (LEA) proteins

Approximately half of the Arabidopsis NHL proteins including NHL4, NHL6, and NHL25, which are central to this study, belong to a specific subgroup of the LEA proteins. These proteins were first identified in cotton (*Gossypium hirsutum*) seeds and are highly abundant at the late stage of embryogenesis (Dure III et al., 1981). In Arabidopsis, the LEA family covers many groups of proteins based on different criteria of classification, and the nomenclature of this family was inconsistent in the literature for a long time, raising difficulties in gene annotation (Dure et al., 1989; Bray, 1993; Dure III, 1993; Wise and Tunnacliffe, 2004). According to the Pfam domain database (http://pfam.xfam.org/), sequence motifs and biased amino acid composition, LEA members identified in Arabidopsis have been classified into nine different subgroups, including, for instance, dehydrin (PF00257) and LEA_2 (PF03168) (Hundertmark and Hincha, 2008). Their subcellular localization was also predicted in various subcellular compartments, e.g. the cytosol, nucleus, chloroplasts, and mitochondria (Hundertmark and Hincha, 2008). The Arabidopsis LEA_2 subgroup consists of 51 members, out of these 27 proteins belong to the Arabidopsis NHL family (NHL1 – 6, 9 – 15, 17 – 23, 25, 26, 30, 36, and 39 – 41; Nguyen, Khan, and Reumann, unpubl. data). Genome-wide sequence analyses have identified LEA homologs in many other different species, e.g. *Zea mays* (Amara et al., 2012), *Sorghum bicolor* (Nagaraju et al., 2019), and *Oryza sativa* (Wang et al., 2007). Interestingly, LEAs are not fully plant-specific, as they have been found in bacteria, such as *Bacillus subtilis* (Stacy and Aalen, 1998), *Deinococcus radiodurans* (Battista et al., 2001), and cyanobacteria (Close and Lammers, 1993) as well as in animals (see review by Hand et al., 2011).

Apart from seeds, Arabidopsis LEAs were also found in roots, buds, and reproductive organs (Hundertmark and Hincha, 2008). Several *LEAs* are highly expressed under ABA and abiotic stress conditions, e.g. low temperature, dehydration, and high salinity (Curry et al., 1991; Romo et al., 2001; NDong et al., 2002; Bies-Etheve et al., 2008; Kosová et al., 2008), indicating a role in plant mechanisms to deal with such environmental changes. Indeed, studies of transgenic plants overexpressing *LEAs* revealed diverse functions of LEAs, which enhance the plant tolerance under abiotic stress conditions (NDong et al., 2002; Brini et al., 2007).

To reveal their functions, several studies have used heterologous expression of yeast and *E. coli* and *in vitro* enzymatic assays. Interestingly, plant LEAs often also conferred abiotic stress resistance in yeast and *E. coli* (Swire-Clark and Marcotte, 1999; Liu and Zheng, 2005). Moreover, several *in vitro* assays have been established to investigate a general protective role of LEAs as molecular chaperones. Commercial enzymes (e.g., malate or lactate dehydrogenase) are subjected to heat, drying or low temperature, and the decline in enzymatic activity is measured in the presence or absence of LEAs. Many LEA proteins, primarily of dehydrins and LEA_4, protected the enzymes from denaturation (Hara et al., 2001; Sanchez-Ballesta et al., 2004; Nakayama et al., 2007), implying their functions as stress protective chaperones. Additional commercial enzymes, such as fumarase, rhodanese, catalase, and citrate synthase were stabilized by plant LEAs if subjected to desiccation and freezing (Hara et al., 2001; Goyal et al., 2005; Grelet et al., 2005). Thus, several LEAs have been shown to play a role as a molecular shield and are capable of protecting target proteins *in vivo* from partial denaturation under stress conditions. Structural analyses could perhaps gain further insights into the protective role of LEAs.

Arabidopsis LEA members of different sub-groups often do not share significant sequence similarity with each other, thereby not allowing the conclusion of similar function. Most AtLEAs are highly hydrophilic and intrinsically unstructured (Battaglia et al., 2008). As a result, structural data are hardly available for LEA proteins. By contrast, LEA_2 subgroup members are rather hydrophobic and not intrinsically unstructured, implying sub-group specific functions. As the first member of this subgroup, the structure of AtLEA14 was resolved, showing structural similarity to the fibronectin type III domain group (Singh et al., 2005). In animals, fibronectins function as cell surface binding proteins that are involved in wound healing, cell adhesion, and cell motility, thus, a similar function in plants was suggested for AtLEA14 (Singh et al., 2005). *AtLEA14* is highly induced by several abiotic stresses such as cold, drought, high light, and salt stresses (Kimura et al., 2003) but not by pathogens or defense-related signaling hormones (Schenk et al., 2000). Overexpression of *AtLEA14* resulted in enhanced salt stress tolerance of Arabidopsis (Jia et al., 2014). Altogether, it is suggested that AtLEA14 might share similar structural and functional properties with its Arabidopsis sub-group members, including the 27 NHL paralogs as mentioned earlier.

1.4.3   NHL proteins: Peroxisome targeting analyses and biological functions

To date, none of the plant NDR1 homologs has been proven to be associated with peroxisomes. Previous studies from the Reumann group, however, showed that several NHL homologs are predicted PTS1 proteins and are indeed peroxisome-targeted (Kataya, 2011; Crappe, 2016). These proteins are the members of one specific sub-clade (comprising NHL4, NHL6, and NHL25) which contain a single predicted N-terminal TMD and a central LEA_2 domain (Figure 1.3).
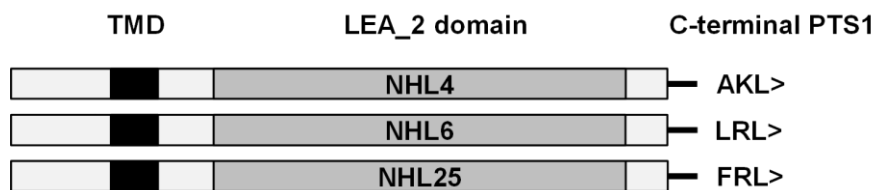
Figure 1.3: Domain structure of NHL4, NHL6, and NHL25

The membrane association of NHL4 and NHL25 was confirmed experimentally in transiently transformed Arabidopsis protoplasts (Crappe, 2016; Chowdhary and Reumann, unpubl. data). Surprisingly, from subcellular localization studies, these proteins did not seem to be directed to peroxisomes by the standard PTS1 pathway for soluble matrix proteins. In onion epidermal cells, the EYFP-tagged fusions of the three NHL proteins were observed to target to vesicle-like structures but not peroxisomes (Kataya, 2011). Notably, in a few exceptional cases of transiently transformed tobacco protoplasts 48 hours post transformation (hpt), these small vesicles (for NHL4) were found in close proximity to mature peroxisomes (Kataya, 2011). In tobacco protoplasts, EYFP-NHL4 was observed occasionally in peroxisomes but only at late expression time 48 hpt (Kataya, 2011). This peroxisome targeting of NHL4 remained rare to observe and difficult to detect 24 hpt in approx. 20% of the transformed Arabidopsis protoplasts from young leaves, while the cell ratio was even lower with approx. 10% for NHL6 and NHL25 (Crappe, 2016). Interestingly, NHL4 was detectable in ER-like network structures in transiently transformed protoplasts (Crappe, 2016). However, when co-expressed with an ER marker, the ER localization of NHL4 could not be convincingly shown, possibly because the ER targeting of NHL4 was finished too rapidly to be observed. Subcellular localization studies of these proteins in tobacco and Arabidopsis protoplasts showed that NHL4, NHL6, and NHL25

were clearly detected in the cytosol, small vesicle-like structures of unknown identity, and peroxisomes, implying a trafficking pathway from the ER *via* budded vesicles to peroxisomes. The peroxisomal targeting pathway *via* the ER and vesicle intermediates has been mostly investigated in mammals and yeasts and merely proposed for plants (1.1.4). The most interesting feature of NHL targeting to peroxisomes, however, was rarely observed and often not reproducible, requiring more detailed comprehensive analyses.

Towards elucidating the biological function of these NHLs, gene expression analyses were carried out for *NHL6* and *NHL25* under pathogen infection. As revealed by qRT-PCR, expression of *NHL6* was upregulated (> 10 fold) by both virulent *Pst* and avirulent *Pst*(*avrRpt2*) 12 and 18 hours post infection (hpi) (Kataya, 2011; Crappe, 2016). In addition, the expression *NHL6* was induced by flg22 and SA (Crappe, 2016). These data suggested an involvement of NHL6 in both the PTI and ETI pathways mediated by SA. Metabolomic analyses of the two double *nhl6-1 x nhl25-1* mutant lines upon the flg22 treatment displayed a significant difference compared to WT in terms of an accumulation of specific lipids and defense molecules (Crappe, 2016). Taken together, the biological function of NHL6 and NHL25 as well as NHL4 in plant immunity remained to be studied in greater details.

1.5   Objectives

A specific subclade of Arabidopsis NHL proteins including three members (NHL4, NHL6, and NHL25) had been indicated to be directed to peroxisomes. These three NHLs represent PMPs but atypically carry a PTS1 which is specifically described for soluble matrix proteins of peroxisomes. Hence, these NHLs are possibly targeted to peroxisomes in a novel targeting pathway, resembling that of PMPs and PTS1 proteins. In addition, the molecular functions of the three NHL proteins in plant defense had not yet been revealed. Therefore, the overall aims of this study were (i) to investigate in depth their peroxisomal targeting pathway, and (ii) to study their predicted functions primarily in plant innate immunity.

The objectives were formulated in the following manner:

(1) To demonstrate reproducibly and reliably that the three NHL proteins of interest were indeed targeted to peroxisomes as their final destination, transient *in vivo* subcellular targeting analyses should be established in intact Arabidopsis seedlings (Li et al., 2009) including comprehensive controls. The functionality of the predicted PTS1 should be investigated by appropriate methodology. In addition, peroxisome targeting should be confirmed in stable Arabidopsis lines by either overexpressing *EYFP*-tagged *NHL* constructs from the strong *CaMV 35S* promoter or by expressing genomic *EYFP*-tagged constructs from the native promoters.

(2) To characterize the hypothesized vesicular trafficking pathway of these NHL proteins from the ER to peroxisomes, trafficking intermediates (e.g., the ER and vesicle-like structures) should be characterized in depth by confocal microscopy and TEM. In addition to full-length proteins, the biogenesis pathway should be investigated by appropriate truncated and mutated constructs.

(3) To investigate the postulated function of NHL4 in abiotic stress resistance, the survival of *E. coli* transformants expressing *NHL4* under osmotic stress conditions should be investigated in an *in vivo* assay, similar to other LEA_2 proteins. The effect of ABA on *NHL* gene expression should be investigated; single KO and OE lines should also be analyzed for altered sensitivity of ABA-dependent inhibition of seed germination.

(4) To investigate the postulated function of the three NHL proteins in plant innate immunity, their gene expression should be studied based on publicly available microarray data and be validated by qRT-PCR with focus on bacterial infection and by stable *GUS* reporter lines using

the endogenous *NHL* promoters. A reverse genetic approach of the single *nhl* KO mutants should be supplemented by double (*nhl6-1 x nhl25-1*) and triple (*nhl4-1 x nhl6-1 x nhl25-1*) mutants. All lines should be phenotypically characterized primarily under pathogen infection by investigating alterations in proliferation of avirulent *Pseudomonas* strains and analyzing the kinetics of HR progression in comparison to WT and *ndr1-1*.

2 MATERIALS AND METHODS

2.1 Arabidopsis cultivation and stress application

2.1.1 Arabidopsis cultivation

Arabidopsis thaliana ecotype Columbia (Col-0) seeds were sown in pots containing a mixture of commercial soil (Einheitserde Profisubstrate 70 liters, Einheitserdwerke Werkverband eV, Uetersen, Germany), sand, and vermiculite in a volume ratio of 7:2:1. Trays with pots after sowing were covered by plastic domes and stratified at 4°C for 4 days to synchronize seed germination. Seeds germinated and plants were grown in a light chamber under standard long-day conditions (21°C, 16 h light/8 h dark, 50 – 100 µmol·m^{-2}·s^{-1} light intensity, approx. 65% humidity), unless specified further. The plants were fertilized once a week with Hoagland nutrient solution (Hoagland and Arnon, 1950).

For experiments requiring sterile conditions, *Arabidopsis thaliana* ecotype Col-0 seeds were surface-sterilized in 70% (v/v) ethanol for one min, followed by 1.5% (w/v) sodium hypochlorite (NaOCl) for 20 min. Seeds were subsequently washed with sterile deionized water five times prior to sowing on 0.5x Murashige and Skoog (MS) medium (Duchefa, Haarlem, Netherlands) supplemented with 1% (w/v) sucrose and 0.8% (w/v) plant agar (pH 6.0). For transient seedling transformation, 0.25x MS medium was used instead. After 4 days of stratification at 4°C (only one day of stratification in transient transformation experiments), seeds were grown in a Percival growth incubator (CLF Plant Climatics, Wertingen, Germany) under standard long-day conditions (21°C, 16 h light/8 h dark, 100 µmol·m^{-2}·s^{-1} light intensity, approx. 65% humidity).

Homozygous single knockout (KO) mutant seeds (*nhl4-1*, SAIL_681_E12; *nhl6-1*, SALK_148523; *nhl25-1*, SALK_113216) were kindly provided by Dr. Kirsti Sørhagen (University of Stavanger, Stavanger, Norway). Two independent lines of double *nhl6-1 x nhl25-1* mutants (KS23, line 1; KS37, line 2) had been created by cross pollination between the two single *nhl6-1* and *nhl25-1* KO mutants (Sørhagen and Reumann, unpubl. data). The *ndr1-1* mutant was kindly provided by Prof. Dr. Sheng Yang He (Michigan State University, Lansing, USA).

2.1.2 Biotic stress application by the bacterial pathogen *Pseudomonas syringae*

To study gene expression under biotic stress conditions, 4- to 5-week-old *Arabidopsis* (Col-0) plants grown in a Percival growth chamber under standard growth conditions (2.1.1) were used to infiltrate different *Pst* strains, e.g. *Pseudomonas syringae* pv. *tomato* strains *Pst*

DC3000 (shorter form, *Pst*), *Pst*(*avrRpm1*), or *Pst*(*avrRpt2*). First, the bacteria were streaked out from a glycerol stock and grown on King's B medium agar plates (Suppl. Table 1) supplemented with appropriate antibiotics (2.2). The bacteria were grown on plates for 2 days at 28°C. From a single colony, a 5-mL overnight culture was made in the same medium (King's B medium plus antibiotics). On the next day, a 20-mL day-culture was prepared in the same medium with the overnight culture to an initial OD_{600} of 0.1 – 0.2. When the day-culture had reached an OD_{600} of 0.6 – 0.8, cells were harvested by centrifugation at 4,500 *g* for 5 min at room temperature (RT). Cell pellets were washed in 10 mM $MgCl_2$ and sedimented again at 4,500 *g* for 5 min at RT. Cell pellets were resuspended in 10 mL of 10 mM $MgCl_2$. The cell optical density was determined in order to prepare 50-mL of bacterial infiltration solution in 10 mM $MgCl_2$ with an OD_{600} of 0.2 (approx. 10^8 CFU·mL^{-1}) (Varet et al., 2002). Infiltrations were done with a needleless 1-mL syringe, infiltrating only one half of each leaf. After infiltration, plants were covered with a plastic dome to increase humidity and maintained under the same growth condition as before. Six bacterium-treated leaves from three different plants were harvested as one biological sample at different time points (i.e., 0, 6, 12, 24, and 48 h post treatment) and frozen immediately in liquid nitrogen. $MgCl_2$-infiltrated leaves were used as mock control. Two biological samples from one experiment were prepared and analyzed. Samples were stored at -80°C for RNA isolation. The experiment was repeated once.

2.1.3   ABA treatment of Arabidopsis seedlings

For treatment of *Arabidopsis* (Col-0) plants with exogenous ABA, the published method (Nakashima et al., 1997) was used with minor modifications. Plants were grown on MS plates for 10 days. Plants with similar size and developmental stage from all genotypes were chosen and transferred to Magenta boxes (MAGENTA®, Illinois, USA) for four to five weeks in a Percival growth chamber. The plants were gently removed from the sterile boxes and carefully transferred to trays floating on 3 L of liquid medium (0.5x MS, 1% (w/v) sucrose, pH 6.0) without ABA for 1 h under the same growth condition (Figure 2.1). After 1 h, ABA was added to a final concentration of 100 μM. At different time points (i.e., 0, 6, 12, and 24 h post treatment), three plants were harvested, pooled as one biological sample, and frozen immediately in liquid nitrogen. Plants floated on 0.5x MS medium (+ 1% sucrose, pH 6.0) but without ABA were used as control. Two biological samples from one experiment were averaged. Samples were stored at -80°C for RNA isolation. The experiment was repeated once.

Figure 2.1: Four- to five-week-old plants removed from sterilized culture medium and subsequently floated on MS medium prior to exogenous addition of ABA

2.2 Cultivation of bacteria

a) *Escherichia coli*

The *E. coli* strains JM109 (Promega, Wisconsin, USA), TOP10 (C3030-03, Invitrogen, California, USA, kindly provided by Prof. Dr. Arp Schnittger, University of Hamburg, Hamburg, Germany), *ccdB* Survival (A10460, Invitrogen, kindly provided by DNA Cloning Service, Hamburg, Germany), and BL21(DE3)RIPL (230280, Agilent Technologies, provided by Prof. Dr. Julia Kehr, University of Hamburg, Hamburg, Germany) were used in this study. They were grown at 37°C in Luria-Bertani (LB) medium (10 g·L^{-1} tryptone, 5 g·L^{-1} yeast extract, and 5 g·L^{-1} NaCl). The wild-type (WT) JM109 strain does not carry any antibiotic resistance gene and was used for subcloning. The *ccdB* Survival strain is resistant to streptomycin (100 µg·mL^{-1}) and was used to propagate Gateway plasmids (pDONR223, pMDC99, pMDC123, and pMDC162) (Curtis and Grossniklaus, 2003). Since the TOP10 strain is *ccdB* sensitive, it was used to obtain positive transformants following BP- and LR-Gateway recombination reactions (2.13.6). The BL21(DE3)RIPL strain is resistant to chloramphenicol and spectinomycin. This strain was used to produce recombinant proteins from pMAL-c2x plasmids.

b) *Agrobacterium tumefaciens* GV3101

The *Agrobacterium tumefaciens* GV3101 strain having a C58 chromosomal background conferring rifampicin resistance (100 µg·mL⁻¹) and carrying the Ti plasmid pmp90 (pTiC58DT-DNA) conferring gentamycin resistance (10 µg·mL⁻¹) was used in this study for transformation with plant expression vectors to generate transient or stable transgenic Arabidopsis plants. *Agrobacterium* was grown at 28°C in LB medium.

c) *Pseudomonas syringae* pv. *tomato* DC3000 (*Pst*), *Pst*(*avrRpt2*), and *Pst*(*avrRpm1*)

The *Pst* and *Pst*(*avrRpt2*) strains were kindly provided by Prof. Dr. Sheng Yang He (Michigan State University, Lansing, USA). *Pst*(*avrRpt2*) is resistant not only to rifampicin (100 µg·mL⁻¹), as is *Pst* but also to spectinomycin (100 µg·mL⁻¹) since the former was modified to express *avrRpt2* from the pMMXR1 vector (Dong et al., 1991). The *Pst*(*avrRpm1*) strain is also resistant to rifampicin but additionally to kanamycin (50 µg·mL⁻¹) due to *avrRpm1* expression from the pVSP61 (kindly provided by Prof. Dr. Stefan Hoth, University of Hamburg, Hamburg, Germany). All *Pseudomonas* strains were grown at 28°C in King's B medium (Suppl. Table 1).

2.3 Construct design for expression vectors

2.3.1 *NHL* construct design for pQE31 and pMAL-c2x vectors for investigation of *E. coli* responses to osmotic stress

To characterize the function of NHL4, NHL6, and NHL25 in osmotic stress responses of *E. coli*, truncated gene sequences encoding the polypeptides lacking the short N-terminal domain and with the transmembrane domain (TMD) of NHL4 (aa 1 – 80), NHL6 (aa 1 – 100), and NHL25 aa (1 – 100) were subcloned with N-terminal 6xHis and maltose binding protein (MBP) tags in the *E. coli* expression vectors, pQE31 and pMAL-c2x, respectively. Both vectors contain the ampicillin resistance gene. The primers used for subcloning the constructs were designed to contain restriction sites of BamHI and PstI (Suppl. Table 2). The TMDs were predicted by TMHMM Server v. 2.0 (http://www.cbs.dtu.dk/services/TMHMM/) and PHYRE2 (http://www.sbg.bio.ic.ac.uk/phyre2/) (2.7.2). This subcloning strategy was designed for Eduardo Muñoz Díaz's MOPS lab rotation (University of Hamburg, Hamburg, Germany) and successfully carried out by him. *E. coli* was transformed with successfully ligated constructs (2.4.1) for recombinant protein production and analyses for osmotic stress tolerance of *E. coli* (2.12).

2.3.2 *NHL* **construct design for** *in vivo* **subcellular localization and functional charac-terization studies in Arabidopsis**

To study *in vivo* the subcellular localization of NHL4, NHL6, and NHL25 in transient trans-formation using Arabidopsis seedlings and/or in stable transgenic Arabidopsis lines, the full-length, mutated, or deletion sequences of NHLs were N-terminally fused with EYFP and/or with monomeric Venus (mVenus) (Suppl. Table 2). EYFP had been previously subcloned into pBA002 (Kataya, 2011). The CDS encoding the WT NHLx were fused to the back of EYFP *via* PacI and SpeI and expressed from the *Cauliflower Mosaic Virus* (*CaMV*) *35S* promoter.

The same subcloning strategy was applied to obtain mutated and deletion constructs of NHL25 fused with EYFP, including EYFP-NHL25ΔPTS1, EYFP-NHL25(SRL>) (i.e., FRL> replaced with SRL>), and EYFP-TMD(NHL25) (i.e., TMD extended downstream and upstream by 20 aa). These constructs were used to investigate the contribution of the PTS1 and the TMD of NHL25 in peroxisome targeting efficiency by subcellular localization studies. To investigate whether these NHLs possess a functional PTS1, the C-terminal 10 aa of each NHL was fused to the back of EYFP *via* PacI and SpeI in pBA002. The primers were designed to amplify *EYFP* with the 3' end extension (in the reverse primer) which encoded the C-terminal 10 aa of NHLx (Suppl. Table 2).

The pBA002 vector contains resistance genes for spectinomycin and glufosinate (BASTA, Bayer, Germany) for bacteria and plant selection, respectively. Since two constructs without a fluorescence tag (pBA002_*35S*$_{pro}$*:NHL4* and pBA002_*35S*$_{pro}$*:NHL6*) had already been created (Kataya, 2011), the remaining *NHL25* construct was subcloned in this study to generate the Arabidopsis overexpressor (OE) lines (pBA002_*35S*$_{pro}$*:NHL25*). For mVenus-NHLx fusions, mVenus was first obtained by introducing a mutation (A206K) into the *Venus* sequence in pSAT6_Ven-C (Arabidopsis Biological Resource Center, ABRC, CD3-1779, donated by Prof. Dr. Stanton Gelvin, Purdue University, USA) by site-directed mutagenesis (SDM) (2.13.2), using appropriate primers (Suppl. Table 2). *mVenus* was then amplified and subcloned in front of *IMMUNE ASSOCIATED NUCLEOTIDE BINDING 12* (*IAN12*) in pBA002 *via* MluI and PacI. In pBA002_*35S*$_{pro}$*:mVenus-IAN12*, *IAN12* was replaced with *NHLx via* PacI and SpeI to obtain pBA002_*35S*$_{pro}$*:mVenus-NHLx*. *mCherry* fusion constructs were also generated for co-locali-zation studies between NHLx. For *mCherry-NHLx* fusion, *mCherry* carrying a multicloning site (MCS plus stop codon) was first subcloned into pBA002 *via* XhoI and SacI. *NHLx* were subcloned in the back of *mCherry via* PacI and SpeI. The primers used and all pBA002

constructs created in this study are listed in Suppl. Table 2. To investigate peroxisomal targeting, a blue peroxisome marker, *mCerulean-PTS1* (*mCer-PTS1*), subcloned into pBA002 vector by Pierre Endries and Christian Falter (both University of Hamburg, Hamburg, Germany) was used (Falter et al., 2019). The endoplasmic reticulum (ER) marker, pBIN20_*Wak2:CFP:HDEL*, was obtained from ABRC (CD3-953; Nelson et al., 2007).

To generate *EYFP* fusion of *NHLs*, the expression of which was driven by the endogenous *NHL* promoters (in stable transgenic Arabidopsis plants and Arabidopsis complementation lines), the genomic sequences of *NHL4* (AT1G54540.1, 20367301 – 20369650, reverse)*, NHL6* (AT1G65690.1, 24431167 – 24434202, reverse)*,* and *NHL25* (AT5G36970.1, 14603949 – 14606979, reverse) that contained the endogenous promoter and the gene of interest were amplified by PCR and first integrated into pDONR223 by homologous recombination (Gateway cloning; 2.13.6). The intergenic region (i.e., the non-coding DNA region between the start codon of the gene of interest and the next gene located upstream) was defined as the maximum promoter length of the gene of interest. The primers used to amplify the genomic sequence, the so-called "the full genomic sequence" of *NHL4*, *NHL6*, and *NHL25,* are shown in Suppl. Table 2. Before introducing the full genomic sequences into two different plant expression vectors, pMDC123 and pMDC99 (Curtis and Grossniklaus, 2003), the integrated regions in pDONR223 were sequenced (2.13.12).

These pDONR223 vectors also served for subcloning of N-terminal and internal *EYFP* fusion constructs driven by endogenous *NHL* promoters. These EYFP fusion constructs were designed for the two Master thesis projects and successfully conducted by Eduardo Muñoz Díaz (for *NHL4*, Díaz, 2020) and Kashmery Khan (for *NHL6* and *NHL25*, Khan and Reumann, unpubl. data) under my lab work supervision. To generate Arabidopsis complementation lines of *nhl* KO mutants (2.8.2), the correct genomic constructs in pDONR223 were selected for further Gateway cloning to insert the full genomic sequences into the plant expression vectors (2.13.6).

To analyze tissue expression pattern and promoter activity of *NHL4, NHL6,* and *NHL25* (2.9), stable transgenic Arabidopsis lines expressing *GUSA* from the corresponding endogenous promoter of *NHL4, NHL6,* or *NHL25* were generated. The upstream intergenic region was chosen as the most suitable promoter region of *NHL4* (1,229 bp), *NHL6* (1,304 bp), and *NHL25* (1,785 bp). Primers are listed in Suppl. Table 2. The first homologous recombination reaction served to introduce the endogenous promoters into pDONR223 which were subsequently

confirmed by sequencing (2.13.12) prior to being transferred in front of the *GUSA* CDS in the plant expression vector pMDC162 (Curtis and Grossniklaus, 2003), *via* the second homologous recombination reaction of Gateway cloning (2.13.6).

2.3.3   *NHL* constructs for yeast two-hybrid (Y2H) analyses

To investigate interaction between full-length NHL4, NHL6, and NHL25 and their C-terminal PTS1 domains and AtPex5 by the Y2H method, the sequences encoding the C-terminal 30 amino acids of NHL4, NHL6, and NHL25 as well as the long protein peptide (lacking the short N-terminal domain and the TMD; for TMD prediction, see 2.7.2) were N-terminally fused to the GAL4 activation domain (AD) *via* NcoI and BamHI in the pACT2 vector. The CDS encoding the tetratricopeptide repeat (TPR) domain or full-length of AtPex5 was fused to the back of the GAL4 DNA binding domain (BD) in the pGBKT7 vector. Both vectors were kindly provided by Prof. Dr Danja Schünemann (Ruhr-Universität Bochum, Bochum, Germany) (Funke et al., 2005). PTS1 peptides (e.g., ARL>, SRL>) and peptides without PTS1 (e.g., DML>, GDA>) of approx. 15 – 16 aa in length, which were identical to those used by Kragler et al. (1998), were subcloned into pACT2 to obtain positive and negative interactions with AtPex5 in pGBKT7, respectively. To subclone the short-peptide constructs (approx. 15 – 16 aa), part of the *GAL4 AD* was amplified and appended at the 3' end with sequence encoding these short peptides (introduced to the flanking region of reverse primers). The amplified sequences were subcloned into pACT2 *via* MluI and BamHI, replacing the redundant *GAL4 AD* in the vector. The constructs and primers are listed in Suppl. Table 2. Successful ligated constructs were transformed into the Y190 yeast strain (2.4.3) to analyze protein-protein interactions (2.11).

2.4   Transformation of different organisms

2.4.1   *E. coli* transformation by heat shock

The plasmids (10 – 100 ng) or 5 µL of a ligation reaction were mixed with 100 µL of competent *E. coli* cells in a 2-mL reaction tube, and the mixture was incubated on ice for 30 min. Heat-shock was performed for 60 s at 42°C followed by 2 min on ice. Super optimal broth with catabolites repression (SOC, Suppl. Table 3) medium (500 µL) was added to recover transformants for 1 h at 37°C on a shaker (190 rpm). The transformation was spread on two LB plates (10% and 90%) containing appropriate antibiotics, as defined by the *E. coli* strain (2.2) and the plasmid (2.3.1 and 2.3.2) used for transformation. The plates were incubated for 24 h at 37°C.

2.4.2 *Agrobacterium* transformation by electroporation

The plasmids (10 – 100 ng) were mixed with 50 µL of competent *Agrobacterium* cells in a 2-mL reaction tube, and the mixture was transferred to a cuvette (2-mm gap) and incubated on ice for 30 min. The electroporation was carried out at 1,800 V by applying PULSE twice (Electro-porator 2510, Eppendorf, Hamburg, Germany). SOC medium (500 µL) was added to the mixture to recover transformants when growing them at 28°C on a shaker (190 rpm) for 2 – 4 h. The bacteria were spread on two LB plates (10% and 90%) containing 100 µg·mL^{-1} rifampicin, 10 µg·mL^{-1} gentamycin (for resistance genes, see 2.2), and additional appropriate antibiotics which were defined by the plasmid used for transformation (2.3.1 and 2.3.2). The plates were incubated for 48 h at 28°C.

2.4.3 *Saccharomyces cerevisiae* transformation

From an overnight culture *S. cerevisiae* strain Y190, a 100-mL day culture of yeast peptone dextrose adenine hemi-sulfate (YPDA, Suppl. Table 4) medium was inoculated to an OD$_{600}$ of approx. 0.2, which was sufficient for 10 transformations. This culture was kept shaking at 28°C for 3 – 5 h until it reached an OD$_{600}$ of 0.45 - 0.6. Cells were harvested in two 50-mL tubes by centrifugation at 2,000 rpm at RT for 5 min and subsequently washed in 30 mL of sterile deionized H$_2$O. The cell resuspension was again centrifuged at 2,000 rpm for 5 min at RT. Each cell pellet was dissolved in 1 mL of 0.1 M Li-Acetate (LiAc) and transferred into a sterile 1.5-mL reaction tube. A quick centrifugation was performed at 14,000 rpm for 15 s. Each cell pellet was resuspended in 500 µL 0.1 M LiAc, and all were combined in one tube (approx. 1 mL). Of each plasmid (pGBKT7 and pACT2) 1.5 µg (for plasmid purification, see 2.13.3) were diluted in sterile deionized H$_2$O to a final volume of 48 µL in a 2-mL reaction tube. Next, 100 µL of the yeast cell resuspension was added to that DNA mixture. The remaining reagents were added, followed by 480 µL PEG (50% w/v), 72 µL 1 M LiAc, and 20 µL of salmon sperm DNA (10 mg·mL^{-1}). The tube was vigorously vortexed for 1 min and rotated on a wheel at 28°C for 30 min. Seventy-two µL of dimethyl sulfoxide (DMSO) was added to each tube and mixed gently, followed by a centrifugation at 6,000 rpm for 15 s. The supernatant was removed with a pipette, and the pellet was subsequently resuspended in 300 µL of sterile deionized H$_2$O. The cell suspension was spread on one so-called "-LT plate" (i.e., synthetic defined (SD) medium without/minus leucine (Leu) and tryptophan (Trp, T erroneously stands for Trp; Suppl. Table 5) and one -LTH plate (additionally lacking histidine, His). The plates were incubated for 5 days at 28°C. Yeast double transformants grown on -LTH plates indicated possible protein-protein

interaction and were subjected to the colony-lift filter assay (2.11). Those grown on -LT plates were further selected for the protein-protein interaction analyses by serial dilution (2.11).

2.4.4 Arabidopsis transformation

a) Transient transformation in Arabidopsis seedlings

The transient transformation was performed by the fast *Agrobacterium*-mediated seedling transformation (FAST) method (Li et al., 2009) with minor modifications to study the sub-cellular localization of fluorophore-tagged NHL4, NHL6, and NHL25 *in vivo* by co-trans-formation with two *Agrobacteria* carrying two different fluorophore constructs. In brief, Arabidopsis seeds (approx. 50 seeds per 4-cm Petri dish) were sown on 0.25x MS medium (supplemented with 1% (w/v) sucrose, 0.8% (w/v) agar, pH 6.0), stratified for one day at 4°C in dark, and seeds were germinated for 4 days in a Percival incubator (see 2.1.1) until co-cultivation with *Agrobacteria*. As a modification of the original method, seedlings were kept in the dark for 3 – 4 h prior to co-cultivation with *Agrobacterium* (GV3101) to slow down seedling growth, which was often observed to result in higher transformation efficiency. From the overnight culture of *Agrobacteria* transformed with different plant expression vectors, 20-mL day cultures (LB supplemented with appropriate antibiotics) were prepared with an initial OD_{600} of 0.35 – 0.4, which should reach an OD_{600} of approx. 1.5 prior to cell harvesting at 4,500 g for 5 min. Cell pellets were then washed in 10 mM $MgCl_2$ freshly supplemented with acetosyringone to a final concentration of 100 µM (to activate expression of *Agrobacterium virulence* genes), followed by a second centrifugation at 4500 g for 5 min. The pellets were resuspended in 1 mL of the above washing solution and incubated until further use. The OD was determined and used to calculate the required volume of resuspended *Agrobacteria* to be mixed with co-cultivation medium (0.25x MS, 1% (w/v) sucrose, pH 6.0, 0.005% (v/v) Silwet L-77, 100 µM acetosyringone) in order to obtain OD_{600} of 0.5. A total volume of 5 mL of this *Agrobacterium* resuspension solution was used to co-cultivate with 4-day-old Arabidopsis seedlings (approx. 50), previously removed from agar plates by fine forceps, in 4-cm Petri dishes. Arabidopsis seedlings and *Agrobacterium* were co-cultivated in the dark in a Percival incubator (growth conditions see 2.1.1). Two days after co-cultivation, seedlings were washed with sterile water containing 50 µg·mL^{-1} carbenicillin (for suppressing *Agrobacterium* growth) and subsequently kept in 5 mL of co-cultivation solution without acetosyringone and Silwet L-77. Microscopic analyses were performed 2 – 6 days after the beginning of co-cultivation with *Agrobacterium*.

b) <u>Stable transformation of Arabidopsis (by floral dip)</u>

For transformation by floral dip, initial inflorescences from 3- to 4-week-old Arabidopsis (Col-0) plants cultivated under standard growth conditions (2.1.1) were removed to produce more inflorescences (Clough and Bent, 1998). Plants with many inflorescences and flowers were used for transformation. *Agrobacterium* (GV3101) carrying the desired plant expression vectors was grown overnight at 28°C in 200 mL LB medium supplemented with appropriate antibiotics (2.2 and 2.4.2). The next day, cells were sedimented by centrifugation (4,500 g for 30 min), and the cell sediments were resuspended in sterile dipping solution (5% (w/v) sucrose and 0.05% (v/v) Silwet L-77 in sterile deionized water) to obtain an OD_{600} of 0.8. Plants were then dipped in the resuspended bacterium solution for 1 min and covered with plastic domes. Dipped plants were kept in the dark for 24 h before transferring them back to the growth chamber. A few weeks later, the harvested T_1 seeds (each representing either an independent line or an embryo developing from an untransformed female gametophyte) were sown and screened for transgenic T_1 plants. Then, T_2 seeds were harvested for plant genotyping in further generations (2.8.2).

2.5 Fluorescence microscopy

2.5.1 Confocal microscopy

Confocal microscopy was performed with a Leica DMi8 inverted microscope coupled to a confocal spinning disc unit CSU-X1 (Yokogawa Electric Corporation, Musashino, Japan). Two laser beams were used to excite the fluorophores used in this study, namely CFP and mCer at 445 nm and EYFP and mVenus at 515 nm. The confocal spinning disc unit CSU-X1 was equipped with the emission filters for CFP or mCerulean (mCer) (480/40 nm) and EYFP or mVenus (542/27 nm). Confocal images were captured as single planes with a QImaging OptiMOS sCMOS (scientific Complementary Metal–oxide–semiconductor) camera system (OptiMOS, Surrey, Canada). Image acquisition and co-localization analyses were performed using the VisiView software v3.0 (Visitron Systems, Puchheim, Germany). For co-localization analyses, the blue CFP fluorescence was later changed to red prior to overlaying images. The images of the two channels were merged using the "Overlay" tool in the VisiView software.

2.5.2 Epifluorescence microscopy

Samples co-expressing mCherry and EYFP fusions were analyzed by epifluorescence microscopy. The analysis was performed with the same Leica DMi8 inverted microscope

equipped with the white light source (380 – 680 nm, LED, Sola SM 5-LCR-SB, Lumencor Inc., Oregon, USA) and filter cubes for the excitation and emission wavelength of EYFP (EX500/20 nm, EM535/30 nm) and mCherry (EX560/40 nm, EM630/75 nm). The filter sets also included dichroic beam splitters for EYFP (515 nm) and mCherry (585 nm) each. Images were captured with a PCO Edge 4.2 sCMOS-LT digital camera (PCO AG, Kelheim, Germany). Image acquisition and co-localization analyses were done as described above (2.5.1) keeping the color of fluoro-phores.

2.5.3 Object counting and size determination by ImageJ

To determine the quantity and the percentage of NHL-labeled puncta that co-localized with ER-derived vesicles, images of cells co-expressing *EYFP* alone or with the ER marker *ER-CFP* were acquired by confocal microscopy (2.5.1). Prior to counting puncta per cell in a single confocal plane image (tiff file), the scale was first set up in ImageJ based on the scale bar previously generated by VisiView during image processing. A line of identical length was drawn along the scale bar. Under "Analyze function > Set Scale", the value of the scale bar was assigned to the "known distance" value of the drawn line, followed by changing the unit length, e.g. to μm. Then, the scale setting was confirmed by pressing "OK".

For puncta counting, noisy signals and background fluorescence were minimized to avoid their unwanted counting as puncta by applying the "Image > Brightness/Contrast > Adjust" tools. The image was then converted to 8-bit with "Image > Type > 8-bit" function and subsequently to binary color with "Process > Binary > Make Binary" function. To precisely define the cell or region for vesicle/puncta counting, the "Polygon Selection" tool was applied. Thereby, all puncta within the defined region were counted automatically by applying "Analyze > Analyze Particles" function. A new window then appeared with information of the total number of puncta as well as the diameter of individually counted puncta, referred to as the Feret value in the output result.

2.6 Transmission electron microscopy (TEM)

To study the targeting of NHLs to membrane-bound vesicles, 4-day-old Arabidopsis seedlings 3, 4, and 5 dpc with *Agrobacterium* carrying the pBA002 plant expression vector, which was either "empty" (no insert/gene of interest (GOI)) or contained *EYFP-NHL4, EYFP-NHL6,* or *EYFP-NHL25,* for expression from the *CaMV 35S* promoter, were used for the TEM analyses. First, the transformed Arabidopsis seedlings expressing *EYFP-NHLx* were screened for EYFP fluorescence by confocal microscopy. Seedlings with strong EYFP fluorescence in both cotyledons

(approx. 5 seedlings – 10 cotyledons) were chosen for TEM. The seedlings co-cultivated with *Agrobacterium* carrying the empty pBA002 vector were used as control not expressing *EYFP* and/or *NHLs*.

2.6.1 TEM by immunogold labeling

a) <u>Chemical fixation</u>

The samples were subjected to chemical fixation (2% (v/v) paraformaldehyde, 0.1% (v/v) glutaraldehyde in 1x microtubule stabilizing buffer (MSB), pH 6.8 (see Suppl. Table 6 for 2x MSB) for 2 h at RT and incubated at 4°C overnight. On the next day, the samples were washed three times with 1x MSB (1:2 dilution of 2x MSB, pH 6.8). To better handle the tiny seedlings in the following step, the samples were then embedded in blocks of 2% (w/v) agar (prepared in 1x MSB). Next, the samples were incubated for 1 h on ice with 0.25% (w/v) osmium tetroxide (OsO_4) (prepared in 1x MSB), followed by washing three times with 1x MSB, and kept at 4°C. Osmium tetroxide stains phospholipids of biological membranes.

b) <u>Dehydration, LR White resin infiltration, and polymerization</u>

The next day, the samples were dehydrated by incubation with increasing concentration series of ethanol, i.e. 30, 50, 70, 90, and 100% (v/v, prepared in H_2O) at 4°C. Each incubation was approx. 20 – 30 min in duration. Next, the samples were infiltrated with increasing concentrations of the LR White resin (v/v, prepared in ethanol), i.e. 30% (1 h), 50% (1 h), 70% (2 h), and 100% (overnight). On the next day, the samples were embedded in gelatin capsules prior to polymerization for 36 h at 50°C (O_2-free atmosphere).

c) <u>Ultrathin section preparation</u>

The gelatin capsule blocks were trimmed with a razor blade under a binocular until reaching the specimen. To obtain ultrathin sections (70 – 80 nm), the block was placed in a microtome (Ultracut E, Leica-Reichert-Jung, Nußloch, Germany) equipped with a diamond knife for sectioning. Sections were then captured by nickel grids. The grids were mounted with 0.3% (v/v) polyvinyl butyral (prepared in chloroform) to stabilize the section under the beam.

d) <u>Antibody labeling</u>

The grids with the sections were incubated upside down in drops of 1x MSB for 30 min and followed by incubation with the blocking solution (3% (w/v) bovine serum albumin (BSA) and 0.2% (w/v) acetylated BSA in 1x MSB (AURION BSA-c™ (10%), Cat. 900.022, Generon, Slough,

UK)) for 30 min. To determine the best antibody dilution, the grids were incubated with drops of different dilutions (i.e., 1:400, 1:800, 1:1,000, and 1:1,500) of the rabbit polyclonal anti-GFP antibody (Ab290, Abcam, Berlin, Germany) in blocking solution for 1 h. Washing was performed five times in 30 min in drops of the blocking solution diluted with 1x MSB at 2:1 (v/v) ratio. Next, the grids were incubated in drops of anti-rabbit polyclonal secondary antibody (produced in goat, G7402, Sigma-Aldrich) conjugated with 10-nm gold particles for 1 h (1:50 dilution in 1x MSB). Washing was done with five times in drops of 1x MSB for 30 min. The grids were fixed for 10 min in 1% (v/v) aqueous glutaraldehyde and followed by washing three times in H_2O for $5-10$ min. Unspecific binding of the secondary antibody to the specimen was investigated by omitting the primary anti-GFP antibody.

e) Contrast generation of specimen

To visualize better the specimen by TEM, the grids were subjected to 2% (w/v) uranyl acetate for 10 min, followed by washing four times with H_2O. Uranyl acetate can enhance the contrast of specimen by interacting with lipids and proteins. The contrast of specimen was further improved by incubating the grids in 0.2% (v/v) of aqueous lead citrate ($C_{12}H_{10}O_{14}Pb_3$) for 15 min and washed four times with H_2O. Lead citrate can improve the contrast of specimen as it binds to osmium and uranyl acetate and enhances contrast in many cellular structures (Reynolds, 1963).

f) TEM

The grids were stored at RT until TEM observation (LEO 906 E TEM, LEO, Oberkochen, Germany), and image acquisition was performed with a multiscan CCD (Charge-coupled device) camera system (Model 794, Gatan, Munich, Germany) and analyzed by a digital micrograph software (v 2.0.2, Gatan). The TEM was operated at 100 kV.

2.6.2 TEM without immunogold labeling for ultrastructural analyses

Samples were processed as described above for TEM with immunogold labeling (2.6.1) but without the two steps of antibody labeling and contrast generation of specimen. Furthermore, several differences in chemicals and buffers for fixation and resin infiltration are described in detail below.

a) Chemical fixation

The samples were subjected to chemical fixation at 4°C overnight using 2% (v/v) glutar-aldehyde in 75 mM (w/v) sodium cacodylate trihydrate buffer (pH 7.0 adjusted with 1 M HCl).

On the next day, the samples were washed three times with the same cacodylate buffer (1x quick, 1x 5-min washing, and 1x 10-min washing). The samples were then embedded in blocks of 2% (w/v) agar (prepared in cacodylate buffer). After washing, the samples were incubated with 1% (w/v) OsO_4 (prepared in cacodylate buffer) for 2.5 h on ice, followed by washing three times with cacodylate buffer (1x quick, 1x 5-min washing, 1x 15-min washing). This sample processing method helped to strongly stain the phospholipid membrane structure but prevented the efficiency of antibody labeling, hence, were only analyzed without antibodies.

b) Dehydration, Spurr resin infiltration, and polymerization

On the same day, the samples were dehydrated by incubation with increasing concentration series of acetone, i.e. 30, 50, 70, 90, and 100% (v/v, prepared in H_2O) at 4°C for 10 min. The dehydration was continued with two more times of 100% acetone incubation at RT, 10 min each. After dehydration step, the samples were then infiltrated with increasing concentration series of the Spurr resin (Spurr, 1969) (v/v, prepared in acetone), i.e. 25% (1 h), 50% (3 h), 75% (overnight), and 100% (28 h, replaced twice after 6.5 and 24 h). The samples were embedded in silicone embedding molds (E4015, Sigma-Aldrich) prior to polymerization for 16 h at 70°C.

Ultrathin section preparation and TEM analyses were performed as described above for immunogold labeling. Copper but not nickel grids were used to mount the ultrathin sections.

2.7 *In silico* analyses

2.7.1 LEA_2 domain prediction

LEA_2 domains were predicted by the Pfam database (http://pfam.xfam.org/) for the protein sequences of NHL4, NHL6, and NHL25 retrieved from TAIR (https://www.arabidopsis.org/). The output result that showed a bit score value higher than the sequence and domain gathering thresholds of 25.4 for the LEA_2 protein family (PF03168 Pfam annotation) indicated a reliable prediction (Punta et al., 2011).

2.7.2 Transmembrane domain prediction

To generate TMD deletion constructs of *NHLs* for *in vivo* subcellular localization studies and heterologous expression in yeast and *E. coli* (2.3), the location of the single TMD were predicted by TMHMM Server v. 2.0 (http://www.cbs.dtu.dk/services/TMHMM/) and by

protein structure modelling in extensive mode by PHYRE2 (http://www.sbg.bio.ic.ac.uk/~phyre2/).

2.7.3 Gene expression analyses using publicly available transcriptomics data

Expression of genes of interest through developmental stages of Arabidopsis and under abiotic and biotic stress conditions was analyzed using Genevestigator (Hruz et al., 2008) with two transcriptomic datasets (Arabidopsis ATH1 genome arrays and large-scale mRNA sequencing). Compared to untreated samples (control), only gene expression data derived from Arabidopsis Col-0 with 3-fold change and supported by *p* values < 0.05 were presented.

2.7.4 *Cis*-regulatory element prediction

To gain further insights into the regulation of *NHL4*, *NHL6*, and *NHL25* expression, a promoter analysis was performed. The gene annotation of *NHL4* (At1g54540), *NHL6* (At1g65690), and *NHL25* (At5g36970) retrieved from the Arabidopsis Information Resource (TAIR) (https://www.arabidopsis.org/) was used as an input query for searching for *cis*-regulatory elements. The search was performed against the Arabidopsis *cis*-regulatory element database, the Arabidopsis Gene Regulatory Information Server (https://agris-knowledgebase.org/ AtcisDB/).

2.8 Plant genotyping

2.8.1 Genotyping of homozygous T-DNA insertion mutants

To characterize the function of NHL4, NHL6, and NHL25 in plant responses to biotic and abiotic stress, the homozygous mutants (i.e., *nhl4-1*, *nhl6-1*, *nhl25-1*, *nhl6-1 x nhl25-1* (line 1 and 2)) were confirmed with correct T-DNA insertion alleles and the gene expression level. Leaves of 4- to 5-week-old mutant and WT (Col-0) plants grown under standard condition (2.1.1) were used for genotyping.

a) Genotyping by PCR

A leaf square (0.4 x 0.4 cm) was excised and ground in 20-µL dilution buffer provided by the Phire Plant Direct PCR Master Mix kit (F160L, Thermo Scientific, Vilnius, Lithuania). The presence of T-DNA in mutants was confirmed by PCR using Phire Hot Start II DNA polymerase (2.13.1) in which the appropriate T-DNA left border primer, either for SAIL or SALK lines, was used in combination with the gene-specific reverse primer. Gene-specific primer pairs were used to detect if any the WT alleles were present in the mutant line. Primer sequences (for WT

and mutant allele detection) are shown in Suppl. Table 7. Five plants per genotype were screened.

b) Confirmation of gene expression in homozygous single and double mutants by qRT-PCR

Six leaves from an individual plant were harvested and frozen immediately in liquid nitrogen (approx. 100 – 200 mg). Samples were stored at -80°C for further RNA isolation (2.13.8). cDNA synthesis and the gene expression analyses by qRT-PCR were performed according to 2.13.9 and 2.13.10, respectively. Primers used for qRT-PCR are listed in Suppl. Table 8. Three plants per genotype were used as three biological replicates for statistical analysis.

2.8.2 Genotyping of transgenic Arabidopsis lines

a) Transgenic Arabidopsis lines overexpressing *NHL4*, *NHL6*, and *NHL25* with and without EYFP tag

T_1 seeds harvested from Arabidopsis (Col-0) plants transformed with pBA002 vectors containing different inserts (i.e., *35S$_{pro}$:NHL4, 35S$_{pro}$:NHL6, 35S$_{pro}$:NHL25, 35S$_{pro}$:EYFP-NHL4, 35S$_{pro}$:EYFP-NHL6,* and *35S$_{pro}$:EYFP-NHL25*) were sown and grown on soil under standard long-day condition (see 2.1.1). Glufosinate ammonium (200 mg·L^{-1} BASTA, Bayer, Germany) was applied three times to 2-week-old plants by spraying (with an interval of every two days). Surviving plants represented independent transgenic T_1 lines. Seeds from these plants were harvested for further BASTA screening in the T_2 and T_3 generation. Transgenic lines overexpressing *EYFP-NHL4*, *EYFP-NHL6,* and *EYFP-NHL25* were also grown on MS plates containing 15 µg·mL^{-1} BASTA (Møller et al., 2003). Seven-day-old seedlings were screened for EYFP fluorescence by confocal microscopy. To identify homozygous T_2 lines, the segregation ratio (i.e., the absence of BASTA sensitive WT progeny) was analyzed in the T_3 generation.

For expression analyses, seeds from 4- to 5-week-old homozygous OE lines (at least 5 – 6 independent lines) and WT (Col-0) were grown on soil under optimal growth conditions (2.1.1). For each independent line, six leaves from an individual plant were harvested, immediately frozen in liquid nitrogen, and stored at -80°C for RNA extraction. cDNA synthesis and the gene expression analyses by qRT-PCR were performed according to 2.13.9 and 2.13.10, respectively. Primers used for qRT-PCR are listed in Suppl. Table 8. Two individual plants were used as biological replicates for statistical analysis.

b) Transgenic Arabidopsis lines expressing _GUSA_ from the endogenous promoter of _NHL4,_
NHL6, or _NHL25_

T_1 seeds harvested from Arabidopsis (Col-0) plants transformed with constructs in pMDC162
(i.e., _NHL4$_{pro}$:GUSA, NHL6$_{pro}$:GUSA,_ and _NHL25$_{pro}$:GUSA_) were grown on MS plates supple-
mented with 25 µg·mL^{-1} hygromycin under optimal growth condition in a Percival growth
chamber (for only 6 h after 4-day stratification at 4°C). Seedlings were then kept in the dark for
two days in a Percival growth chamber under optimal growth conditions (2.1.1). Seedlings with
prolonged hypocotyls and green cotyledons 7 – 10 days after germination were defined as
hygromycin-resistant. These seedlings, representing independent transgenic T_1 lines (at least 5
– 6 lines needed), were subsequently transferred to soil under the same growth conditions for
subsequent GUS histochemical analyses (2.10.1) and for T_2 seed production. The determin-
ation of the segregation ratio in the T_2 and T_3 generation was used to select homozygous
parental lines.

c) Transgenic Arabidopsis lines carrying genomic promoter-gene construct of _NHL4, NHL6_, or
NHL25 for future complementation analyses

T_1 seeds were harvested from homozygous Arabidopsis (Col-0) mutant plants (_nhl4-1_:
SAIL_681_E12; _nhl6-1_: SALK_148523; _nhl25-1_: SALK_113216) transformed with the corres-
ponding complementation constructs (i.e., pMDC123_NHL4$_{pro}$:NHL4, pMDC123_NHL6$_{pro}$:NHL6,
and pMDC99_NHL25$_{pro}$:NHL25). Transformed seeds of two lines (pMDC123_NHL4$_{pro}$:NHL4 and
pMDC123_NHL6$_{pro}$:NHL6) were sown on soil and grown under standard growth condition for
BASTA screening as described above (2.8.2, section a) since the pMDC123 vector carries the
BASTA resistance gene (_Bar_) for transformant selection. Seeds transformed with the
pMDC99_NHL25$_{pro}$:NHL25 construct were sown on MS plates for screening hygromycin-
resistance seedlings as mentioned above (2.8.2, section b).

2.8.3 Generation and genotyping of triple _nhl_ mutants

One homozygous single _nhl4-1_ and one double _nhl6-1 x nhl25-1_ KO mutant (line 2, for mutant
information see 2.1.1) were used for cross-pollination in order to generate the triple _nhl4-1_ x
nhl6-1 x nhl25-1 mutant. The double _nhl6-1 x nhl25-1_ mutant was used as a pollen recipient
while the _nhl4-1_ mutant was the pollen donor. Before cross-pollination, stamens in flower
buds of the pollen recipient were removed. If the stamens were still shorter than the stigma in
a flower bud, this indicated that no self-pollination had taken place. Stamens with anthers and
pollens from the pollen donor were used to transfer its pollen to the stigmas of the pollen

recipient. Cross-pollinated stigmas were wrapped in parafilm for a few days until the initial formation of siliques was observed. Seeds from these siliques (T_1) were harvested for further genotyping by PCR (2.13.1). According to Mendel's law, the homozygous triple mutant could only be obtained in the T_2 generation (1:64 segregation ratio). Therefore, 100 plants (T_2) were screened by PCR to successfully identify at least one homozygous triple mutant.

2.9   Promoter activity analyses using *GUS* reporter lines

2.9.1   Developmental and tissue-specific promoter analyses

The expression patterns of *NHL4*, *NHL6*, and *NHL25* in term of *GUSA* expression were analyzed at different developmental stages using six independent transgenic lines transformed with the same *GUS* reporter construct (T_2 generation). For early developmental stages, transgenic Arabidopsis seeds were sterilized and sown on MS agar plates (2.1.1), and seedlings were harvested for the GUS histochemical assay (2.10.1) after defined days of germination (i.e., 0.5, 4, and 8 days after germination). These transgenic lines were simultaneously grown on soil in a Percival growth chamber and were used to analyze the expression patterns of *NHL4*, *NHL6*, and *NHL25* 14 days after germination and at the flowering stage. Part of the inflorescence was used for GUS histochemical assay.

2.9.2   Promoter analyses under biotic stress treatments

Four- to five-week-old transgenic Arabidopsis plants (carrying *GUS* reporter constructs) grown on soil in a Percival growth chamber (21°C, 12 h light/12 h dark, 100 µmol·m^{-2}·s^{-1}, 65% humidity) were used to apply different types of biotic stress. Of six transgenic Arabidopsis lines expressing *GUSA* from the native promoters, three lines showing similar expression patterns through different developmental stages were chosen. The following biotic stressors were applied: virulent (*Pst*) and avirulent strain *Pst*(*avrRpt2*), wounding, elf18, and flg22. For GUS histochemical assay, three to four treated leaves were harvested at different time points (e.g., 30 min, 6 and 24 h after treatment). Two independent experiments were performed.

a) <u>Infiltration of *Pst* and *Pst*(*avrRpt2*)</u>

The infiltration method and preparation of the bacterial suspension were performed according to 2.1.2. Leaves were infiltrated in a circular area (0.5 cm in diameter) to observe gene expression. MgCl$_2$-infiltrated leaves were used as control.

b) <u>Infiltration of elf18 and flg22</u>

The elf18 and flg22 peptides (synthesized by EZBiolab Inc., Parsippany, New Jersey, USA) were dissolved and diluted in sterile Milli-Q water to obtain 1 µM as working concentration prior to syringe infiltration of the leaves. Like the above description, leaves were infiltrated in a circular area (0.5 cm in diameter). H_2O-infiltrated plants were used as control.

c) <u>Wounding</u>

To wound leaves, the edge of one half of a leaf was cut at several sites using a pair of scissors. The other half of the leaf was punctually wounded using a needle of a syringe. Untreated plants were used as control.

2.10 Plant assays

2.10.1 GUS histochemical assay

The *GUSA* gene encodes β-glucuronidase which converts a specific soluble colorless substrate (i.e., 5-bromo-4-chloro-3-indolyl glucuronide, X-Gluc) into the insoluble, colored product 5, 5'-dibromo-4, 4'-dichloro-indigo. As *GUSA* expression was driven by the promoter of the GOI, color formation showed where the promoter was active.

The plant samples expressing *GUSA* to be analyzed for tissue-specific expression pattern (2.9.1) and for the effect of stress treatment (2.9.2) were first incubated in ice-cold 90% (v/v) acetone for 30 min prior to being washed 3 times for a total of 30 min with GUS buffer (50 mM sodium phosphate buffer, pH 7.0, 2.5 mM ferricyanide, 2.5 mM ferrocyanide, 0.05% (v/v) Triton X-100). Samples were subsequently incubated in GUS substrate solution (GUS buffer supplemented with 0.5 mg·L^{-1} X-Gluc, Duchefa, Haarlem, Netherlands) and vacuum-infiltrated at -70 kPa for 30 min (vacuum stopped briefly every 10 min). Then, samples were incubated at 37°C for 16 h for colored product formation. Finally, samples were dehydrated by rinsing with gradually increasing ethanol concentrations (i.e., 25%, 50%, 75%, 90%, and 95% (v/v)). During the dehydration step, also chlorophyll was extracted and released from samples. For observation and imaging under a stereomicroscope or a light microscope equipped with a camera (Axio Cam 105 0.5x or Axio Cam MRc5 0.63x, respectively, Zeiss, Oberkochen, Germany), samples were briefly rehydrated with 50% (v/v) glycerol.

2.10.2 Bacterial proliferation assay

This assay is used to monitor bacterial proliferation in the apoplast of plants and to investigate difference in plant susceptibility and resistance in mutants. The more bacteria proliferate, the more susceptible the plant is.

The preparation of bacteria has been described above (2.1.2) with the exception that the bacteria cells harvested from day cultures of $Pst(avrRpt2)$ or $Pst(avrRpm1)$ were diluted in 10 mM $MgCl_2$ to an OD_{600} of 0.002 (approx. 10^6 $CFU \cdot mL^{-1}$) rather than 0.2 (2.1.2), referred to as infiltration solution (see below).

Four- to five-week-old Arabidopsis (Col-0) plants grown on soil under short-day condition (21°C, 12 h light/12 h dark, 100 $\mu mol \cdot m^{-2} \cdot s^{-1}$ light intensity, approx. 70% humidity) were used. For each treatment, nine individual plants were used in one independent experiment, which was sufficient for three biological replicates. Bacterial infiltration was performed in one half of a leaf by using a needleless 1-mL syringe containing infiltration solution (OD_{600} = 0.002 in 10 mM $MgCl_2$). Six young mature leaves from each plant were infiltrated (two leaves from each needed). The infiltrated plants were sprayed with water and covered by a plastic dome (to maintain high humidity, facilitating bacterial infection). The leaf discs were harvested at different time points (i.e., 0, 2, and 3 days post infection). For one biological replicate, six leaf discs from three infiltrated plants were excised using a cork borer (0.4 cm in diameter, area of six leaf discs = 0.75 cm^2), pooled, and then ground in 1 mL of 10 mM $MgCl_2$ using a micro pestle. Depending on the time point of sample harvesting, four to six serial 10-fold dilution were made in 200 μL of 10 mM $MgCl_2$, and twice independently to yield two technical replicates of counting. Ten microliters of each dilution were spotted on King's B medium plates (Suppl. Table 1) supplemented with appropriate antibiotics. The number colony forming units (CFUs) were determined by counting single colonies grown in one spot at an appropriate dilution with 5 – 40 CFUs. Thus, bacterial proliferation per leaf area ($CFU \cdot cm^{-2}$) was calculated according to the equation below.

$$\text{Bacteria number per area (CFU} \cdot cm^{-2}) = \frac{\text{CFU x Dilution factor}}{V_{spotting} \text{ (mL)}} \times \frac{V_{grinding} \text{ (mL)}}{\text{Leaf area (cm}^2)}$$

Here, CFU is the mean of the colony numbers determined for the two technical replicates. For statistical analysis, the data from three biological replicates in one experiment were included, and the One-way ANOVA, Tukey's test ($p < 0.05$) was performed using the SPSS 16 (Statistical Package for the Social Sciences 16) software (IBM, New York, USA).

2.10.3 Seed germination analyses in the presence of ABA

Seeds of identical age and storage conditions of WT Arabidopsis (Col-0), different KO mutants, and two OE lines (*35S$_{pro}$:NHL4*) were harvested from parental lines cultivated in parallel, sterilized, and sown on MS plates with and without ABA (0.5 and 1 µM) to investigate the optimal inhibitory concentration of ABA on seed germination (Bao et al., 2016). In each treatment (with and without ABA), 70 seeds of each genotype were sown, followed by 4-day stratification at 4°C, and subsequently transferred to long-day condition (2.1.1). The appearance of two cotyledons was defined as seed germination (Tran et al., 2007). Phenotyping was performed until day 6 of incubation at long-day condition. Three independent experiments were conducted, and their data were used for statistical analysis using the SPSS 16 software (One-way ANOVA, Tukey's test, $p < 0.05$).

2.10.4 Electrolyte leakage measurement

Plants were cultivated under short-day condition in a Percival growth chamber (12 h light/12 h dark, 100 µmol·m^{-2}·s^{-1}, 65% humidity). Thirty-five to forty-five leaf discs from ten different 4- to 5-week-old plants of each genotype were harvested for the electrolyte leakage measurement. Leaf discs were vacuum-infiltrated with bacterial suspension (OD$_{600}$ of 0.2, equal to approx. 10^8 CFU·mL^{-1}; 2.1.2) for 15 min at -70 kPa (vacuum stopped briefly every 3 – 5 min). Leaf discs were then washed three times with sterile Milli-Q water (18.2 MΩ·cm purity). For each biological replicate, ten leaf discs were transferred to a 5-cm Petri dish containing 10 mL of sterile Milli-Q water and incubated at RT. Right after transfer, 6 mL of solution from each petri dish were collected to a separate 15-mL Falcon tube for measurement 0 h post infection prior to being returned to the appropriate dish. The Falcon tubes were kept for later measurement of the same sample. Electrolyte leakage measurement was performed for 6 and 8 h in case of infection with *Pst*(*avrRpm1*) and *Pst*(*avrRpt2*), respectively. In detail, 1-h interval readings were performed during the time course. For the first 4 h (*Pst*(*avrRpm1*)) or from 2 to 6 h (*Pst*(*avrRpt2*)), the measurements were carried out every 30 min.

Total ion contents in samples were determined after 20-min autoclaving and 5-h shaking at 28°C. Raw data of electrolyte leakage were normalized to the total electrolyte content and expressed in percentage, thereby giving the relative electrolyte leakage. The normalized data were fitted with the model of the Weibull equation with Box-Cox transformation (equation 1) (Johansson et al., 2015).

$$F(t) = min + (max - min)(1 - e^{-e^{a+b\frac{t^{c-1}}{c}}}) \tag{1}$$

t: time after vacuum infiltration

min: the lower asymptote

max: the upper asymptote

a, b, c: additional parameters describing the curve

To investigate the speed of electrolyte leakage change in each genotype, the velocity (V) was analyzed by using the derivative of the equation (1).

$$V = \frac{dF(t)}{dt} = (max - min)b(e^{a+b\frac{t^{c-1}}{c} - e^{a+b\frac{t^{c-1}}{c}}})t^{c-1} \tag{2}$$

To compare the kinetics of electrolyte leakage among genotypes, the time point at which the velocity value reached its maximum was analyzed. This value was named t_{max} in this study and determined by the Excel solver tool. The algorithm used in this tool allows the estimation of the time point at which equation (2) has the maximum value.

2.11 Protein-protein interaction analysis by the Y2H method

To investigate the interaction between NHLx and AtPex5, the Y2H method was performed in two steps. First, the *S. cerevisiae* strain Y190 was double transformed to carry the pGBKT7 and the pACT2 vectors (2.4.3). Subsequently, the auxotrophic growth analysis of yeast transformants carrying the reporter genes was performed to investigate the protein-protein interaction. Different double transformed yeast Y190 cells were grown overnight in SD medium without Leu and Trp (Suppl. Table 5). After one to two days, five transformants (containing the same plasmids) were mixed and concentrated to an OD_{600} of 10, and four 10-fold serial dilutions were made. Of these, 10 µL were spotted on SD plates without Leu, Trp, and His (supplemented with 25 mM 3-amino-1,2,4-triazole (3-AT)). The plates were incubated at 28°C for 5 days. The formation of the fully functional GAL4 transcription factor activates the transcription of two reporter genes involved in histidine biosynthesis (*HIS3*) and coding for β-galactosidase (*LacZ*). Therefore, if the interaction between two investigated proteins takes place in yeast cells, this enables growth on these plates within 5 days. The cellular activity of β-galactosidase was analyzed by the qualitative so-called colony lift filter assay, in which the colonies were transferred to filter paper (VWR, Pennsylvania, USA) followed by freezing in liquid nitrogen. The side of the filter paper with the colonies was placed right-side up on top of

other two filter papers that had been wetted with reaction solution. The reaction solution contained 50 mL Z buffer (Suppl. Table 9), 135 µL of β-mercaptoethanol, and 835 µL of 5-bromo-4-chloro-3-indolyl-β-D-galactopyranoside (X-gal; stock conc. of 20 mg·L^{-1} in dimethylformamide). The activity of β-galactosidase was visualized within 6 h. The enzyme β-galactosidase converts the substrate, X-gal, to galactose and 5-bromo-4-chloro-3-hydroxyindole, which is oxidized to a dark blue pigment. The supplement of 25 mM 3-AT helped to inhibit the background expression of the *HIS3* gene in this yeast strain.

2.12 Osmotic stress tolerance assay in *E. coli*

a) Recombinant protein production in *E. coli*

After transformation of *E. coli* BL21(DE3)RIPL (2.4.1), nine colonies carrying the same pMAL-c2x expression vector were grown separately overnight at 37°C in 5-mL LB medium containing suitable antibiotics (i.e., 35 µg·mL^{-1} chloramphenicol and 100 µg·mL^{-1} spectinomycin for strain, and 100 µg·mL^{-1} ampicillin for transformant selection). For the day-culture, 200 µL overnight culture served as inoculum of 20-mL LB medium containing appropriate antibiotics. When the day-cultures had reached an OD$_{600}$ of 0.6, 1 mL was collected as uninduced sample prior to adding IPTG at a final conc. of 0.3 mM. This uninduced sample was centrifuged at 8,000 *g* for 10 min, and the pellet was resuspended in 100 µL of 1x sample loading buffer. For SDS-PAGE (sodium dodecyl sulfate–polyacrylamide gel electrophoresis) (2.13.14), 10 µL of uninduced samples were loaded per lane (equal to an OD$_{600}$ of approx. 0.6). The IPTG induction was done at 15°C for 16 h. *E. coli* cells were harvested by centrifugation at 8,000 *g*, 4°C for 10 min. Each cell pellet was resuspended in 500 µL of lysis buffer (20 mM Tris-HCl pH 7.4, 200 mM NaCl, 1 mM EDTA, 1 mg·mL^{-1} DNase I, 1x cocktail protease inhibitors (cOmplete Protease Inhibitor Tablets, 4693116001, Roche, Basel, Switzerland). The resuspended bacteria were transferred to pre-cooled 2-mL cryo-tubes that already contained an equal volume of 0.1-mm glass beads (N029.1 Carl Roth, Karlsruhe, Germany). Cells were disrupted by vortexing at 2,700 rpm for 3 min (Disrupter Genie, Scientific Industries, New York, USA) and then cooled on ice for 3 min. Cell disruption was repeated twice. After disruption, cryo-tubes were placed on ice for a few minutes to sediment the glass beads. The supernatant (approx. 200 µL) was transferred to a 1.5-mL reaction tube for subfractionation at 20,000 *g* for 20 min. The supernatant containing soluble proteins was transferred to a new 1.5-mL reaction tube while the cell debris and insoluble proteins were resuspended in the same volume as the supernatant. The protein concentration of the supernatant fraction was determined by Bradford (Bradford, 1976;

2.13.13). For SDS-PAGE analysis, 10 µg of total protein of the supernatant were loaded per lane, and an equal volume of the pellet per sample was used.

b) Osmotic stress tolerance assay in *E. coli*

After the above-mentioned pre-screening of *E. coli* transformants for recombinant protein production, the best three were analyzed. The transformants were grown overnight at 37°C in 5-mL LB containing appropriate antibiotics (2.12, section a). On the next day, the overnight cultures were diluted 100-fold in the 20-mL LB liquid containing appropriate antibiotics to prepare the day-culture. When the day-culture reached the OD_{600} of 0.6, IPTG was added to the final concentration of 0.3 mM to induce the production of recombinant proteins for 6 h at 37°C (i.e., w/o additional osmoticum). After this step, three different *E. coli* transformants expressing the same construct were mixed in equal proportions, concentrated, adjusted to a total OD_{600} of 5 (in 3 mL), and serially diluted six times 10-fold in 100 µL LB (to $1:10^6$ dilution). The last three dilutions (10 µL) were spotted onto both standard LB plates and LB plates supplemented with either NaCl or KCl (0.4, 0.5, and 0.6 M) or with sorbitol (0.8, 1.0, and 1.2 M). Technical replicates were as described above. After 1, 2, and 3 d of incubation at 37°C, the CFU numbers were determined by counting single colonies grown on plates. Three independent experiments were performed and analyzed statistically using the SPSS 16 software (One-way ANOVA, Tukey's test, $p < 0.05$).

c) Detection of recombinant MBP and MBP-NHLx in *E. coli* by immunoblotting

The cell pellet was generated from the pooled day cultures (a total OD_{600} of 5) of three different transformants per construct and subsequently lysed, prior to subfractionation and protein quantification as described above (2.12, section a). Constant protein was loaded (1 µg of total protein) for SDS-PAGE and followed by immunoblotting using a mouse monoclonal primary anti-MBP antibody (1:5,000 dilution, CSB_MA000061M0m, Cusabio Technology, Houston, Texas, USA, supplied by Dianova GmbH Hamburg, Germany) (2.13.15 for more method details). To verify equal loading of total soluble protein per lane, a second SDS-PAGE gel (5 µg each lane) was stained with colloidal Coomassie Brilliant Blue G-250.

2.13 Molecular biology methods

2.13.1 Polymerase chain reaction (PCR)

For subcloning constructs in plasmids, DNA inserts were amplified by a high-fidelity DNA polymerase, namely Phusion DNA polymerase (F530S, Thermo Scientific, Vilnius, Lithuania).

Reagents for one reaction are shown in Table 2.1. The annealing temperature (T_a) and extension time were determined based on the sequences of primers used and the sizes of amplicons, respectively.

Table 2.1: PCR components for Phusion DNA polymerase

Reagent	Volume (µL)	Final concentration
5x Phusion HF buffer	10	1x
10 mM dNTPs	1	0.2 mM
Forward primer (10 µM)	1	0.2 µM
Reverse primer (10 µM)	1	0.2 µM
Phusion High–Fidelity DNA Polymerase (2 U·µL^{-1})	0.5	0.02 U·µL^{-1}
DNA template (30 ng)	x	
Nuclease-free H$_2$O	ad 50 µL	

PCRs used for positive *E. coli* transformant (colony PCRs) and plant genotyping were carried out by using DreamTaq DNA polymerase (K1082, Thermo Scientific, Vilnius, Lithuania) and Phire Hot Start II DNA polymerase (F130WH, Thermo Scientific, Vilnius, Lithuania), respectively. Reagents in one PCR run by each DNA polymerase are shown in Table 2.2 and Table 2.3. Thermal cycler parameters were followed by the manufacturer's instruction.

Table 2.2: PCR components for DreamTaq DNA polymerase

Reagent	Volume (µL)	Final concentration
2x DreamTaq Green PCR Master Mix (includes DreamTaq DNA Polymerase, 2x DreamTaq Green buffer, dNTPs, and 4 mM MgCl$_2$)	12.5	1x
Forward primer (10 µM)	0.5	0.2 µM
Reverse primer (10 µM)	0.5	0.2 µM
DNA template (30 ng) or o/N bacterial culture	x µL of DNA or 1 µL of culture	
Nuclease-free H$_2$O	ad 25 µL	

Table 2.3: PCR components for Phire Hot Start II DNA polymerase

Reagent	Volume (µL)	Final concentration
2x Phire Plant Tissue PCR Buffer (includes dNTPs and MgCl$_2$)	5	1x
Forward primer (10 µM)	0.5	0.5 µM
Reverse primer (10 µM)	0.5	0.5 µM
Phire Hot Start II DNA Polymerase	0.2	
Plant sample prepared in dilution buffer	0.5	
Nuclease-free H$_2$O	ad 10 µL	

2.13.2 PCR-based site-directed mutagenesis (SDM)

Site-directed mutagenesis (SDM) was performed according to Edelheit et al. (2009) and was used to generate pSAT_*mVenus-C* from the parental plasmid pSAT6_*Venus-C*, thereby obtaining monomeric Venus (mVenus), which later could be subsequently used as the template for generating reporter constructs. In detail, the A206 residue of Venus was mutated to K (Zacharias et al., 2002) by SDM specific primers. These two primers, complementary to each other, were designed to contain the point mutation and to have a very high melting temperature of 72 – 85°C and a GC content of 40 – 70%. The plasmid template (0.5 µg) was amplified by Phusion DNA polymerase. The reaction components are shown in Table 2.1 except that only one primer was used per reaction in a total volume of 25 µL and performed according to the manufacturer's instruction (F530S, Thermo Scientific, Vilnius, Lithuania). Particularly, the annealing temperature was 55°C, and elongation was performed at 72°C for 2.5 min. After combination of the two reactions, the two DNA strands were annealed by a specific cooling-down cycle as shown in Table 2.4. Subsequently, the DNA was incubated with 1 µL of FastDigest DpnI (Thermo Scientific, Vilnius, Lithuania) overnight at 37°C, followed by inactivation at 80°C for 5 min. *E. coli* was then transformed with 10 µL of the reaction (2.4.1). Because the parental plasmid/template (1 µg), which had been propagated and methylated in *E. coli*, was digested by DpnI, the amplified plasmids, which were not digested by DpnI and contained nicks near the point mutation, were taken up by *E. coli* after transformation.

Table 2.4: Annealing cycle

Temperature (°C)	Time duration (min)
95	5
90	1
80	1
70	0.5
60	0.5
50	0.5
40	0.5
37	Hold

2.13.3 DNA purification from agarose gels

To subclone constructs into plasmids, PCR products and digested plasmids were purified from 1% agarose gel according to the manufacturer's instructions (GeneJET Gel Purification Kit, Thermo Scientific, Vilnius, Lithuania).

2.13.4 Restriction digest using FastDigest enzymes

For subcloning constructs into plasmids, DNA molecules (e.g., 1 μg of gel-purified DNA insert and 2 μg of plasmids) were enzymatically digested by FastDigest (FD) restriction enzymes (Thermo Scientific, Vilnius, Lithuania). Components in one 20-μL restriction reaction are shown in Table 2.5. For plasmid digestion, alkaline phosphatase was additionally used to catalyze the release of 5'-phosphate groups from DNA in order to avoid plasmid re-ligation with itself without inserts in a ligation reaction. Restriction reactions were incubated at 37°C for 2 h, followed by a thermal inactivation that was defined by FD enzymes used. Analytical reactions, which were performed to confirm the presence of transgene or inserts in plasmids, were incubated at 37°C for only 30 min prior to DNA electrophoresis.

Table 2.5: Components in restriction digestion reaction using FD enzymes

Reagent	Volume (μL)	Note
10x FD buffer	2	
FD enzyme 1	0.2	
FD enzyme 2	0.2	
FastAP (1 U·μL^{-1})	1	Only for plasmid digestion reaction to remove 5'-phosphate groups
DNA (1 μg)	x	
Nuclease-free H$_2$O	ad 20 μL	

2.13.5 DNA Ligation

Plasmid backbone and DNA inserts, which were digested by the same FD enzymes (1:5 or 1:10 molar ratio), were ligated in a 10-µL ligation reaction including 1 µL of T4 ligase (1 U·µL^{-1} as a final concentration) and 10x T4 ligase buffer (1x as a final concentration, Thermo Scientific, Vilnius, Lithuania). For ligation, 30 ng of plasmids backbone were used. The reaction mixture was incubated overnight at 4°C. The next day, 5 to 10 µL of the reaction was used for transformation of *E. coli*.

2.13.6 Gateway cloning

The Gateway technology (Thermo Scientific, California, USA) was used to generate the complementation and *GUS* reporter constructs. In general, the first step was to amplify a DNA insert using primers flanked by the *att*B sequences. To create the entry clone pENTR223, a BP reaction was done overnight at 25°C using BP clonase enzyme mix to recombine regions between *att*B and *att*P sites (forming *att*L sites), replacing the toxic *ccdB* gene between the two *att*P sites of pDONR223 vector by the insert. The *ccdB*-sensitive *E. coli* strain TOP10 was transformed with the BP reaction products to obtain transformants with positive recombinant pENTR223.

Sequencing of inserts in pENTR223 was carried out to confirm correct sequences of inserts (2.13.12). A second recombination reaction for 3 h at 25°C using LR clonase enzyme mix was performed to recombine regions between *att*L sites (e.g., pENTR223) and *att*R sites in a destination plant expression vector (e.g., pMDC99, pMDC123, or pMDC162). This reaction, called the LR reaction, enables the transfer of the inserts into a plant expression vector to generate transient and stable transgenic *Arabidopsis* plants *via Agrobacterium*-mediated transformation.

2.13.7 Plasmid isolation and purification

Plasmids were isolated and purified using GeneJET Plasmid Miniprep Kit (K0503, Thermo Scientific, Vilnius, Lithuania) according to the manufacturer's instructions.

2.13.8 RNA extraction

The method was adapted from the protocol developed by Nina Kassner (Gertrud Lohaus research group, Germany). Samples were strictly kept on ice in all steps. All standard centrifugation steps were performed at 14,000 rpm. Six leaves (approx. 100 – 200 mg in total) of 4- to 5-week-old plants were ground in liquid nitrogen using a sterile mortar and pestle to a

fine powder. One milliliter of Trizol™ (Invitrogen, California, USA) was added, and the plant powder was immediately vortexed. After centrifugation for 10 min at 4°C, the supernatant was collected and subsequently mixed with 200 μL chloroform, followed by inversion for 15 s to extract RNA. Samples were kept on ice for 3 min and centrifuged for 15 min at 4°C. Phase separation yielded an upper aqueous phase containing the total RNA and an organic phase, with a thin layer of proteins in between the two. The upper phase was transferred carefully to a new 1.5-mL Eppendorf tube which contained ½ volume (of aqueous phase) isopropanol and ½ volume of salt solution (0.8 M trisodium citrate and 1.2 M sodium chloride prepared in DEPC-treated H_2O). After 10-min incubation on ice, samples were centrifuged for 10 min at 4°C. The white pellet containing precipitated RNA was washed twice with freshly prepared 75% (v/v) ethanol in DEPC-treated H_2O. Ethanol was gently removed after centrifugation, and excess ethanol was removed using a pipette. The pellet was dried at 65°C for 3 − 5 min and subsequently dissolved in 50 − 100 μL of DEPC-treated H_2O at 65°C for 3 − 5 min.

The quantity and purity of the RNA were determined by using a spectrophotometer (Eppendorf, Hamburg, Germany) based on the absorbance ratios A260/A280 and A260/A230. Samples were either treated with DNase I (1 U·μL^{-1}) to remove gDNA or stored at -80°C until further use.

Before cDNA synthesis, RNA samples were treated with DNase I to completely digest any gDNA contamination. As *NHL4* is a single exon gene, it was necessary to eliminate all gDNA from the purified RNA in order to quantify gene expression accurately. Thus, an optimized DNase I treatment was performed in which the amount of DNase I was doubled (to 2 U for 1 μg of purified RNA) (Díaz, 2020). The purified-RNA sample (1.5 μg) was digested in a 30-μL reaction including 3 U of DNase I (1 U·μL^{-1}, Thermo Scientific, Vilnius, Lithuania), 30 U of Ribolock RNase inhibitor (40 U·μL^{-1}, Thermo Scientific, Vilnius, Lithuania), and 1x Reaction Buffer with $MgCl_2$ (B43, Thermo Scientific, Vilnius, Lithuania). Samples were incubated at 37°C in a water bath for 45 min, 3 μL of 50 mM EDTA were added (final conc. approx. 4.5 mM), followed by an incubation at 65°C for 10 min. The quantity and purity of the RNA were determined by spectrometry. Isolated RNA was either stored at -80°C until further use or analyzed by RNA electrophoresis to judge its quality. To this end, 500 ng of DNase I-treated RNA was mixed with an equal volume of 2x RNA loading dye (1x final conc.) and 2 μL of 2% GelRed (41003, Biotium, California, USA), followed by heating up at 70°C for 10 min. The RNA electrophoresis was carried out at 100 V for 50 min.

2.13.9   cDNA synthesis

To minimize the gDNA contamination and other components from the previous applications, which could interfere with qRT-PCR, only 200 ng (rather than 1 µg) of RNA after DNase I treatment was used for cDNA synthesis. First-strand cDNA synthesis was carried out with RevertAid H Minus Reverse Transcriptase (200 U·µL^{-1}; Thermo Fisher, Vilnius, Lithuania). The first three components including RNA, the oligo(dT) primer, and DEPC-treated H$_2$O were prepared in a 0.2-mL tube in a final volume of 12.5 µL (Table 2.6). The mixture was incubated at 65°C for 5 min in a thermal cycler. The remaining reagents were added as also shown in Table 2.6, and cDNA synthesis was conducted following a thermal cycle as shown in Table 2.7. cDNA samples were stored at -20°C until further use.

Table 2.6: cDNA synthesis reaction components

Reagent	Volume (µL)	Final concentration
In a preincubation step		
RNA (200 ng)	x	
Oligo(dT) primer (100 µM)	1	50 µM
DEPC-treated H$_2$O	ad 12.5 µL	
After preincubation		
5x Reaction buffer	4	1x
RiboLock RNase Inhibitor (40 U·µL^{-1})	0.5	1 U·µL^{-1}
10 mM dNTPs	2	1 mM
RevertAid H Minus Reverse Transcriptase (200 U·µL^{-1})	1 µL	10 U·µL^{-1}

Table 2.7: Thermo cycle for cDNA synthesis

Temperature	Time duration
25 °C	5 min
42 °C	60 min
70 °C	5 min
4 °C	∞

2.13.10 Gene expression analysis by qRT-PCR

To study the gene expression level in the KO mutants, the relative quantification method ($2^{-\Delta\Delta Ct}$) was used (Livak and Schmittgen, 2001). qRT-PCR was prepared in a 96-well plate. In a 15-µL reaction, 7.5 µL of 2x FastStart Essential DNA Green Master Mix (Roche, Mannheim, Germany) was mixed with two primers (final conc.: 0.3 µM for each), 1 µL of cDNA template, and nuclease-free H$_2$O. The thermal profile of the qRT-PCR was 95°C for 10 min, 45 cycles of

95°C for 10 s, 60°C for 10 s, and 72°C for 18 s (LightCycler® 96 System, Roche, Mannheim, Germany). Melting curves were obtained using the following thermal melting profile performed after the qRT-PCR cycle: 95°C for 10 s, followed by a constant increase in the temperature range between 60 to 97°C. Gene-specific primer pairs for *NHL4, NHL6,* and *NHL25* used in this study are shown in Suppl. Table 8 with reference to Mwaanga (2011). For qRT-PCR of *NHL* genes, the housekeeping gene *ACT2* (At3g18780) was used as reference gene (Maruyama et al., 2013). The C_t values of both genes (*NHLx* and *ACT2*) were calculated by LightCycler® 96 software (v1.1.1320, Roche, Mannheim, Germany) and used to calculate the relative gene expression (vs. *ACT2*) in the corresponding *nhl* mutants using the $2^{-\Delta Ct}$ method (Livak and Schmittgen, 2001). Subsequently, the fold change of relative target gene expression between genotypes (KO mutant or OE line vs. WT which was set to 100%) and two treatments (stress vs. non-stress) was determined by the so-called "ΔΔCt" method ($2^{-\Delta\Delta Ct}$) (Livak and Schmittgen, 2001). The mean values of the fold change were used to plot figures (n ≥ 2). The data were analyzed by Student's t-test in Microsoft Excel 2016 (one tail, unpaired, equal variance) to identify the statistical significance of differential gene expression between genotypes and treatments with $p < 0.05$.

Different cDNA concentrations in serial dilutions of cDNA samples (in triplicates) were used to verify the primer amplification efficiencies. The standard curves generated from undiluted cDNA, 10-fold cDNA dilutions (i.e., undiluted to 10^{-3}) and corresponding Ct values were used to generate the regression equation with a slope value in order to calculate the amplification efficiency of primer pairs ($E = 10^{-1/slope}$). For genes which have a very low basal expression level (for *NHL4*, *NHL6* and *NHL25*), ABA- or *Pst*(*avrRpt2*)-induced samples were used to analyze the primer amplification efficiency.

The binding specificity of qRT-PCR primer pairs was also verified by analyzing the melting curves of each reaction. The unique appearance of one melting peak in each reaction represents the dissociation of only one product that was amplified in the reaction, indicating the specificity of the used primer pair.

2.13.11 Nucleic acid electrophoresis

DNA and RNA samples were prepared in 1x appropriate loading dye and 1 – 2 μL of 2% (v/v) Gel Red (Biotium) prior to gel loading. DNA and RNA molecules migrated in 1% (w/v) agarose gels that was prepared in 1x TAE buffer (40 mM Tris, 20 mM acetic acid, 1 mM EDTA pH 8.5) at

a constant voltage of 100 V in 1x TAE buffer. DNA or RNA molecules were visualized by UV light (E-Box VX5, Vilber, Marne-la-Vallée, France).

2.13.12 Sequencing analysis

DNA sequencing was performed using the Sanger sequencing service from Microsynth Seqlab (Göttingen, Germany). DNA samples (minimum conc. at 80 ng·μL^{-1}) were mixed with 3 μL of the sequencing primers (2.5 μM as final conc.) in a final volume of 12 μL prior to sending samples for sequencing. Sequencing primers used for verifying subcloned constructs in different plasmids are listed in Suppl. Table 10.

2.13.13 Protein quantification by Bradford

The protein concentration was determined by the Bradford method. The free dye Coomassie Brilliant Blue G-250 (CBB-G250) molecule is blue but shifts in absorbance maximum from 465 to 595 nm. Therefore, protein concentration can be quantified by measuring the absorption at 595 nm if bound to proteins. To quantify the protein concentration in samples, a standard curve of different bovine serum albumin concentrations (0 – 20 μg·mL^{-1} of BSA) was generated. For measurement, standard samples were prepared with Milli-Q water in a final volume of 100 μL, and 900 μL of Bradford reagent (0.01% (w/v) CBB-G250, 5% (v/v) ethanol (molecular grade), 8.5% (v/v) orthophosphoric acid) was further added. After 5-min incubation, the samples were transferred to a 1-mL cuvette for measuring the absorbance at 595 nm. Based on linear regression analysis and the resulting linear equation, the absorption value of protein samples was used to determine protein concentration of samples.

2.13.14 SDS-PAGE

Proteins migrate in SDS-PAGE gels (Laemmli, 1970) which were made of the upper 4% (w/v) acrylamide stacking gel and the lower 12.5% (w/v) acrylamide separating gel (Table 2.8) using Hoefer gel caster system (e.g., 8.5 x 7.5 x 0.1 cm; width x height x depth, SE245, Hoefer, Inc., Massachusetts, USA). Solidified gels were placed into a Hoefer SE250 electrophoresis unit, filled with 1x electrophoresis buffer (25 mM Tris, 192 mM glycine, and 0.1% (w/v) SDS).

To a total sample volume of 20 – 30 μL, 5x sample buffer (300 mM Tris-HCl pH 6.8, 10% (w/v) SDS, 50% (v/v) glycerol, 0.125% (w/v) bromophenol blue, and 25% (v/v) 2-mercaptoethanol) was added to obtain 1x as a final concentration, and the proteins were dissolved by pipetting. Proteins were denatured by heating samples at 95°C for 5 min in a thermo-block, followed by a brief centrifugation at 14,000 rpm prior to loading.

Protein electrophoresis was performed at a constant voltage of 200 V for approx. 1 –
2 h. After running, SDS-PAGE gels were washed three times with deionized H_2O and incubated
with colloidal Coomassie solution (0.02% (w/v) CBB-G250, 5% (w/v) aluminum sulfate-(14-18)-
Hydrate, 10% (v/v) ethanol, 2.35% (v/v) orthophosphoric acid) on an orbital shaker at RT
overnight.

Table 2.8: Gel preparation for SDS-PAGE

Solution	Volume (mL) for 12.5% separating gel	Volume (mL) for 4% stacking gel
30% Acrylamide/Bisacrylamide solution	5	0.67
1.5 M Tris-HCl pH 8.8 (0.375 M final conc.)	3	--
0.5 M Tris-HCl pH 6.8 (0.125 M as final conc.)	--	1.25
10% (w/v) SDS	0.12	0.05
M_Q H_2O	4	3
APS (10% w/v)	0.06	0.03
TEMED	0.01	0.005
Total volume	12.19	5.005

2.13.15 Immunoblotting

Total protein extract (1 – 20 µg) separated by SDS-PAGE was transferred from the gel to a
nitrocellulose membrane (pore size 0.2 µm, protein binding capacity 209 µg·cm^{-1}, BioTrace NT,
Pall Life Sciences, Portsmouth, USA) by tank blotting. The membrane, gel, and blotting papers
were assembled in a tank (Mini-PROTEAN® Tetra Vertical electrophoresis Cell, Bio Rad,
Hercules, California, USA) that contained the cold 1x transfer buffer (4.9 mM Tris, 3.9 mM
glycine, 20% (v/v) ethanol, 0.04% (v/v) SDS in M_Q H2O). Transfer was performed at 70 mA for
2 h at 4°C. After transfer, the membrane was washed with PBS-T (10 mM Na_2HPO_4, 1.8 mM
KH_2PO_4, 137 mM NaCl, 2.7 mM KCl, 0.1% (v/v) Tween 20, pH 7.4). To reduce unspecific binding,
the membrane was incubated in blocking solution (5% (w/v) dry milk powder dissolved in
PBS-T, Carl Roth, Karlsruhe, Germany) while shaking on an orbital shaker at RT for 1 h. The
membrane was then washed six times in PBS-T for a total of 15 min (3x quick, 3x 5-min
washing). The membrane was subsequently incubated overnight at 4°C in 10 mL of mouse
monoclonal primary anti-MBP antibody (1:5,000 in cold PBS-T; CSB-MA000061M0m, Cusabio
Technology, Houston, Texas, USA; supplied by Dianova GmbH Hamburg, Germany). The
primary antibody was re-used several times. On the next day, the membrane was washed
again six times with PBS-T, as described above, followed by an incubation in 10 mL polyclonal

secondary anti-mouse IgG (whole molecule)-peroxidase antibody produced in rabbit (1:20,000 dilution in cold PBS-T; A9044-2ML, Sigma-Aldrich Chemie GmbH, Schnelldorf, Germany) on an orbital shaker for 1.5 h. The membrane was washed six times with PBS-T (see above) prior to the detection. The presence of MBP-tagged proteins was detected by exposing the membrane to a 1:1 volumetric mixture of luminol and peroxide (Amersham ECL Prime Western Blotting Detection Reagent, GE Healthcare, Chicago, USA). Image acquisition was done using a ChemiDoc™ Touch Imaging System (Bio-Rad, California, USA).

3   RESULTS

3.1   Selection of specific fluorophore combinations for reliable *in vivo* peroxisome targeting analyses in Arabidopsis seedlings

Apart from their enhanced fluorescence, yellow (EYFP) and blue (CFP) fluorescent proteins display very distinct emission spectra at 520 – 550 and 475 – 503 nm, respectively, compared to the red autofluorescence of chloroplasts (648 – 709 nm). Therefore, for *in vivo* subcellular targeting studies of peroxisomal proteins, blue fluorescent peroxisomal marker proteins and yellow fluorescent fusions with the proteins of interest have been widely used for more than a decade in different transient plant expression systems, including onion epidermal cells and protoplasts of tobacco and Arabidopsis mesophyll cells (Fulda et al., 2002; Ma et al., 2006; Reumann et al., 2007; Kataya and Reumann, 2010; Lingner et al., 2011; Chowdhary et al., 2012). Both fluorescent proteins are GFP variants and have been reported to have a reduced but still detectable very weak tendency of dimerization (Zacharias et al., 2002). The property might become problematic particularly in peroxisome research. As previously shown, proteins with a deletion of their PTS were still imported into peroxisomes *via* dimerization with peroxisomal full-length proteins, demonstrating the capability of peroxisomes in importing fully folded and oligomeric proteins (1.1.3; Glover et al., 1994; McNew and Goodman, 1994). This mechanism is referred to as piggy-back import (Glover et al., 1994) and was reported to occur also for few native proteins, i.e. lacking PTS (Islinger et al., 2009; Kataya et al., 2015).

Because the method of fast transient transformation of Arabidopsis seedlings (Li et al., 2009) was newly established in this study, the piggy-back import could be more problematic due to higher expression rates in this homologous and intact system compared to others, e.g. the heterologous onion epidermal cells and stressed protoplasts. To verify cytosolic and non-peroxisomal targeting of non-peroxisomal proteins, untagged EYFP versions or EYFP fusions with a non-PTS peptide were routinely used in onion epidermal cells and protoplasts (Kataya and Reumann, 2010; Chowdhary et al., 2012). In these two systems, this control also verified the absence of unspecific peroxisomal import of non-peroxisomal proteins, allowing the reliable interpretation of peroxisome targeting of novel peroxisomal proteins. Likewise, in a system such as Arabidopsis seedlings with high expression rates, an untagged yellow fluorophore should be expressed together with a peroxisomal marker labeled with a blue fluorophore as a standard negative control for peroxisome targeting. This control is only meaningful

if untagged yellow fluorophores fully remain in the cytosol and the nucleus and are not imported into peroxisomes to any extent.

Besides the combination of EYFP and CFP and in order to minimize any weak dimeri-zation between GFP variants, a fully monomeric yellow fluorescent protein, monomeric Venus (mVenus), was generated by mutating A206 of Venus to K by site-directed mutagenesis (2.3.2 and 2.13.2; Zacharias et al., 2002), and a pre-existing fully monomeric blue fluorophore, mono-meric Cerulean (mCerulean), was used (2.3.2). To investigate whether a cytosolic yellow fluorescent GFP variant was co-imported into peroxisomes together with a blue peroxisome marker due to fluorophore dimerization and *via* piggy-back mechanism, *EYFP* or *mVenus* lacking any peptide or protein tags was co-expressed with a blue peroxisome marker, either *CFP-PTS1* or *mCerulean-PTS1* (*mCer-PTS1*) in transiently transformed Arabidopsis seedlings. This method is based on the co-cultivation of 4-day-old seedlings with *Agrobacteria* carrying the constructs of interest for approx. 2 d before observation by confocal microscopy. The co-cultivation solution containing acetosyringone and Silwet L-77 (2.4.4) facilitates the transient transformation of both epidermal and mesophyll cells by *Agrobacterium*. To verify the lack of unspecific peroxisomal import of untagged EYFP variants, the untagged fluorophore was simultaneously expressed alone. In the following paragraphs, the results performed by myself and those which are part of my publication (Falter et al., 2019) are described.

In single transformed Arabidopsis epidermal cells, untagged EYFP and mVenus were found exclusively in the cytosol and nucleus, as expected (data not shown). However, when they were co-expressed with *CFP-PTS1*, EYFP became detectable in peroxisomes 2 days post co-cultivation (dpc) (data now shown) and also 3 dpc (Figure 3.1A). The results demonstrated that untagged EYFP was imported unspecifically into peroxisomes in the presence of CFP-PTS1 due to weak but sufficient fluorophore dimerization. The same finding was observed for mVenus (Figure 3.1B), indicating that the introduction of the A206K mutation was not sufficient to completely abolish the dimerization between mVenus and CFP. Similar results were found in transiently transformed tobacco leaf epidermal cells (by infiltration with *Agrobacterium*), as EYFP and mVenus were also detected in peroxisomes specifically after co-expression with *CFP-PTS1* (Falter et al., 2019). In contrast and consistent with previous results (Kataya and Reumann, 2010; Chowdhary et al., 2012), such unspecific peroxisome targeting of untagged fluorophore was not observed in other commonly used expression systems, such as onion epidermal cells and protoplasts (Falter et al., 2019). Piggy-back import was indeed

problematic in the intact plant systems. The data indicated that neither EYFP nor mVenus in combination with CFP-PTS1 could be used as the standard negative controls of peroxisome targeting analyses in transiently transformed Arabidopsis seedlings and tobacco leaf epidermal cells.
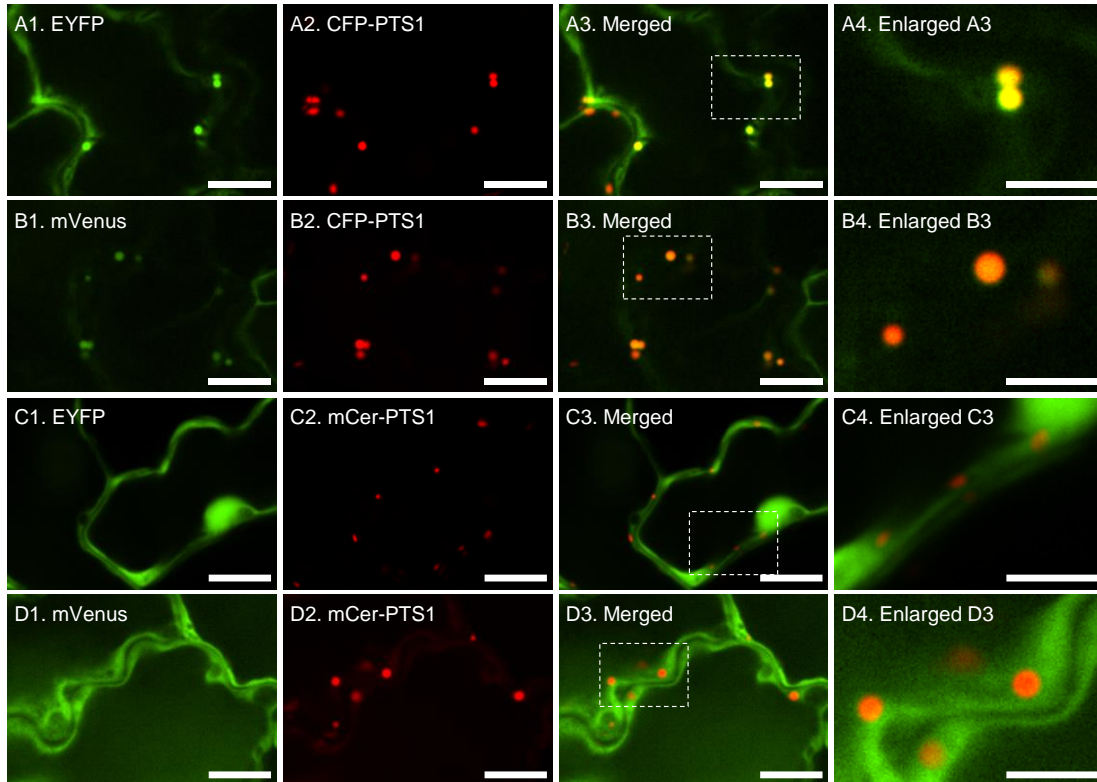
Figure 3.1: Peroxisomal and cytosolic targeting of untagged EYFP and mVenus when co-expressed with either *CFP-PTS1* or *mCer-PTS1*

Four-day-old seedlings were transiently transformed by co-cultivation with *A. tumefaciens*. Peroxisomal localization of (A) EYFP and (B) mVenus was observed in epidermal cotyledon cells of double transformants co-expressing the untagged yellow fluorophore together with *CFP-PTS1.* Upon co-expression with *mCer-PTS1,* however, (C) EYFP and (D) mVenus remained fully cytosolic without any detectable peroxisome targeting. Images were taken 3 dpc. Representative images of several inde-pendent experiments are shown (n > 3). The blue fluorescence was converted to red. The white dashed boxes indicate enlarged regions. Scale bar = 10 μm (5 μm for enlarged region). Data are very similar but not identical to those presented in the study of Falter et al. (2019).

Contrary to previous *in vivo* subcellular targeting analyses in onion epidermal cells and protoplasts (Ma et al., 2006; Kataya and Reumann, 2010; Lingner et al., 2011), where the transformed cells were rather uniform in showing either cytosolic or peroxisomal targeting for diverse proteins of interest, the transformed epidermal cells of Arabidopsis seedlings were heterogeneous in terms of peroxisome targeting of EYFP and mVenus. Moreover, the

percentage of double transformed cells showing peroxisome targeting for the yellow fluorophores increased with expression time, as expected for a mechanism depending on cytosolic protein concentrations. To quantify the relationship between the extent of piggy-back import and expression time, a large number of double transformed cells were quantitatively analyzed at different time points of expression for peroxisomal localization of EYFP or mVenus. A minimum number of 100 double transformed cells were investigated to calculate the percentage of cells with peroxisome targeting of untagged yellow fluorophore at different expression time points. This value was averaged from two independent experiments. When co-expressed with *CFP-PTS1*, untagged EYFP was targeted to peroxisomes in approx. 10% of double transformed cells 3 dpc (Figure 3.2). The percentage increased up to 45% 5 dpc. When mVenus was co-expressed with *CFP-PTS1*, even more cells were observed with peroxisomal mVenus (3 d: 45%; 5 d: 59%). The results revealed that the extent of piggy-back import increased with the time of expression, consistent with the hypothesized import mechanism which should become more relevant with increased expression level of EYFP or mVenus.

As mentioned above of using mVenus, heterodimerization with CFP-PTS1 still occurred (Figure 3.1B). However, if peroxisomes were labeled with *mCer-PTS1*, peroxisome targeting of EYFP or mVenus was not detected at all 3 dpc (Figure 3.1C, D) and even not at later time point 5 dpc (data not shown). The same result was also obtained in transiently transformed tobacco leaf epidermal cells (Falter et al., 2019). Altogether, the heterodimerization occurred between one of the yellow fluorophores EYFP or mVenus with CFP-PTS1, but not with mCer-PTS1. Therefore, to study *in vivo* peroxisomal localization of proteins of interest in transiently transformed Arabidopsis seedlings, it was strongly recommended that mCer-PTS1 in combination with EYFP or mVenus must be used to obtain reliable results of peroxisome targeting.
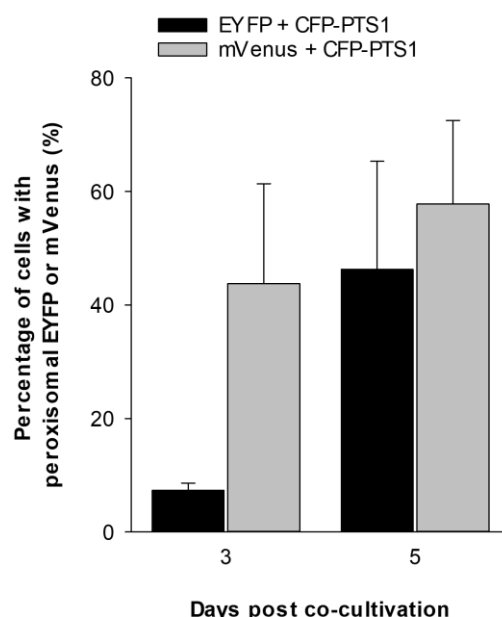
Figure 3.2: Percentage of double transformed Arabidopsis cells showing peroxisomal EYFP or mVenus upon co-expression with *CFP-PTS1*

Four-day-old Arabidopsis seedlings were co-cultivated with *Agrobacterium*. Epidermal cells displaying peroxisome targeting of untagged EYFP (black) or mVenus (grey) when co-expressed with *CFP-PTS1* were counted and expressed in percentage of double transformed cells (> 100 per experiment). For quantification, a minimum of 100 double transformed cells was analyzed per experiment. Data represent the mean value and standard error from two independent experiments. This figure is adapted from the one published in Falter et al. (2019).

3.2 Characterization of a novel endoplasmic reticulum-mediated biogenesis pathway of peroxisome-targeted NHL proteins

Previous studies in the research group had revealed that NHL4 and NHL25 are membrane proteins and carry a functional PTS1 domain that was sufficient to target EYFP to peroxisomes in onion epidermal cells 18 hours post transformation (hpt) (Kataya, 2011; Crappe, 2016; Chowdhary, Sørhagen, and Reumann, unpubl. data). In tobacco and Arabidopsis protoplasts, only full-length EYFP-NHL4 was occasionally observed in peroxisomes, but the results were not robust and hardly reproducible (Kataya, 2011; Crappe, 2016). Detectable peroxisome targeting was even weaker for EYFP-NHL6 and EYFP-NHL25 (Crappe, 2016). The three NHLs were primarily detected in the cytosol and vesicle-like structure, few of which (labeled by NHL4) were occasionally found in close physical association with peroxisomes (Kataya, 2011). Thus, the three NHL proteins were considered to be putative class II peroxisomal membrane proteins

(PMPs) that are targeted to peroxisomes *via* the endoplasmic reticulum (ER) and a vesicular pathway and possess the atypical and novel feature of a functional PTS1 domain.

To describe and characterize the intriguing multi-step biogenesis pathway of the three NHL proteins of interest (NHL4, NHL6, and NHL25) in greater depth, a transient expression system preferentially of intact Arabidopsis plants of very high biogenetic activity, i.e. with high endogenous rates of cell proliferation and organelle biogenesis was considered advantageous and sought. Seedlings represent an early developmental stage with these features. Hence, intact Arabidopsis plants (i.e., seedlings) were chosen as the transient expression system, referred to as FAST assay (Li et al., 2009; 3.2.1 and 3.2.2). Peroxisome targeting was investigated in-depth not only for NHL4 but also for NHL6 and NHL25 using live cell imaging, and the analyses were further extended by TEM. Additionally, stable transgenic Arabidopsis plants expressing *NHLs* either from the strong constitutive *Cauliflower Mosaic Virus* (*CaMV*) *35S* promoter or from the genes' endogenous promoters were created and used to verify the results (3.2.3).

3.2.1 NHL4, NHL6, and NHL25: *In vivo* subcellular targeting analyses and functional characterization of PTS1 domains

To study the subcellular localization of NHL4, NHL6, and NHL25 in Arabidopsis seedlings, the CDS of the full-length proteins were fused to the back of different fluorescent proteins (EYFP, mVenus, or mCherry) and co-expressed with organelle markers from the strong constitutive *CaMV 35S* promoter. In addition, EYFP appended with the C-terminal 10 aa of NHLs was used to investigate whether the PTS1 alone could sufficiently target the protein to peroxisomes and how efficient the peroxisome targeting was compared to that of the full-length protein. The peroxisome marker *mCer-PTS1* (3.1) was transiently co-expressed with *EYFP-* or *mVenus-NHLs* in 4-day-old Arabidopsis seedlings upon co-cultivation with *Agrobacterium*. Fluorescence was analyzed at different time points (2 – 6 dpc).

3.2.1.1 Peroxisome targeting analyses of the C-terminal decapeptides of NHL4, NHL6, and NHL25

According to present knowledge derived from fungi, animals, and plants, PTS1s are specific for soluble peroxisomal proteins and not found in PMPs. To investigate whether the three NHLs represent a novel type of PMPs carrying functional PTS1 domains that are sufficient to direct a reporter protein to peroxisomes, EYFP was extended C-terminally by the C-terminal decapeptides of the three NHLs. A relatively high prediction score of 0.906 for peroxisome targeting

with a targeting probability of 100% (> prediction threshold 0.412 and probability threshold 50%; http://ppp.gobics.de) had been calculated for NHL4 and its canonical and presumably strong PTS1 (AKL>) (Kataya, 2011; Lingner et al., 2011; Reumann et al., 2012). By contrast, NHL6 (LRL>) and NHL25 (FRL>) were predicted to possess PTS1 domains with the lower scores of 0.492 and 0.536, respectively, indicating a slightly lower peroxisome targeting probability (NHL6: 87.3%; NHL25: 94.9%) and presumably a weaker peroxisome targeting efficiency (Reumann et al., 2012).
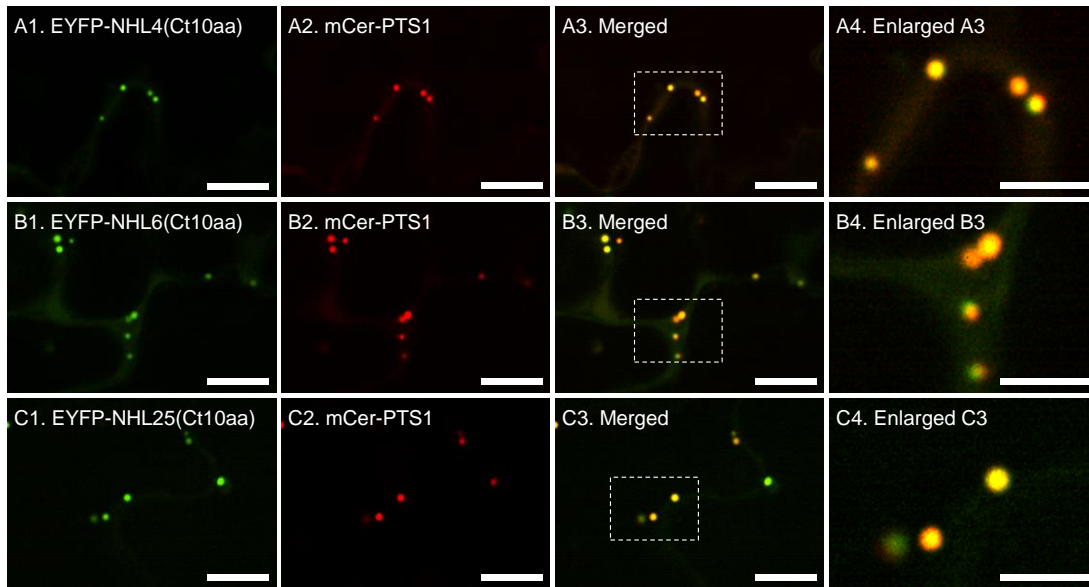
Figure 3.3: Functional analysis of the predicted PTS1 domains of NHL4, NHL6, and NHL25 by *in vivo* subcellular localization targeting analyses

(A – C) The C-terminal 10 aa of NHL4 (A), NHL6 (B), and NHL25 (C) targeted EYFP to peroxisomes in double transformed epidermal cotyledon cells co-expressing *mCer-PTS1* 2 dpc. Four-day-old seedlings were transiently transformed by co-cultivation with *Agrobacterium*. Images are representative for two independent experiments. White dashed boxes show enlarged regions. Scale bar = 10 μm (5 μm for enlarged region).

Upon co-expression of *mCer-PTS1* with the three EYFP constructs, strong EYFP fluorescence was detected in peroxisomes in all double transformed cells at a very early time point 2 dpc (Figure 3.3). Only very weak fluorescence was observed in the cytosol. Notably, and as expected for the three standard soluble PTS1 proteins, targeting to non-peroxisomal puncta was not observed. The results verified that the three NHL proteins possess functional PTS1 domains that are sufficient to direct a reporter protein to peroxisomes. Despite slightly different prediction scores of peroxisome targeting for the canonical PTS1 of NHL4 compared

to the non-canonical PTS1s of NHL6 and NHL25, all three PTS1 domains were characterized as strong and efficient in these *in vivo* analyses.

3.2.1.2   Protein-protein interaction analyses between NHL4, NHL6, and NHL25 and AtPex5

Similar to Pex5 orthologs from human and fungi (Stanley et al., 2006; Hagen et al., 2015), plant Pex5 from tobacco and Arabidopsis are reported to bind PTS1s in the C-terminal tetratricopeptide repeat (TPR) domain (Kragler et al., 1998; Bonsegna et al., 2005; Khan and Zolman, 2010; Skoulding et al., 2015). To investigate whether the PTS1 domains of NHL4, NHL6, and NHL25 can bind to AtPex5, protein-protein interaction analyses by the yeast two-hybrid (Y2H) method were performed. Any transmembrane domains (TMDs) of proteins should be removed to allow nuclear translocation of the protein complex. By TMHMM 2.0 (2.7.2) the TMD was predicted from aa $55-75$ (NHL4), aa $67-87$ (NHL6), and aa $66-86$ (NHL25). Therefore, the short N-terminal domain and the predicted TMD of NHL4 (80 aa), NHL6, and NHL25 (both 100 aa) were not included in the fusion constructs. Hence, the remaining LEA_2 domain and the PTS1 were N-terminally fused with the activation domain (AD) of the GAL4 transcription factor (TF) in the yeast expression vector, pACT2 (2.3.3; Figure 3.4A). In addition, their C-terminal 30 aa residues that contained the PTS1s were similarly fused in pACT2. In parallel, the CDS encoding full-length AtPex5 or its TPR domain (i.e., aa 451 to 728) were N-terminally fused with the GAL4 DNA binding domain (BD) in the yeast expression vector, pGBKT7 (2.3.3; Figure 3.4A). Both GAL4 domain constructs are generally expressed at moderate (pACT2) to high (pGBKT7) rate in *S. cerevisiae* strain Y190 from two different (truncated) versions of the constitutive promoter of *ALCOHOL DEHYDROGENASE 1* (Clontech Protocol No. PT3024-1; Tornow and Santangelo, 1990; Ruohonen et al., 1995). After protein synthesis in the cytosol, the fusion proteins are targeted to the nucleus by nuclear localization signals located nearby the N-termini of both the GAL4 BD and AD. If the two proteins of interest interact with each other, the GAL4 TF can fully function, thereby activating the transcription of the two reporter genes, *HIS3* and *lacZ*, which encode enzymes involved in histidine biosynthesis and β-galactosidase, respectively. Thus, the double transformants producing two interacting proteins of interest are able to (i) grow on synthetic defined (SD) plates lacking Leu, Trp, and His (-LTH) and containing 3-AT (to minimize basal *HIS3* expression) and to (ii) hydrolyze X-gal, which subsequently leads to the formation of an intensively blue colored reaction product (2.11). In addition, to verify Y2H functionality and with reference to the study of Kragler et al. (1998), two positive control PTS1 peptides of humans containing

canonical PTS1s (e.g., ARL>, SRL>) were used in addition to the full-length Arabidopsis macrophage migration inhibitory factor 1 (MIF1, SKL>) and its C-terminal decapeptide (Munder, 2017, 2020). As non-interacting negative controls two previously used non-PTS1 peptides were used (Kragler et al., 1998).

In transformed yeast cells and in the absence of cargo PTS1s, the full-length AtPex5 but not the TPR domain alone caused auto-activation of transcription of the reporter genes (data not shown), as reported previously (Kragler et al., 1998). Hence, the subsequent Y2H analyses focused on usage of the TPR domain only (Figure 3.4). Indeed, the TPR(AtPex5) domain interacted strongly with full-length MIF1 (Figure 3.4B). The C-terminal decapeptide of MIF1 (SKL>) also bound strongly to TPR(AtPex5) (Figure 3.4B), as did the positive control peptides (Hs27, ARL>; Hs19, SRL>; Figure 3.4B, C). As expected, the negative control peptides (Nk03, DML>; Nk02, GDA>) did not interact with TPR(AtPex5) (Figure 3.4B, C). These results confirmed correct expression and folding of TPR(AtPex5) in yeasts and that the receptor was capable of binding known PTS1 but not non-PTS1 peptides.

The LEA_2 domain of NHL4 including the predicted PTS1 domain (AKL>) indeed showed an interaction with the TPR domain of AtPex5; however, it was relatively weak, as revealed by growth analysis of yeast on -LTH SD plates (plus 3-AT) and minimal detectable β-galactosidase activity (Figure 3.4B). By contrast, the C-terminal 30-aa peptide of NHL4 interacted strongly with TPR(AtPex5) (Figure 3.4C). On the other hand, neither the PTS1 domains nor the LEA_2 domains including the predicted non-canonical PTS1 domains of NHL6 (LRL>) and NHL25 (FRL>) showed interaction with TPR(AtPex5) (Figure 3.4B, C). Their interaction could have been below the detection limit. In summary, the Y2H data further confirmed that NHL4 indeed possesses a correctly predicted PTS1 that could be recognized and bound by the TPR domain of AtPex5 *in vivo*. Hence, in addition to the subcellular targeting results, the Y2H results provided a second independent line of evidence that at least NHL4 as one member of this phylogenetic subclade of studied NHLs possesses a functional PTS1.
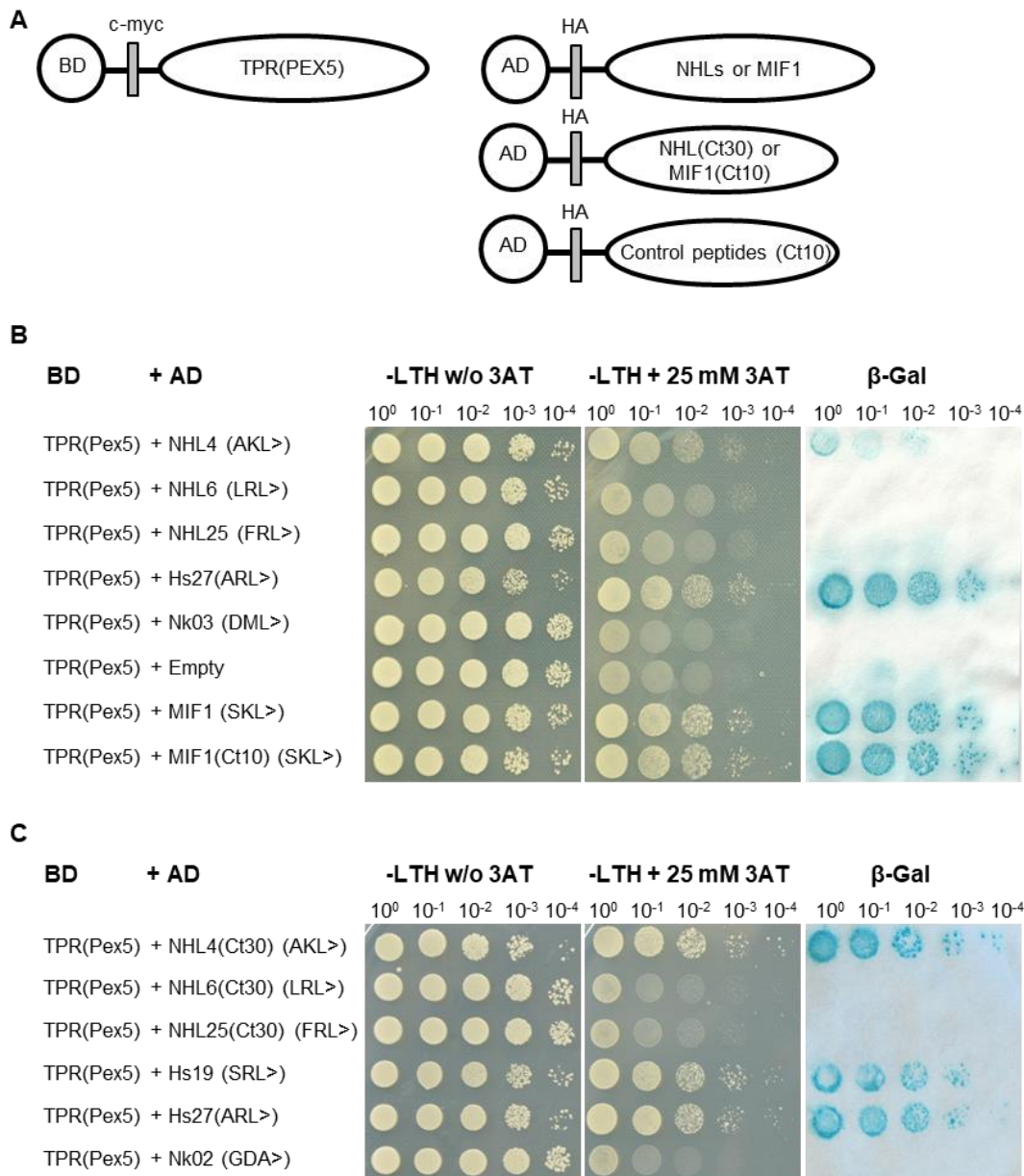
Figure 3.4: Y2H studies of NHLs with the TPR domain of AtPex5

(A) The TPR domain of AtPex5 and different proteins or peptides of interest are depicted as GAL4 BD and AD fusions in the pGBKT7 and pACT2 vectors, respectively. Interactions were investigated between the TPR domain of AtPex5 either with (B) the LEA_2 domain constructs of NHLs containing a C-terminal PTS1 (lacking the short N-terminal domain and the TMD) or with (C) the C-terminal 30 aa of NHLs. Protein-protein interactions are shown by growth of transformed *S. cerevisiae* strain Y190 on SD medium lacking Leu, Trp, and His (-LTH) and containing 25 mM 3-AT and by β-galactosidase activity, which was detected by the colony-lift filter assay. The LEA_2 domain construct with C-terminal PTS1 and the 30 aa of NHL4 alone showed interaction with TPR (AtPex5). Similar to two positive control PTS1 peptides (HS27, ARL>; Hs19, SRL>; Kragler et al. 1998), also full-length MIF1 and its C-terminal decapeptide interacted with TPR(AtPex5). There was no interaction between TPR(AtPex5) and the negative control peptides (Nk03, DML> and Nk02, GDA>). Data are representative of two independent experiments. Yeast transformants expressing only BD-TPR(AtPex5) did not show any autoactivation of reporter gene transcription. Data (B) and (C) were produced independently.

3.2.1.3 Peroxisome targeting analyses of full-length NHL4, NHL6, and NHL25

If the full-length NHL proteins could reliably and reproducibly be demonstrated to be targeted to peroxisomes as their final destinations, these membrane proteins would indicate a novel type of PMPs. Peroxisome targeting of full-length NHL4, NHL6, and NHL25 was firstly studied in single transformants. Because the PTS1 needed to be placed at the extreme C-terminus in the fusion protein and because the NHLs lacked a predicted ER signal peptide, N-terminal reporter fusions were created, as used previously (Kataya, 2011; Crappe, 2016). In single transformants overexpressing *EYFP-NHLx* alone, the EYFP fusion was detected 3 dpc in the cytosol and in strongly fluorescent puncta of varying sizes (0.2 – 1.3 µm in diameter; Figure 3.5A – C), of which the larger had the typical size of peroxisomes. Primarily in cells of high expression level, EYFP fusions were also found in aggregate-like structures (2 – 3 µm in diameter; Figure 3.5D – F). The latter observation was similar to that of other membrane proteins as they are prone to aggregation upon overexpression due to their hydrophobicity. Among the three, EYFP-NHL4 (but not EYFP-NHL6 and EYFP-NHL25) was occasionally observed in ER-like structures (Figure 3.5G).

When co-expressed with *mCer-PTS1*, primarily non-peroxisomal puncta were observed for EYFP-NHLs (Figure 3.6A – C). The targeting of EYFP-NHLs to non-peroxisomal puncta could be distinguished from the targeting to mature peroxisomes by mCer-PTS1. These non-peroxisomal puncta were reminiscent of vesicles and referred to as "vesicle-like structures". This observation were consistent with previous reports in onion epidermal cells and protoplasts (Kataya, 2011; Crappe, 2016). The reliable and reproducible detection of the three NHLs in non-peroxisomal puncta further stimulated the hypothesis that these structures could represent ER-derived vesicles and trafficking intermediates of the targeting pathway to peroxisomes. Hence, they were characterized in greater depth in terms of size, number, and mobility. First, the size of the non-peroxisomal puncta ranged 0.2 – 0.7 µm in diameter (Figures 3.5A – C and 3.6A – C). Second, the puncta labeled by EYFP-NHL4 and EYFP-NHL6 were generally very bright in fluorescence, well detectable and very high in number (> 100 per cell, data not shown; for methodology of object counting per cell, see 2.5.3). Third, the NHL4- and NHL6-labeled non-peroxisomal puncta were mobile and moved passively within the cytosol at relatively high speed due to cytoplasmic streaming. Fourth and most intriguingly, specific puncta labeled by EYFP-NHL4 and EYFP-NHL6 were occasionally detected in very close proximity to peroxisomes (Figure 3.6A, B).
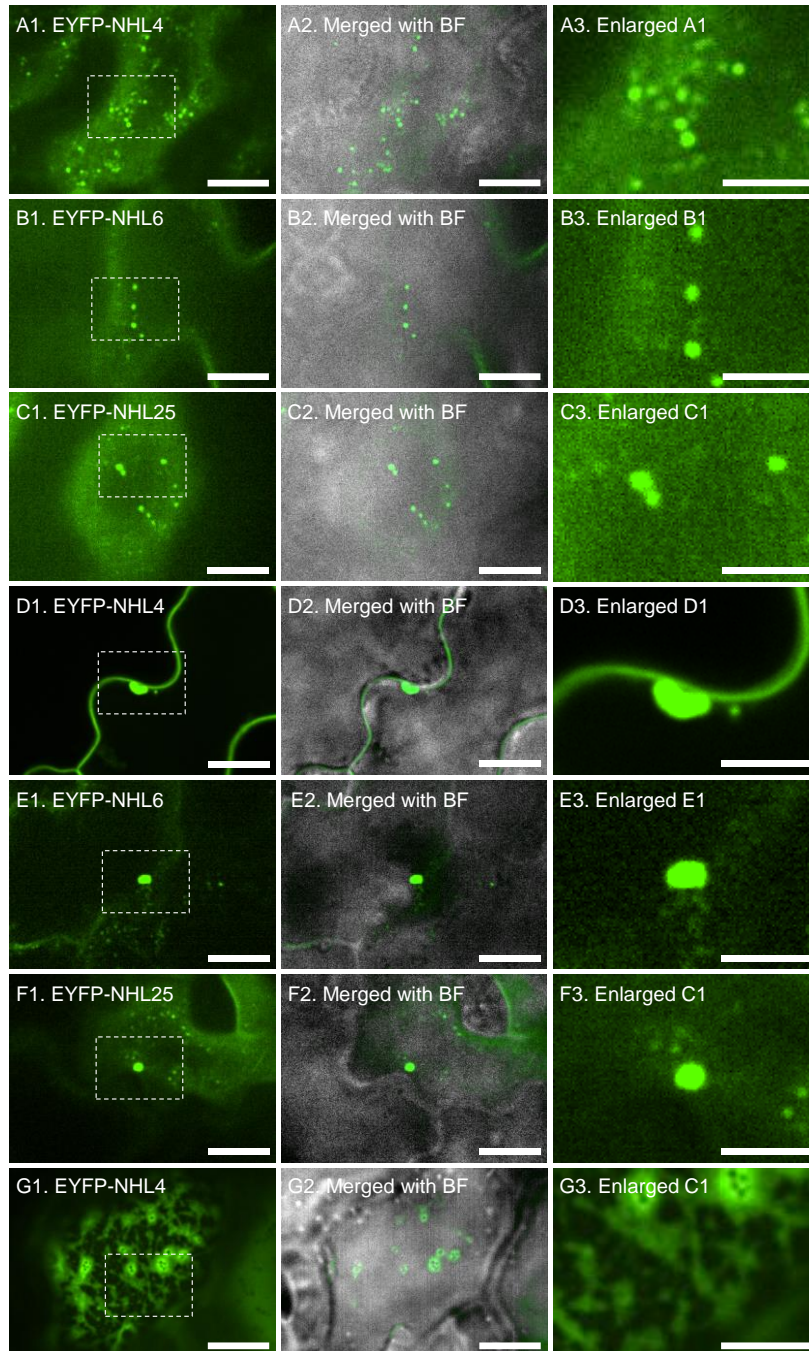
Figure 3.5: Subcellular targeting of full-length NHL4, NHL6, and NHL25 to puncta, aggregate- and ER-like structures in single transformed cells

(A – C) In single transformants of epidermal cotyledon cells, EYFP-NHLs were localized in puncta of different sizes, the larger of which were reminiscent of peroxisomes, with some cytosolic background fluorescence. (D – F) Occasionally, epidermal cotyledon cells expressing *EYFP-NHL4* (D), *EYFP-NHL6* (E), or *EYFP-NHL25* (F) alone 3 dpc showed EYFP fluorescence in aggregate-like structures. (G) EYFP-NHL4 was found in ER-like structures that differed from normal cytosolic fluorescence shown in (A). Images were taken 3 dpc (A – F) and 4 dpc (G). Representative confocal images of > 3 independent experiments are shown. For information on the transformation method, scale bar, and image enlargement, see legend of Figure 3.3.

The non-peroxisomal puncta labeled by EYFP-NHL25, however, showed only weak fluorescence and were often very tiny in size close to the detection limit, preventing reliable counting. Nevertheless, the results indicated that the puncta might represent transient trafficking intermediates in the form of cargo vesicles that carry the NHL proteins from the ER to peroxisomes. Such a pathway had previously been postulated for peroxisomes of fungi, animals, and plants but transient vesicles had hardly been documented in any model organism (1.1.4).
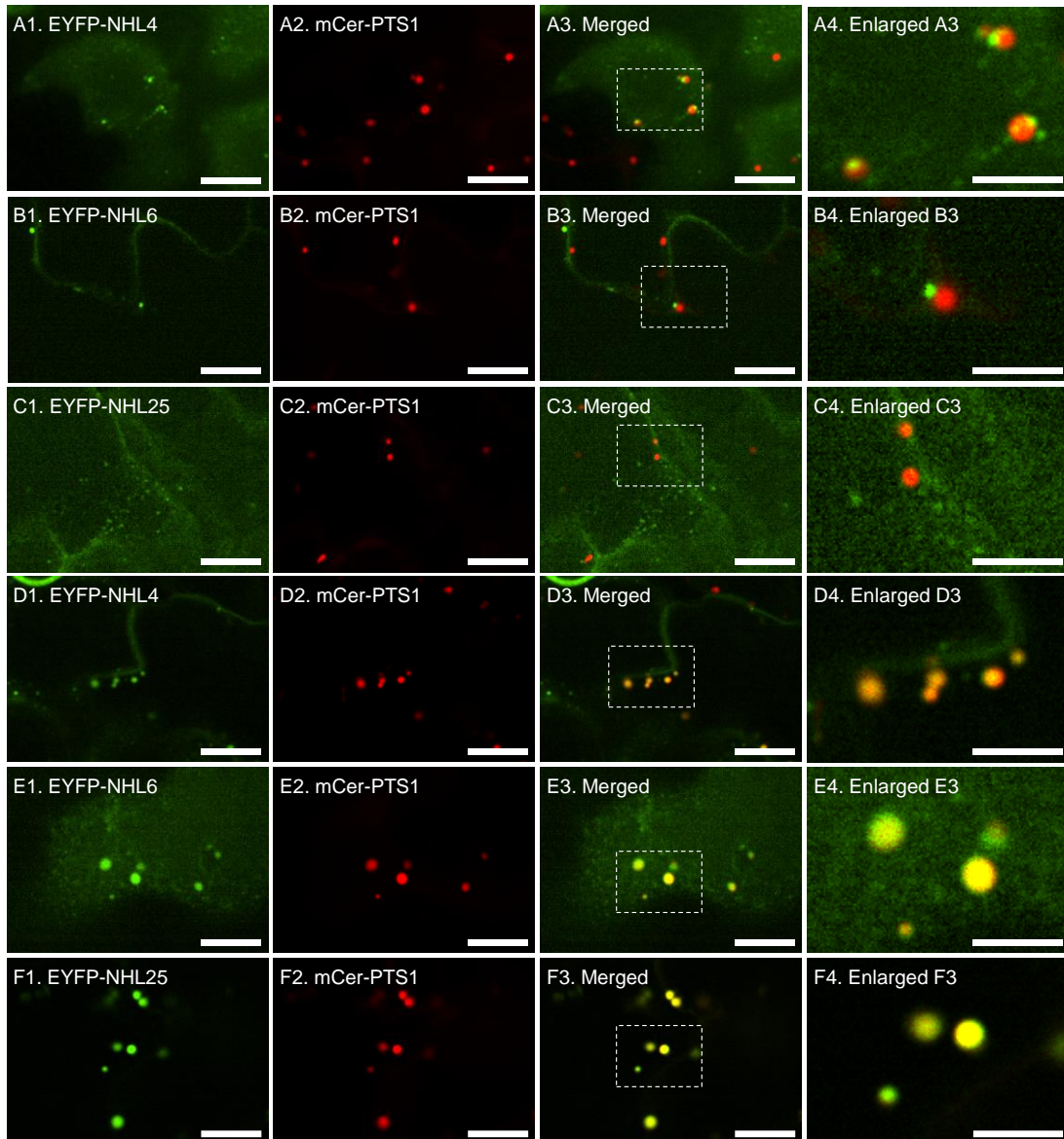
Figure 3.6: *In vivo* subcellular targeting of the three NHLs to peroxisomes and non-peroxisomal puncta in double transformed cells

EYFP was observed in non-peroxisomal puncta in double transformed cells co-expressing (A) *EYFP-NHL4*, (B) *EYFP-NHL6*, or (C) *EYFP-NHL25* together with *mCer-PTS1* 2 dpc. Close physical association of NHL4- and NHL6-labeled puncta with peroxisomes is shown but was not observed for NHL25, possibly due to

weaker fluorescence. (D – F) In several double transformed cells co-expressing *EYFP-NHLs* and *mCer-PTS1,* peroxisome targeting was observed for (D) NHL4, (E) NHL6, and (F) NHL25 3 dpc, shown in yellow in merged images. Images are representative for > 3 independent experiments. Four-day-old seedlings were transiently transformed by co-cultivation with *Agrobacterium*. The white dashed boxes indicate regions selected for enlargement. Scale bar = 10 µm (5 µm for enlarged region).

Moreover, in several double transformed cells co-expressing *mCer-PTS1,* the yellow fluorescent fusion proteins (EYFP-NHL4/6/25) indeed coincided with mCer-PTS1 labeled peroxisomes, which had a size of approx. 0.7 – 1.7 µm in diameter (Figure 3.6D – F). The negative control of untagged EYFP analyzed in parallel remained exclusively in the cytosol (and nucleus) when co-expressed with *mCer-PTS1*, demonstrating that peroxisome targeting of EYFP-NHL4/6/25 was reliably interpreted. When EYFP was exchanged against the fully monomeric Venus (3.1), peroxisome targeting was reproduced for NHL6 and NHL25 3 dpc (Suppl. Figure 1). Only peroxisome targeting of NHL4 could not be confirmed for the mVenus reporter protein due to technical problems. Targeting to non-peroxisomal puncta could be observed also for mVenus-NHL fusions (NHL4, Suppl. Figure 1; NHL6 and NHL25, data not shown). By contrast, targeting of NHLs to aggregate-like structures was not detectable for mVenus fusions. However, mVenus fluorescence was much weaker compared to EYFP for unknown reasons and only few double transformed cells were detectable, limiting subcellular localization analyses of the mVenus fusions. Thus, all three full-length NHLs were reproducibly targeted to peroxisomes in transiently transformed Arabidopsis seedlings as EYFP and/or mVenus fusions. Their peroxisomal targeting at slightly later expression time points compared to mCer-PTS1 was fully consistent with a more complex trafficking pathway and peroxisomes as the proteins' final destination.

Unlike the C-terminal 10-aa NHL reporter fusions, all of which were targeted to peroxisomes with high efficiency (3.2.1.1), the three full-length NHLs differed in their targeting speed to peroxisomes. NHL25 started localizing to peroxisomes relatively early (2 dpc), with approx. 5% of double transformed cells showing peroxisome targeting (data not shown). By contrast, at the same time point of expression NHL4 and NHL6 were not yet observed in peroxisomes but only in small non-peroxisomal puncta (Figure 3.6). To investigate the different efficiency in peroxisome targeting of the three NHLs, a quantitative analysis of the peroxisome targeting efficiency of each NHL was carried out at different time points of expression or co-cultivation (Figure 3.7). For NHL25, peroxisome targeting increased from approx. 5% (2 dpc) to 20% (3 dpc) and further to 34% (4 dpc) in double transformed epidermal cells, before

71

decreasing slightly to 25% (5 dpc). For EYFP-NHL6, the percentage of double transformed cells with detectable peroxisome targeting showed a similar trend in terms of an increase over time (e.g., approx. 3% after 3 d, 12% after 4 d, and 27% after 5 d). For EYFP-NHL4, however, peroxisome targeting could only be detected in approx. 5 – 10% of cells independent of the expression time and, hence, was too low to allow significant differences to be resolved. Taken together, the subcellular targeting data for full-length NHL4, NHL6, and NHL25 strongly indicated that peroxisomes are the final destination and vesicles are a transient stage.
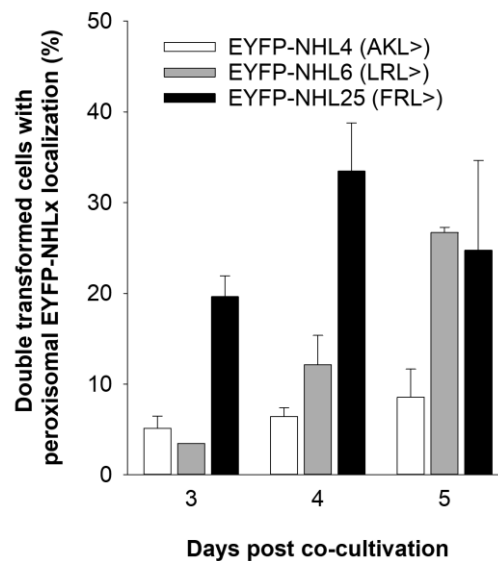
Figure 3.7: Quantitative analysis of transiently double-transformed Arabidopsis cells showing peroxisome targeting of EYFP-NHL4, NHL6, and NHL25

To calculate the percentage of double transformed cells showing peroxisomal localization of EYFP-NHLs, cells of one cotyledon co-expressing *EYFP-NHLs* and *mCer-PTS1* were analyzed (at least total ≥ 20 cells 3 dpc and ≥ 100 cells 4 and 5 dpc). Error bars represent the standard deviation for the mean values calculated for three different cotyledons in one experiment. Data were reproduced in a second independent experiment.

In comparison to the quick peroxisome targeting of the C-terminal 10 aa of the three NHLs (3.2.1.1) and of soluble matrix proteins (Skoulding et al., 2015), the peroxisome targeting efficiency of full-length NHLs in nearly all transformed cells was lower (i.e., after longer expression time) and only detectable in few epidermal cells. Both predominant NHL targeting to puncta, reminiscent of vesicle-like structures at very early expression times, and progress-

sively increasing peroxisome targeting with longer expression time indicated a multi-step vesicular biogenesis pathway *via* vesicle-like structures to peroxisomes.

3.2.1.4 Characterization of the non-peroxisomal vesicle-like structures labeled by EYFP-NHLx and their peroxisome association

Because the EYFP-NHL4 labeled puncta were most numerous and best to visualize, they were used representatively to verify the hypothesized vesicle attachment to peroxisomes. In general, puncta labeled by EYFP-NHL4 were mobile. If the puncta were attached to peroxisomes, they were expected to move together with peroxisomes in a coordinated manner. The movement of two selected peroxisomes, each of them with one EYFP-NHL4 labeled vesicle-like structure in close proximity, was analyzed over time in a single confocal plane extracted from a time-lapse video (Figure 3.8).
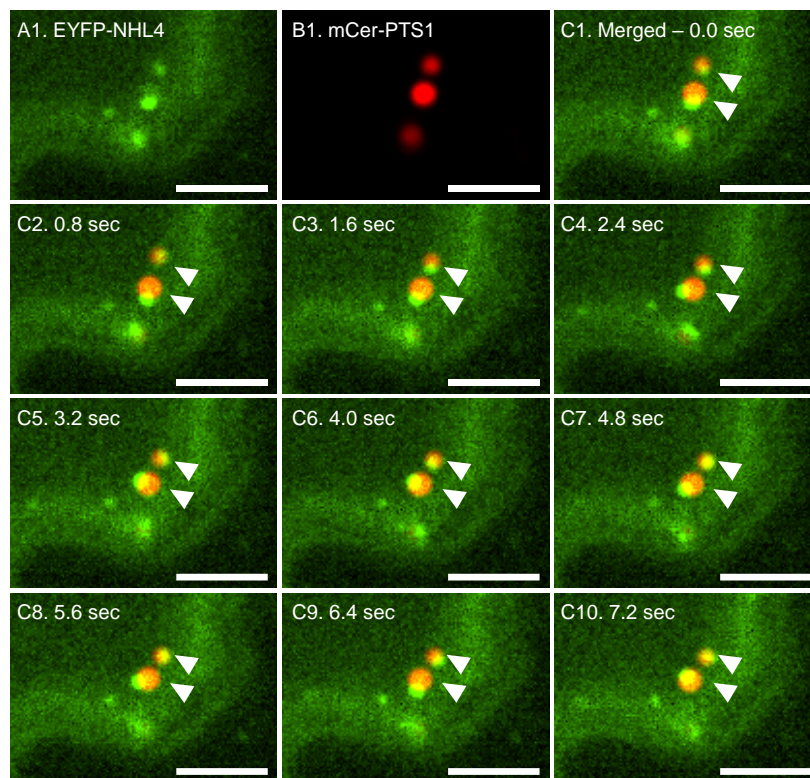
Figure 3.8: Documentation of the physical attachment between EYFP-NHL4 labeled vesicle-like structures with peroxisomes by time-lapse video

Four-day-old seedlings were transiently transformed by co-cultivation with *Agrobacterium*. The confocal images of epidermal cotyledon cells showed (A, B, C1) NHL4 localization in vesicle-like structures in close proximity to peroxisomes, and (C2 – C10) the coordinated joint movement of these structures together with the neighboring peroxisome. A single confocal plane was retrieved from a time-lapse video. The time-lapse video was taken 3 dpc and is representative for > 3 independent experiments. Peroxisomes were labeled with mCer-PTS1, converted to red for co-localization studies. Arrows indicate the vesicle-

like structure localization at the start (C1) and remained in constant place to visualize their lateral movement. Scale bar = 5 μm.

The rotation of both peroxisomes could only be seen in the time lapse video but not in Figure 3.8. Despite detectable peroxisome rotation, each of the vesicle-like structures located in close proximity to one mature peroxisome stayed next to the same peroxisome, as shown for a time span of 7 sec (n > 3). This coordinated movement occurred also over a longer time period (i.e., 47 sec, n > 3, data not shown). The data documented a physical association between a subset of NHL4-labeled vesicle-like structures and peroxisomes *in vivo* and was referred to as "docking structures". This result implied that the vesicle-like structures were attached and docking to peroxisomes possibly prior to fusion with the peroxisomal membrane, supporting the hypothesis (3.2.1.3) that NHL4 (and most likely also NHL6 and NHL25) traffics to peroxisomes through carrier vesicles.

To determine whether the vesicle-like structures observed by confocal microscopy were indeed vesicles, i.e. were surrounded by a bilayer membrane, the same transiently transformed Arabidopsis seedlings were analyzed by TEM. Moreover, peroxisome targeting as well as the vesicle-like structure association with mature peroxisomes were intended to be verified by TEM, as a second line of evidence. To this end, Arabidopsis seedlings were co-cultivated with *Agrobacterium* carrying the binary vector pBA002 with or without *EYFP-NHL* cassette (as a negative control), harvested after 3 – 5 days, and the seedlings were fixed in paraformaldehyde and glutaraldehyde (2.6.1). The tissue was either labeled by the primary polyclonal anti-GFP antibody to detect EYFP-NHLs or analyzed without immunogold labeling. The principle of immunogold labeling is that the primary antibody binds to target proteins, and the secondary antibody conjugated with 10-nm gold particles is detected by TEM (2.6.1). The dilution of the primary polyclonal anti-GFP antibody (Abcam, Cat. Ab290) was initially 1:400, however, this dilution showed much unspecific labeling in the WT sample (data not shown). Thus, to determine the best concentration lacking unspecific EYFP detection in WT seedlings, the lower concentrations were tested, i.e. 1:800, 1:1,000, and 1:1,500. With increasing dilution of the primary antibody, unspecific gold labeling was indeed reduced. Nevertheless, even at the highest dilution of 1:1,500 of primary antibody, chloroplasts, mitochondria, ER, and peroxisomes still remained labeled unspecifically by 1 – 2 gold particles per organelle in nearly each cell of WT seedlings (Suppl. Figure 2). In addition, no strong labeling of vesicles or peroxisomes by gold particles was observed even when using seedlings overexpressing *EYFP-*

NHLs, indicating that the EYFP fusions could possibly be degraded during sample processing for TEM. Hence, subcellular targeting of EYFP-NHLs could not be analyzed by immunogold labeling combined with TEM.

To overcome the problem of unspecific binding and to investigate whether overexpression of EYFP-NHLs led to any differences in ultrastructure, TEM was performed without immunogold labeling. In the fixation step a higher concentration of osmium tetroxide was used, i.e. 1% vs. 0.25%, and glutaraldehyde was added at 2% (2.6.2). Glutaraldehyde and osmium tetroxide react with amino groups of proteins and lipids, respectively, and thereby protein and phospholipid containing structures such as membranes become more visible in TEM. However, this fixation step could cause unsuccessful binding of primary antibodies to membranes.

The transformants (overexpressing *EYFP-NHLs*) and WT control (see above) harvested at 5 dpc were fixed, dehydrated, infiltrated with Spurr resin, and sectioned prior to observation by TEM without immunogold labeling (Figure 3.9). Interestingly, numerous single vesicles and clustered vesicles were observed in the cytosol of mesophyll cells of seedlings overexpressing *EYFP-NHL4* (Figure 3.9A). These vesicles in clusters had high protein content (black labeled) and were surrounded with a membrane (Figure 3.9A2). They were found not only in mesophyll cells but also in epidermal cells (data not shown). Such high number of vesicles was detected in 10 cells out of hundreds of cells (approx. 300 – 600 cells) in the observed TEM sections (n = 2 sections), thus in approx. 2 – 5 % of cells. The vesicles had a size of 0.1 – 0.2 μm in diameter, and the vesicle clusters ranged from 1.5 to 3 μm in diameter. By contrast, similar vesicle clusters were not detected in many screened sections of the WT control. Even though single small vesicles were occasionally also detected in the WT control, the clusters of 20 to 100 vesicles in transformed seedlings were never observed when approx. 500 different cells were analyzed (n = 10 sections) (Figure 3.9B). Therefore, the data indicated that those vesicles are specific to *EYFP-NHL4* overexpression. Like *EYFP-NHL4*, the same vesicle clusters were also observed for seedlings overexpressing either *EYFP-NHL6* or *EYFP-NHL25* alone (Suppl. Figure 3). In conclusion, the vesicle clusters detected by TEM specifically in transiently transformed *EYFP-NHLx* seedlings might correspond to the strongly fluorescent aggregate-like structures labeled by EYFP-NHLs that had been observed occasionally in some cells by confocal microscopy (approx. 2 – 3 μm; Figure 3.5D – F). Furthermore, the phenome-

non of vesicle clustering was possibly a consequence of the overexpression of the *NHLs*, as reported previously for other membrane proteins.
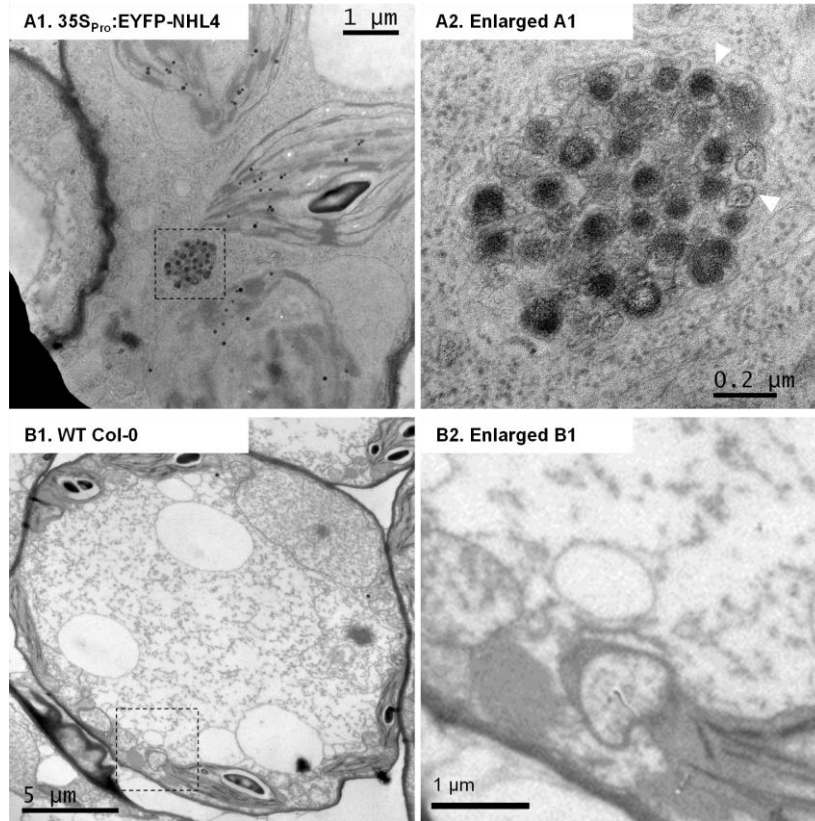
Figure 3.9: TEM analyses of vesicle clustering in transiently transformed Arabidopsis seedlings

Four-day-old seedlings were transiently transformed by co-cultivation with *Agrobacterium*. Cotyledons of Arabidopsis seedlings harvested at 5 dpc were subjected to chemical fixation (2% glutaraldehyde and 1% osmium tetroxide), dehydration, and infiltration with Spurr resin. Samples were then embedded in a silicone mold, sectioned, and subsequently analyzed by TEM (2.6.2). Proteins and lipids were stained with glutaraldehyde and osmium tetroxide, respectively. In few mesophyll cells of cotyledons of transiently transformed Arabidopsis seedlings overexpressing *EYFP-NHL4*, clusters of vesicles were found (A) but not in (B) WT control. The images are representative of hundreds of cells analyzed, and approx. 10 cells showed the clusters (obtained from two sections). Arrows indicate vesicles surrounded with a well visible membrane. The sample fixation, embedding, sectioning, and TEM were performed with technical assistance by Ms. Elke Woelken (University of Hamburg, Hamburg, Germany).

3.2.1.5   Analysis of NHLx targeting to the ER and to ER-derived vesicles

To investigate whether (i) NHL4, NHL6, and NHL25 are targeted first transiently to the ER, as reported for class II PMPs on their trafficking route to peroxisomes, and (ii) whether the NHL-labeled vesicle-like structures originated from the ER and partially co-localized with the ER-

derived vesicles, the ER marker, Wak2-CFP-HDEL referred to as ER-CFP, was used (2.3.2; Nelson et al., 2007). In this construct, CFP is extended N- and C-terminally with the ER signal peptide of AtWak2 and the protein's ER retention signal, respectively (He et al., 1999). Indeed, the ER marker labeled the typical fine ER network made of tubules and cisternae (Figure 3.10C2). This ER pattern was very distinct from the cytosolic fluorescence of untagged EYFP (Figure 3.10G – H, compare G1 with G2). Additionally, the ER marker labeled another ER-derived structure, known as the ER body (approx. 5 µm in length and 1 µm in width), which was prominent particularly in epidermal cotyledon cells (Figure 3.10C2, E2), as reported earlier (Matsushima et al., 2003). Most importantly, the ER marker also occasionally labeled small puncta of unknown identity (0.2 – 0.5 µm in size, approx. 50 – 100 per cell), referred to as "ER-derived vesicles", that appeared to be associated with the ER tubules (Figure 3.10D2, F2) and moved together with the ER due to cytoplasmic streaming (data not shown). The detection of small vesicles labeled by the ER marker allowed addressing the question whether NHL-labeled vesicle-like structures co-localized with ER vesicles, thereby providing evidence for their ER origin.

Next, the kinetics of ER localization of NHL4, NHL6, and NHL25 were investigated (2 – 4 dpc). Although numerous double transformed cells were well visible at later time points (e.g., 4 dpc), only few cells displayed co-localization of EYFP-NHL4 with the ER marker, namely in the perinuclear ER (Figure 3.10A, B), but this was not detected for EYFP-NHL6 and EYFP-NHL25 (data not shown). None of the EYFP-NHL fusions could be found in the tubular and cisternal ER of either epidermal or mesophyll cells (Figure 3.10C – F; data not shown for NHL6 and NHL25). Notably, and as shown in single transformed cells (Figure 3.5G), EYFP-NHL4 could indeed be observed in ER-like structures but for unknown reasons its fluorescence was weak and rapidly vanished. Similarly, in double transformed cells, the signal of EYFP-NHL4 in the ER was not sufficiently stable to allow the ER co-localization studies. However, perinuclear ER targeting of EYFP-NHL4 could occasionally and briefly be detected, but its fluorescence started declining after 3 sec, thereby increasing cytosolic fluorescence (Figure 3.10A, B). The data indicated a very weak and rapid removal of EYFP-NHL4 from the perinuclear ER.
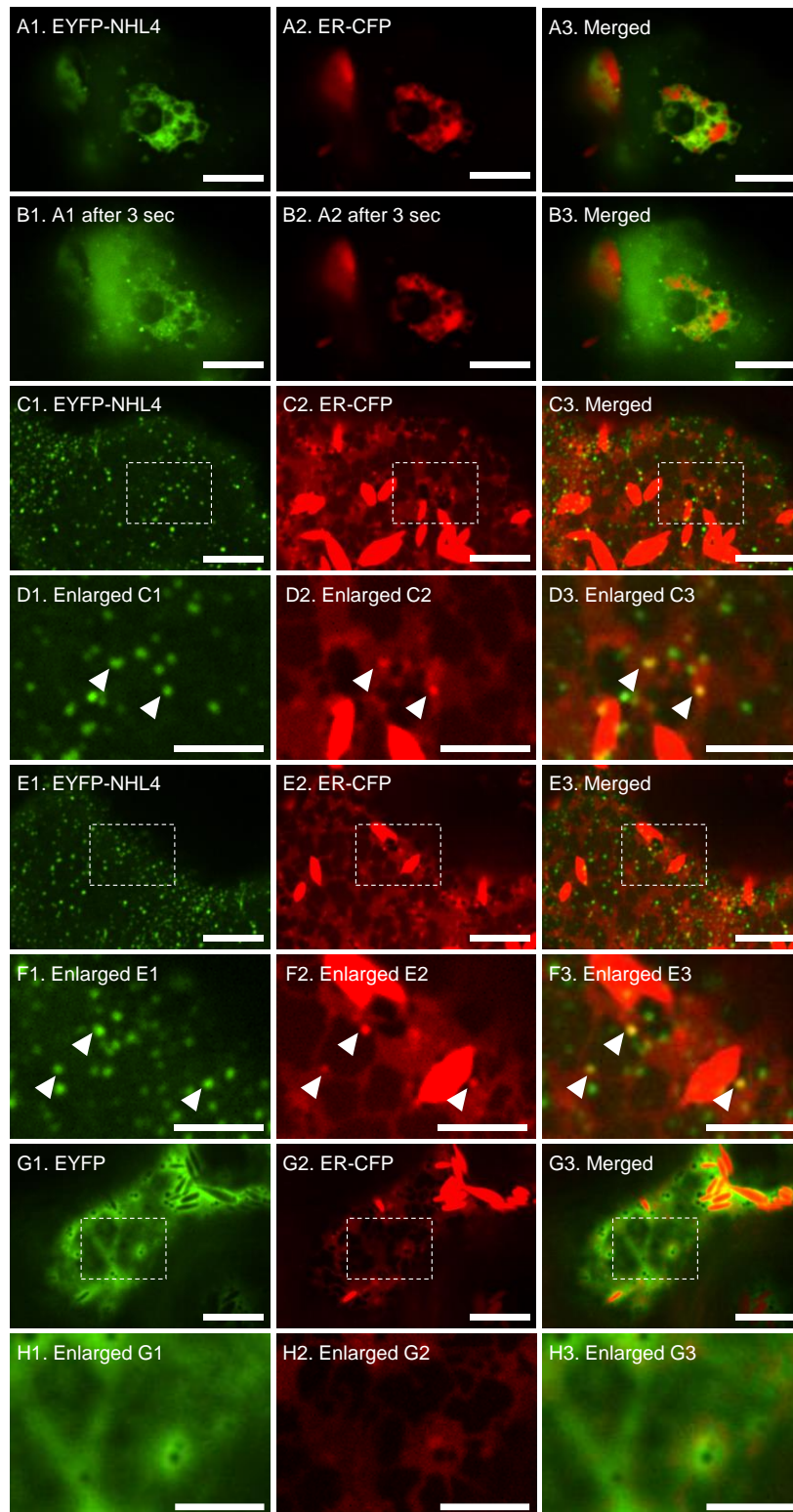
Figure 3.10: ER targeting analyses of EYFP-NHL4 and co-localization of a sub-population of the EYFP-NHL4 labeled vesicle-like structures with ER-derived vesicles

Four-day-old seedlings were transiently transformed by co-cultivation with *Agrobacterium*. (A) Perinuclear ER targeting of EYFP-NHL4 was detected by fast image acquisition. (B) The EYFP fluorescence

started to become diffuse in the cytosol. Arrows indicate (C – F) co-localization of NHL4 in ER-derived vesicles. (G – H) The typical cytosolic fluorescence of untagged EYFP was distinct from that of CFP labeling the ER. Confocal images of epidermal cotyledon cells co-expressing (A – F) *EYFP-NHL4* or (G – H) *EYFP* with *ER-CFP* 3 dpc (A – B) and 4 dpc (C – H) are shown. Images are representative for two independent experiments. CFP fluorescence was converted to red. To better visualize the ER network, which was often very dim, the fluorescence of the ER bodies was visualized oversaturated. Scale bar = 10 µm (5 µm for enlarged regions).

On the other hand, strong cellular fluorescence of EYFP-NHL4 found in puncta and having more double transformed cells at later time point of expression allowed vesicle co-localization analyses. In a few epidermal cells co-expressing *ER-CFP* and *EYFP-NHL4* and showing vesicles labeled by the ER marker, few of the large population of NHL4-labeled vesicle-like structures indeed coincided with some of the CFP-labeled ER-derived vesicles (approx. < 0.5 µm in diameter; Figure 3.10C – F). It needs to be pointed out that this co-localization of vesicles was rarely seen (in approx. < 2% of double transformed cells) due to a very low number of transformed cells showing these CFP-labeled ER vesicles. With these cells, the efficiency of EYFP-NHL4 targeting to ER-derived vesicles was determined by the percentage of vesicles with co-localization. In a double transformed cell, 18 out of 380 NHL4-labeled vesicle-like structures (i.e., approx. 5%) co-localized with the ER-derived vesicles. With respect to 102 ER-derived vesicles detected in that cell, 18% coincided with the NHL4-labeled vesicle-like structures. This low efficiency of EYFP-NHL4 targeting to the ER-derived vesicles was reproduced in the second cell. Nevertheless, the low number of tested cells was not appropriate for statistical analysis. However, the results showed that a sub-population of EYFP-NHL4 labeled vesicle-like structures indeed coincided with ER-derived vesicles labeled by ER-CFP. In conclusion, the data indicated (i) the identity of these vesicle-like structures with ER-derived vesicles and (ii) their origin from the ER.

3.2.1.6 NHL4 and NHL6 targeting to the same kind of vesicle-like structures

The high homology between Arabidopsis NHL4, NHL6, and NHL25 in one phylogenetic sub-clade (1.4.3) and the detection of their EYFP fusions in very similar non-peroxisomal vesicle-like structures suggested that these unknown structures might be identical. Indeed, EYFP-NHL25 was found to fully co-localize with CFP-NHL4 in the same kind of non-peroxisomal puncta in onion epidermal cells, the system in which the peroxisome targeting had not been observed for the three NHLs (Kataya, 2011). In the same study, EYFP-NHL6 and CFP-NHL4 had been found to partially co-localize in non-peroxisomal puncta. The observations of co-localization between NHLs in the same non-peroxisomal puncta were also reported when using

Arabidopsis protoplasts (Crappe, 2016). To investigate the identity of the vesicle-like structures in Arabidopsis seedlings, NHL4 and NHL25 were N-terminally fused with mCherry to allow co-localization analyses among the three NHLs by epifluorescence microscopy. Although the emission spectra of EYFP and mCherry partially overlap, the fluorophores could be specifically detected by usage of appropriate filters (EYFP: EM535/30 nm; mCherry: 630/75 nm; Suppl. Figure 4).

Similar to EYFP-NHL4, mCherry-NHL4 was also detected in the cytosol and in mobile puncta. Upon co-expression with *EYFP-NHL6*, the red fluorescent puncta indeed coincided with those labeled by EYFP-NHL6 (Figure 3.11). Because both proteins were known to be targeted to peroxisomes as their final destination, it had to be ascertained that these puncta were not peroxisomes. Notably, both NHL4 and NHL6 were generally not yet targeted to peroxisomes at this very early time point of expression, i.e. 2 dpc (3.2.1.3; Figure 3.6A, B). Additionally, these puncta labeled by NHL4 and NHL6 were with 0.2 to 0.5 µm significantly smaller than the typical size of peroxisomes (approx. 0.7 – 1.7 µm), supporting the idea that both NHL4 and NHL6 were targeted to the same non-peroxisomal vesicle-like structures on their trafficking route to peroxisomes. As mCherry-NHL25 was hardly detectable by both epifluorescence and confocal microscopy, co-localization analyses were impossible for these fusion proteins. Fluorophore exchange between NHL4/NHL6 and NHL25 did not solve the problem. Nevertheless, the data indicated that NHL4 and NHL6 are recruited to the same type of vesicle-like structures and might share the same vesicular trafficking pathway from the ER to peroxisomes.
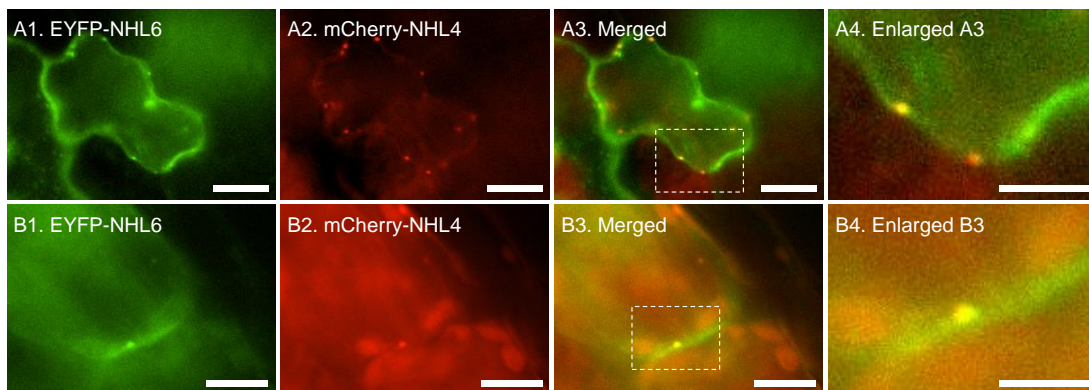
Figure 3.11: Co-localization analyses of EYFP-NHL6 and mCherry-NHL4 in vesicle-like structures

The epifluorescent images of epidermal cotyledon cells (A) 2 dpc and (B) 3 dpc with *Agrobacterium* show co-localization of EYFP-NHL6 and mCherry-NHL4 in vesicle-like structures. Images are representative for two independent experiments. Scale bar = 10 µm (5 µm for enlarged regions).

3.2.2 Characterization of a second PTS in NHL25 in transient transformed Arabidopsis seedlings

All three NHLs possessed functional PTS1 domains that were sufficient to direct EYFP to peroxisomes (3.2.1.1; Figure 3.3), but the peroxisome targeting efficiency of full-length NHLs was relatively slow, consistent with a complex vesicular pathway (3.2.1.3; Figure 3.7). The data suggested that peroxisome targeting of the NHLs did not solely depend on their PTS1s and that another signal, predicted to be located close to the TMD, was the major signal influencing the peroxisome targeting efficiency. Among the three NHL proteins, NHL25 was targeted to peroxisomes most quickly and efficiently with approx. 34% of the cells showing peroxisome targeting 4 dpc (3.2.1.3; Figure 3.7). Therefore, NHL25 was used, representatively for NHL4 and NHL6, to study the contribution of the PTS1 to peroxisome targeting, which could possibly be determined by its deletion. Hence, several deletion constructs of NHL25 were made in order (i) to verify the function of the PTS1 in directing NHL25 to peroxisomes and address whether the TMD possessed another signal for peroxisome targeting, (ii) to investigate whether the replacement of the non-canonical PTS1 (FRL>) of NHL25 to a canonical one (SRL>) could enhance peroxisome targeting, and (iii) to identify the second PTS likely needed for peroxiso-mal localization of NHL25 (Figure 3.12A). The predicted TMD of NHL25 (by TMHMM 2.0; aa 66 – 86) was extended at both sides by 20 aa to include possible neighboring targeting signals (i.e., aa 46 – 106; 2.7.2). The mutated and deletion constructs of *NHL25* were N-terminally fused with EYFP and expressed individually with *mCer-PTS1*.

First, upon of PTS1 deletion (EYFP-NHL25ΔPTS1), EYFP fluorescence was observed in the cytosol and weakly in puncta (data not shown), similar to full-length NHL25 (3.2.1.3; Figure 3.5C). However, the number of cells with peroxisomal localization dropped significantly from approx. 26% and 14% for full-length NHL25 3 and 4 dpc, respectively, to less than 8% (Figure 3.12B), further confirming the involvement of the PTS1 in peroxisome targeting of NHL25. By contrast, the replacement of the non-canonical PTS1 (FRL>) of NHL25 with the canonical tripeptide (SRL>) did not detectably enhance peroxisome targeting of NHL25. NHL25(SRL>) targeted EYFP to the cytosol and puncta with weakly detectable fluorescence (data not shown), and did not show significantly enhanced peroxisome targeting, approx. 24% (3 dpc), very similar as that of unmutated NHL25 (3 d: 26%) (Figure 3.12B). The data demonstrated that the non-canonical PTS1 (FRL>) of NHL25 indeed had an important function *in vivo* in peroxisome targeting. The data also raised a further question which signal other than

the PTS1 still targeted EYFP to peroxisomes in the PTS1 deletion construct. When shortening NHL25 to its TMD (aa 66 – 86) and the neighboring 20-aa peptides, peroxisome targeting was significantly reduced to approx. 2% 3 dpc (11 out of 480 double transformed cells) and to approx. 4% 4 dpc (18 out of 456 double transformed cells) compared to WT NHL25 (Figure 3.12B). Nevertheless, peroxisome targeting was still detectable. The results indicated that this TMD of NHL25 likely contains an additional PTS in addition to the predominant PTS1.
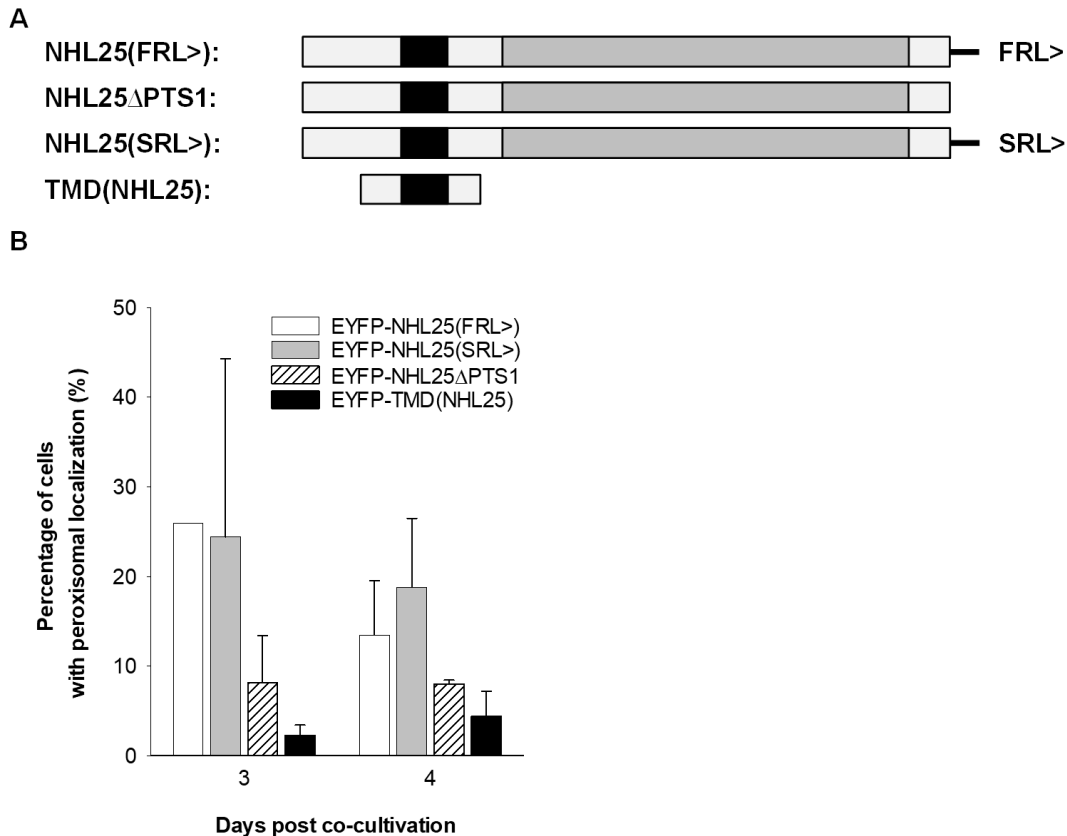
Figure 3.12: Quantitative analyses of peroxisome targeting of mutated and deletion constructs of NHL25

(A) Construct overview of truncated and mutated NHL25 and (B) quantitative analysis of peroxisomal localization of the respective proteins in double transformed cells of Arabidopsis seedlings. The percentage of epidermal cotyledon cells with peroxisomal localization was determined for NHL25(FRL>) (26% for 3 dpc; 14% for 4 dpc), NHL25(SRL>) (24% for 3 dpc; 19% for 4 dpc), NHL25ΔPTS1 (8% for 3 dpc; 8% for 4 dpc), and TMD(NHL25) (2% for 3 dpc; 4% for 4 dpc). Cells in one cotyledon co-expressing full-length *NHL25* (n = 25 for 3 dpc; n = 100 – 200 for 4 dpc), mutated or deletion constructs of *NHL25* together with *mCer-PTS1* (n = 50 – 200, 3 and 4 dpc) were counted to calculate the percentage of cells showing peroxisomal NHL25 localization. Error bars represent the standard deviation of three cotyledons in one experiment. Data are representative for two independent experiments.

Interestingly, in many cells expressing *EYFP-TMD(NHL25)* alone (Figure 3.13A, B) or with *mCer-PTS1* (data not shown), EYFP was detected in three compartments, namely in structures resembling the ER network, ER bodies, and small vesicle-like structures (approx. 0.5 µm in diameter). The latter were often in close proximity to the putative ER network (Figure 3.13B) and better visible compared to full-length NHL25 due to stronger fluorescence (data not shown). Because it was possible to clearly discriminate the ER network targeting from cytosolic fluorescence (Figure 3.10G, H), the ER targeting could be confirmed for EYFP-TMD(NHL25) even without the ER marker (Figure 3.13A, B). When co-expressed with *ER-CFP*, EYFP-TMD(NHL25) was indeed targeted to the ER and the membrane of ER bodies in epidermal cells (Figure 3.13C – F). Taken together, it was concluded that NHL25 possesses a TMD in this domain that acts as a signal anchor and directs NHL25 first to the ER, from where the protein traffics further to peroxisomes by a vesicular pathway (1.1.4). Hence, the information for NHL25 concentration at ER exist sites and for vesicle budding must be in the protein domains outside of this TMD construct. As NHL4 and NHL6 also contain a similar N-terminal TMD in this domain and belong to the same subclade with NHL25, their predicted TMDs very likely function as a signal anchor as well.
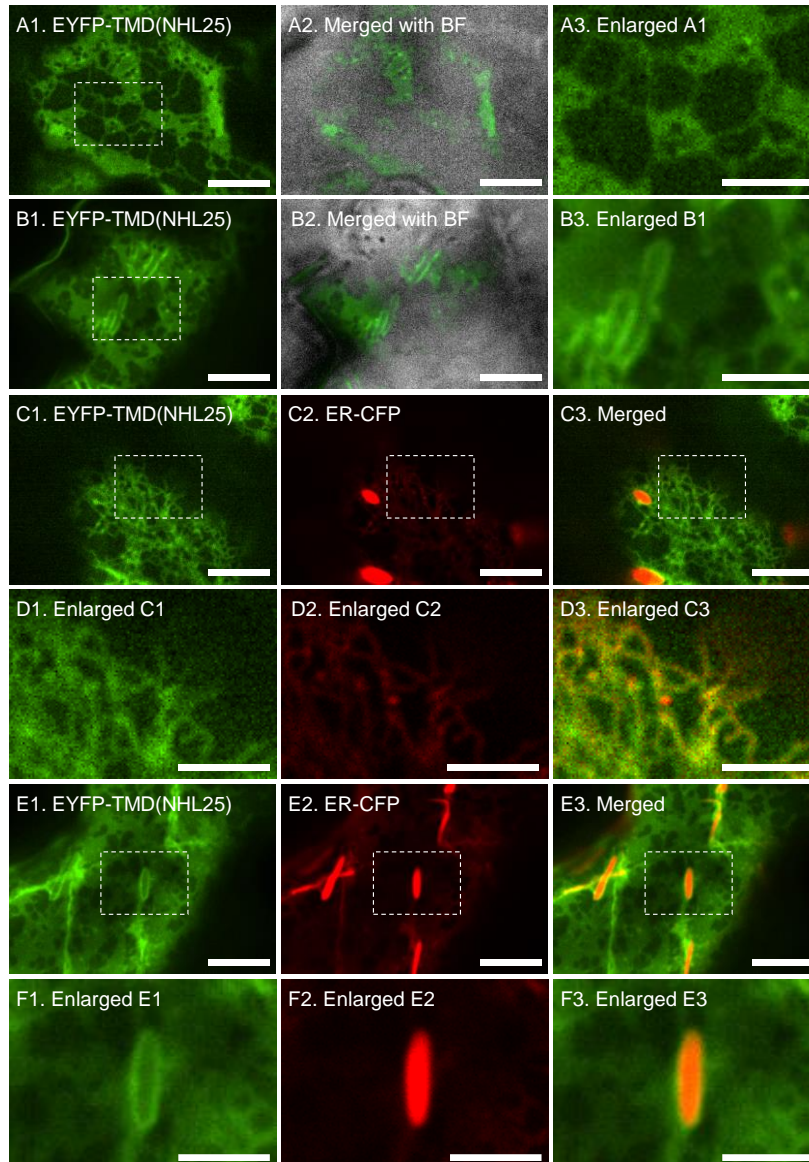
Figure 3.13: ER targeting analyses of the TMD of NHL25 in transiently transformed Arabidopsis seedlings

Four-day-old seedlings were transiently transformed by co-cultivation with *Agrobacterium*. The confocal images of epidermal cotyledon cells show (A – B) the expression of *EYFP-TMD*(*NHL25*) alone and (C – F) the co-expression of *EYFP-TMD*(*NHL25*) with the luminal ER marker (*ER-CFP*). The TMD with the neighboring 20 aa of NHL25 was localized in ER-derived structures, including (A, C, D) the ER network, (B, E, F) the membrane of ER bodies, and (B) vesicle-like structures in a physical association with the ER network. The ER body targeting was observed because this is the default pathways, further strengthening the idea that NHL25 is no longer correctly recruited to the ER exit sites where the NHL vesicles are formed. Blue fluorescence was converted to red for co-localization studies. Images were taken (A, C, D) 2 dpc and (B, E, F) 4 dpc, and are representative for two independent experiments. Scale bar = 10 µm (5 µm for enlarged regions).

3.2.3 *In vivo* subcellular localization analyses in transgenic Arabidopsis plants representatively for NHL4

To verify peroxisome targeting of NHLs detected in transiently transformed Arabidopsis seedlings (3.2.1.3), stable transgenic Arabidopsis lines overexpressing *EYFP-NHL*s from the *CaMV 35S* promoter were generated (2.3.2 and 2.4.4). Transgenic plants resistant to BASTA were screened for well detectable yellow fluorescence in mature leaves (T$_3$). For each NHL protein, approx. 30 independent overexpressor (OE) lines were screened for EYFP fluorescence. Five independent lines showed detectable EYFP fluorescence. However, none of the BASTA resistant plants transformed with EYFP-NHL6 or EYFP-NHL25 showed detectable EYFP fluorescence for unknown reasons. Next, the expression level of *NHL4* was analyzed by qRT-PCR, using the relative quantification method ($2^{-\Delta\Delta Ct}$) with *ACT2* as reference gene and the WT as a calibrator (Livak and Schmittgen, 2001). The five *EYFP-NHL4$_{OE}$* lines were screened for moderate and high *NHL4* expression levels (Suppl. Figure 5) by the M.Sc. student Muzaffer Emre Gül (University of Hamburg). *NHL4* was highly expressed up to approx. 7,000 – 520,000 fold compared to WT. Line 25 had the second lowest expression level of *NHL4* (approx. 9,600 fold), but EYFP fluorescence detected by confocal microscopy was much stronger compared to other lines (data not shown). Therefore, this line together with the line of the highest expression level of *NHL4* (line 19: 520,000 fold) were used to study the subcellular localization of NHL4.

In 5-day-old seedlings of the two *EYFP-NHL4$_{OE}$* lines, EYFP-NHL4 fluorescence was generally observed in the cytosol and puncta of various sizes, ranging from approx. 0.2 to 1.3 µm in diameter (Figure 3.14A, B). Additionally, strongly fluorescent small vesicle-like structures were captured when they started attaching to and moving toward the larger puncta (Figure 3.14A4 – A9), reminiscent of peroxisome-vesicle association, and this was observed pending for 4 sec and even longer, e.g. 12 sec for others (Figure 3.14; A4 – A9 and B1 – B3). Hence, these results were consistent with the results obtained from the transiently transformation system (3.2.1.3; Figure 3.5A), thereby further supporting their reliability in regard to the observation of small vesicle-like structures. Moreover, the results also highlighted that NHL4 was targeted to small vesicle-like structures in attachment with larger puncta and presumably peroxisomes. Thus, the data were repeatedly observed in both of transient transformation system and stable transgenic lines.
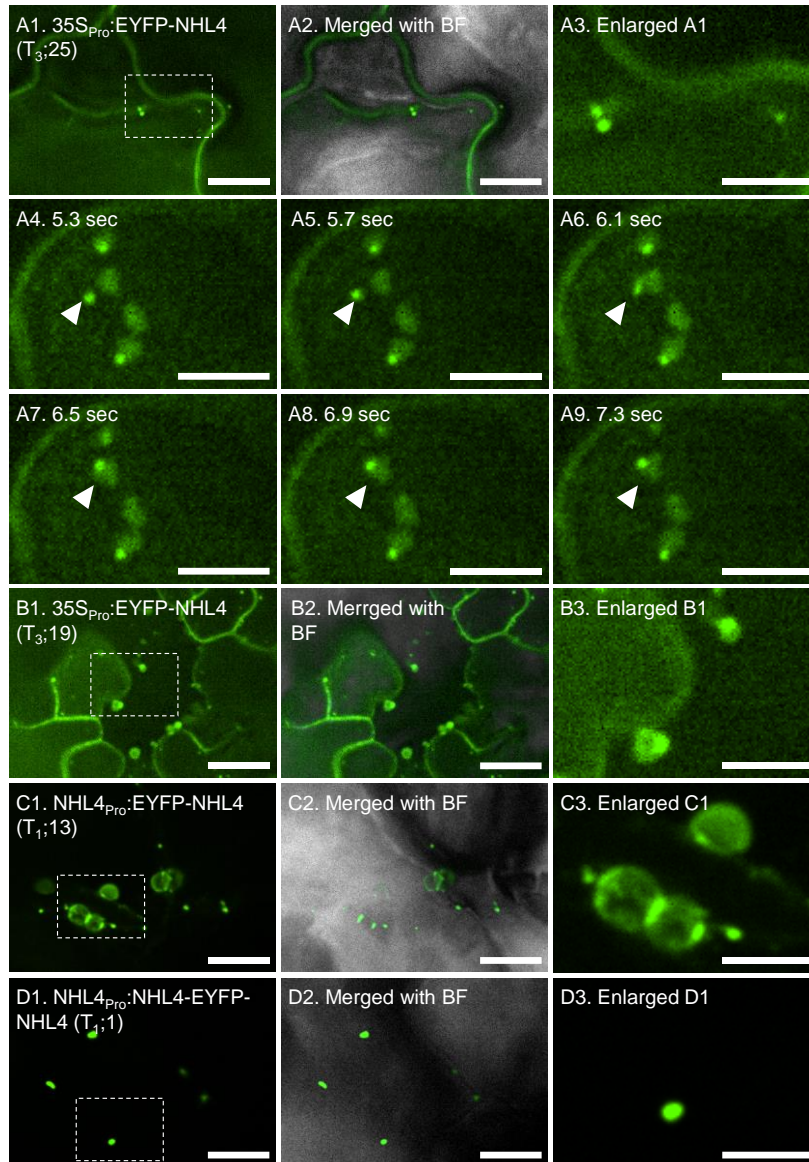
Figure 3.14: *In vivo* **subcellular localization analyses of N-terminal and internal EYFP fusions with NHL4 in stable transgenic Arabidopsis plants**

NHL4 targeted EYFP to (A, B) free puncta and puncta in association with larger spherical structures reminiscent of peroxisomes in epidermal cells of 5-day-old Arabidopsis seedlings of stable transgenic *EYFP-NHL4$_{OE}$* plants (T$_3$, line 25 and line 19). (C, D) Punctate and ring-like structures in epidermal cells of mature leaves of 6-week-old stable transgenic lines (T$_1$) expressing *EYFP-NHL4* (line 13) or *NHL4$_{(1-21)}$-EYFP-NHL4$_{(22-239)}$* (line 1) from the endogenous *NHL4* promoter. (A4 – A9) Small vesicle-like structures moved toward and along the larger structures are shown in a single confocal plane retrieved from a time-lapse video (scale bar = 5 μm). Apart from A4 – A9 images, scale bar = 10 μm (5 μm for enlarged regions).

In general, expression from the strong *CaMV 35S* promoter bears the risk of mistargeting of proteins of interest due to their high expression. To overcome this limitation, *NHL4* constructs with N-terminal (*EYFP-NHL4*) and internal fusion of EYFP (*NHL4$_{(1-21)}$-EYFP-NHL4$_{(22-239)}$*) under the control of the *NHL4* promoter were designed as part of the Master thesis conducted by Eduardo Muñoz Díaz (University of Hamburg; Díaz 2020) supervised by myself and Prof. Dr. Sigrun Reumann (University of Hamburg). To verify construct correctness and sufficient promoter activity, the EYFP fusions were transiently expressed in Arabidopsis seedlings co-cultivated with *Agrobacterium*. However, first trials were unsuccessful (Díaz, 2020). Therefore, transgenic Arabidopsis plants stably transformed with the same two constructs (*NHL4$_{Pro}$:EYFP-NHL4* or *NHL4$_{Pro}$:NHL4$_{(1-21)}$-EYFP-NHL4$_{(22-239)}$*) were generated. Due to their very low constitutive expression levels, only one suitable line was obtained for each construct, and both were used to investigate subcellular protein targeting *in vivo*. In mature leaves of 6-week-old plants, NHL4 with N-terminal and internal EYFP fusions was detected in the cytosol and in puncta of different sizes, very similar to the results for the *EYFP-NHL4$_{OE}$* lines (Figure 3.14C-D). In many cells, EYFP-NHL4 was newly seen in large ring-like structures of 2 – 3 µm in diameter and in small vesicles associated with the former (i.e., *NHL4$_{pro}$:EYFP-NHL4*; line 13; Figure 3.14C). As these large ring-like structures were most prominent in the mature leaves of old plants and resembled vacuoles based on their size, they could represent autophagic vacuoles. For the internal EYFP fusion, primarily puncta of 0.5 – 1 µm were seen (i.e., line 1; Figure 3.14D). Hence, this NHL4 fusion was likely targeted to peroxisomes due to their typical size of approx. 1 µm in diameter.

To verify peroxisome targeting of NHL4 by co-cultivation of Arabidopsis seedlings with *Agrobacterium*, the stable line expressing the internal EYFP fusion construct (T$_2$, line 1) was transiently transformed to express the peroxisome marker, *mCer-PTS1*. As a result, EYFP fluorescence was observed in peroxisomes labeled with mCer-PTS1 (Figure 3.15). In addition to peroxisome targeting, NHL4 was also found in free vesicles-like structures (data not shown) and in those attached to peroxisomes (Figure 3.15A). The attachment was documented for 7.5 sec (Figure 3.15B4 – 12) and even longer observed (for more than 14 sec; data not shown). In conclusion, the data demonstrated that NHL4 is a true novel peroxisomal protein and most likely is targeted to peroxisomes *via* the docking event between cargo vesicle-like structures and peroxisomes. Because many properties of NHL4 are conserved in NHL6 and NHL25 (an N-terminal TMD, a LEA_2 domain, and a C-terminal PTS1) and because several trafficking

intermediates were similar (vesicle-like structures, the ER, and ER-derived vesicles), NHL6 and NHL25 most likely use the same trafficking pathway as NHL4.
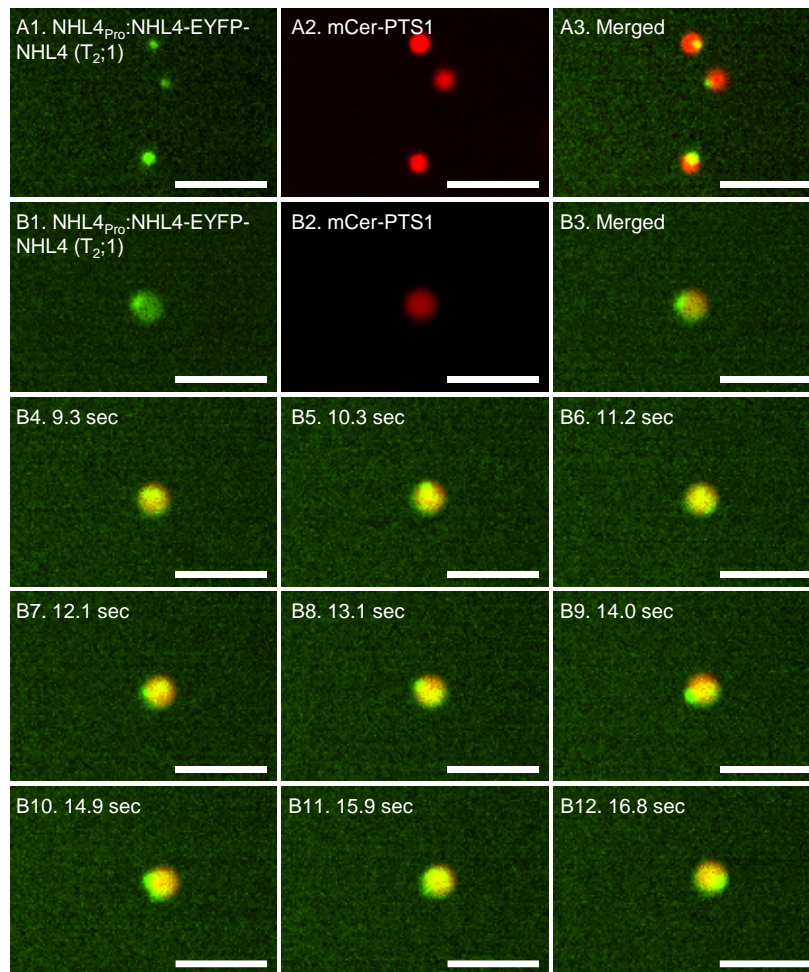
Figure 3.15: Targeting analyses of NHL4 to peroxisomes and vesicle-like structures in stable transgenic Arabidopsis plants

In 4-day-old Arabidopsis seedlings of the stable transgenic line *NHL4$_{Pro}$:NHL4$_{(1-21)}$-EYFP-NHL4$_{(22-239)}$* (T$_2$, line 1) that had been transiently transformed with *Agrobacterium* and expressed *mCer-PTS1*, (A) targeting of NHL4 to vesicle-like structures was observed in epidermal cotyledon cells 3 dpc. All three vesicle-like structures were in very close proximity to mature peroxisomes, thus peroxisome attachment was observed at very high frequency. (B) NHL4 was targeted to peroxisomes and to vesicle-like structures in proximity to peroxisomes. Co-movement of mature peroxisomes and vesicle-like structures is documented in a single confocal plane retrieved from a time-lapse video (B4 – B12) and indicates physical attachment. Peroxisomes were labeled with mCer-PTS1 and converted to red. Scale bar = 5 μm.

3.3 Functional characterization of the three peroxisomal NDR1 homologs

3.3.1 Promoter and expression analyses of *NHL4*, *NHL6*, and *NHL25*

To start investigating the biological functions of the first three NDR1 homologs (NHL4, NHL6, and NHL25) that had been demonstrated to be targeted to peroxisomes as their final destination (3.2.1.3), it was considered important to know their expression profile in different tissues and under diverse stress conditions. *NHL25* expression had already been reported to be induced upon infection of Arabidopsis leaves by avirulent *Pst* carrying one of four avirulence genes (*avrRpm1*, *avrRpt2*, *avrB*, or *avrRps4*) but not by the virulent *Pst* strain (1.4.1; Varet et al., 2002). Expression of *NHL4* and *NHL6* was found to be ABA-inducible in imbibed seeds (Goda et al., 2008) and in seedlings (Bao et al., 2016), respectively (1.4.1). In this study, computational analyses of the promoter regions of these *NHLs* (700 – 1,300 bp; 2.7.4) indicated that they shared predicted *cis*-regulatory elements, namely binding site motifs for well-known transcription factors (TFs), including ABA-INSENSITIVE PROTEIN 3/VIVIPAROUS 1 (ABI3/VP1), MYELOBLASTOSIS domain protein 4 (MYB4) and MYB-related TFs (Suppl. Figure 6). While MYB TFs are known to control gene expression in secondary metabolism and plant cell morphogenesis (Jin and Martin, 1999; Stracke et al., 2001), ABI3/VP1 TFs are regulators of ABA signaling and seed maturation (Suzuki et al., 1997). The *NHL6* and *NHL25* promoters also included predicted binding site motifs for BASIC LEUCINE ZIPPER (bZIP) TFs which regulate seed maturation and flower development as well as plant responses to pathogens and stress (Jakoby et al., 2002). In the *NHL6* promoter, additionally several predicted binding site motifs for WRKYGQK motif-containing (WRKY) TFs, which function typically in plant responses to wounding and pathogens (Eulgem et al., 2000), were found (Suppl. Figure 6). Hence, these predictions suggested that expression of the three *NHL* genes might be regulated by these TFs, which are activated by ABA, wounding, and pathogen infection.

To validate the predicted gene regulation, the expression profiles of the three *NHLs* were analyzed first based on publicly available expression data (Genevestigator database; Hruz et al., 2008) in the following section (3.3.1.1). Tissue expression of *NHLs* using the native *NHL* promoters in *GUS* reporter lines was analyzed in depth at different developmental stages using stable transgenic Arabidopsis *GUS* reporter lines (3.3.1.2). The most relevant and informative expression data were validated experimentally by qRT-PCR (3.3.1.3.1) and by promoter analyses using stable transgenic Arabidopsis *GUS* reporter lines (3.3.1.3.2) under different biotic and abiotic stress conditions.

3.3.1.1 Expression analyses of *NHL4*, *NHL6,* and *NHL25* deduced from publicly available transcriptomics data

The expression data for *NHL4* and *NHL6* had been generated by Arabidopsis ATH1 genome arrays and large-scale mRNA sequencing projects, which were combined and made publicly by Genevestigator (Hruz et al., 2008; 2.7.3), while those for *NHL25* were restricted to the latter dataset. For developmental analyses of *NHL* gene expression, the mRNA dataset was chosen (Figure 3.16A). As reference gene, the prototypical NHL protein, NDR1, was included due to its relatively well characterized signal transduction function in plant immunity (1.4.1). Unlike *NDR1*, which was constitutively expressed, the expression of all three *NHLs* fluctuated at rather low level throughout the developmental stages. These data suggested that NHL4, NHL6, and NHL25 might function as regulatory proteins, which often are weakly expressed.

NHL gene induction was investigated for physiologically relevant plant treatments, such as phytohormone, pathogen, elicitor application, and abiotic stress conditions (Figure 3.16B). Only those data derived from Arabidopsis Col-0 with > 3-fold change in gene expression (vs. untreated) and supported with a *p* value < 0.05 were analyzed. The expression of *NHL4* was strongly and quickly induced in seedlings treated with ABA (10 µM, approx. 12 fold; 3 h post treatment). Interestingly, another online microarray data source (ArrayExpress, ATH1-121501) showed that loss of function of three ABA-activated kinases, which play important roles in ABA signal transduction (1.3), in the triple mutant *srk2dei*, caused a reduced expression of *NHL4* (7.5 fold) under the same ABA treatment (data not shown). *NHL6* (but not *NHL25*) showed considerable but lower ABA induction (4- and 6.6-fold). The mRNA seq data also showed an ABA-inducible expression of *NHL4* and *NHL6* (both 6.6 fold) in 14-day-old plants after 6 h treatment (sprayed with 100 µM ABA). *NHL6* expression was also found to be induced 7 fold upon leaf spraying with SA (2 mM, 24 h, Figure 3.16B). By contrast, the other plant defense hormones (e.g., ethylene, JA) did not cause significant (> 3 fold) changes in *NHL* gene expression (data not shown). Among different abiotic conditions, *NHL6* expression was induced by cold with 40-fold increase, whereas *NHL4* and *NHL25* were unaffected. Taken together, the data indicated that NHL4 plays a physiological role primarily in plant responses mediated by ABA signal transduction. On the other hand, NHL6 had an indicated physiological role also in SA-mediated plant responses.
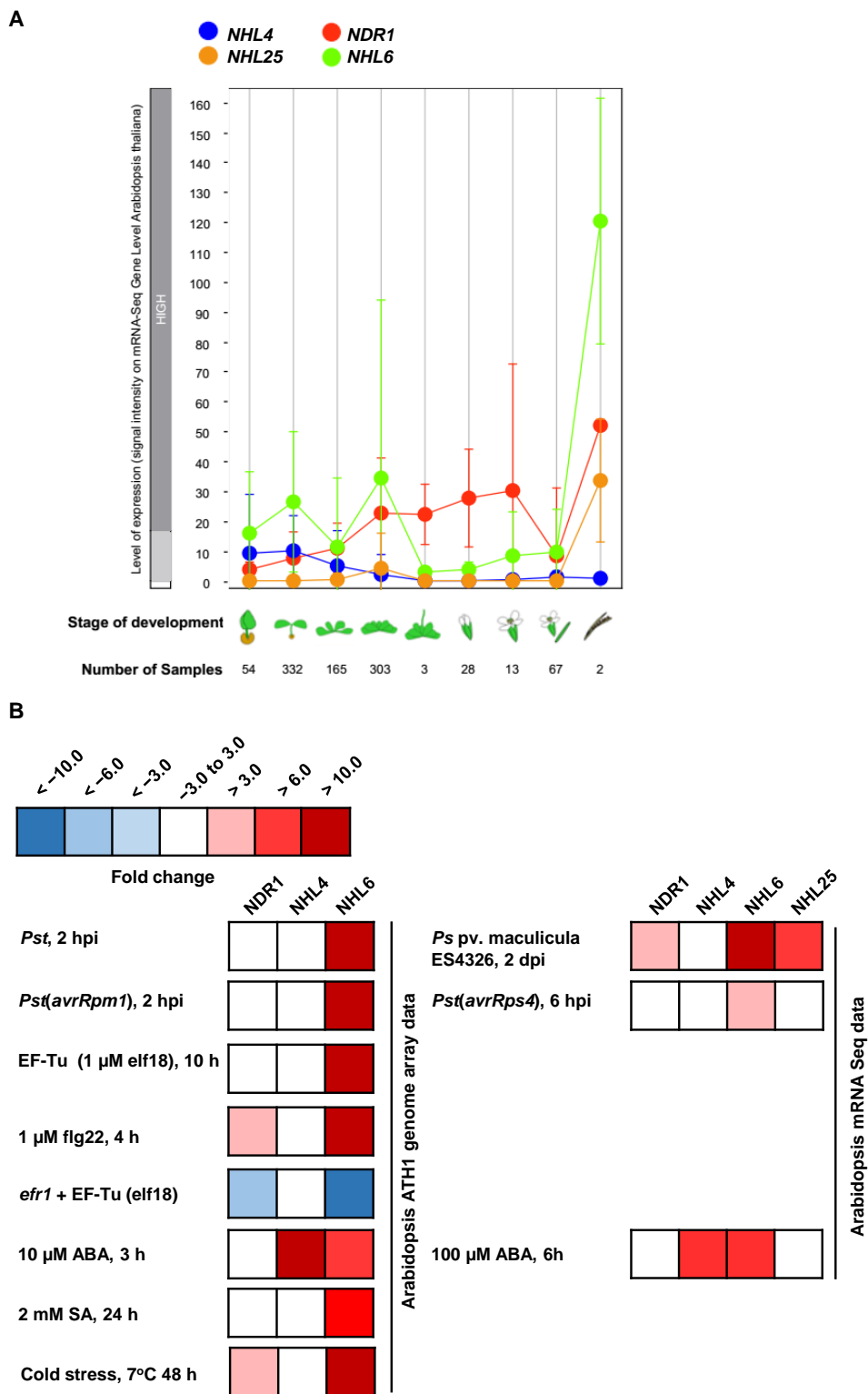
Figure 3.16: Gene expression analyses of *NHL4, NHL6, NHL25* and *NDR1* by Genevestigator

Gene expression was analyzed in different plant developmental stages (A) and upon biotic stress treatment and ABA application (B).

The genes encoding proteins involved in innate immunity are typically induced by pathogen infection (Li et al., 2016). Particularly *NHL6* was strongly induced by elicitor treatment with elf18 (29 fold) and flg22 (35 fold). The Arabidopsis plasma membrane-located EF-Tu receptor1 (EFR1) binds elf18, which triggers PTI (1.2.1). Consistently, elf18-induced expression of *NHL6* was suppressed in the *efr1* mutant, showing that *NHL6* expression was induced upon elf18 perception by EFR1. Considerable gene induction of *NHL6* and *NHL25* was also observed for specific elicitors of fungi (data not shown), indicating that the defense function of both proteins is extended beyond bacterial pathogens.

If infiltrated into mature leaves, two virulent *Pseudomonas* strains including *Pst* (at a concentration of 10^8 CFU·mL^{-1}) and *Pseudomonas syringae* pv. *maculicola* (*Psm*) ES4326 (at $1.6·10^6$ CFU·mL^{-1}) strongly induced expression of *NHL6* (12 and 38 fold, respectively; Figure 3.16B). Avirulent strains, which also possess EF and flagellin, are expected to cause at least the same gene induction as virulent strains. Upon infection with two avirulent strains, *NHL6* induction remained at high level (*Pst*(*avrRpm1*): 12 fold; *Pst*(*avrRps4*): 6 fold) similar to infection with virulent *Pst*. The data suggested that *NHL6* is induced by a signal transduction pathway of PTI that is blocked neither by AvrRpm1 nor by AvrRps4. Despite limited large-scale mRNA sequencing data for *NHL25*, they indicated a strong gene induction (7 fold) after virulent *Psm* ES4326 infection. By contrast, *NDR1* was hardly induced by *Psm* or flg22 treatment. The data demonstrated that *NHL6* and *NHL25* are induced by virulent and avirulent bacterial pathogens, strongly suggesting that they play a physiological role in plant innate immunity. Among the three NHLs, NHL6 seemed to play a dual role in stress responses to both of biotic and abiotic stress.

3.3.1.2 Analyses of the tissue-specific expression patterns of *NHL4*, *NHL6,* and *NHL25* at different developmental stages

To investigate the stress-responsive expression of *NHLs* experimentally in *planta* and at high tissue-specific resolution, promoter-*GUSA* lines were created. The upstream intergenic regions (non-coding DNA region between the start codon of the gene of interest and the next gene located upstream) of *NHL4* (1,229 bp), *NHL6* (1,304 bp), and *NHL25* (1,785 bp) were cloned to obtain the desired *NHL*$_{Pro}$*:GUSA* constructs and to generate stable transgenic lines (Figure 3.17A; 2.3.2). Besides the *NHL*$_{Pro}$*:GUSA* cassette, the expression vector also carried a second cassette expressing the hygromycin resistance gene, which allowed to select stable transgenic lines (Figure 3.17A). For each *GUSA* construct, three out of six stable transgenic lines were

selected as representative lines in terms of *GUSA* expression as these three lines showed very similar expression patterns. The enzyme β-glucuronidase encoded by the *GUSA* gene was analyzed by a histochemical approach in which the *GUS* reporter lines were vacuum-infiltrated with a buffer containing the substrate (X-Gluc, 2.10.1), leading to formation of an insoluble blue reaction product, whose local cell concentration correlated with the *NHL* promoter activity.

The promoters of *NHL4*, *NHL6*, and *NHL25* were predominantly active in vascular tissue of cotyledons and roots (0.5- and 4-day-old seedlings). *NHL6* expression was slightly lower compared to *NHL4* and *NHL25* (Figure 3.17B). Pronounced *GUSA* gene expression in vascular tissue was also observed in rosette leaves of older plants (8- and 14-day-old). *GUSA* expression in vascular tissue indicated that the three *NHL* promoters must be active in the living cells of this tissue type, i.e. phloem cells. GUS staining was also visible at the periphery of cotyledons and leaves. Most interestingly with respect to the hypothesized function of NHL6 and NHL25 in innate immunity, the three *NHL* promoters were constitutively highly active in hydathodes of both cotyledons and leaves (Figure 3.18). Hydathodes are structures located at the leaf margins and form water pores. The bacterial pathogen, *Xanthomonas campestris* pv. *campestris* (*Xcc*), which causes the black rot disease in cruciferous plants, infects its host primarily by entering the leaves through these pores (Onsando, 1992; Hugouvieux et al., 1998). Therefore, the activity of the *NHL* promoters in hydathodes indicated a constitutive general defense functions of the NHLs at these pathogen entry sites and their important defense role against *Xcc*. Moreover, the *NHL6* promoter activity was observed in stomata and trichomes (Figure 3.18B, C). For many plant pathogenic bacteria like *Pseudomonas*, stomata are the primary entry point to the plant apoplast. Hence, the data suggested a function specifically of NHL6 in trichomes and stomata against pathogens using this entry route.

A

GGGGACAAGTTTGTACAAAAAAGCAGGCT - **Promoters of NHLs** - ACCCAGCTTTCTTGTACAAAGTGGT
*att*B1   ~ 1.2 – 1.8 kb   *att*B2

B

NHL4*Pro*:GUSA   NHL6*Pro*:GUSA   NHL25*Pro*:GUSA

B1. Seedling (0.5 days old)

B2. Seedling (4 days old)

B3. Root tip (4-day-old seedling)

B4. Rosette (8-day-old plant)

B5. Old lateral root (8-day-old plant)

B6. Rosette (14-day-old plant)
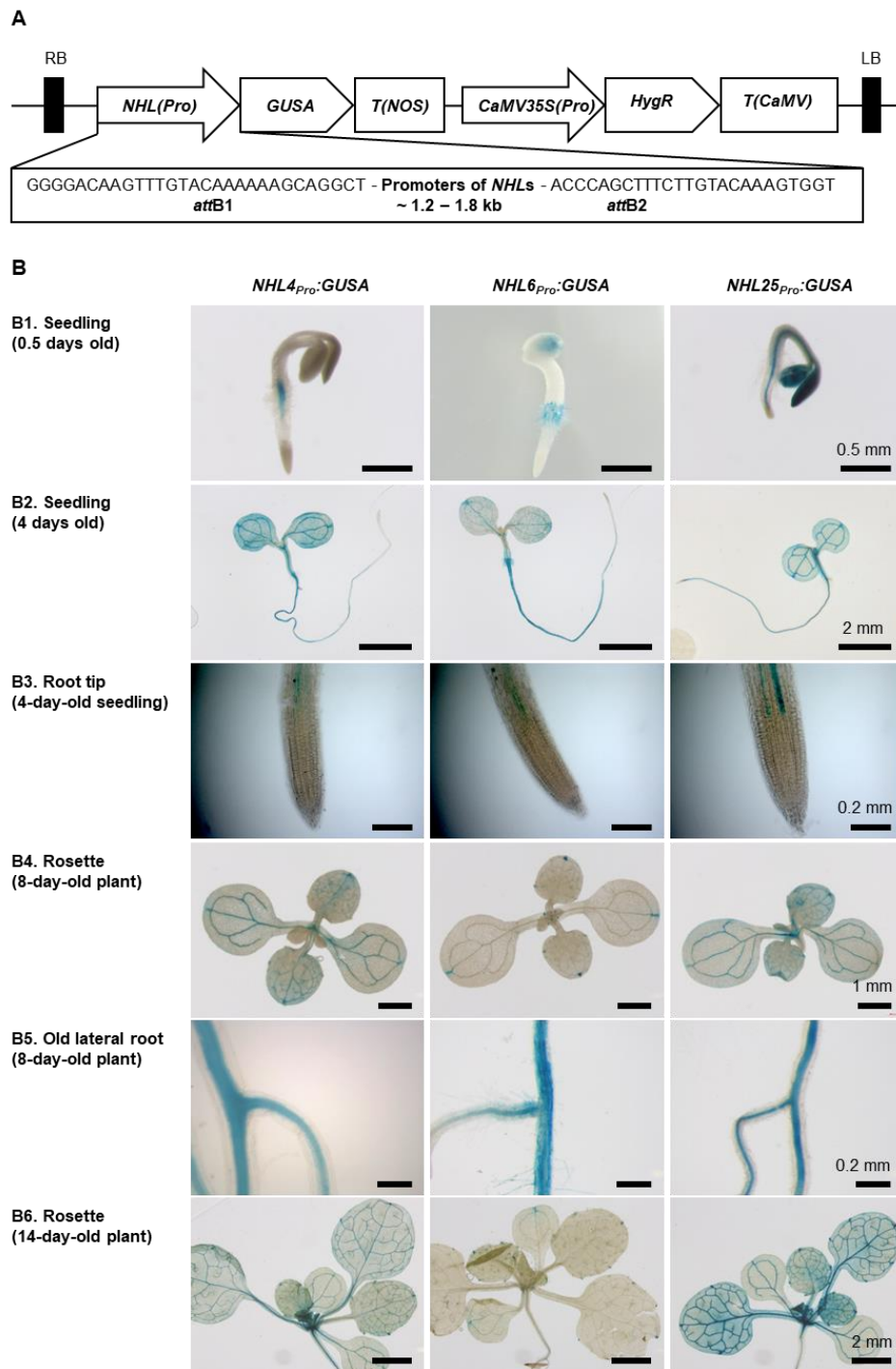
Figure 3.17: *GUSA* expression analyses from the native *NHL* promoters during plant development in stable transgenic *Arabidopsis* lines

(A) The schematic diagram shows the *GUS* reporter cassettes constructed in this study. The T-DNA of the pMDC162 vector includes the *GUSA* CDS under control either of the *NHL4,* the *NHL6* or the *NHL25* promoter, the *NOS* terminator T(*NOS*), and a hygromycin resistance (*HygR*) cassette (with *CaMV 35S* promoter and *CaMV* terminator). (B) The tissue-specific activation of the three *NHL* promoters is indicated by blue color at the site of *GUSA* expression and enzymatic activity and was analyzed in depth at different developmental plant stages. All three promoters were active in seedlings, and the GUS staining was most pronounced in vascular tissue of cotyledons, mature leaves, and roots. Six indepen-

94

dent transgenic lines per *NHL$_{pro}$:GUSA* construct (T$_2$ generation) were screened for *GUSA* expression of which three lines displaying the most similar tissue-specific *GUSA* expression were chosen for this analysis. Representative data of three independent lines per promoter construct and of two independent experiments are shown. Promoter and constructs were designed by the thesis author. GUS assay optimization, experimental analyses of the reporter lines, and image documentation were kindly performed by Dr. Thanh-Hao Nguyen (University of Hamburg, Hamburg, Germany).

At the late developmental stage (approx. 6 weeks old), both the *NHL4* and *NHL25* promoters were active in various floral parts (e.g., style, valve, gynophore, sepals, petals), in the stamen of flowers, in specific parts of mature siliques, and in young pedicels and their junctions (Suppl. Figure 7). In these tissue types, the activity of the *NHL6* promoter was considerably weaker (e.g., in sepals, petals, the stamen, and main pedicel).

Altogether, the constitutive expression of *NHL4*, *NHL6*, and *NHL25* in vascular tissue, hydathodes, and stomata strongly indicated a fundamental defense function of three NHLs in combatting microbial pathogens that enter leaves *via* these infection routes. Together with the identical subcellular localization of all three NHLs in peroxisomes, the results indicated that the proteins might have partly redundant physiological functions.
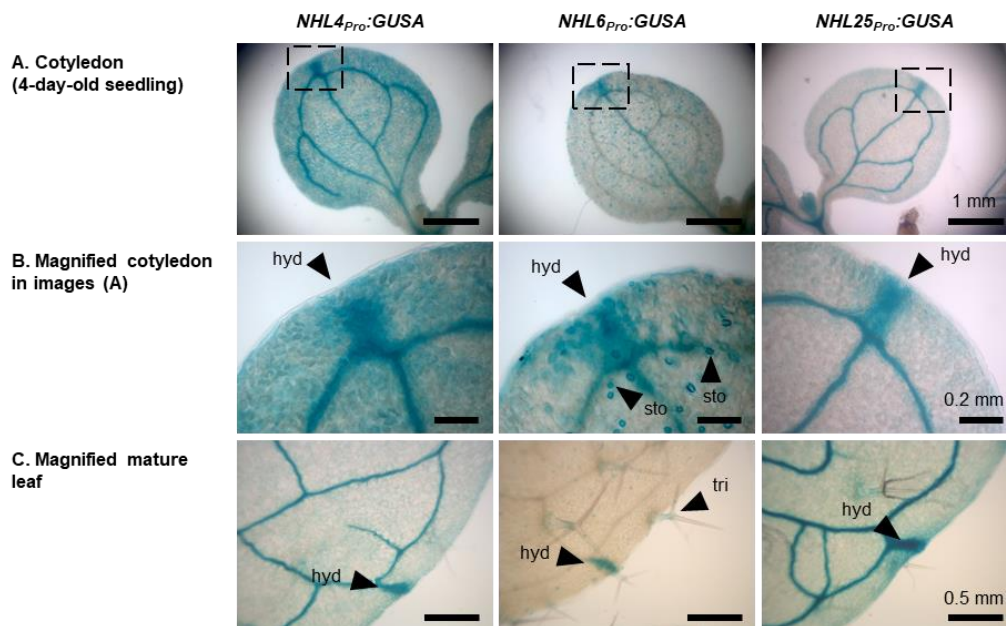
Figure 3.18: Pronounced constitutive *GUSA* expression in hydathodes and the vascular system of cotyledons and mature leaves

(A) *GUSA* expression driven by the promoters of *NHL4, NHL6,* and *NHL25* was found in hydathodes and the vascular tissue in cotyledons. (B) Enlarged regions as indicated in (A) show magnified leaf structures with better visible hydathodes and vascular tissue where the promoters of the three *NHLs* were active. The *NHL6* promoter activity was revealed also in stomata. (C) Magnification of mature leaves showed similar patterns of *NHL* promoter activity in hydathodes and vascular tissue as observed in cotyledons.

The *NHL6* promoter activity was additionally observed in trichomes of mature leaves. Information of expression cassettes and experiments is provided in Figure 3.17.

3.3.1.3 Experimental expression analyses of *NHL4*, *NHL6,* and *NHL25* under biotic and abiotic stress conditions by qRT-PCR and GUS histochemical approach

The publicly available expression data had revealed a pronounced inducible *NHL* expression under particular biotic stress conditions, such as elicitor treatment (i.e., elf18 and flg22) and bacterial infection as well as by ABA (Figure 3.16; 3.3.1.1). To experimentally validate the large-scale data, expression analyses by qRT-PCR and GUS histochemical analyses are the most widely used methods of choice and were applied in this study.

3.3.1.3.1 Analyses of *NHL* gene expression by ABA and *Pseudomonas* infection

To verify *NHL* expression by qRT-PCR, the same experimental conditions of plant treatment underlying the most relevant transcriptomics data published in the Genevestigator database were used with few minor modifications (2.1.2, 2.1.3, and 2.7.3). For ABA application, the roots of sterile 4- to 5-week-old plants were treated with 100 µM ABA by floatation on liquid MS medium (Nakashima et al., 1997). For bacterial infection, three different *Pseudomonas* strains, *Pst*, *Pst* (*avrRpm1*), and *Pst*(*avrRpt2*), were syringe-infiltrated into leaves of 4-week-old plants at a relatively high concentration of ~ 10^8 CFU·mL^{-1} (i.e., OD$_{600}$ of 0.2). The treated leaves were harvested at different time points to analyze *NHL* gene expression (2.1.2 and 2.1.3). As negative controls (i.e., mock treated plants), either 0.5x MS medium without ABA supplement or 10 mM MgCl$_2$ were used for plant incubation and infiltration, respectively.

Most procedures of RNA isolation are prone to contamination by gDNA, which would disturb expression analyses of single exon genes such as *NHL4*. In this study, specific precautions such as an intensified DNase I treatment were undertaken (2.13.8). As a result, the negative control (200 ng RNA, without cDNA synthesis) did not show significant amplicon generation (Ct > 40, data not shown), confirming successful removal of gDNA. Relative expression of *NHL*s was determined using *ACT2* as the reference gene for normalization and the $2^{-\Delta Ct}$ method (Livak and Schmittgen 2001; 2.13.10). Under stress conditions, fold changes in gene expression compared to mock-treated plants were calculated by the $2^{-\Delta\Delta Ct}$ method (Livak and Schmittgen 2001; 2.13.10). For both methods, primer amplification efficiencies of the target genes (*NHL4*, *NHL6,* and *NHL25*) and the reference gene must be close to 100% and very similar (i.e., differing by < 10%, Schmittgen and Livak, 2008). Due to low constitutive

expression of *NHL* genes in mature leaves under standard conditions (3.3.1.1), preventing template detection at high cDNA dilutions, stressed leaves (treated by ABA and *Pst*(*avrRpt2*)) were used for RNA isolation (Suppl. Figure 8; 2.1 and 2.13.10). The amplification efficiency (E) of the *ACT2* and the three *NHL* primer pairs were very similar (E = 1.8 – 1.9, equal to 90 to 95% (Suppl. Figure 8). Moreover, amplicon generation was specific for all four genes, as deduced from single peaks in melting curve analyses (Suppl. Figure 9). The expression of *ACT2* remained constant upon treatments, allowing its usage as a reference gene. The constant expression of *NHLs* relative to *ACT2* for mock treatments between time points (data not shown) allowed the evaluation of hormone or pathogen effects on the *NHL* expression level.

Under ABA treatment, the expression of *NHL4*, *NHL6*, and *NHL25* was significantly induced (Figure 3.19A). *NHL4* induction was the strongest and fastest (6 – 7 fold 6 and 12 h post treatment). Gene induction was minimal but still significant for *NHL6* (2.2 and 2.4 fold) and *NHL25* (3.6 and 2.5 fold). Hence, the expression data confirmed that primarily NHL4 played a role in ABA-mediated plant responses.

Upon Arabidopsis infection with virulent *Pst* or avirulent *Pst* expressing either *avrRpm1* or *avrRpt2* (Figure 3.19B – D), the expression of *NHL6* was induced more than 3 fold 6 hours post infection (hpi). A very high up-regulation of *NHL6* was observed 48 hpi. *NHL6* expression was highest with 84-fold induction for the virulent strain *Pst*, and to a lower extent for the avirulent strains, e.g. 23-fold and 44-fold increase by *Pst*(*avrRpm1*) and *Pst*(*avrRpt2*), respectively (data not shown)*. NHL25* was also highly and significantly up-regulated by *Pst* (6 hpi: 19 fold, 48 hpi: approx. 350 fold). Both avirulent strains also strongly induced *NHL25* expression, with interesting differences among them and compared to the virulent strain. *Pst*(*avrRpt2*) induced *NHL25* expression 92 fold (6 hpi) and 230 fold (48 hpi). By contrast, *NHL25* was most strongly up-regulated by *Pst*(*avrRpm1*) (6 hpi: approx. 270 fold) compared to the other two strains, and this extreme induction declined (48 hpi, 70 fold). These expression data for *NHL25* suggested a differential regulation of *NHL25* expression by different kinds of pathogenic *Pst* strains and probably by specific defense responses that sequentially take place upon infection. However, *NHL4* expression was unaffected by any of the *Pst* strains, which was consistent with the microarray data (Figure 3.16B). The results further strengthened the indications that NHL6 and NHL25 (but not NHL4) play a role in plant innate immunity.
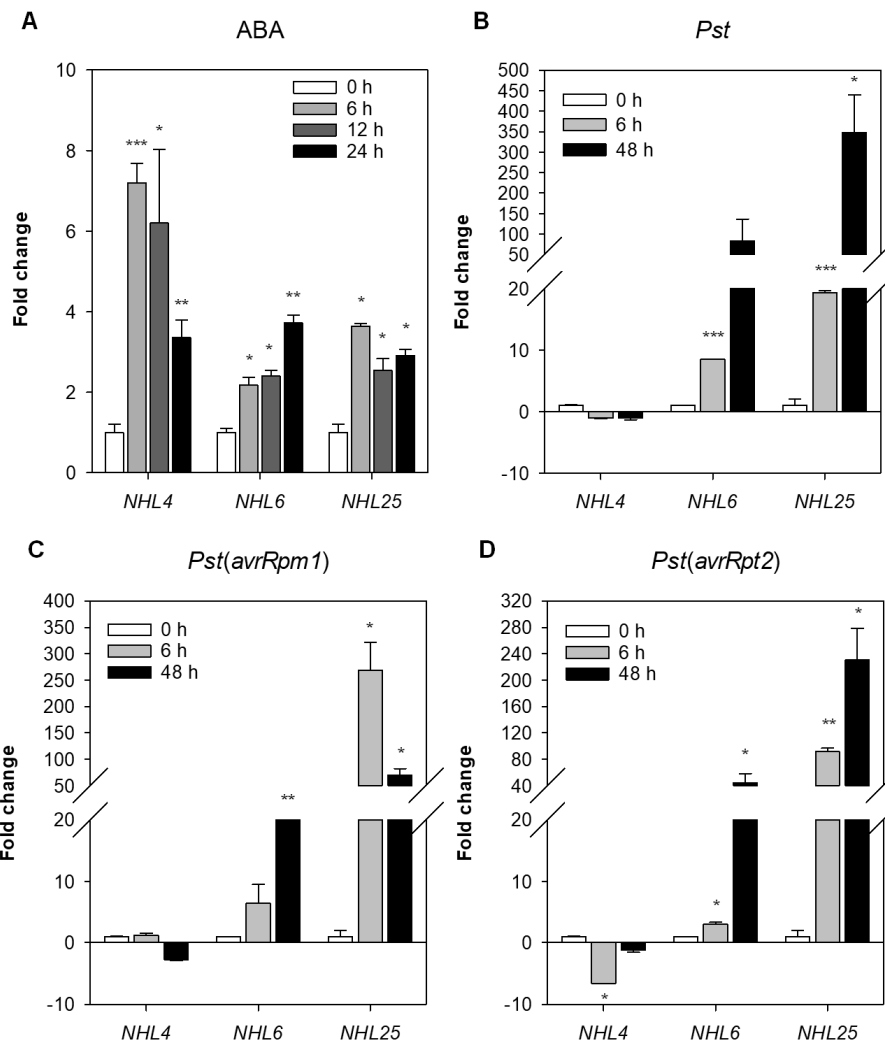
Figure 3.19: Expression analyses of *NHLs* upon treatment with ABA or *Pseudomonas* strains by qRT-PCR

(A) *NHL4, NHL6,* and *NHL25* expression was induced by ABA. (B – D) Changes in *NHL* gene expression were observed by virulent and avirulent *Pst* expressing either *avrRpm1* or *avrRpt2*. *NHL6* and *NHL25* expression were upregulated by *Pseudomonas* strains while that of *NHL4* remained unchanged. At the indicated time points, the fold change of *NHL* gene expression in ABA- or bacteria-treated samples was quantified relative to that in the mock-treated samples (0.5x MS-treated or MgCl$_2$-infiltrated plant samples, respectively) by the $2^{-\Delta\Delta Ct}$ method. Data represent the mean of fold change and standard errors of at least two biological samples. Each biological sample was analyzed by three technical replicates. Statistical analysis was performed by t-test (one tail, equal variance). Asterisks indicate statistically significant differences to the mock treated samples at the same time point ($p < 0.05$ (*), < 0.01 (**), and < 0.001 (***)).

3.3.1.3.2 Inducibility analyses of *NHL* promoters by *GUS* reporter gene analyses

The transgenic *NHL*~*Pro*~*:GUSA* lines, which had revealed constitutive *NHL* promoter activity in hydathodes, vascular tissue, and reproductive organs (3.3.1.2), were next used to analyze the inducibility of the *NHL* promoters upon different biotic treatments including wounding, infiltration with bacterial elicitors (flg22 and elf18), and infection with different *Pst* strains. Leaves were wounded by cutting the leaf edges and piercing the leaf surfaces. As a result, the *NHL25* promoter was most inducible by wounding, followed by that of *NHL4*, while activity of the *NHL6* promoter was not detectable (Figure 3.20). The data suggested that NHL4 and NHL25 could be engaged in plant defenses against tissue wounding by pathogens and/or herbivores. Upon flg22 and elf18 infiltration into the leaves, both the *NHL6* and *NHL25* promoters (but not that of *NHL4*) were induced (6 and 24 hpi), fully consistent with the transcriptomics data (3.3.1.1). Similar to gene expression analyses by qRT-PCR (3.3.1.3.1), virulent and avirulent *Pst*(*avrRpt2*) induced the activity of the *NHL6* promoter and more intensively that of the *NHL25* promoter (6 and 24 hpi). The *NHL4* promoter showed the weakest response to *Pst* application. Hence, NHL6 and NHL25 were implicated in playing a role in signal transduction of PTI in a pathway that was not blocked by AvrRpt2.
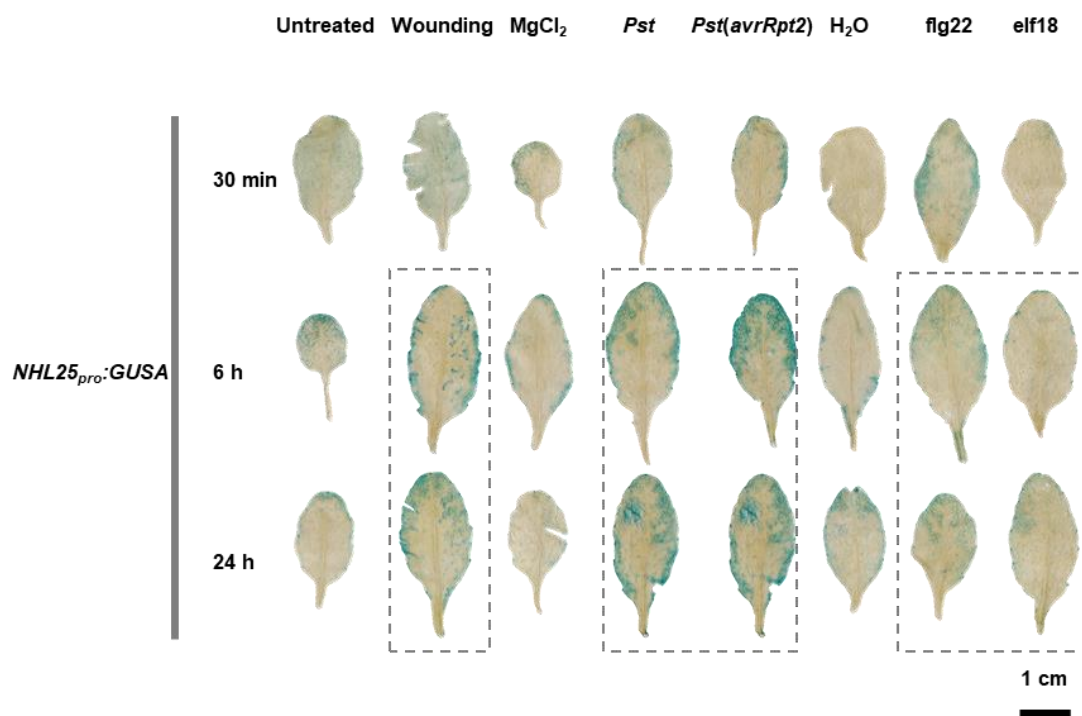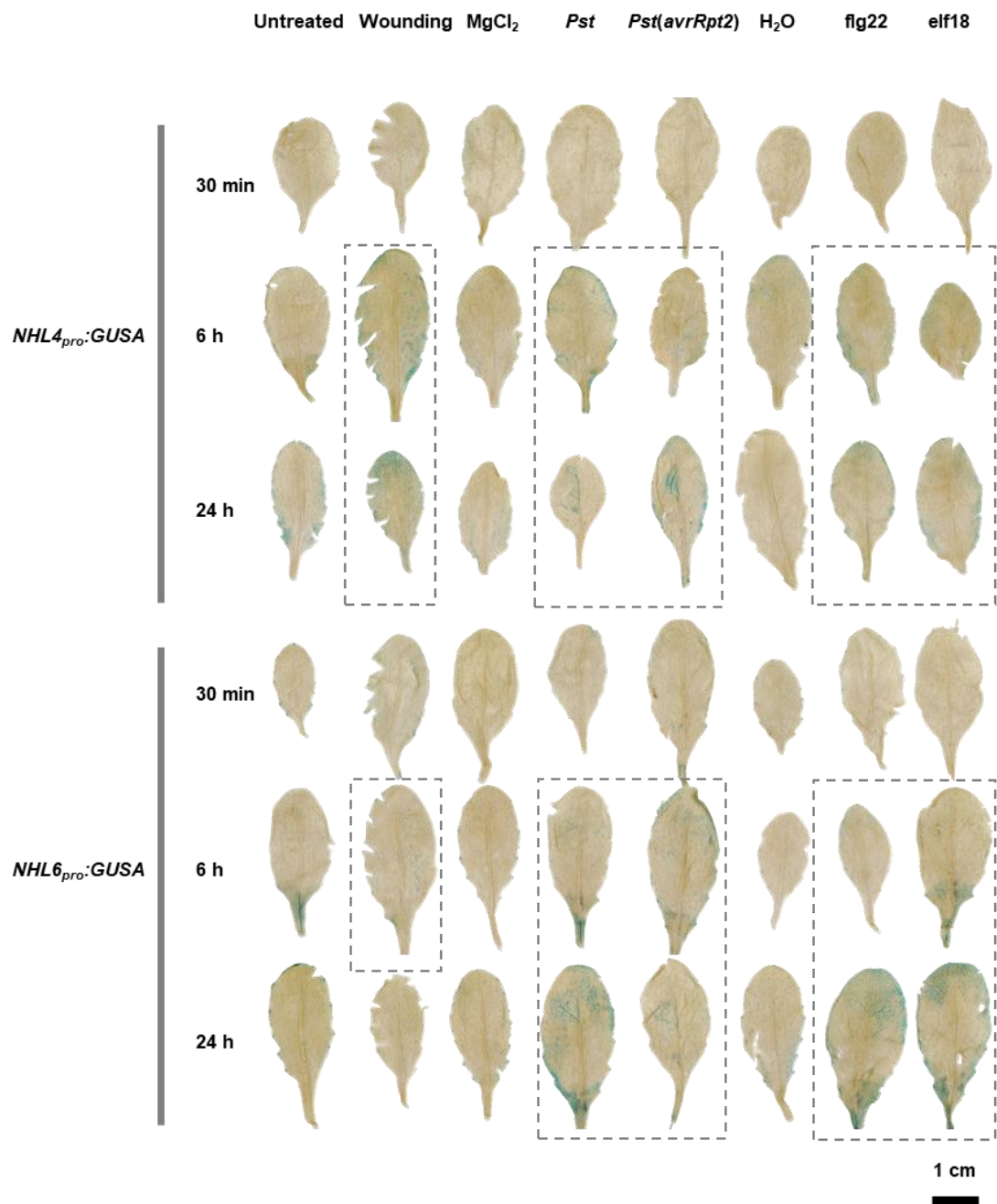
Figure 3.20: Inducibility analyses of *NHL* promoters by wounding, *Pseudomonas* strains, and elicitors using *GUS* reporter lines

For details on the *GUS* reporter lines, see Figure 3.17. One representative leaf of six analyzed leaves is shown for each treatment at the indicated time points. Bacterial elicitors (flg22 or elf18, 1 µM) were applied by syringe-infiltration. Bacteria at an OD_{600} of 0.2 (approx. 10^8 CFU·mL^{-1}) were used for infiltration. Untreated leaves, $MgCl_2$- and H_2O-infiltrated leaves were used as controls for wounding, bacterial infection, and elicitor infiltration, respectively. Dashed boxes indicate *GUSA* expression induced by a treatment. Experiments were repeated once and conducted with major assistance by Dr. Thanh Hao Nguyen (University of Hamburg, Hamburg, Germany), who also performed image documentation.

3.3.2 Functional analyses of NHL4, NHL6, and NHL25 in plant responses to biotic and abiotic stress by reverse genetics

NHL gene expression and promoter analyses strongly indicated a role of NHL4 in abiotic stress responses and of NHL6 and NHL25 in biotic stress responses. To characterize their functions in greater depth *in vivo*, a reverse genetic approach was applied. Homozygous single mutants (kindly provided, together with the two double mutants, by Dr. Kirsti Sørhagen, University of Stavanger, Norway) were confirmed with the sequenced T-DNA insertion site; the *nhl4-1* mutant (SAIL_681_E12) contained the T-DNA inserted in the 5'-UTR (-2 position), while the *nhl6-1* (SALK_148523) and *nhl25-1* (SALK_113216) mutants had the insertion in the first and second exon, respectively (Figure 3.21). The suppression of *NHL* gene expression was quantified in the three single *nhl* mutants and in two lines of the double *nhl6-1 x nhl25-1* mutant (2.8.1). Accordingly, despite being very low in WT plants, the basal gene expression of *NHL4*, *NHL6*, and *NHL25* was sufficient to observe a reduction to less than 1% in mature leaves of the corresponding mutant lines (Suppl. Figure 10), demonstrating that the three *nhl* genes were knocked out and that the lines represented loss-of-function mutations in NHLs.
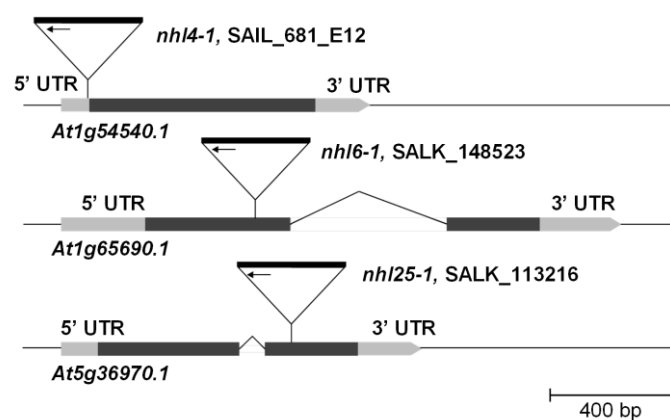
Figure 3.21: Schematic diagram of the Arabidopsis T-DNA insertion mutants

The schematic diagram of the exon/intron structure, UTR length and T-DNA insertion position in *nhl* mutants was based on ABRC stock center information (https://abrc.osu.edu/; TAIR) and was confirmed by sequencing. Arrows indicate the right border of the T-DNA.

Because the three NHLs might be partly redundant in plant immunity, a triple mutant (*nhl4-1* x *nhl6-1* x *nhl25-1*) was generated in this project by the cross-pollination between *nhl4-1* as a pollen donor and *nhl6-1 x nhl25-1* (line 2) as the mother line. From segregation analysis

of heterozygous triple mutants (T_1 generation), two offspring individuals (T_2) that were homozygous in all three mutated alleles were identified by PCR-based genotyping (data not shown). Simultaneously, the *ndr1-1* mutant, which is more susceptible to infection by *Pst*(*avrRpm1*) and *Pst*(*avrRpt2*) than WT (Century et al., 1995; 1.4.1), was used for comparative phenotyping analyses.

3.3.2.1 Analyses of *nhl4-1* and *nhl6-1* mutants for ABA sensitivity of seed germination

Besides the physiological roles of ABA in plant growth and responses to water shortage, ABA plays a prominent role in regulating seed dormancy and germination (1.3; Hilhorst, 1995; Kermode, 2005). Both negative and positive regulators of the core ABA signaling pathway were identified by screens for mutants that were ABA-hypersensitive or -insensitive in seed germination, respectively (Koornneef et al., 1984; Gosti et al., 1999; Fujii and Zhu, 2009; Nakashima et al., 2009). Bao et al. (2016) showed that the *nhl6-1* mutant is less sensitive to ABA in seed germination and seedling growth, suggesting its important role in abiotic stress-induced ABA signaling. In this study, the three single mutants were analyzed for alteration in ABA sensitivity of seed germination together with the two independent *NHL4* OE lines (T_5, line 5 and 10). Due to the extremely low constitutive expression level of *NHL4* in mature WT Arabidopsis leaves, the relative overexpression level of *NHL4* from the *CaMV 35S* promoter in these two OE lines was very high (line 5: approx. 12,000-fold increase; line 10: approx. 39,000-fold increase) compared to that of WT, as determined by Eduardo Muñoz Díaz (Díaz, 2020).

First, the optimal ABA concentration to inhibit germination was investigated (0.5 or 1 μM) for WT seeds. Seeds were sown on MS plates and stratified for 4 days at 4°C followed by cultivation under long-day condition. The appearance of two cotyledons was considered as germination (2.10.3; Tran et al., 2007). Germination of 5-day-old WT seeds was significantly reduced to 33% (for 0.5 μM ABA) and to 13% (1 μM ABA), in comparison to a germination rate of 98% in the absence of ABA (Figure 3.22). Thus, WT showed higher ABA sensitivity at 1.0 μM ABA versus 0.5 μM ABA. The inhibitory effect of 0.5 μM ABA on WT seed germination was also observed after 6 days but resulted in an increase of the WT seed germination rate from 33% (day 5) to 59%, and, hence, in a reduction of the inhibitory effect. By contrast, after 6 days 1 μM ABA showed the most significant effect, as only 32% of WT seeds could germinate. Hence, 1 μM ABA was considered the most suitable concentration for further analyses of the ABA sensitivity of germination of the *nhl* mutants.
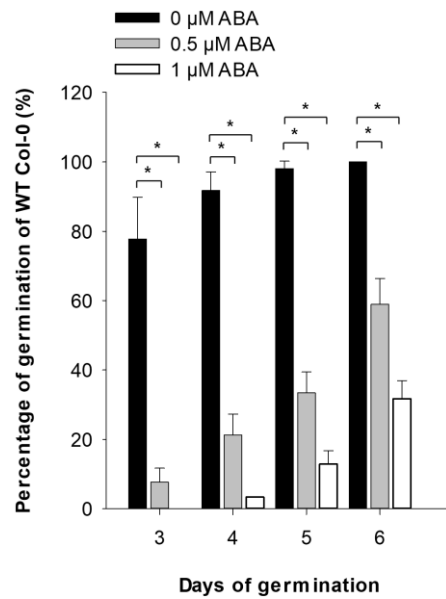
Figure 3.22: Analyses of an inhibitory effect of different ABA concentration on WT seed germination

To choose the optimal concentration, the inhibitory effect of ABA of WT seed germination was quantified in the presence of 0.5 and 1 µM ABA. The inhibitory effect was most pronounced for 1 µM ABA (5 d: 13% seeds germinated; 6 d: 32%) compared to 0.5 µM ABA (5 d: 33%; 6 d: 59%), and 1 µM ABA was chosen for the subsequent mutant analyses. The germination assays were conducted on 0.5x MS medium supplemented with 1% (w/v) sucrose (pH 6.0) and 0.8% (w/v) agar (Bao et al., 2016). Data represent mean value and standard deviation of three independent experiments (each with 70 seeds per treatment). Statistical analysis was performed with One way ANOVA (Tukey's test). Asterisk indicates statistically significant differences ($p < 0.05$).

All seeds had the same age. Analyses of seed gemination of the mutants and WT in the absence of ABA showed a rate of 100% (6 d), confirming high and equal seed quality (Figure 3.23A, B). In the presence of 1 µM ABA, the germination of *nhl4-1* was with 31% (4 d) significantly higher compared to WT and the *nhl6-1* and *nhl25-1* mutants ($p < 0.05$, data not shown), all of which showed only approx. < 3% germination (Figure 3.23A). The putative two *NHL4* OE lines (lines 5 and 10) showed an ABA hypersensitivity due to their low germination rate of < 2% (4 d), which was significantly lower compared to *nhl4-1* (Figure 3.23A, B; for 4 d, $p < 0.05$, data not shown).

A

B

Days of germination

- ●— 0 µM ABA WT
- ■— 0 µM ABA *nhl4-1*
- ▲— 0 µM ABA *nhl6-1*
- ▼— 0 µM ABA *nhl25-1*
- ○— 1 µM ABA WT
- □— 1 µM ABA *nhl4-1*
- △— 1 µM ABA *nhl6-1*
- ▽— 1 µM ABA *nhl25-1*

Days of germination

- ●— 0 µM ABA WT
- ◆— 0 µM ABA $NHL4_{OE}$ (T_5, line 5)
- ●— 0 µM ABA $NHL4_{OE}$ (T_5, line 10)
- ○— 1 µM ABA WT
- ◇— 1 µM ABA $NHL4_{OE}$ (T_5, line 5)
- ○— 1 µM ABA $NHL4_{OE}$ (T_5, line 10)

C
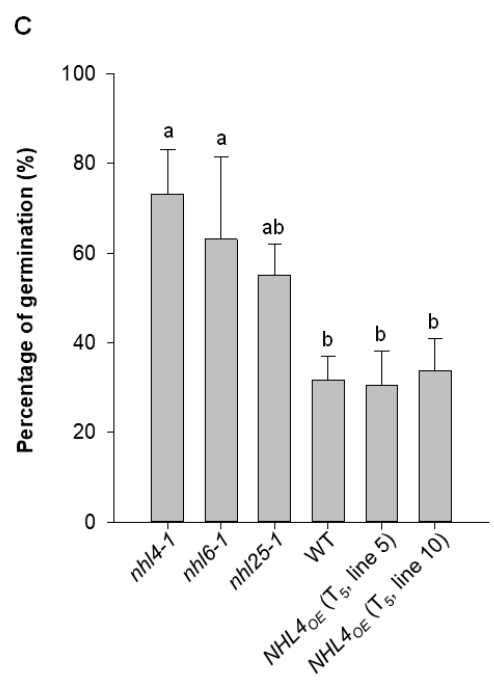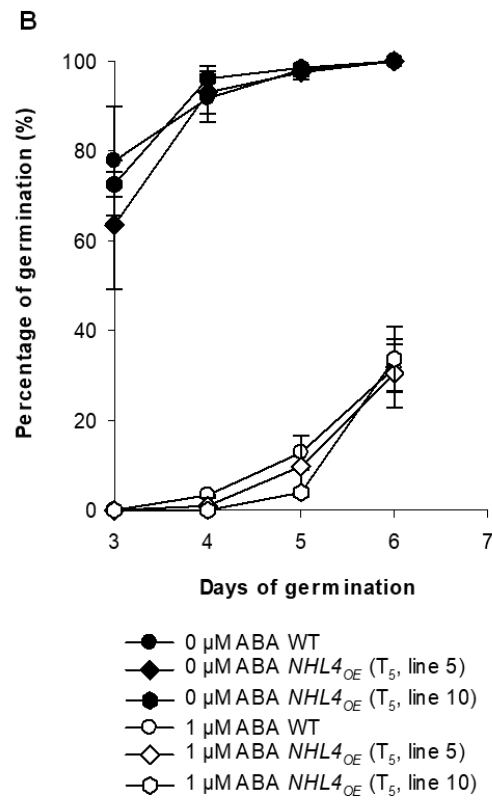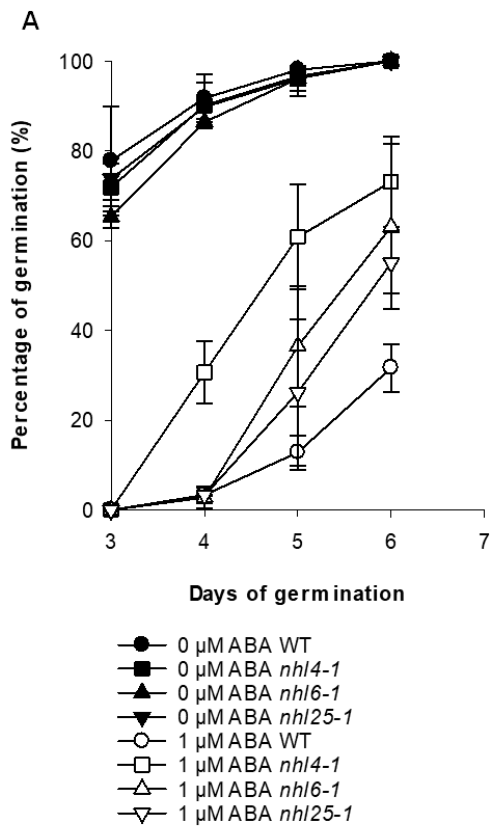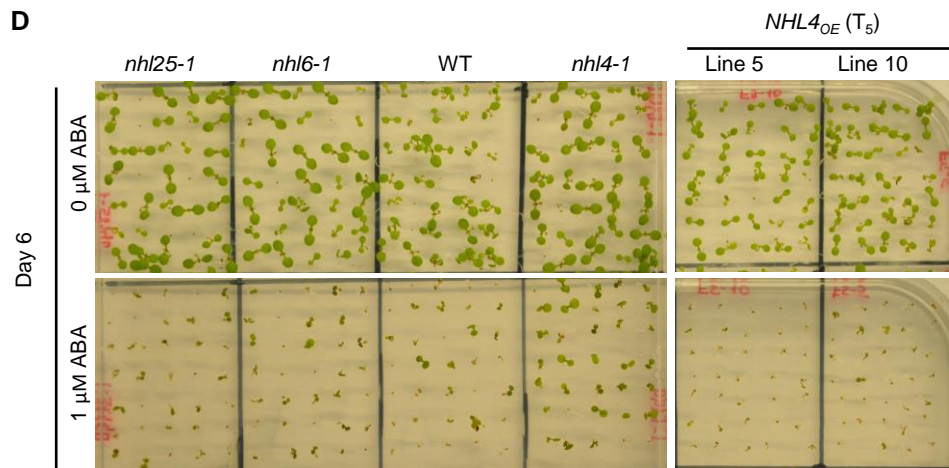
Figure 3.23: Analyses of an inhibitory effect of 1 µM ABA on seed germination of WT and T-DNA insertion lines

(A) The percentage of germination of WT and single *nhl* mutants was analyzed at 0 µM (filled symbols) and 1 µM ABA (open symbols) between 3 to 6 d. The three *nhl* mutants showed a higher rate of germination compared to WT at days 5 and 6, corresponding to a loss of ABA sensitivity and that was observed primarily for *nhl4-1* and to a lower degree for *nhl6-1* and *nhl25-1*. (B) By contrast, the degree of ABA inhibition of germination was similar for the WT and the two *NHL4* OE lines (T_5, line 5 and 10). (C) The percentage of seed germination of all genotypes in the presence or absence of 1 µM ABA was statistically analyzed at day 6 of germination. *nhl4-1* and *nhl6-1* displayed a significant difference in seed germination rate compared to WT and the other genotypes. Different letters indicate statistical differences. For detailed statistical analysis see Figure 3.22. (D) Exemplary plates are shown 6 d of germination. Seeds of all genotypes had the same age and were stored in the same manner. Data represent mean value and standard deviation of three independent experiments (each with 70 seeds per treatment).

The observation of the ABA sensitive phenotype was further supported at 6 d of germination. While WT germination was inhibited by ABA to 32%, that of *nhl4-1, nhl6-1,* and *nhl25-1* was less inhibited, with a rate of up to 73, 63, and 55%, respectively (Figure 3.23A, C, D). By contrast, germination of the two *NHL4* OE lines was significantly more sensitive to ABA, as only 31% (line 5) and 34% (line 10) could germinate compared to *nhl4-1* (73%). However, the two lines did not statistically differ from WT (Figure 3.23B, C). The results confirmed that loss of function of *NHL4* rendered the mutant less sensitive to ABA. Although *nhl6-1* and *nhl25-1* also displayed a detectable but lower degree of ABA sensitivity compared to WT, only that of *nhl6-1* was confirmed with statistical analyses, consistent with the study of Bao et al. (2016). Taken together, the data showed that seed germination of *nhl4-1* and *nhl6-1* was less sensitive to ABA, indicating that NHL4 and NHL6 play a role in ABA-regulated seed dormancy. The data further suggested that both proteins have possible functions in plant responses to abiotic conditions mediated by ABA.

3.3.2.2   The role of NHL4 in protecting *E. coli* against salt stress

The NHL proteins of interest contain the water stress and hypersensitive response (WHY) domain as previously described (Ciccarelli and Bork, 2005; Kataya, 2011). According to a Pfam domain search (2.7.1), one LEA_2 domain (PF03168 Pfam annotation) was detected with sufficiently high bit scores in NHL4 (38.4, threshold 25), NHL6 (44.3), and NHL25 (45.3). The function of several proteins with LEA_2 domains has been revealed (1.4.2). The protective function of LEA proteins under stress was proven by *in vitro* enzymatic activity analyses of labile model enzymes, such as LDH, MDH, and citrate synthase (Hara et al., 2001; Sanchez-Ballesta et al., 2004; Goyal et al., 2005) and by studies of abiotic stress tolerance of *E. coli* transformants (He et al., 2012). Hence, the three NHL proteins of interest were hypothesized to possibly stabilize temperature-sensitive enzymes, as investigated by Díaz (2020), and to confer tolerance in *E. coli* against osmotic and high temperature stress. To this end, *NHL4, NHL6,* and *NHL25* were constructed as His_6 or MBP-tagged fusions in the bacterial expression vectors, pQE31 and pMAL-c2x, respectively, for recombinant protein production in *E. coli*. NHL4, NHL6, and NHL25 lacking the N-terminal region and the predicted TMD (i.e., deleting the N-terminal approx. 80 – 100 aa, 2.3.1) were N-terminally fused with either one of the above-mentioned tags (Figure 3.24A). Gene expression was induced by IPTG, and solubility of recombinant *NHL* proteins were optimized (Crappe, 2016; Díaz, 2020). Preliminary experiments had shown that the His_6-tagged NHL proteins were largely insoluble and that the MBP tag indeed enhanced solubility up to 50% (Díaz, 2020). Hence, in subsequent osmotic stress analyses, the MBP tag was used.

To investigate the effect of *NHL* expression in *E. coli* on the organism's osmotic stress tolerance, nine *E. coli* transformants expressing the same *NHL* construct were analyzed for best expression and protein solubility (2.12). For stress application and tolerance analyses, three transformants were grown in liquid cultures to the exponential phase (OD_{600} of 0.6), and recombinant gene expression was induced by IPTG for 6 h at 37°C. Next, cells were harvested, sedimented, and adjusted to constant cell concentration (OD_{600} of 5.0) prior to combining the three transformants. Six 10-fold dilutions were performed, and the last three dilutions of cells were spotted (10 µL) on standard LB plates containing either only IPTG (0.3 mM) or additionally NaCl or KCl (0.4 – 0.6 M) or sorbitol (0.8 – 1.2 M). After 1 – 3 d, the number of CFUs was counted at an appropriate dilution, and the concentration ($CFU \cdot mL^{-1}$) was calculated. The final concentrations of osmoticum, e.g. 0.5 M (for NaCl and KCl) and 1 M (for sorbitol), at

which the concentration of *E. coli* cells expressing *MBP* alone started being reduced (data not shown) and were chosen to study osmotic stress tolerance of *E. coli* cells expressing *MBP-NHLs*.
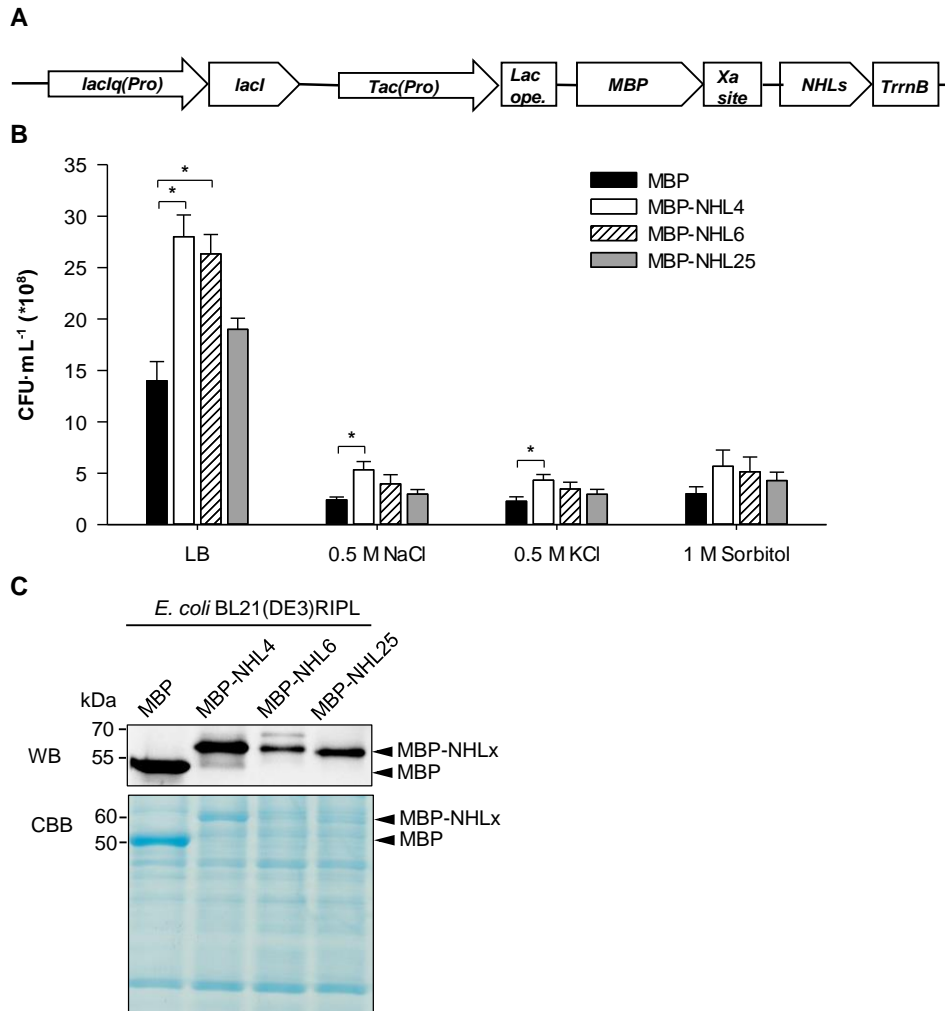
Figure 3.24: Analysis of osmotic stress tolerance of *E. coli* BL21(DE3)RIPL conferred by recombinant MBP-NHL proteins

(A) Illustration of the two expression cassettes of the *lactose inhibitor* (*lacI*) and the *MBP* fusion in the bacterial expression vector pMAL-c2x. The NHLs lacking the N-terminal region and the predicted TMD (deletion of the N-terminal 80 – 100 aa) were fused N-terminally with MBP to enhance recombinant protein solubility. The expression of *MBP-NHLs* was tightly regulated by the lacI repressor and the *Tac* promoter (a hybrid form of the *tryptophan* and *lac* promoters) and only induced in the presence of IPTG. (B) The growth of *E. coli* BL21(DE3)RIPL (in CFU·mL^{-1}) producing MBP alone or MBP-tagged NHLs was quantified on LB plates with and without supplementation of additional NaCl, KCl, or sorbitol. After 6 h of IPTG induction at 37°C in liquid LB cultures (w/o additional osmoticum), three different *E. coli* transformants expressing the same construct were mixed at equal proportions and concentrated to a total OD$_{600}$ of 5, and 10 µl of three 10-fold dilutions in LB (10^{-4} to 10^{-6}) were spotted on LB plates containing 0.3 mM IPTG and with or without osmoticum. Two independent dilutions were performed, spotted, counted, and referred to as technical replicates. After 1 – 3 d of incubation at 37°C, the number of CFU was counted at an appropriate dilution. Data represent mean and standard deviation from three

independent experiments, with three different transformants per construct analyzed in each. For statistical analyses see Figure 3.22. (C) For comparative analyses of soluble recombinant protein levels, the concentrated cell mixture of three transformants carrying the same construct were lysed by vortexing and sonication and subfractioned to isolate the soluble proteins (2.12). For immunoblotting, 1 µg of total soluble protein was loaded. Equal protein loading was verified by a second SDS-PAGE gel (5 µg each lane) and was stained with colloidal Coomassie Brilliant Blue. Recombinant MBP-tagged proteins were detected using a primary anti-MBP antibody. The recombinant proteins had the follow calculated molecular masses: MBP-NHL4 (60.6 kDa), MBP-NHL6 (60.5 kDa), MBP-NHL25 (59.8 kDa), and MBP (50.8 kDa). For immunoblotting, representative data of one of three independent experiments are shown. *MBP-NHL4* and *MBP* alone were better expressed compared to *MBP-NHL6* and *MBP-NHL25*.

Even in the absence of any stress application, *E. coli* expressing *MBP-NHL4* and *MBP-NHL6* showed significantly higher proliferation with higher CFU concentration ($2.8 \cdot 10^9$ and $2.6 \cdot 10^9$ CFU·mL^{-1}, respectively) than the cells expressing *MBP* alone ($1.4 \cdot 10^9$ CFU·mL^{-1}) or *MBP-NHL25* ($1.9 \cdot 10^9$ CFU·mL^{-1}) (Figure 3.24B). In the presence of 0.5 M NaCl, *E. coli* expressing *MBP-NHL4* formed significantly more CFUs ($5.4 \cdot 10^8$ CFU·mL^{-1}) compared to those expressing *MBP* alone ($2.4 \cdot 10^8$ CFU·mL^{-1}), *MBP-NHL6* ($3.9 \cdot 10^8$ CFU·mL^{-1}), or *MBP-NHL25* ($2.9 \cdot 10^8$ CFU·mL^{-1}). A similar tendency of the highest CFU was also observed for the *E. coli* expressing *MBP-NHL4* at 0.5 M KCl. *E. coli* cells expressing *MBP-NHL6* or *MBP-NHL25* also displayed higher cell proliferation compared to those expressing *MBP* alone in 0.5 M NaCl or KCl, but the differences were not statistically significant (Figure 3.24B). In the presence of 1 M sorbitol, the expression of *MBP-NHL4* in *E. coli* conferred osmotic stress tolerance better than *MBP* alone, as demonstrated by a higher CFU concentration, i.e. $5.7 \cdot 10^8$ CFU·mL^{-1} vs. $3 \cdot 10^8$ CFU·mL^{-1}. However, this result was not conclusive due to the insignificant difference revealed by statistical analyses. The same was observed for *E. coli* expressing *MBP-NHL6* ($5.2 \cdot 10^8$ CFU·mL^{-1}) or *MBP-NHL25* ($4.3 \cdot 10^8$ CFU·mL^{-1}). In conclusion, if *MBP-NHL4* was expressed, *E. coli* cells showed higher tolerance to osmotic stress caused by NaCl and KCl.

The apparent salt tolerance conferred specifically by NHL4 could be caused by higher concentrations of soluble NHL4 compared to NHL6 and NHL25. To investigate whether the three recombinant proteins differed in concentrations and solubility, immunoblotting was performed using primary anti-MBP antibody (2.12). Equal amounts of total soluble protein extracted from the concentrated and combined three transformants (OD$_{600}$ of 5.0) were used (1 µg). All three MBP-tagged NHL proteins were produced in *E. coli* in their correct apparent size as the cross-reactive bands corresponded to the expected molecular masses of the recombinant NHL proteins (MBP-NHL4: 60.6 kDa; MBP-NHL6: 60.5 kDa; MBP-NHL25: 59.8 kDa) (Figure 3.24C). Importantly, the concentration of MBP-NHL4 was higher compared to those of

MBP-NHL6, and MBP-NHL25 and similar to MBP alone (Figure 3.24C). Taken together, the results demonstrated that MBP-NHL4 indeed conferred a higher survival rate in *E. coli* under salt stress conditions compared to MBP alone. The result that the closely related paralogs, NHL6 and NHL25, did not have the same effect, was most likely caused by technical problems in producing similar concentrations of soluble proteins.

3.3.2.3 Analyses of the functions of NHL4, NHL6, and NHL25 in plant responses to bacterial pathogens

3.3.2.3.1 Analyses of *nhl* mutants for alterations in resistance to avirulent *Pseudomonas* strains

Arabidopsis NDR1 is the best characterized member of the NHL protein family and has been shown to play an important role in ETI (1.4.1). A relevant physiological function was proposed here for NHL4, NHL6, and NHL25 in innate immunity due to (i) their homology to NDR1, (ii) their constitutive expression in hydathodes, trichomes, stomata, and vascular tissue (3.3.1.2; Figure 3.18) as well as (iii) their strong up-regulation of expression in leaves by bacterial elicitors and infection with *Pseudomonas* strains (3.3.1.3, Figures 3.19 and 3.20). To address this hypothesis, the single, double (*nhl6-1 x nhl25-1*), and triple (*nhl4-1 x nhl6-1 x nhl25-1*) mutants were investigated for altered resistance to bacterial pathogens. The so-called bacterial proliferation assay is the most common method to investigate changes of the plant immune system. A defined concentration of bacteria is introduced into the apoplast of mature leaves by several possible methods, e.g. dipping, spraying, vacuum- or syringe-infiltration. Thereafter, the proliferation of bacteria is monitored over time (2.10.2; Katagiri et al., 2002) with a positive correlation between bacterial proliferation and plant susceptibility. As the *ndr1-1* mutant is highly susceptible to several different avirulent *Pseudomonas* strains (*avrB, avrRpm1, avrRpt2,* and *avrPph3*; 1.4.1), the mutant was included as positive control. As previously reported, *ndr1-1* showed an increase of *Pst*(*avrRpm1*) and *Pst*(*avrRpt2*) concentration (expressed as CFU·cm^{-2} leaf area) by a factor of approx. 10,000 between 0 and 2 dpi (Century et al., 1995). By contrast, the same avirulent strains proliferated much less in WT *A. thaliana* Col-0, i.e., showing only an approx. 1,000-fold and 30-fold increase, respectively, in the same time period, demonstrating that WT is resistant to these avirulent bacteria (Century et al., 1995).

Similarly, in this study, both avirulent *Pseudomonas* strains proliferated only weakly in WT (~ 34 – 87 fold until 3 dpi, Figure 3.25), while the *ndr1-1* mutant exhibited the reported

increased susceptibility towards *Pst*(*avrRpm1*) (at 3 dpi). Bacterial proliferation was approx. 690 – 1,400 fold higher compared to day 0 (Figure 3.25A, B). In case of *Pst*(*avrRpt2*) infection, the *ndr1-1* mutant also showed its reported susceptibility with an increase of bacterial concentration of approx. 1,500 – 1,800 fold (Figure 3.25C, D). These data were consistent with previous findings on the high susceptibility of *ndr1-1* to these two avirulent bacteria.
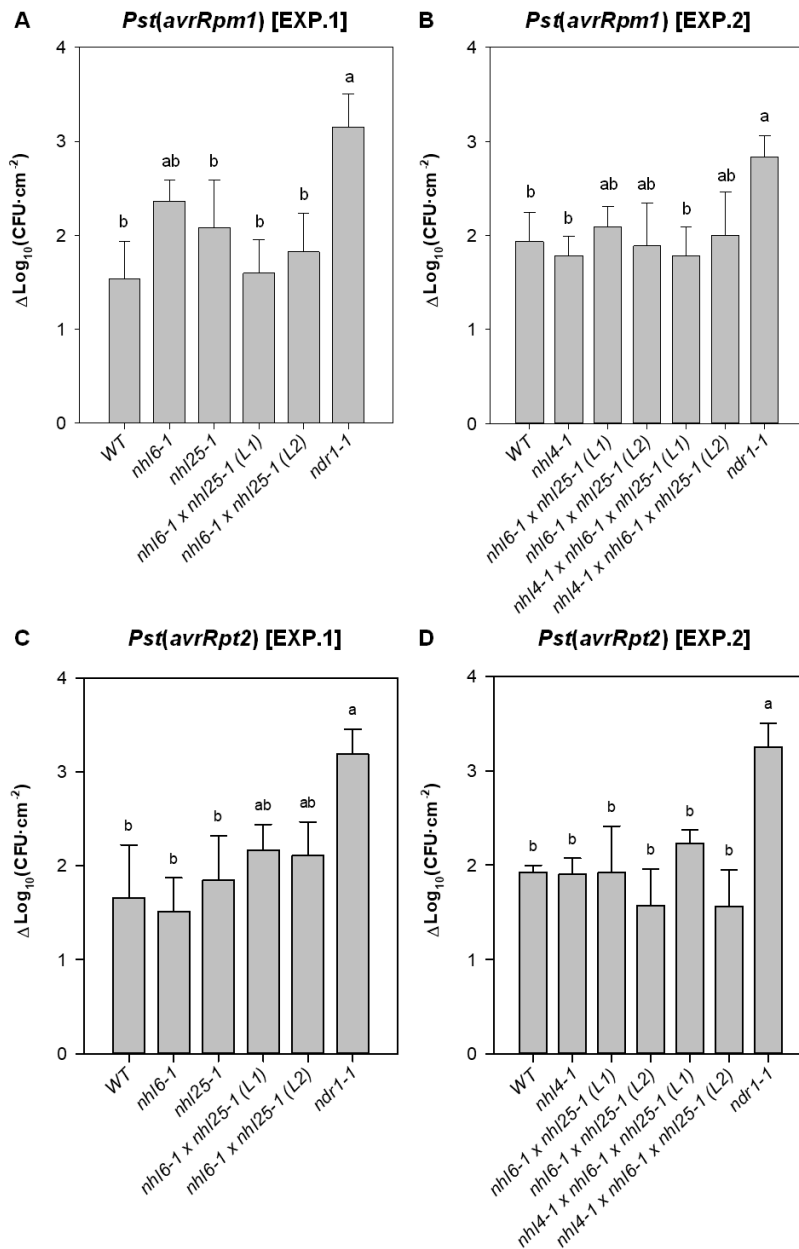
Figure 3.25: Analysis of altered innate immunity of different *nhl* mutants by determination of avirulent bacteria proliferation

Bacterial proliferation was quantified in two independent experiments (exp.; i.e., studies using different batches of plant genotypes) for *Pst*(*avrRpm1*) (in A and B) and for *Pst*(*avrRpt2*) (in C and D). Proliferation

of the avirulent *Pseudomonas* strains *Pst*(*avrRpm1*) (A, B) and *Pst*(*avrRpt2*) (C, D) was quantified 3 dpi. For each biological sample, six leaf discs taken from infiltrated leaves of three individual plants were harvested, pooled for grinding, and adjusted to a constant volume. Two serial 10-fold dilutions were performed as technical replicates. The number of CFU was counted right after infection (0 dpi) and 3 dpi. Data were converted to the decadic logarithm, and the change of bacterial concentration per area of leaf disc, i.e. $\Delta\log_{10}$ of (CFU·cm^{-2}) were plotted. Data represent the mean value and standard deviation of three biological samples per experiment. Statistical analysis was performed with One way ANOVA (Tukey's test). Different letters indicate statistically significant differences ($p < 0.05$). Representative results of two independent experiments are shown.

The single, double, and triple *nhl* mutants also showed increased concentrations of *Pst*(*avrRpm1*) 3 dpi compared to 0 dpi. The *nhl4-1* mutant resembled WT in its relatively low degree of bacterial proliferation (60 fold), while the higher bacterial proliferation in *nhl6-1* (240 fold) and *nhl25-1* (120 fold) compared to WT (34 and 87 fold) indicated a partial loss of ETI resistance (Figure 3.25A, B). In the two double *nhl6-1* x *nhl25-1* mutants, the same bacterial strain also proliferated more slowly, namely 39 fold (line 1) and 66 fold (line 2) (Figure 3.25A), which was lower compared to *nhl6-1* and *nhl25-1*, but the data were not statistically significant. In an independent experiment, the two double mutants showed a bacterial increase of approx. 123 (line 1) and 78 fold (line 2) (Figure 3.25B), but that was not statistically different from WT (84 fold). In the same experiment, the two triple mutants showed a bacterial increase by a factor of 61 (line 1) and 100 (line 2) (Figure 3.25B); thereby, both were not significantly different from WT, the two double mutants, and *nhl4-1*. The data showed that additional disruption of *NHL4* in the double mutant did not render the triple mutants more susceptible to *Pst*(*avrRpm1*), and that the *nhl* mutants did not show any statistically significant phenotypic differences in terms of increased susceptibility to *Pst*(*avrRpm1*) compared to the WT, based on this assay.

Upon infection with *Pst*(*avrRpt2*), the three single *nhl* mutants showed bacterial proliferation by a factor of 80 (*nhl4-1*), 33 (*nhl6-1*), and 70 (*nhl25-1*) within three days, but these values were not significantly different from WT (46 and 83 fold) (Figure 3.25C, D). The two double (*nhl6-1* x *nhl25-1*) mutants displayed higher bacterial proliferation (line 1: 145 fold; line 2: 130 fold; Figure 3.25C), but the differences were also not statistically from WT. Also, *Pst*(*avrRpt2*) proliferation was detected in the triple mutants with increases by a factor of 170 (line 1) and 36 (line 2) but were not significantly higher than WT (83 fold) (Figure 3.25D). Similar to *Pst*(*avrRpm1*), the proliferation of *Pst*(*avrRpt2*) in all *nhl* mutants was much lower compared to that in *ndr1-1*, but the differences between any *nhl* mutants and WT showed only a trend of increased susceptibility but were not significantly different. These data indicated

111

that the three NHLs might not play an essential role in resistance mechanism of plants to *Pst*(*avrRpm1*) and *Pst*(*avrRpt2*).

3.3.2.3.2 Hypersensitive response analyses of *nhl* mutants upon infection by avirulent *Pseudomonas* strains

Cell death caused by HR is an early and the most important ETI response to restrict avirulent pathogens to the infection site (1.2.2). To investigate the possible function of NHLs in ETI, the kinetics and intensity of HR upon infection with avirulent *Pst* strains were analyzed in different *nhl* mutants. *Pst*(*avrRpm1*) and *Pst*(*avrRpt2*) strains were chosen, and *ndr1-1* served as a negative control as NDR1 mediates HR triggered by two R proteins of the CC-NBS-LRR class (RPM1 and RPS2) against the two pathogenic avirulence effectors, AvrRpm1 and AvrRpt2, respectively (Century et al., 1995; Aarts et al., 1998; Hofius et al., 2009). The most common method to monitor the kinetics and intensity of HR is the measurement of total ion concentration released ("leaked out") from excised leaf discs into an external solution over time after infection by measuring the changes in conductance of the solution, referred to as electrolyte leakage (2.10.4; Johansson et al., 2015). To consider differences determined in total ion content of the leaf discs between different genotypes (data not shown), which would have affected the absolute electrolyte concentrations of the medium, the data were normalized. The total ion content of genotype-specific leaf discs was determined by autoclaving and set to 100% as maximum ion leakage. The absolute values were expressed in percentage to indicate the relative degree of HR-induced cell death. In addition, the velocity of electrolyte leakage was analyzed as the derivative of relative electrolyte leakage over time, presenting the speed of HR progression at the given point in time (2.10.4). This novel methodology of HR analyses allowed differences in HR progression to be resolved at very high resolution. After initial HR analyses, which had spanned 24 h and had revealed that the major electrolyte leakage occurred within the first 6 to 8 h after inoculation (data not shown), subsequent analyses focused on this period for *Pst*(*avrRpm1*) and *Pst*(*avrRpt2*), respectively.

For *Pst*(*avrRpm1*), electrolyte leakage started quickly in all genotypes 0.5 h post infection (0.5 hpi) and reached saturation after approx. 3 hpi but at different levels of 50 to 70% of maximal ion leakage (Figure 3.26A, B). Preliminary experiments, in which leaf discs from $MgCl_2$-infiltrated leaves of each genotype (as a control) were used, had shown that ion leakage was less than 5% over the time course experiment (data not shown), indicating the observed maximal leakage of 50 to 70% in bacteria-infiltrated samples was specific to the

infection. The *ndr1-1* mutant was relatively slow in ion leakage but reached the highest value of approx. 70 – 74% (6 hpi) compared to the other genotypes (Figure 3.26A – D). The instantaneous velocity of electrolyte leakage over time clearly showed a delay in HR progression in the *ndr1-1* mutant compared to WT (Figure 3.26E, F). The single *nhl* mutants differed slightly in the kinetics of electrolyte leakage compared to both *ndr1-1* and WT (Figure 3.26A, B). For instance, *nhl25-1* showed significantly lower relative ion leakage 6 hpi (61% compared to 74% for *ndr1-1*; Figure 3.26A, C). However, the difference was not statistically significant when compared to the WT (61%; Figure 3.26A, C). By contrast, in one experiment (Figure 3.26A, C), the two double (*nhl6-1 x nhl25-1*) mutant lines reached a relative electrolyte leakage of 66% (line 1) and of 70% (line 2) 6 hpi, and this was significantly higher than WT (61%) and the corresponding single mutants. In the second experiment (Figure 3.26B, D), a similar tendency of higher ion leakage in the double mutant lines was observed but not statistically significant. In the two triple mutant lines, electrolyte leakage was further increased compared to the two double mutant lines, e.g. to 63% (line 1) and 65% (line 2) (Figure 3.26B, D), and reached the level of *ndr1-1*. Thereby, electrolyte leakage of the triple mutant was significantly higher than that of the WT (Figure 3.26B, D).

114
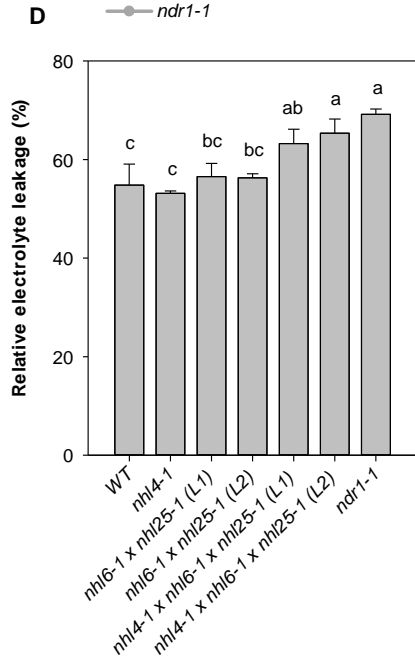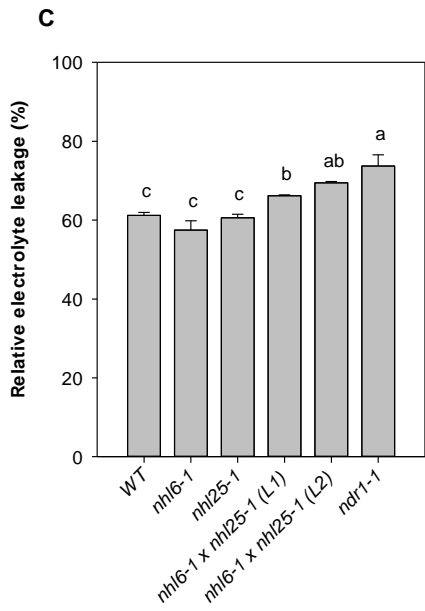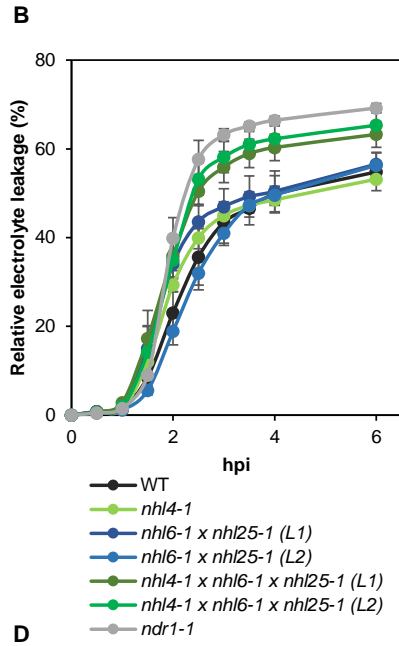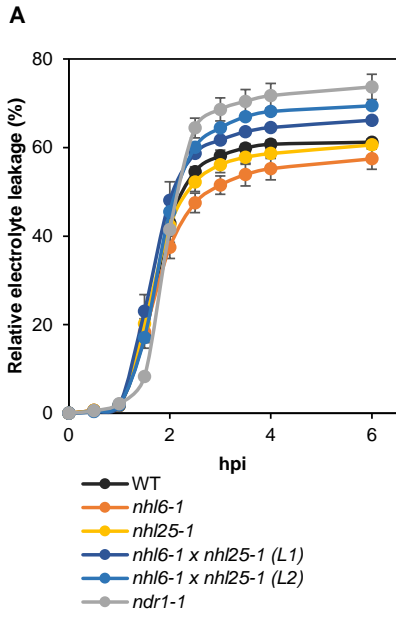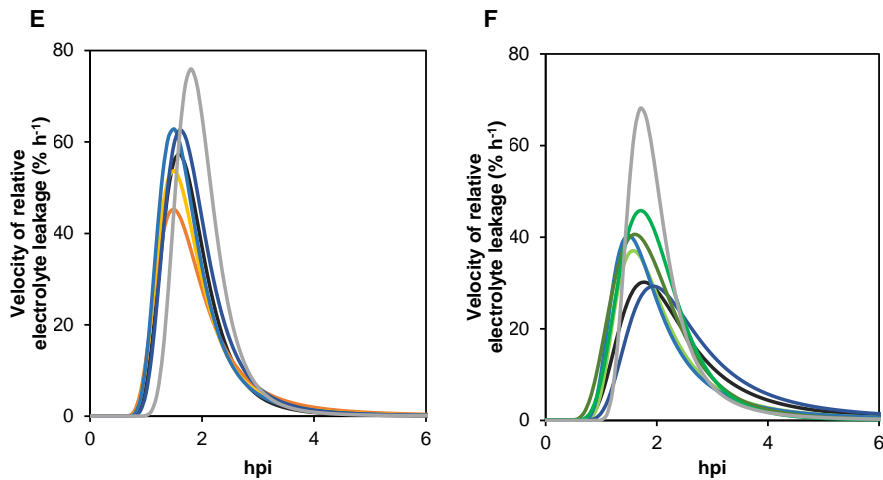
Figure 3.26: Kinetic analyses of electrolyte leakage upon infection of *nhl* mutants by avirulent *Pst*(*avrRpm1*)

(A, B) Kinetic analyses of relative electrolyte leakage were performed over 6 hpi. Thirty leaf discs from ten different plants were vacuum-infiltrated with bacterial suspension (in 10 mM $MgCl_2$), and three biological sets of ten leaf discs each were investigated per genotype. The total ion leakage, defining the maximum ion conductance per genotype (100%), was determined for autoclaved samples (2.10.4). The data for 0 hpi were obtained right after infiltration. $MgCl_2$-infiltrated samples served as negative controls and showed very low electrolyte leakage (< 5%, data not shown). Different batches of plants were used in two independent experiments shown in A and B. (C, D) The relative electrolyte leakage of different genotypes shown in A and B was statistically analyzed for 6 hpi. (E, F) The kinetics of velocity change of electrolyte leakage was analyzed as the derivative function using the data from A and B, respectively. Different letters indicate statistically significant differences (One-way ANOVA, Tukey's test, $p < 0.05$). Data are representative for two independent experiments. Method establishment and experiments were carried out with major contributions of Dr. Thanh-Hao Nguyen (University of Hamburg, Hamburg, Germany).

Analyses of the temporal changes in relative electrolyte leakage indicated a higher maximal velocity of electrolyte leakage of the double and triple mutants vs. WT, and that the time needed to reach the maximal velocity (i.e., t_{max}) was shorter (Figure 3.26E, F), however, these points of time were not significantly different in statistical analyses (data not shown). Taken together, the double and triple *nhl* mutants (contrary to the single mutants) showed a detectable phenotype upon *Pst*(*avrRpm1*) infection in terms of elevated relative ion leakage (6 hpi) suggesting that (i) NHL4, NHL6, and NHL25 have partly redundant functions in innate immunity and (ii) they play a role in restricting cell death induced by HR in RPM1-triggered ETI.

For avirulent *Pst*(*avrRpt2*), electrolyte leakage was initiated more slowly and showed interesting differences in kinetics for WT and *ndr1-1* compared to *Pst*(*avrRpm1*) (Figure 3.27A – D). The *ndr1-1* mutant showed very low relative electrolyte leakage over time that

progressed at roughly constant velocity (Figure 3.27), which is consistent with the reported major reduction of HR in this mutant (Century et al., 1995). HR mediated by RPS2 is strictly NDR1-dependent and largely suppressed in *ndr1-1* (Century et al., 1995; Aarts et al., 1998; Hofius et al., 2009). By contrast, electrolyte leakage apparently developed in WT but was initiated more slowly compared to that caused by *Pst*(*avrRpm1*).
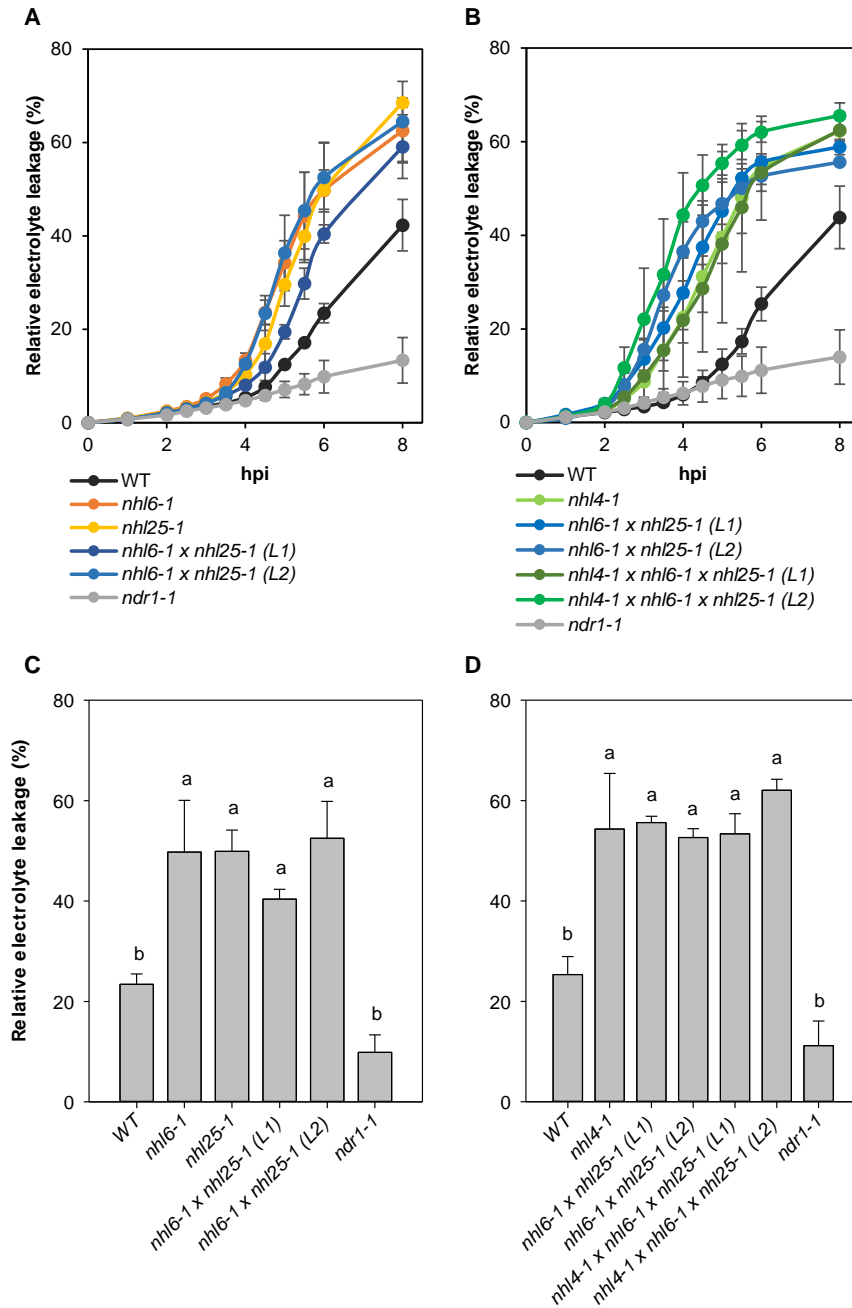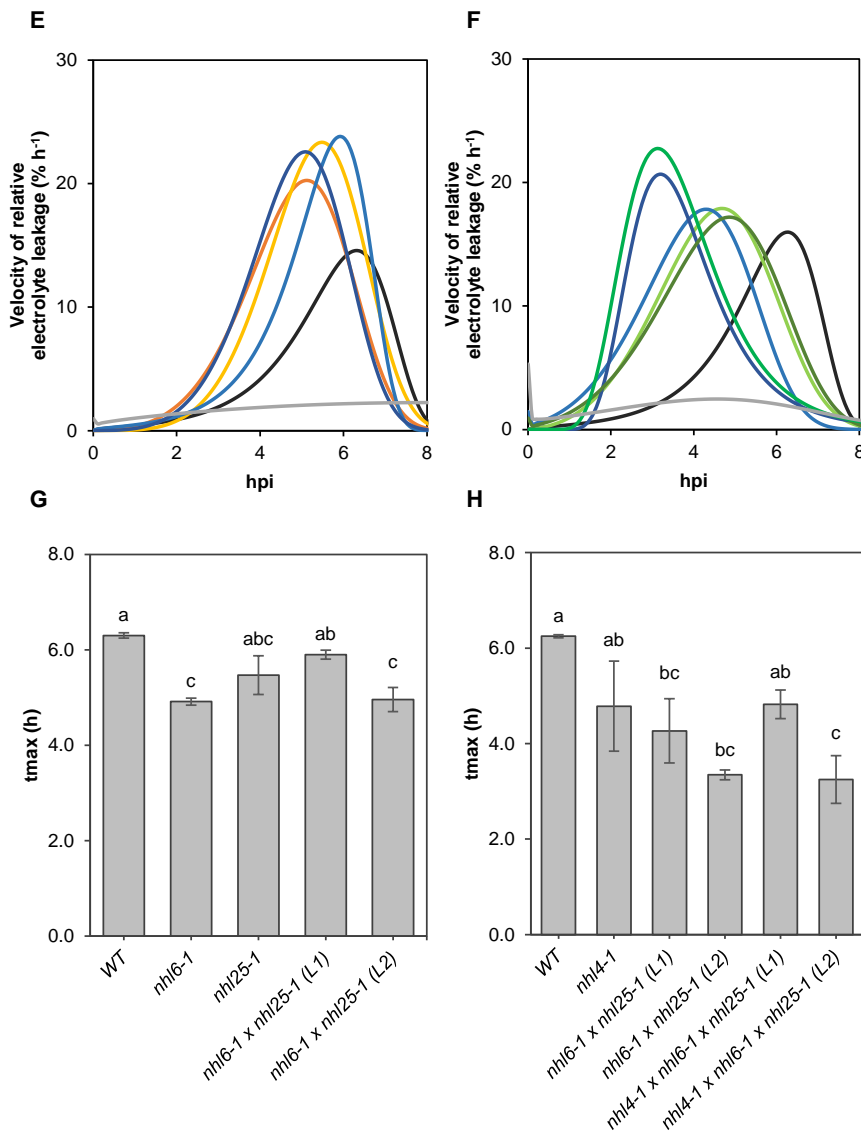
Figure 3.27: Kinetic analyses of electrolyte leakage upon infection of *nhl* mutants by avirulent *Pst*(*avrRpt2*)

(A, B) Kinetic analyses of relative electrolyte leakage were performed over 8 hpi. Relative electrolyte leakage was higher for the single, double, and triple *nhl* mutants compared to WT and *ndr1-1*. For details of the experimental design, see Figure 3.26. (C, D) The relative electrolyte leakage in different genotypes 6 hpi was statistically analyzed. (E, F) The kinetics of velocity change of electrolyte leakage was analyzed as the derivative function using the data from A and B, respectively. (G, H) The time point at which the change of electrolyte leakage was at maximum (t_{max}), was determined for the *nhl* mutants in comparison with WT. Data are representative for two independent experiments. The method of statistical analysis is explained in Figure 3.26. Experiments were carried out with major contributions of Dr. Thanh-Hao Nguyen (University of Hamburg, Hamburg, Germany).

Differences in the kinetics of relative electrolyte leakage progression were observed between WT, *ndr1-1*, and *nhl* mutants. Most intriguingly, the single, double, and triple mutants developed electrolyte leakage more rapidly compared to WT (Figure 3.27A, B). For instance,

the three single mutants already showed higher relative electrolyte leakage 6 hpi, e.g. 54% for *nhl4-1* (Figure 3.27D) and approx. 50% for *nhl6-1* and *nhl25-1* (Figure 3.27C), compared to WT (< 25%) and the *ndr1-1* mutant (< 11%). The differences were statistically significant. Here, however, electrolyte leakage did not differ significantly between the single mutants (*nhl6-1* and *nhl25-1*) and their two double mutants (Figure 3.27C). As expected, the additional disruption of *NHL4* did not cause a further increase of electrolyte leakage (Figure 3.27D). These data indicated a non-redundant function of NHL4, NHL6, and NHL25 in negatively regulating HR.

Because the time-point at which the change in relative electrolyte leakage was maximum (referred to as t_{max}) differed between WT and *nhl* mutants (Figure 3.27E, F), the values were statistically analyzed (Figure 3.27G, H). Due to its minimal degree and constant velocity in electrolyte leakage increase, *ndr1-1* was excluded from this analysis. The *nhl6-1* mutant showed a t_{max} of 4.8 h, while it was 6.3 h for WT. Upon statistical analysis among biological replicates, the RPS2-triggered HR occurred significantly earlier in *nhl6-1* than in WT (Figure 3.27G). Likewise, the *nhl4-1* (t_{max} = 4.8 h) and *nhl25-1* mutants (t_{max} = 5.5 h) showed accelerated electrolyte leakage and HR development than WT (Figure 3.27G, H), respectively, but these differences were not statistically significant. One of the two double (*nhl6-1 x nhl25-1*) mutant lines acted like *nhl6-1* with significantly earlier HR (line 2, t_{max} = 4.9 h; Figure 3.27G). In the second independent experiment, even both double mutant lines showed significantly faster acceleration of HR compared to WT (4.3 and 3.3 h for line 1 and line 2 vs. 6.3 h for WT; Figure 3.27H). The data suggested that primarily the loss of function of *NHL6* rather than of *NHL25* caused HR acceleration in the two double mutant lines.

As the single, double, and triple mutants showed similar magnitude of electrolyte leakage, the results suggested that NHL4, NHL6, and NHL25 play important, non-redundant, and non-additive roles in restricting and slowing down the cell death during HR triggered by RPS2. Kinetic analyses of changes in HR revealed that NHL6 might play the most important role in the restriction of HR acceleration against *Pst*(*avrRpt2*).

4 DISCUSSION

4.1 The monomeric blue fluorophore mCer in combination with the yellow fluorophore EYFP or mVenus is sufficient to prevent fluorophore-dimerization based piggy-back import

In live cell imaging, GFP variants are widely used as reporter genes and cellular markers in subcellular localization studies (Tsien, 1998). The most common application of GFP is to investigate the targeting of proteins to organelles, their trafficking pathways, and molecular interactions between proteins. In peroxisome research, novel peroxisomal proteins are commonly found by proteome or bioinformatics analyses and experimentally verified by *in vivo* subcellular localization studies using different GFP variants. However, precautions must be undertaken because some GFP variants are reported to dimerize at high concentration (Zacharias et al., 2002). This is particularly relevant in peroxisome research because the organelle is capable of piggy-back import (1.1.3; Glover et al., 1994; Islinger et al., 2009; Kataya et al., 2015). If using different spectral variants of GFP for labeling both, the protein of interest and the peroxisomal matrix marker, this could possibly result in piggy-back import of a non-peroxisomal protein of interest into peroxisomes due to heterodimerization of the GFP variants. Hence, thorough negative controls need to be routinely performed in peroxisome research, such as using an unmodified version of the same fluorophore that needs to remain cytosolic (and possibly partly nuclear) and shall not be imported into peroxisomes to any degree (Skoulding et al., 2015). When publishing the FAST method (Li et al., 2009), however, such negative controls were not suggested to be required nor the problem of unspecific piggy-back import into peroxisomes due to fluorophore dimerization was mentioned and discussed.

It was first discovered in this study and published by our group that unmodified EYFP and EYFP-AtIAN13, both lacking any PTS, were co-imported into peroxisomes in the presence of the peroxisomal marker CFP-PTS1 in two specific plant expression systems, namely Arabidopsis seedlings (Figures 3.1A and 3.2) and tobacco leaves (Falter et al., 2019). Conversely, co-expression of two monomeric fluorophores, *mVenus* and *mCer-PTS1*, prevented the artificial peroxisomal import of untagged mVenus (Figure 3.1D). The reason underlying this mechanism could be explained by an inverse correlation between protomer dimerization and the K_D. The presence of the A206K mutation in both mCer-PTS1 and mVenus increases the K_D from 0.1 to 70 mM and thereby reduces homodimerization significantly (Zacharias et al., 2002). Thus, the

A206K mutation prevented heterodimerization between these two fluorophores and the import of mVenus into peroxisomes.

Due to their enhanced fluorescence, EYFP fusions have been widely used in plant peroxisome research, thus many EYFP-containing expression vectors are available for sub-cloning of the gene of interest (GOI) and for *in vivo* subcellular localization studies. To be able to continuously take advantage of this material, we next asked whether one monomeric fluorophore (mCer-PTS1) was sufficient in combination with EYFP to avoid fluorophore heterodimerization. Indeed, incorrect targeting of untagged EYFP to peroxisomes was abolished in the presence of mCer-PTS1 (Figure 3.1C). Likewise, EYFP-AtIAN13 was no longer peroxisomal upon replacement of CFP-PTS1 by mCer-PTS1 (Falter et al., 2019). The data revealed that co-expression of *mCer-PTS1* with one of two yellow fluorophores (*EYFP* and *mVenus*) fully prevented the piggy-back import of non-peroxisomal proteins into peroxisomes and allowed reliable analyses of pre-existing EYFP fusion proteins.

The underlying mechanism of how the A206K mutation in mCer-PTS1 could abolish fluorophore heterodimerization with EYFP was revealed by analyzing the dimeric structure of GFP. Dimerization of GFP variants occurs in a head-to-tail fashion mediated by two hydro-phobic interfaces of the β-barrels of the two protomers (Figure 4.1). A206 together with L221 and F223, all located in one hydrophobic interface between the protomers, form the main hydrophobic dimer contact (Yang et al., 1996). The A206 residue in the β-strand 10 of one protomer interacts with L221 and F223 in the β-strand 11 of the other protomer. Thus, the dimer structure shows a twofold axis of symmetry in which the two A206 residues of both protomers are located nearly below each other, forming two contact sites (Figure 4.1). A number of hydrophilic residues are also involved in strengthening the dimer (Yang et al., 1996). Therefore, the A206K mutation in mCer disrupts one of two contact sites in the heterodimer, increases the K_D of this heterodimer, and sufficiently abolishes fluorophore dimerization under the cytosolic protein concentrations generated in Arabidopsis seedlings (Zacharias et al., 2002; Falter et al., 2019).
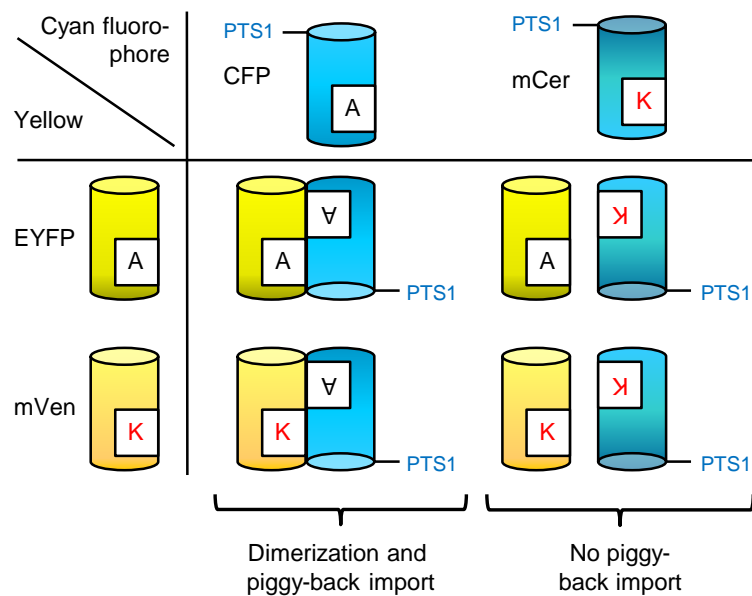
Figure 4.1: Prevention of piggy-back import of untagged yellow fluorophores into peroxisomes by usage of a monomeric peroxisome marker.

Two untagged yellow fluorophores, EYFP and mVen, were imported into peroxisomes by piggy-back import upon co-expression with *CFP-PTS1* (but not with *mCer-PTS1*) in transiently transformed Arabidopsis seedlings and tobacco leaves. Heterodimerization is mediated by A206 located in one hydrophobic interface of each monomer. The EYFP:CFP interaction could be abolished if A206 was replaced by K in both mCer and mVen. Application of the peroxisome marker mCer-PTS1 was sufficient to prevent piggy-back import of EYFP or mVen into peroxisomes due to fluorophore-dimerization. The image is taken from Falter et al. (2019) with permission from the publisher.

Even though the K_D of mVenus is very high (Zacharias et al., 2002), co-expression of untagged *mVenus* with *CFP-PTS1* caused piggy-back import (Figure 3.1B). This is in contrast to EYFP and mCer-PTS1 which showed abolished piggy-back import. Thus, it seemed that the impact of the A206K mutation on heterodimerization was fluorophore dependent. Two reasons may account for this phenomenon: (i) the high cytosolic concentration of the mVenus monomer due to abolished homodimer formation (Falter et al., 2019) and (ii) the T203 residue (characteristic for mVenus) is located closely to the dimer interface, thereby slightly enhancing the interaction strength with CFP-PTS1 (Nagai et al., 2002). Notably, as peroxisomal protein import is a quick process for the peroxisome marker CFP-PTS1 containing the canonical PTS1 SKL>, compared to untagged mVenus, the cytosolic concentration of CFP-PTS1 is lower, thereby minimizing the homodimer formation of CFP-PTS1 in the cytosol. Together with the high cytosolic abundance of the mVenus monomer, heterodimerization between mVenus:CFP-

PTS1 must have occurred at a low level in the cytosol and was further increased by peroxisomal import, which takes the heterodimer out of cytosolic equilibrium. Conversely, EYFP lacking the A206K mutation (low K_D of 0.1 mM) favors homodimerization over heterodimerization with mCer-PTS1, and thus EYFP:mCer-PTS1 heterodimerization might have been significantly reduced compared to that of mVenus:CFP-PTS1, as the former remained undetectable by peroxisomal targeting analysis (Falter et al., 2019).

Notably, this unexpected piggy-back import of untagged EYFP and mVenus into peroxisomes was only observed in two of five common transient expression systems, Arabidopsis seedlings and tobacco leaves, but not in onion epidermal cells, Arabidopsis and tobacco protoplasts (Falter et al., 2019). As mentioned above, the degree of piggy-back import is determined by the cytosolic concentrations of the fluorophores, which are determined by the rates of transcription (here driven by the *CaMV 35S* promoter), protein synthesis, protein import into peroxisomes, and protein degradation. Contrary to protoplasts and onion epidermal cells, which represent stressed systems, gene expression in entire Arabidopsis seedlings and tobacco plants is likely more efficient, thereby generating higher protein concentrations and promoting fluorophore dimerization and piggy-back import (Falter et al., 2019).

Taken together, it was concluded that monomeric fluorophores are the variants of choice for subcellular localization studies in transiently transformed Arabidopsis seedlings and tobacco leaves. These fluorophores allow reliable analyses of peroxisome targeting of the protein of interest. In addition, EYFP fusions can continuously be used in combination with the monomeric peroxisome marker mCer-PTS1 to benefit from the pre-existing constructs and the enhanced fluorescence characteristic of EYFP in applications of confocal microscopy. Furthermore, to detect possible unspecific peroxisome targeting, proper controls including single transformation using EYFP-tagged proteins of interest and double transformations co-expressing untagged EYFP with the peroxisome marker should always be performed simultaneously (Falter et al., 2019).

4.2   Description of a novel vesicular trafficking pathway

Based on the findings of peroxisome targeting and several trafficking intermediates for NHL4, NHL6, and NHL25 in this study, a novel multi-step vesicular targeting pathway to peroxisomes has been described for these proteins. The following chapters discuss (i) the significance of the PTS1 of these NHLs in peroxisome targeting (4.2.1 and 4.2.2), (ii) the targeting of NHLs to non-

peroxisomal vesicles as an intermediate step before reaching peroxisomes as the final destination (4.2.3), and (iii) the role of the transmembrane domain (TMD) and its proximal 20 aa in endoplasmic reticulum (ER) targeting and the involvement of ER-derived vesicles in carrying these signal anchor proteins to peroxisomes (4.2.4).

4.2.1 NHL4, NHL6, and NHL25 possess functional PTS1 domains

The three proteins of interest harbor a single predicted N-terminal TMD and also possessed the novel feature of a predicted C-terminal PTS1. Up to now, in addition to the PTS2 and few internal signals, the PTS1 is the major signal that directs soluble matrix proteins to their peroxisomal destination (1.1.3; Reumann, 2004). Only a single membrane protein, glucose-6-phosphate transporter 1 (GPT1), which carries the PTS1 (AKL>), has been very recently reported to be dually targeted to the peroxisomal membrane (Baune et al., 2020), next to its predominant localization and function in the inner plastidic membrane. Except for this protein, none of the known peroxisomal membrane proteins (PMPs) from plants, animals, and fungi are reported to carry a PTS1 and/or to require it for peroxisome targeting. The targeting efficiency of PTS1 proteins depends on the nature of the PTS1 tripeptide and the neighboring residues (Neuberger et al., 2003a). To investigate whether a protein indeed possesses a functional PTS1 domain that is sufficient to direct a reporter protein to peroxisomes, the C-terminal 10-15 aa are generally fused N-terminally with EYFP (Reumann et al., 2007; Ma and Reumann, 2008). In this study, the function and strength of the predicted PTS1s in peroxisome targeting was investigated in intact Arabidopsis seedlings. Indeed, the three C-terminal decapeptides of NHL4, NHL6, and NHL25 were sufficient to direct EYFP to peroxisomes. Peroxisome targeting was observed nearly quantitatively in all cells and as quickly as the marker at early time points, i.e. 2 days post co-cultivation (dpc), and was well detectable against only a weakly cytosolic fluorescent background (Figure 3.3). This data demonstrated that the three NHL proteins indeed possess functional PTS1 domains of relatively high strength, particular in case of the non-canonical PTS1 tripeptides of NHL6 (LRL>) and NHL25 (FRL>). The results further supported the previous data obtained in onion epidermal cells (for NHL6 and NHL25, Kataya 2011; for NHL4, Sørhagen and Reumann, unpubl. data).

The canonical PTS1 motif, (S/A/C)-(K/R/H)-L>, is largely conserved between yeasts, mammals, and plants but also displays sequence variation between kingdoms (1.1.3). For instance, canonical plant PTS1 tripeptides match the consensus sequence of the above-mentioned PTS1 motif and allow considerable sequence variations (Reumann, 2004; Reumann

et al., 2016). Moreover, with the advantages of bioinformatics tools, many novel plant peroxisomal matrix proteins were predicted to contain non-canonical PTS1s and were experimentally validated to be targeted to peroxisomes *in vivo* (Lingner et al., 2011). Non-canonical PTS1s display a non-canonical amino acid in one of the three positions of the PTS1 tripeptide. According to the peroxisome targeting prediction algorithm (Lingner et al., 2011; Reumann et al., 2012), NHL6 (LRL>) and NHL25 (FRL>) carry non-canonical PTS1s with moderate prediction scores of 0.49 and 0.54, respectively, slightly above the prediction threshold (0.41), translating into a peroxisome targeting probability of 87% (NHL6) and 95% (NHL25), which is higher than the so-called balanced targeting probability threshold (50%). As predicted, with respect to peroxisomal targeting efficiency, the C-terminal 10 aa containing the PTS1 tripeptides of NHL6 and NHL25 were capable of targeting EYFP to peroxisomes as efficiently as that of NHL4 (prediction score: 0.91; targeting probability: 100%) (3.2.1.1; Figure 3.3).

The peroxisome targeting pathways and mechanisms are widely conserved in eukaryotes. Regarding the import mechanism of PTS1 proteins, the C-terminal TPR domain of Pex5 binds and guides PTS1 cargos to peroxisomes (Gatto et al., 2000; Stanley et al., 2006; Hagen et al., 2015). The N-terminal domain of AtPex5 is responsible for the interaction with the PTS2 receptor AtPex7 and with AtPex14, one component of the membrane docking complex (Nito et al., 2002). In this study, it was reasoned that if NHL4 (AKL>), NHL6 (LRL>), and NHL25 (FRL>) possess functional PTS1s, their C-terminal PTS1s should be recognized and bound by the cytosolic PTS1 receptor AtPex5 or the yet unknown homolog of yeast Pex9. Hence, the yeast two-hybrid (Y2H) approach was used to investigate NHLx:AtPex5 interaction. Notably, the recombinant C-terminal TPR domain of AtPex5 alone has a similar binding affinity for PTS1 peptides as the recombinant full-length AtPex5 (Skoulding et al., 2015). Thus, both AtPex5 constructs were N-terminally fused with the GAL4 DNA binding domain. Their putative interacting proteins, i.e. full-length NHLs, the C-terminal 30 aa domain of NHLs, and the short control PTS1 peptides (for positive and negative interaction) were N-terminally fused with the GAL4 activation domain (AD). The full-length AtPex5 had shown autoactivation (data not shown), but this was not observed when using the TPR domain of AtPex5. The TPR domain of AtPex5 indeed interacted with the canonical PTS1 of NHL4, as other canonical PTS1s used as positive controls (Figure 3.4). A different interaction strength was observed between the longer NHL4 protein construct (150 aa lacking the short N-terminal domain and the TMD, i.e. 80 aa) (Figure 3.4B) and the short peptide of NHL4 comprising its C-terminal 30 aa (Figure

3.4C). The latter displayed a stronger interaction with the TPR domain of AtPex5 as the yeast cells grew better in the absence of His and showed detectable β-galactosidase activity. Such difference in interaction strength could result from differences in (i) correct native folding, (ii) sterical hindrance of protein-protein interactions, and (iii) cellular protein concentration of the two NHL4 variants. First, in the elegant and widely applied Y2H system, the two constructs differ in native folding. In the longer construct, the N-terminal deletion of the short N-terminal domain and the single TMD are unlikely to have affected protein folding. Second, the shorter C-terminal 30-aa construct possibly leads to an enhanced surface exposure of the PTS1 in the fusion protein due to the lacking tertiary structure, thereby facilitating the AtPex5 interaction. Third, the synthesis rate depends on the transcript length and ribosome density. The translation is more efficient if transcripts have a high ribosome density. The longer the transcript, the smaller the ribosome density, meaning that the translation is less efficient (Fernandes et al., 2017). Therefore, due to higher translation efficiency the shorter construct might lead to a slightly higher concentration of the C-terminal 30 aa fusion protein in the nucleus compared to the longer fusion protein.

The TPR domain of tobacco Pex5 was shown to bind many PTS1 variants, from which a plant PTS1 motif was deduced ((A/C/G/P/S/T)-(H/K/L/N/R)-(I/L/M/Y)>; Kragler et al., 1998). In addition, tobacco Pex5 could also bind weakly non-canonical PTS1s that deviated from the PTS1 motif such as SQL>, SML>, SSL>, and SAL> (Kragler et al., 1998). Consistently, the TPR domain of AtPex5 also bound peptides ending with the PTS1 tripeptides in this study, i.e., AKL>, ARL>, SKL>, and SRL> (Figure 3.4). However, the C-terminal 30 aa constructs of NHL6 and NHL25 were not detectably bound by TPR(AtPex5) in the Y2H assay. This was surprising because the shorter C-terminal decapeptides had directed EYFP to peroxisomes (Figure 3.3), most likely due to interaction with AtPex5. Three explanations are possible. First, the C-terminal 30-aa domains of NHL6 (LRL>) and NHL25 (FRL>) containing non-canonical PTS1s, which indicated a low affinity to AtPex5, might interact weakly with TPR(AtPex5), and this interaction might have been below the detection limit of the Y2H assay. Second, in Y2H analyses, the fusion proteins of interest may accumulate at different levels due to the different expression control by different truncated versions of the *ALCOHOL DEHYDROGENASE 1* promoter in pGBKT7 and pACT2, which generally results in high and moderate expression level of the GOI, respectively (Clontech Protocol No. PT3024-1; Tornow and Santangelo, 1990; Ruohonen et al., 1995). Hence, nuclear concentration of the GAL4 AD fusion with the C-terminal 30 aa was probably lower than its counterpart TPR(AtPex5). This issue could

significantly influence the interaction strength of two proteins if the interaction is natively weak as here. Third, the residues preceding of the C-terminal decapeptides in NHL6 and NHL25 (pos. -11 to -30) could have reduced the weak binding affinity of NHL6 and NHL25 to the receptor AtPex5. This argument, however, is unlikely because the length known to be important in PTS1 protein import is 12-14 aa.

Similar to the 30-aa domain, the longer NHL6 and NHL25 fusion proteins (lacking the short N-terminal domain and the single TMD) did not interact with TPR(AtPex5) (Figure 3.4) possibly because of the same reasons discussed above for the longer NHL4 protein construct: (i) the unequal nuclear abundance between these long NHL6 and NHL25 fusions and TPR(AtPex5), and (ii) the efficiency of synthesis rate depending on the transcript length. Thus, these long NHL6 and NHL25 fusions might occur at lower concentrations compared to the C-terminal 30-aa domain, limiting the interaction possibility with TPR(AtPex5). Altogether, an immunoblotting analysis could be conducted to confirm such low protein levels; to verify the interaction between NHL6 and NHL25 with AtPex5, it is suggested to use additional methods such as bimolecular fluorescence complementation and *in vitro* co-immunoprecipitation assays.

4.2.2   NHL4, NHL6, and NHL25 constitute a novel family of peroxisomal proteins

The above-mentioned characterization of functional PTS1 domains by *in vivo* subcellular targeting analyses (for NHL4, NHL6, and NHL25) and by Y2H TPR(AtPex5) interaction studies (for NHL4) strongly suggested that the full-length proteins are peroxisomal despite their unusual nature as PMPs. Indeed, peroxisome targeting of the full-length proteins could be well detected for all three NHLs in Arabidopsis seedlings, even though at a slightly later expression time point of 3 dpc (Figure 3.6D – F) compared to mCer-PTS1, which was quantitatively targeted to peroxisomes 2 dpc. Only NHL25 was already detectable in peroxisomes 2 dpc but at a low percentage of double transformed cells (approx. 5% of cells showing peroxisome targeting; data not shown) compared to 3 dpc (20%; Figure 3.7). Altogether, the present data indicated that NHL4, NHL6, and NHL25 are localized in peroxisomes, but the targeting was more slowly and was well detectable for all the three at a later expression time point, i.e. 3 dpc.

The relatively slow protein targeting to peroxisomes in transiently transformed Arabidopsis seedlings was similarly observed in preliminary results obtained in tobacco and Arabidopsis protoplasts (Kataya, 2011; Crappe, 2016). While the marker clearly labeled

peroxisomes after 24 hours post transformation (hpt), the NHLs became detectable in peroxisomes only 48 hpt (Kataya, 2011; Crappe, 2016). The peroxisomal import efficiency of PTS1 proteins depends on of the method of transient transformation. In general, peroxisome targeting is observed rapidly after transient transformation, e.g. 5 – 8 h for yeasts (Faber et al., 2002), 18 h in mammalian cells (Walton et al., 1992), 18 – 24 h in onion epidermal cells (Skoulding et al., 2015), 18 – 48 h in Arabidopsis protoplasts (Pan et al., 2018), and 48 h for *Agrobacterium*-mediated transient transformation of tobacco leaves (Reumann et al., 2009). As not all double transformed cells were observed with EYFP-NHL-labeled peroxisomes, the peroxisome targeting efficiency was < 35% of the double transformed cells 3 and 4 dpc (Figure 3.7). Consistently, in Arabidopsis protoplasts, EYFP-NHL4 was found in peroxisomes in 20% of double transformed protoplasts, and this ratio was approx. 10% for NHL6 and NHL25 48 hpt (Crappe, 2016). These data indicated that the population of double transformed cells displays an atypically high heterogeneity in terms of the speed of the entire NHL protein biogenesis pathway to peroxisomes. Those cells with detectable peroxisome targeting of NHLs must have been faster in NHL biogenesis. On the other hand, those cells with non-peroxisomal targeting of NHL4, NHL6, and NHL25 were delayed in NHL biogenesis. The relatively slow peroxisome targeting of NHL4, NHL6, and NHL25 compared to standard PTS1 matrix proteins is fully consistent with the description of a complex multi-step vesicular targeting pathway of these NHLs to peroxisomes. Notably, other than containing functional PTS1s, these NHL proteins were validated to represent integral membrane proteins (NHL4: Chowdhary and Reumann, unpubl. data; NHL25: Crappe, 2016). Hence, these proteins were deduced to traffic to peroxisomes *via* a novel peroxisomal targeting pathway.

The above-mentioned results were obtained *in vivo* upon transient gene expression from the *CaMV 35S* promoter. Especially for genes that are hardly expressed constitutively, as are the *NHL* genes, this promoter is the method of choice to visualize these proteins in subcellular targeting analyses. However, there are also important advantages of GOI expression from the native promoter. First, this produces a reporter protein at a level very similar to that of the endogenous protein. Second, the activity of the native promoter ensures cell and/or tissue type-specific expression of the GOI. These two advantages help preventing any intracellular changes caused by inappropriate GOI expression sites and/or by overproduction of the protein of interest.

In addition, N-terminal or C-terminal fusions of the reporter protein could result in masking a targeting signal located at the same position. Internal fusions of fluorescence tags have been suggested to circumvent this problem (Tian et al., 2004). Furthermore, stable transgenic lines expressing the GOI could prevent possible ambiguities, of transient transformation systems. Therefore, as shown by Díaz (2020), NHL4 (representatively chosen) was internally fused with EYFP, and the construct was expressed from the native promoter in transgenic Arabidopsis lines. One transgenic line with moderate EYFP fluorescence in the T_2 generation was selected and used to transiently express the peroxisome marker *mCer-PTS1* in this study. Indeed, peroxisome targeting of NHL4 was detected (Figure 3.15), fully consistent with the data previously derived from transiently transformed Arabidopsis seedlings (Figure 3.6). Taken together, these data provide conclusive evidence for peroxisomal localization of NHL4, NHL6, and NHL25.

Interestingly, NHL25 was targeted to peroxisomes most efficiently and was best detectable compared to the other two. The protein was peroxisomal in 20% (3 dpc), 34% (4 dpc), and 25% (5 dpc) of double transformed cells (Figure 3.7). Therefore, the PTS1-dependency of peroxisome targeting of NHL25 was further characterized in greater detail representatively for the entire sub-clade. The peroxisome targeting efficiency of NHL25 was indeed dependent on its non-canonical PTS1 (FRL>), because its deletion caused a reduction from 26% (3 dpc) and 14% (4 dpc) for full-length NHL25 to less than 8% for the PTS1-lacking protein (Figure 3.12B). Hence, the PTS1 (FRL>) is the major signal for peroxisome targeting but is not the only signal, as peroxisome targeting of the deletion construct was not completely abolished. In the opposite way, it was not possible to increase peroxisome targeting of NHL25 by replacing the non-canonical and presumably relatively weak PTS1 with a canonical PTS1, SRL> (EYFP-NHL25(SRL>); Figure 3.12A). The peroxisome targeting efficiency remained rather constant, i.e. 24% 3 dpc compared to 26% for WT NHL25 (Figure 3.12B). Taken together, peroxisome targeting of NHL25 relied on its PTS1 (FRL>) and a second PTS to be identified.

To identify the second PTS in NHL25, it was hypothesized to be located next to the single N-terminal TMD, as found in other PMPs, e.g. AtPex3-2 (Hunt and Trelease, 2004). Therefore, the TMD of NHL25 predicted by TMHMM 2.0 and extended on each side by 20 aa (aa 46 – 106; Figure 4.2), was used to investigate whether the construct contained the information sufficient for ER targeting and possibly also for peroxisome targeting. When fused N-terminally with EYFP, the protein remained largely in the ER (Figure 3.13), demonstrating

that (i) this 61-aa domain of NHL25 including the TMD serves as a signal anchor that is sufficient to direct a reporter to the ER and (ii) an NHL25 domain located outside of this construct reduces the residence time of NHL25 in the ER membrane, most likely by active NHL25 concentration in defined ER subdomains and by carrier vesicle budding off from the ER. Moreover, peroxisome targeting was nearly completely abolished for this TMD construct of NHL25 (approx. 2% of double transformed cells; Figure 3.12B). This low efficiency could not be considered reliable, therefore, the TMD of NHL25 (predicted by TMHMM 2.0) and its proximal 20 aa were not sufficient to direct a reporter protein to peroxisomes. Instead, the second unknown PTS of NHL25 might be located in other domains, including the short N-terminal domain, the LEA_2 domain, and the C-terminal domain upstream of the PTS1. Future studies shall reveal the localization of this second signal for peroxisome targeting. Additionally, based on the PHYRE2 prediction (Figure 4.2), an atypically long TMD of 30 aa with only 11 aa upstream and 20 aa residues downstream were included. Interestingly, the four C residues in the beginning of the PHYRE2-predicted TMD are highly conserved between NHL4, NHL6, and NHL25, possibly indicating a regulatory role of intra- or intermolecular disulfide bridges in NHL function.
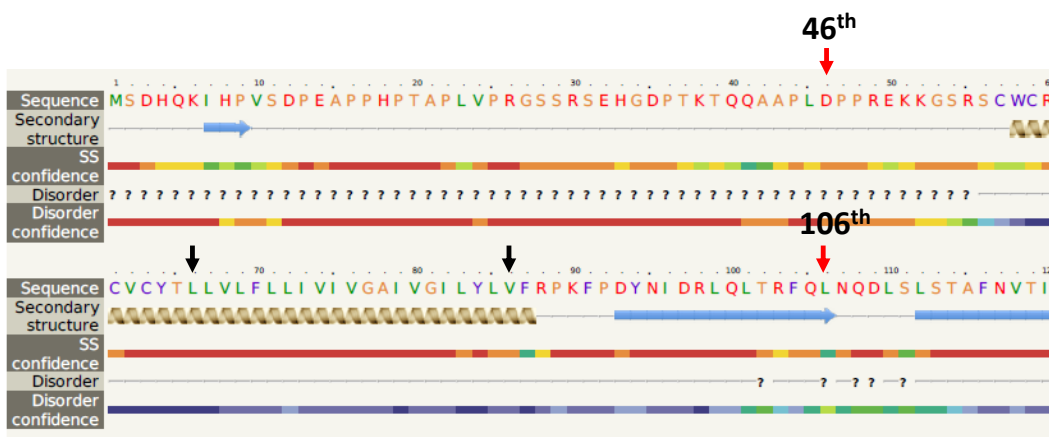
Figure 4.2: Secondary structure prediction of the first 120 aa of NHL25

The TMD of NHL25 was predicted from aa 66 to 86 (length 21 aa) by TMHMM 2.0 (indicated by black arrows) and from aa 58 to 87 (atypically long α-helix of 30 aa) by PHYRE2. The red arrows indicate the chosen protein region, including the TMHMM-predicted TMD and the proximal 20 aa (aa 46 – 106).

4.2.3 The representative subclade member, NHL4, is targeted to peroxisomes *via* vesicle-like structures

As discussed above, the three NHLs, each contains an N-terminal TMD, were predicted to traffic to peroxisomes *via* a novel targeting pathway that involves a PTS1 (4.2.1 and 4.2.2). Notably, in yeasts and mammals, class II PMPs have been experimentally found to be targeted to the ER and to traffic in pre-peroxisomal vesicles to peroxisomes (1.1.4). Reliable data, however, are largely missing for plants. In this study, in cells expressing *NHLx* alone, the three NHLs were observed in puncta with a size of 0.2 – 1.3 µm in diameter (Figure 3.5A – C). In double transformed cells, the NHLs were targeted to peroxisomes and non-peroxisomal puncta (Figure 3.6A – F). In the majority of double transformed cells the NHLs were targeted to non-peroxisomal puncta rather than to peroxisomes, namely in approx. of 95% (NHL4), 96% (NHL6), and 80% (NHL25) 3 dpc (values were calculated based on the quantitative data in Figure 3.7). Such structures could be derived either from the ER or the endosomal system. As these structures displayed a high mobility (shown for NHL4 in Figure 3.8; for NHL6 and NHL25: data not shown), which are unlike protein aggregates. The shape of these structures was round with a relatively large size of approx. 0.2 – 0.7 µm (Figures 3.5A – C and 3.6A – C). Therefore, this data implied that the non-peroxisomal puncta could be intermediate vesicles carrying NHLs to peroxisomes, which would be quite similar to what had been described for class II PMPs. For instance, Pex14p, a class II PMP in yeast, started to be localized in non-peroxisomal puncta in the first 1.5 – 2 h after inducible expression of Pex3p in *Δpex3* yeast cells. Pex14p accumulated in peroxisomes 5 h later (van der Zand et al., 2010). Also, in Arabidopsis and tobacco suspension cells, the class II PMP Pex16 was found in both non-peroxisomal structures and peroxisomes 2 – 8 h after biolistic bombardment (Karnik and Trelease, 2007). Taken together, the relatively specific targeting of NHLs to non-peroxisomal puncta of similar small size argued against unspecific targeting and protein aggregates, which generally are larger or vary more in size. The data also suggested that the puncta represented ER-derived cargo vesicles that delivered NHLs from the ER to peroxisomes.

This hypothesis was strongly supported by other experimental evidence in this study, which showed that a small portion of the small NHL4-labeled puncta was in close physical association with mCer-PTS1-labeled peroxisomes in transiently transformed Arabidopsis seedlings (Figures 3.6A and 3.8). The attachment of non-peroxisomal puncta with mature peroxisomes was observed for 7 sec (Figure 3.8) and even longer for more than 47 sec (n > 3;

data not shown), unequivocally demonstrating a real docking state of NHL4-labeled non-peroxisomal puncta. A similar physical association had been rarely observed in tobacco protoplasts, but the findings were inconclusive due to the lack of result reproduction and mobility characterization (Kataya, 2011; Crappe, 2016). This physical association was also found in stable transgenic lines expressing the internal NHL4 EYFP fusion constructs from the native promoter (*NHL4$_{pro}$:NHL4$_{1-21}$-EYFP-NHL4$_{22-239}$*) when additionally expressing the peroxisome marker *mCer-PTS1* transiently (Figure 3.15). In addition, the localization of EYFP-NHL4 in small puncta associated with a larger spherical structure observed in stable transgenic lines expressing the fusion construct either from the *CaMV 35S* (Figure 3.14A4 – B3) or from the native *NHL4* promoter (Figure 3.14C) resembled the above-mentioned docking structure.

It should be noted that a similar structural complex between peroxisomes and ER-derived vesicles has not yet been documented in the literature for any class II PMP in yeast and plants. In a *pex3* mutant of human cell lines, it has been recently shown that, when constitutively expressing *Pex3*, the protein was first and exclusively detected in mitochondria and later accumulated in presumably pre-peroxisomal vesicles. The pre-peroxisomal vesicles were shown to fuse with ER-derived vesicles containing Pex16 and further developed into mature peroxisomes, suggesting that peroxisomes could be *de novo* synthesized from both the ER and mitochondria (Sugiura et al., 2017). In this study, the observation of the docking structures was reliable, as it was confirmed not only in transiently transformed Arabidopsis seedlings but also in stable transgenic lines, in which either the *CaMV 35S* or the native promoter was used to control GOI expression. In the docking structure the puncta is thought to be pre-peroxisomal structures due to their small size, mobility, the lack of the peroxisomal matrix marker, and their docking to mature peroxisomes.

Notably, the TEM analyses investigating transiently transformed Arabidopsis seedlings overexpressing *EYFP-NHLs* from the *CaMV 35S* promoter for differences in vesicular compartments revealed a pronounced accumulation of small membrane-bound vesicles ($0.1 – 0.2$ µm) and few vesicle clusters (Figure 3.9A). Such vesicle clusters were undetectable in the seedlings transformed with the empty pBA002 vector (WT control; Figure 3.9B), indicating that the overexpression of *EYFP-NHLs* was the reason. As this kind of control did not express EYFP and could not be screened for successful transformants prior to sample fixation, it remained unclear transformed or untransformed cells were analyzed. For future ultrastructure analyses, a better control of *CaMV 35S* expression of EYFP alone would be needed. Such clusters of

vesicles were also observed in stable transgenic lines overexpressing *EYFP-NHL4* from the *CaMV 35S* promoter (data not shown). Furthermore, by confocal microscopy this kind of vesicle aggregation was also occasionally observed in transiently transformed Arabidopsis seedlings overexpressing *EYFP-NHLs* (Figure 3.5D – F) but not in transgenic lines expressing *NHL4* from its native promoter (data not shown). Hence, the vesicle clusters were likely caused by *NHL* overexpression. Altogether, the TEM data indirectly showed that the observed small membrane-bound vesicles (in clusters) could be carriers of NHLs. Nevertheless, the presence of NHLs in these vesicles remain to be demonstrated at the ultrastructure level in future studies. Thus, by TEM with immunogold labeling, it is suggested to use the two transgenic lines expressing *EYFP-NHLs* from their native promoters, which will not yield overexpression artifacts such as non-physiological vesicles. Altogether, the data supported the hypothesis that NHL4 is targeted to peroxisomes by a vesicular trafficking pathway.

To characterize whether the three NHLs indeed use the same vesicular trafficking pathway and identical vesicle intermediates, a co-localization study was conducted in which each of the *NHLs* was fused with either *EYFP* or *mCherry* and transiently co-expressed from the *CaMV 35S* promoter in Arabidopsis seedlings and analyzed by epifluorescence microscopy. Indeed, NHL6 co-localized in NHL4-labeled puncta 2 dpc (Figure 3.11), the time point when peroxisome targeting was not yet observed for one of the single proteins, implying that the fluorescent structures were not peroxisomes but represented non-peroxisomal vesicles. The data indicated that NHL4 and NHL6 use the same vesicular trafficking pathway, in good agreement with previous data of onion epidermal cells and Arabidopsis protoplasts (Kataya, 2011; Crappe, 2016). Similar to NHL4, the NHL6-labeled vesicle-like structures were sometimes observed in association with peroxisomes (Figure 3.6B). This data showed that not only NHL4 but also NHL6 traffics *via* vesicles to peroxisomes. The punctate fluorescence pattern (expressed from the *CaMV 35S* promoter) of EYFP and the NHL25 fusions with mVenus or mCherry, however, was very weak for unknown reasons and more challenging to observe by epifluorescence microscopy. The constraints prevented not only conclusive studies of co-localization together with either NHL4 or NHL6 but also the detection of fluorescent puncta in close physical association with peroxisomes. The cellular level of proteins with a regulatory function is often tightly regulated depending on the physiological conditions. Therefore, even though *EYFP-NHL25* was expressed from the *CaMV 35S* promoter, its weakly detectable fluorescence could result from its regulation at the protein level due to its regulatory function in plant immunity. In future studies, the expression of *NHL25* from a moderate, inducible or

native promoter might overcome the limitation of the *CaMV 35S* promoter observed here. Therefore, the generation of stable transgenic lines expressing EYFP-tagged variants of genomic *NHL6* and *NHL25* from their native promoters was initiated (Khan, Nguyen, and Reumann, unpubl. data).

4.2.4   NHL4 is targeted to peroxisomes *via* the ER and ER-derived vesicles

As proposed but hardly documented by live-cell imaging for yeasts, mammals, and plants, class II PMPs are targeted to the ER and subsequently to pre-peroxisomal vesicles prior to reaching peroxisomes (1.1.4). In previous studies, ER sorting of class II PMPs was observed to occur rapidly. For example, Pex14p started to be localized in the perinuclear ER and in puncta at the periphery of the ER 60 to 90 min after expression induction by galactose in *Δpex3* yeast cells (van der Zand et al., 2010). After 120 min, these ER proximal puncta were found in greater distance from the ER. Human Pex16 was visualized in peroxisomes 15 h after transfection without any trafficking intermediates and could only be detected in the ER in cells lacking peroxisomes (Kim et al., 2006). In Arabidopsis and tobacco suspension cells, AtPex16 was first detected in the perinuclear and reticular ER 2 – 4 h post bombardments and later in peroxisomes (Karnik and Trelease, 2007).

In this study, EYFP-NHL4 was detected in ER-like structures in Arabidopsis seedlings upon transient expression (Figure 3.5G). These structures, however, often vanished rapidly during imaging, maybe due to their weak signal intensity or because of very fast turnover and sorting in the ER. Fortunately, fast image acquisition was successful and enabled the capturing of yellow fluorescent ER-like structures labeled by EYFP-NHL4 4 dpc (Figure 3.5G). Interestingly, in cells containing these labeled ER-like structures, the puncta targeting of EYFP-NHL4 was not detectable, indicating that NHL4 was sorted to the ER first at the earliest stage of the trafficking pathway and was further directed to the vesicles which might originate from the ER. This data supported the hypothesis of the ER origin of NHL4-labeled vesicles. To verify the ER localization of NHL4, both *EYFP-NH4* fusions and the *ER-CFP* marker were transiently co-expressed in Arabidopsis seedlings, allowing co-localization studies. Similar technical problems, which occurred during imaging of these cells, led to limited data interpretation. However, the occasional observation of EYFP-NHL4-labeled perinuclear ER, which coincided with ER-CFP fluorescence (Figure 3.10A, B), provided evidence for the ER traffic of NHL4.

With the same ER-CFP marker, few ER-associated vesicles of unknown identity and a small size of approx. 0.2 – 0.5 µm in diameter were detected in addition to the tubular and

cisternal ER. Similarly, a low number of ER-associated vesicles was also observed in the study of Faso et al. (2009). The ER marker consists of the signal peptide of AtWak2 (He et al., 1999), CFP, and a C-terminal retention signal (HDEL>) to allow sufficiently high marker concentration in the ER lumen (Nelson et al., 2007). Thus, it is likely that the marker-labeled ER puncta observed in this study were vesicles trafficking between the ER and Golgi and consisting of coat protein complex II (COPII)- and/or COPI-coated vesicles. The size of the vesicles facilitated their characterization. According to TEM studies, plant COPI-coated vesicles are very tiny with 30 – 60 nm in diameter (Pimpl et al., 2000), invisible by light microscopy and restricted to the periphery of *cis* Golgi in higher plants (Hwang and Robinson, 2009). By contrast, the COPII-coated vesicles are larger with a diameter of 0.3 – 0.5 µm (Takagi et al., 2020) and thus are above the resolution limit of light microscopy. These COPII vesicles form at the so-called ER exit sites (ERES) where the COPII components are recruited to mediate the budding off of vesicles carrying secretory proteins. While the COPI-coated vesicles take part in the retrograde transport of proteins from *cis* Golgi to the ER, the COPII-coated vesicles mediate anterograde protein transport from the ERES to the *cis* Golgi (Brandizzi and Barlowe, 2013). Knockdown of Sec16B, an ERES-localized protein in mammals, resulted in disruption of the transport of Pex16 from the ER to peroxisomes, suggesting the involvement of Sec16B in the biogenesis of mammalian peroxisomes as well as of class II PMPs from the ER (Tani et al., 2011; Yonekawa et al., 2011). Also, earlier evidence of the involvement of the ER transport system was shown for the plant PMP, ascorbate peroxidase 3, which accumulated in the ER instead of peroxisomes after brefeldin A treatment, an inhibitor of the ER transport system (Mullen et al., 1999). Brefeldin A causes the disassembly of the Golgi complex and thus the Golgi redistributes to the ER, thereby directly preventing the formation of COPI- and indirectly also of COPII vesicles (Chardin and McCormick, 1999). Based on the vesicle size and the close tubular and cisternal ER association, it is likely that the detected ER-associated and CFP-labeled vesicles could represent COPII vesicles formed at the ERES (Figures 3.10D2 and F2).

Co-localization between ER-derived vesicles and EYFP-NHL4-labeled vesicles was additionally analyzed but challenging. Among approx. 100 analyzed double transformed cells, only a very low number of cells (2 per experiment, n = 2) contained ER-derived vesicles. This could be explained by a preferential labeling of tubular and cisternal ER by the ER-CFP marker over ER-derived vesicles (Nelson et al., 2007). In one cell, 5% of the total number of EYFP-NHL4-labeled vesicles (18 out of 380 vesicles) co-localized with 18% of the ER-derived vesicles labeled with ER-CFP (18 out of 102 vesicles) (Figure 3.10), indicating a partial localization of

EYFP-NHL4 in ER-derived vesicles. Altogether, these data provided evidence that NHL4 is partly localized in the ER-derived vesicles. It should be noted that these vesicles were observed to be restricted to the ER and appeared not to be dissociated yet, suggesting that these structures represent ERES rather than fully budded vesicles. The remaining 95% of the EYFP-NHL4-labeled vesicles that did not co-localize with the mobile vesicle population labeled by ER-CFP had already budded off from the ER (the value subtracted from the data given in 3.2.1.5, Figure 3.10). The 82% of visibly ER-associated vesicles labeled by ER-CFP but not by EYFP-NHL4 could be the ERES. These data indicated that NHL4 is quickly sorted to the ER where it accumulates in ERES and is rapidly transferred to ER-derived vesicles. The complete assembly of the COPII coat is dynamic and depends of inner and outer coat components, for example AtSec23/24 and AtSec13/31, respectively (Hanton et al., 2009; Brandizzi and Barlowe, 2013). Earlier studies revealed that the COPII binding of tomato LeSec13 has a short half-life of 10 sec, thus resulting in rapid appearance like blinking of fluorescence (Yang et al., 2005). Among the COPII components, AtSec24 is an ideal inner COPII marker as its overaccumulation at the ERES did not affect protein export as well as ERES formation (Hanton et al., 2007; Hanton et al., 2009). Therefore, it is suggested to use AtSec24 (fluorophore labeled) to characterize NHL-labeled vesicles at the ERES. This marker shall allow a more quantitative documentation of ER localization and ER exit of NHL4, as well as of NHL6 and NHL25.

Although the trafficking pathway of class II PMPs starts at the ER, few class II PMPs do not contain a signal peptide, e.g. yeast Pex3p (Fakieh et al., 2013). Pex3p orthologs from different organisms were predicted to contain a signal anchor-like sequence, i.e. a cluster of positively charged aa preceding the TMD (Thoms et al., 2012). Even though Pex3p orthologs have not yet been observed in the ER *in vivo*, Pex3p was proven to pass the ER by *in vitro* reconstitution of ER membrane import and an *N*-glycosylation assay (Thoms et al., 2012). The TMD followed by six aa (KRWLYK) of yeast Pex3p contains an ER signal sequence that was required for the ER insertion (Fakieh et al., 2013). In the downstream 11 aa (aa 87 – 98) of the TMD of NHL25 (predicted by TMHMM 2.0; aa 66 – 86), there are positively charged aa, such as R and K, spaced by hydrophobic residues, such as F and V (Figure 4.2). There were also four positively charged aa, preceding the TMD (pos. 49, 51, 52, 55). Subcellular localization analyses of the NHL25 TMD and its downstream and upstream 20 aa indeed targeted EYFP to the ER (as discussed earlier in 4.2.2). This finding supports the hypothesis that the regions including the TMD of NHL25, possibly also those of NHL4 and NHL6, contains an ER targeting signal. To reveal the presence of an ER targeting signal in the three NHLs, the positively charged and

hydrophobic residues located next to the TMD shall be mutated in future studies, and their effect be further analyzed in regard to ER targeting.

In summary, the biogenesis pathway of this NHL subclade represents for a novel peroxisomal targeting pathway in which the NHLs first are sorted to the ER, are subsequently recruited to ER-derived vesicles, and are targeted *via* docking between cargo vesicles and mature peroxisomes to their final peroxisomal destination (Figure 4.3). This process likely requires the participation of AtPex5 (or a yet unknown Pex5 homolog) in guiding these proteins to peroxisomes *via* PTS1 recognition and binding. Future studies of the membrane topology of the NHL proteins are needed to resolve the question whether NHLs display a cytosolic or a matrix-oriented PTS1 domain.
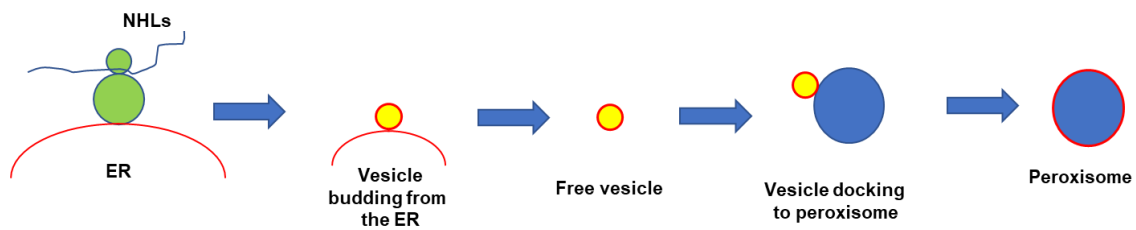
Figure 4.3: A model of the biogenesis of NHL proteins

According to the model, NHLs are first synthesized by ER-bound ribosomes (green) and are sorted co-translationally to the ER (red membrane). Membrane-bound vesicles (yellow cargo vesicle) carrying NHLs bud off from the ER at specific ERES and dock to mature peroxisomes (blue compartment), followed import into the peroxisomal membrane by vesicle fusion.

4.3   First insights into the physiological functions of NHL4, NHL6, and NHL25 in abiotic and biotic stress responses

NHL4, NHL6, and NHL25 belong to the same subclade and share high sequence similarity to Arabidopsis NDR1, which has been well-characterized in its role in plant immunity (1.4.1). The presence of the LEA_2 domain in the NHLs drew further attention to their possible functions in abiotic stress tolerance, as there are many examples of an involvement of LEA_2 containing proteins in abiotic stress responses (1.4.2). In addition to the discussion of NHL functions in plant immunity, a linkage of their functions to abiotic stress responses and their peroxisomal localization is also discussed.

4.3.1 The constitutive tissue- and cell-specific expression patterns of the NHLs link their functions to plant defense

In this study, the tissue expression pattern of the GOIs was investigated using *GUS* reporter lines of Arabidopsis to study at which sites the encoded proteins have a function. The *GUSA* gene was expressed from the native *NHL* promoters to analyze their site of activity. The *NHL* promoters were found to be most active in hydathodes, vascular tissue, stomata and trichomes (the latter only for *NHL6*) (3.3.1.2; Figures 3.17 and 3.18). A highly similar expression pattern was previously detected for the Arabidopsis receptor kinase *FLS2* (Beck et al., 2014). *FLS2* is a key component of the PTI pathway, which is activated upon recognizing the bacterial PAMP flg22 (1.2.1; Gómez-Gómez et al., 1999; Gómez-Gómez and Boller, 2000). As deduced from similar *GUS* analyses, *FLS2* is constitutively expressed in organs vulnerable to bacterial infection, i.e. in hydathodes and stomata, in lateral roots, especially in newly emerged roots, and in the vascular tissue, which are prominent "highways" for bacteria to spread throughout the plant (Beck et al., 2014). Hydathodes and stomata, the natural pores in leaf surfaces, are exploited as infection entry points by different pathogenic bacteria. Also several Arabidopsis leucine-rich repeat receptor-like kinases (*LRR-RLK*s) involved in PTI showed a similar constitutive expression pattern in the same defense cell and tissue types (Wu et al., 2016). Hence, this constitutive expression pattern of NHLs hints towards a function of NHLs in plant immunity. The *NHL* promoters were also active in reproductive organs such as inflorescences (highly for *NHL4* and *NHL25*; Suppl. Figure 7). Interestingly, the receptor EFR, which recognizes the bacterial elongation factor EF-Tu, was predominantly expressed in reproductive tissues, i.e. inflorescences (Wu et al., 2016). Thus, the authors suggested that the inflorescence also represents a defense site. This further confirms a defense function of these NHLs, perhaps also in inflorescences.

Hydathodes are frequently used as entry sites for infection by specific bacterial pathogens, for instance, by *Xanthomonas campestris* pv. *campestris* (*Xcc*), which is a vascular pathogen causing black rot disease in cruciferous plants (Bretschneider et al., 1989; Fargier and Manceau, 2007). Following successful infection, *Xcc* proliferates and moves inside the xylem vessels to the upper leaves and inflorescences (Büttner and Bonas, 2010). This infection site and pathway fully matches the tissue expression pattern of each *NHL*, suggesting their role in these tissue-specific defense responses to *Xcc*. Preliminary data using single *nhl*, double (*nhl6-1 x nhl25-1*), and triple (*nhl4-1 x nhl6-1 x nhl25-1*) mutants infected with avirulent *Xcc*

8004 (expressing *GUSA*) showed a visible infection of *Xcc* in the mutants 10 dpi but not in the WT (data not shown), suggesting an involvement of NHLs in defense responses to *Xcc*. However, these data need to be reproduced to obtain conclusive results. Furthermore, from seedling to flowering stages, the three *NHLs* were constitutively only weakly expressed except for *NHL6* (moderate level in the rosette growth phase) (Figure 3.16), suggesting that the NHLs might have a regulatory function, and that their expression is altered under specific conditions, e.g. under abiotic or biotic stress conditions. Taken together, the constitutive *NHL* expression in "defense tissues" implied a regulatory function of these NHLs in responses to pathogens, e.g. in the defense signaling pathway upon pathogen infection.

4.3.2 The ABA- and pathogen-inducible expression link NHL functions to ABA-regulated and immunity responses

As discussed above (4.3.1), plant gene expression is often changed upon stress application. To gain further insights into the physiological functions of the three NHLs under particular stress conditions including hormone and abiotic stress application, and pathogen infection, gene expression was analyzed using publicly available microarray database (3.3.1.1; Figure 3.16B), and the data were further experimentally validated by qRT-PCR (3.3.1.3.1; Figure 3.19). Among the treatment with hormones, the qRT-PCR data was in agreement with the microarray data, according to which only *NHL4* was significantly induced by ABA (6 – 7 fold 6 and 12 h post treatment) compared to *NHL6* and *NHL25* (< 4 fold). Hence, *NHL4* expression is regulated by ABA, either directly or indirectly by ABA-mediated stress responses. Genes encoding proteins involved in ABA biosynthesis under stress are expressed in diverse tissues such as roots, vascular tissue, leaves, and inflorescence stems, e.g. *ABSCISIC ACID DEFICIENT2* and *ABSCISIC ALDEHYDE OXIDASE3* (Koiwai et al., 2004; Endo et al., 2008; Kuromori et al., 2014). It was also suggested that there is a transfer route of ABA from vascular tissue (phloem companion cells) to guard cells (Kuromori et al., 2014). An ABA-inducible gene in rice (*Oryza sativa*), *rab16A*, showed that its promoter activity increased in vascular bundles after treatment with ABA or upon NaCl stress and desiccation compared to untreated plants (Ono et al., 1996). Interestingly, some LEA proteins of the dehydrin group were also specifically detected in vascular tissues and guard cells (Nylander et al., 2001). Thus, aside from the central role in transporting solutes and macromolecules through the plant, the vascular tissue could also be a place where ABA level is monitored, especially in response to stress, e.g. NaCl and dehydration. Therefore, genes that are expressed in this tissue type and respond to ABA might

function in a similar manner. As the *NHL* promoters were active in vascular tissue and partially also in stomata (for *NHL6*) (3.3.1.2; Figures 3.17 and 3.18), they resembled the pattern of the above-mentioned examples for *LEAs*, ABA biosynthesis and ABA responsive genes. Therefore, it is possible that NHL4 plays a more fundamental function in plant responses to ABA compared to NHL6 and NHL25, and that these responses might take place in vascular tissue. A future study on *NHL4* expression using ABA-insensitive (*abi* and *snrk2*) mutants could give insights into whether *NHL4* expression is mediated by these ABA signal transduction pathways.

Transcription of many signaling proteins involved in PTI and ETI is highly induced by pathogen infection (Li et al., 2016; Meteignier et al., 2017). Thus, it was hypothesized that the NHLs might have a function in plant immunity if their expression is affected by biotic factors. In this study and consistent with the previous data for the flg22-inducible expression of *NHL6* by qRT-PCR (Crappe, 2016), the *NHL6* promoter was more active upon infiltration with the MAMP elf18 in the *GUS* reporter lines (3.3.1.3.2; Figure 3.20). Microarray data revealed a suppression of the elf18-inducible expression of *NHL6* in the *efr1* receptor mutant (3.3.1.1; Figure 3.16B), suggesting a role in PTI. Furthermore, upon infection with two avirulent *Pst* strains, *NHL6* expression was strongly induced 23 fold by *Pst*(*avrRpm1*) and 44 fold by *Pst*(*avrRpt2*) 48 hours post infection (hpi), but the expression levels were lower than upon virulent *Pst* infection (84-fold) (Figure 3.19). This indicated that there was no additional induction of *NHL6* expression during ETI beyond the PTI expression level. The same result was also observed for *NHL25,* where the additional effect of ETI on *NHL25* expression was negligible. Although PTI and ETI display distinct modes in terms of ligand binding and activation, several lines of evidence highlighted the convergence of PTI and ETI in many downstream defense mechanisms such as HR, ROS production, Ca^{2+} influx, and MAPK cascade activation (Yuan et al., 2021b). For example, mutants lacking one of the major PRRs involved in PTI, including FLS2, EFR, and CHITIN ELICITOR RECEPTOR KINASE 1, showed an impaired ETI-associated resistance against *Pst*(*avrRpt2*) (Yuan et al., 2021a). The data suggested that NHL6 and NHL25 have a function that is regulated primarily by PTI rather than ETI. The *NHL25* promoter was activated by flg22 and much less by elf18 (Figure 3.20). Notably, *Pst*-inducible expression of *NHL25* (approx. 350 fold 48 hpi) was in line with previous data (Crappe, 2016), but was inconsistent with an earlier study (Varet et al., 2002). Although the bacterial concentration was similar (i.e., 10^8 CFU·mL^{-1}), the strong inducible expression of *NHL25* detected in this study and that of Crappe (2016) compared to that of Varet et al. (2002) could result from differences in experimental design, e.g. tissue types, plant age, and detection method. The pronounced virulent and avirulent *Pst*-

induced expression of *NHL6* and *NHL25* (but not of *NHL4*) detected by qRT-PCR (Figure 3.19) and by the GUS histochemical approach (Figure 3.20) indicated a function of these two NHLs in plant immunity. This conclusion is further supported by tissue expression analyses (Figures 3.17 and 3.18) as discussed above (4.3.1), thereby implying a defense function in leaf stomata (for NHL6) and in hydathodes (NHL6 and NHL25) (Cerutti et al., 2017). To further resolve the involvement of the two NHLs in PTI or ETI, mutants compromised in either PTI (e.g., *fls2* and *efr1*) or ETI (e.g., *ndr1* and *eds1*) need to be analyzed in future studies.

4.3.3 NHL4 and NHL6 play a role in ABA-mediated seed dormancy

The core components involved in ABA biosynthesis and signal transduction have long been identified and functionally well-characterized (Koornneef et al., 1982; Koornneef et al., 1984; Fujii and Zhu, 2009). Many of these proteins were identified by a fundamental screening method, which is based on a less ABA-sensitive phenotype of the mutants during seed germination. In the presence of ABA, a reduced dormancy of the mutant seed compared to WT means a less ABA-sensitive phenotype of the mutant and indicates an ABA-responsive protein function. In this study, the *nhl4-1* mutant showed the lowest ABA sensitivity compared to the WT during seed germination (Figure 3.23). A significantly higher number of germinated *nhl4-1* mutant seeds (73%) was observed 6 d after germination in comparison with the WT with only 32% of germinated seeds ($p < 0.05$). By contrast, in the two *NHL4* overexpressor (OE) lines, the degree of inhibition by ABA remained similar to the WT (Figure 3.23). Together these data showed that loss of function of *NHL4* renders WT seed germination less sensitive to seed dormancy induced by ABA. Together with the *NHL4* inducibility by ABA (Figures 3.16B and 3.19A, 4.3.2), NHL4 was shown to play a role in ABA-induced seed dormancy.

Several studies have highlighted the important role of core regulators of ABA signaling in regulating abiotic stress response mechanisms (Yoshida et al., 2015). Genes whose expression is regulated by ABA are frequently involved in ABA-mediated abiotic stress responses. For instance, the expression of many *LEA* genes is induced by ABA (Bies-Etheve et al., 2008), and several LEAs were shown to confer enhanced salt and osmotic stress tolerance to transgenic plants (Brini et al., 2007; Jia et al., 2014). Hence, NHL4 with its pronounced upregulation by ABA, was postulated in the beginning of this study to play a second role in regulating abiotic stress responses. As hypothesized, during seed germination and in the seedling stage, the *nhl4-1* mutant showed a significantly higher sensitivity to salt stress (200 mM NaCl) than the WT (Khan, Nguyen, and Reumann, unpubl. data). However, transgenic lines

overexpressing *NHL4* from the *CaMV 35S* promoter displayed the same degree of reduction in seed germination and seedling development as the WT (Khan, Nguyen, and Reumann, unpubl. data). In summary, these data suggested an indispensable function of NHL4 in Arabidopsis in tolerating the effects of salt stress mediated by ABA.

The *nhl6-1* mutant was also less sensitive ABA inhibition of seed germination (63%) compared to the WT (32% at 6 d, *p* < 0.05), but to a lower degree compared to *nhl4-1* (Figure 3.23A, C, D). The data implied that NHL6 and NHL4 have similar functions in seed dormancy induced by ABA, consistent with their high sequence similarity, classification in the same subclade and identical peroxisome localization. This *nhl6-1* phenotype is in agreement with an earlier study (Bao et al., 2016). Both loss of function and overexpression of *NHL6* conferred salt hypersensitivity during seed germination compared to the WT, and this response was regulated by high levels of ABA (Bao et al., 2016). Also in the same study, ABA-induced *NHL6* expression was shown to be mediated by the ABA signal transduction pathway, particularly by ABA INSENSITIVE 1, as in the *abi1-1C* mutant, the ABA-induced expression of *NHL6* was reduced. Thus, NHL6 plays an important role, similarly to NHL4, in regulating abiotic stress responses in an ABA-dependent manner. On the contrary, the *nhl25-1* mutant displayed an insignificantly lower sensitivity of seed germination to ABA inhibition (Figure 3.23), indicating that the protein's function is more specialized on innate immunity.

4.3.4 The protective effect of NHL4 on bacterial stress tolerance upon expression in *E. coli*

Compared to other LEA groups, the LEA_2 subgroup is the largest and most diverse in the plant lineage (Artur et al., 2019). The LEA_2 domain is atypical due to its high hydrophobicity and its defined structure in solution, which has been determined at 0.6 Å by nuclear magnetic resonance for Arabidopsis LEA14 (Singh et al., 2005). It reveals structural similarity to the fibronectin type III domain in animal cells. Fibronectins are involved in cell motility, wound healing, cell adhesion, and maintenance of cell shape (Singh et al., 2005). Plant LEA_2 proteins have been shown to confer stress tolerance not only in transgenic plants (Wang et al., 2014; Sharma et al., 2016) but also in *E. coli* cells *in vivo* under diverse abiotic stress conditions, such as high salinity, freezing, and low temperature (He et al., 2012; Paul et al., 2014).

In this study, the function of the three NHLs in conferring stress tolerance in *E. coli in vivo* under osmotic stress was investigated. Recombinant NHL proteins were produced in *E. coli* following IPTG induction. MBP-tagged NHLs were partly soluble in *E. coli* cells (50%) compared to those tagged with 6xHis (approx. 20%) (data not shown), confirming that the

MBP tag often improves the solubility of the fusion proteins. Hence, *E. coli* transformants expressing each *MBP*-tagged *NHL* were subjected to osmotic stress, including NaCl, KCl (both at 0.5 M) or 1 M sorbitol. The three experiments were conducted independently, and the data were statistically analyzed. The expression of *NHL4* tagged with *MBP* indeed conferred stress tolerance, as indicated by a significantly higher cell concentration under salt stress conditions (NaCl: $5.4 \cdot 10^8$ CFU·mL^{-1}, KCl: $4.3 \cdot 10^8$ CFU·mL^{-1}) compared to MBP alone (NaCl: $2.4 \cdot 10^8$ CFU·mL^{-1}, KCl: $2.3 \cdot 10^8$ CFU·mL^{-1}) (Figure 3.24). The same tendency was observed for 1 M sorbitol but was not statistically significant. The osmolarity was identical between the media. Thus, rather than being involved in the osmotic stress responses, NHL4 might contribute to *E. coli* survival against toxicities specifically caused by high concentration of Na$^+$ and K$^+$ ions that may lead to cellular dehydration. Thus, the data strongly indicated that NHL4 could confer salt stress tolerance in *E. coli*, most likely by protecting specifically sensitive proteins from aggregation due to cellular dehydration.

This assumption is supported by a previous study on the molecular chaperone-like function of the *Citrus unshiu* LEA dehydrin, which belongs to a different LEA sub-group but showed the cryoprotection of catalase and lactate dehydrogenase *in vitro* (Hara et al., 2001). Similar results have been reported for the mitochondrial fumarase and rhodanese (Grelet et al., 2005). In the presence of MBP-NHL4, the reduction of commercial lactate dehydrogenase activity at 42°C was much lower than that in the presence of MBP alone (Khan, Nguyen and Reumann, unpubl. data). Therefore, especially NHL4 might play a role as a molecular chaperone of peroxisomal proteins that are vulnerable to abiotic stress. In addition, despite using similar cell densities at the beginning of the osmotic stress assay, *E. coli* expressing *MBP-NHL4* ($2.8 \cdot 10^9$ CFU·mL^{-1}) and *MBP-NHL6* ($2.6 \cdot 10^9$ CFU·mL^{-1}) proliferated quicklier compared to *E. coli* expressing *MBP* alone ($1.4 \cdot 10^9$ CFU·mL^{-1}) on normal LB medium (Figure 3.24). These data suggested that NHL4 and, to a lesser extent also NHL6, promote cell division and proliferation of *E. coli*, a beneficial effect, allowing more surviving cells under stress conditions.

Immunoblotting analyses showed similar protein concentrations for both MBP-NHL4 and MBP in *E. coli* cells (Figure 3.24C). Since only the cells expressing *MBP-NHL4* conferred increased salt stress tolerance, the data implied that salt stress tolerance of *E. coli in vivo* was caused by NHL4 but not by MBP, and likely by the functional activity of the LEA_2 domain of NHL4 and enzyme protective activity. Also, this stress tolerance of *E. coli* cells could stem primarily from the protection activity of NHL4 against dehydration which was caused by the

high salt concentration. Based on the immunoblotting result, more soluble MBP-NHL4 was produced in the corresponding transformants (Figure 3.24C) compared to MBP-NHL6 and MBP-NHL25. This data indicated that NHL6 and NHL25 could play a similar role as NHL4 in conferring salt stress tolerance in *E. coli* and that could not be revealed due to their lower protein levels.

4.3.5 Towards elucidating the physiological function of NHL4, NHL6, and NHL25 in plant immunity

4.3.5.1 The involvement of NHL4, NHL6, and NHL25 in regulating HR during infection with *Pst*(*avrRpm1*)

Contrary to *NHL4*, the expression of *NHL6* and *NHL25* was strongly induced upon infection of virulent or avirulent *Pst* (Figure 3.19B – D), suggesting a potential role of NHL6 and NHL25 in plant immunity (4.3.2). Functional characterization of NHLs in the HR was performed by measuring the kinetics of electrolyte leakage from leaf discs over 6 or 8 hpi with avirulent *Pst* strains. A large number of leaf discs (i.e., 10 leaf discs mixed from 10 different plants per biological sample per genotype) and the number of three biological samples per experiment allowed recording of reliable data of electrolyte leakage. The experiment was conducted twice, one representative data set of which was statistically analyzed (Figure 3.26). The electrolyte leakage measurements analyzed the speed and intensity of HR execution. It enabled to investigate whether the disruption of GOI led to any effect on HR in the WT. To observe HR-induced cell death and to ensure that the infection could successfully trigger HR, the WT genotype, which is able to effectively develop HR to defend itself against avirulent *Pst* strains (Century et al., 1995), was included as a positive control. The *ndr1-1* mutant was also included as the second positive control of HR, as this mutant was phenotypically observed to maintain residual HR-like symptoms in response to *Pst*(*avrRpm1*) (Century et al., 1995), thus strengthening the reproducibility of the experimental design. Indeed, apart from the expected HR-induced cell death observed in WT plants, electrolyte leakage was still initiated and progressed also in *ndr1-1* (Figure 3.26A – F). As a result, the residual HR, which is triggered by the R protein RPM1 during ETI, was not abolished in absence of NDR1, fully consistent with the report that NDR1 is not essential for RPM1-triggered HR (Century et al., 1995; Hofius et al., 2009). By allowing to precisely visualize HR intensity and progression in WT and *ndr1-1*, the method was considered well-established.

Single *nhl* mutants displayed an HR intensity similar to the WT 6 hpi (3.3.2.3.2; Figure 3.26A – D), while the triple (*nhl4-1* x *nhl6-1* x *nhl25-1*) mutant exhibited a significantly higher degree of HR-induced cell death (line 1: 63%; line 2: 65%) compared to the double mutants 6 hpi (*nhl6-1* x *nhl25-1* line 1: 57%; line 2: 56%). Both genotypes showed an intensity of HR-induced cell death that was significantly higher than that of the WT and single *nhl* mutants (Figure 3.26C, D). The same tendency was repeatedly observed in other independent experiments (n = 3). Altogether, these data suggested an intriguing function of these three NHLs in locally restricting HR-induced cell death with partially redundant functions. However, the kinetics of HR-induced cell death (Figure 3.26E, F) did not differ between genotypes since the maximum change in velocity of ion leakage occurred at nearly the same time point. Taken together, the three NHLs might have a redundant function in reducing HR-induced cell death in terms of intensity rather than kinetics.

Many key components and regulators of innate immunity have been identified based on their strong gene induction by elicitors, pathogens, and defense hormones (e.g., *AvrRpt2-induced gene 1* (*AIG1*)/*IAN8*) (Reuber and Ausubel, 1996). This holds mostly true for positive regulators, while negative regulators vary in their pathogen-induced expression profiles. Few negative regulators of plant resistance have been found in species including Arabidopsis, rice, and chili pepper (Zeng et al., 2004; Wang et al., 2006; Oh et al., 2008). For instance, the transcription factor WRKY54 that was induced by benzothiadiazole treatment, a functional analog of SA, is a negative regulator to prevent SAR induction (Wang et al., 2006). This TF was suggested to repress SA biosynthesis, thereby lowering SAR when the thread of pathogen infection subsides. Also *Capsicum annuum* WRKY1, which negatively regulates plant defense, is highly induced by SA and different pathogens that elicit HR (Oh et al., 2008). These studies show that not only positive but also negative regulators are often highly induced following pathogen attack. Thus, these examples could explain why *NHL6* and *NHL25* were induced upon *Pst*(*avrRpm1*) as well as *Pst*(*avrRpt2*) infection despite the proteins' role as negative regulators of HR. Taken together, the NHLs might act as a "brake" to fine-tune the HR-induced cell death during ETI and to stop programmed cell death when the risk of infection has been eliminated. Moreover, also virulent *Pst* highly induced the expression of *NHL6* (84 fold) and *NHL25* (approx. 350 fold) but not that of *NHL4* 48 hpi (Figure 3.19B). HR is the prime defense response of ETI and was long thought to be specific for ETI. Recently, by using loss of function mutations in PRR co-receptors (involved in PTI), by phenotypic HR observation, and ROS measurement (the luminol-horseradish peroxidase approach), a study convincingly demonstrated that ETI-

associated responses such as HR and ROS production require these PRR co-receptors (Yuan et al., 2021a). Therefore, it is suggested here that NHL6 and NHL25 play a role in restricting the HR-induced cell death, which could be the convergence point between PTI and ETI mediated by virulent and avirulent *Pst*, respectively. These hypotheses remain to be further resolved by electrolyte leakage analyses under infection with virulent *Pst*. In conclusion, this study provides the first indication for a function of these NHL proteins in regulating the HR-induced cell death in response to *Pst*(*avrRpm1*).

It must be noted that the loss of function mutations in *NHLs* did not show any susceptibility to *Pst*(*avrRpm1*) while *ndr1-1* was strongly compromised (3.3.2.3.1; Figure 3.25A, B). This data showed that the three NHLs do not play a primary role in the resistance mechanism against *Pst*(*avrRpm1*) infection. Furthermore, as these proteins might redundantly function in restricting the HR, their loss of function in double and triple mutants potentially renders the plant more resistant to avirulent *Pst*. This explains why a susceptible phenotype had not been observed for the *nhl* mutants in the bacterial proliferation assay (3.3.2.3.1; Figure 3.25A, B). On the other hand, the *NHL* overproduction in OE lines would be expected logically to restrict the HR remarkably, thus could render WT even more susceptible to pathogens. Interestingly, a large number of the stable transgenic lines (approx. 30 – 50 lines) overexpressing *NHL6* and *NHL25* (N-terminally tagged with EYFP) did not show any fluorescence of the EYFP fusion proteins. The *EYFP-NHL6* or *EYFP-NHL25* mRNA levels in these OE lines had not yet been confirmed. However, the expression levels of *NHL6* and *NHL25* in the other OE lines (without EYFP tag) were found to be increased by 10 – 30 fold (in 3 out of 7 lines) and 130 – 280 fold (in 4 out of 5 lines), respectively, by qRT-PCR (data not shown), indirectly suggesting that there must be a considerable expression level of *EYFP-NHL* fusions in the OE lines missing EYFP fluorescence. Thus, although *EYFP-NHL6* and *EYFP-NHL25* must be transcribed in these lines, their protein level was very low. A similar situation might also have occurred in *EYFP-NHL4* OE lines but to a lesser extent, as only five among 30 *EYFP-NHL4* transgenic lines showed sufficient EYFP fluorescence (3.2.3). Interestingly, the line 19 with the highest transcript level of *EYFP-NHL4* (approx. 52,000 fold) displayed weaker EYFP fluorescence (data not shown) compared to the one with much lower transcript level (line 25: approx. 9,600 fold) in 5-day-old Arabidopsis seedlings and mature leaves. These unexpected results together with the constitutively low expression of *NHLs* over developmental stages under normal growth condition (3.3.1.1; Figure 3.16A) suggested that these NHLs, especially NHL6 and NHL25, must be tightly regulated not only at the transcriptional level but also at the protein

level by post-translational regulation, to sophistically control the restriction of the beneficial HR.

4.3.5.2 The involvement of NHL4, NHL6, and NHL25 in regulating HR during infection with *Pst*(*avrRpt2*)

The function of NHLs in attenuating cell death response during HR was also characterized upon infection with avirulent *Pst*(*avrRpt2*). As a positive control, the WT developed HR-induced cell death, as observed by electrolyte leakage with an intensity of 23 – 25% 6 hpi to 42 – 44% 8 hpi (Figure 3.27A – D). This HR response was nearly suppressed in *ndr1-1* (Figure 3.27A – D), in agreement with the previous report (Century et al., 1995). Disruption of *NHLs* resulted in a much more pronounced HR in response to *Pst*(*avrRpt2*). Single, double, and triple *nhl* mutants displayed significantly stronger electrolyte leakage (> 50% relative electrolyte leakage) compared to WT (< 25%) 6 hpi (Figure 3.27A – D). Interestingly, the elevated degree of HR observed in the single mutants without additional effects in the double and triple mutants indicated that the three NHLs function independently in restricting the HR elicited by *Pst*(*avrRpt2*). In terms of kinetics, the HR response in all genotypes required 3.5 – 6 h to reach the highest velocity (Figure 3.27E – H), and this was reached much later than for *Pst*(*avrRpm1*) (1.5 – 2 h) (Figure 3.26E, F). The *nhl* mutants infected by *Pst*(*avrRpt2*) needed less time to reach the maximum change of relative electrolyte leakage (3.3 to 5.9 h) compared to WT (6.3 h) (Figure 3.27E – H). Between the two *nhl25-1* and *nhl6-1* mutants, the latter displayed the faster HR development (t_{max} = 4.9 vs. 5.5 h; Figure 3.27G). Additional disruption of *NHL25* in the double mutants did not accelerate HR any further in the *nhl6-1* mutant (Figure 3.27G). These results suggested that NHL6 plays a much more important role than NHL25 in reducing the speed of HR. In addition, the previous and present expression analyses demonstrated that *NHL6* is induced during PTI (by flg22 and *Pst*) rather than ETI (avirulent *Pst*) (4.3.2; Figure 3.16; Crappe, 2016). An earlier study suggested that PAMPs such as flg22 can induce HR in the callose deposition assay (Naito et al., 2008). Recently, it was shown that loss of function of PRR co-receptors perceiving PAMPs and chitin (*FLS2*, *EFR1*, and *CERK1*) (Yuan et al., 2021a) or endogenous elicitor peptides (*PEPR1* and *PEPR2*) (Ma et al., 2012), impaired HR triggered by *Pst*(*avrRpt2*). These studies highlighted an overlapping regulation of both the PTI and the ETI signal transduction pathway in HR execution. Therefore, together with the inducible expression of *NHL6* by *Pst* observed in this study, the data suggests that NHL6 might function in reducing HR, which is triggered during PTI and/or during ETI. To prove this sophisticated

146

function, the gene expression analyses of *NHL6* upon infection with *Pst*(*avrRpt2*) in the mutants lacking PAMP receptors such as *fls2* should be further studied. Also, whether *Pst*(*avrRpt2*)-triggered HR observed in *nhl6-1* was mediated by PTI could also be resolved in the double (*fls2 x nhl6-1*) mutant.

The expression analysis had shown that *NHL6* and *NHL25* were already upregulated approx. 3 and 92 fold, respectively 6 hpi by the same *Pst* strain (Figure 3.19D). At a later time point, i.e. 48 hpi the transcript level of *NHL6* (44 fold) and *NHL25* (230 fold) were strongly induced. This time-dependent expression upon *Pst*(*avrRpt2*) infection might help the plant to efficiently fine tune the progression of HR-triggered cell death in the infected tissues 6 hpi and to largely suppress the spreading of HR to the cells surrounding the infection site 48 hpi, explaining why HR progression generally declined at this time point. It should be noted that in the inducibility analyses of the *NHL* promoters using *GUS* reporter lines, the *NHL* promoter activity was strongly induced but precisely restricted in the wounded tissues caused by either physical damage or *Pst* or *Pst*(*avrRpt2*) infection, as shown in Figure 3.20. Taken together, the expression of these NHLs was not only strictly controlled at multiple molecular levels, as mentioned above, but also regulated in precise tissue/cells subjected to damage or closely related to damaged tissues. In order to get a better understanding about the role and the accurate function of these NHLs, future research should focus on their precise expression pattern, i.e. in the HR- or wound-affected cells or in the neighboring cells. Recent advances in molecular and cellular technologies, especially the development and the popularity of the single cell sequencing technique, could be a key tool to identify the precise cells where these *NHLs* are active, hence, give an insight into the more precise molecular function of these NHLs.

5 CONCLUSIONS AND FUTURE PERSPECTIVES

In summary, this study showed that the A206K mutation, introduced into Venus and Cer, prevented dimerization of these GFP variants, thereby preventing fluorophore dimerization-based piggy-back import into peroxisomes. This study provided a new guideline for the combination of yellow (EYFP or mVenus) and blue (mCer) fluorescent fusion proteins to label proteins of interest and peroxisomes, respectively, adding a more reliable set of fluorophores to plant peroxisome research.

This study presented detailed analyses on peroxisome targeting of a subclade of NDR1 homologs, including NHL4 (AKL>), NHL6 (LRL>), and NHL25 (FRL>) that carry an N-terminal TMD and a C-terminal PTS1 domain. These proteins were predicted to constitute a novel sub-class of class II PMPs because they were possibly targeted to peroxisomes *via* the ER and a vesicle trafficking pathway, possibly in a PTS1-dependent manner. The PTS1s of these NHLs were confirmed to be functional *in vivo* in this study, and NHL4 was demonstrated to have a detectable binding affinity to the TPR domain of AtPex5. Peroxisome targeting was confirmed to be dependent, to large extent, on the PTS1 (for NHL25) and on a second PTS possibly located in the short N-terminal domain, the LEA_2 domain or the C-terminal domain upstream of the PTS1. Representatively of the subclade, the peroxisomal targeting pathway of NHL4 was analyzed in depth, consisting of rapid ER localization, intermediate vesicle traffic, vesicles in contact with peroxisomes, and peroxisome targeting. Using transient transformation of Arabidopsis seedlings and stable transgenic Arabidopsis lines, this study provided evidence for each targeting intermediate of NHL4, demonstrating a complex and multi-step peroxisomal targeting pathway of these novel peroxisomal NHL proteins. The identification of the unknown NHL-labeled vesicles regarding their characteristics such as actin filament- or microtubule-dependent mobility and stronger evidence for the ER origin of these vesicles by using ER exit site markers remain to be further explored. The regulation of NHL biogenesis would be interesting to address using transgenic lines expressing *EYFP-NHLs* from the native promoters. The use of these transgenic lines will yield more insights into whether the biogenesis of these NHLs in terms of peroxisome targeting could be enhanced under certain circumstances of environmental or cellular stimuli.

These NHL proteins were functionally characterized in this study. Based on reverse genetic studies, the function of NHLs in plant immunity, which had not been reported yet for any member of the NHL protein family, particularly in attenuating HR triggered by RPM1 and

RPS2 upon infection with *Pst*(*avrRpm1*) and *Pst*(*avrRpt2*), respectively, has been first described for NHL4, NHL6, and NHL25 in this study. Their function in plant defense was supported by tissue expression pattern analyses using *GUS* reporter lines that systematically provided information in which tissues the *NHL* promoters are active. The activity of the *NHL* promoters was detected in defense tissue such as hydathodes, vascular tissue, stomata, and trichomes (for *NHL6*), suggesting a defense function of NHLs in plant immunity. The gene expression analyses also showed that the expression of *NHL6* and *NHL25* is pathogen inducible, indicating that they play a role in plant defense, as verified by the HR analyses. Furthermore, this study also highlighted an additional role of NHL4 and NHL6 in regulating seed dormancy, indicating a possible role of these NHLs in ABA-mediated plant responses. The function of the LEA_2 domain revealed for NHL4 in conferring salt stress tolerance in *E. coli in vivo* was first shown in this study. This study provided new findings not only on the biogenesis and defense-related function of these NDR1 homologs, but also established the framework for future studies to further address fundamental questions regarding their biogenesis and function. In future research, other functions of these NHLs in plant immunity, i.e. in the regulation of ROS levels under pathogen infection, could be interesting to address, thus providing evidence directly for a linkage of their functions to their peroxisomal localization.

6 SUPPLEMENTARY DATA

Supplementary Table 1: King's B medium

Ingredient	Amount in 1 L
Peptone	20 g
K_2HPO_4	1.5 g
$MgSO_4 \cdot 7 H_2O$	1.5 g
Glycerol	10 mL
Bacto Agar (for solid medium)	15 g

The pH was adjusted to 7.2 with 1 M KOH.

Supplementary Table 2: Constructs used in this study and the corresponding primers for subcloning

For conventional subcloning, recognition and restriction sites of enzymes (underlined) were introduced into the forward (upper) and the reverse (lower) primers. The primers used for subcloning constructs by Gateway technology contained homologous recombination sites (*att*B1 and *att*B2) as indicated by lowercase letters. To generate pSAT6_mVenus-C, two complementary SDM primers were used to amplify the entire vector pSAT6_Venus-C and introduce the A206K mutation (in bold letters).

Construct	Primer name	Primer sequence (5' → 3')	Destination vector
Bacterial expression vectors			
pQE31_6xHis-ΔNt80aaNHL4	TN91_D80NHL4pQE_BamHI	CGTACG<u>GGATCC</u>TAAACTCCCGAGTTACGAAGTC	pQE31_6xHis
	TN92_NHL4_PstI	AGCCAATGCATTGGTT<u>CTGCAG</u>TCAGAGTTTGGCCTTAAAACTG	
pMAL-c2x_MBP-Xa-ΔNt80NHL4	TN90_D80NHL4_BamHI	CGTACG<u>GGATCC</u>CTAAACTCCCGAGTTACGAAG	pMAL-c2x_MBP
	TN92_NHL4_PstI	AGCCAATGCATTGGTT<u>CTGCAG</u>TCAGAGTTTGGCCTTAAAACTG	
pQE31_6xHis-ΔNt100aaNHL6	TN94_D100NHL6pQE_BamHI	CGTACG<u>GGATCC</u>AGACCGGTTACAGCTCACCC	pQE31_6xHis
	TN95_NHL6_PstI	AGCCAATGCATTGGTT<u>CTGCAG</u>CTATAACCTAAGACGAAATTTGC	
pMAL-c2x_MBP-Xa-ΔNt100NHL6	TN93_D100NHL6_BamHI	CGTACG<u>GGATCC</u>GACCGGTTACAGCTCACCCG	pMAL-c2x_MBP
	TN95_NHL6_PstI	AGCCAATGCATTGGTT<u>CTGCAG</u>CTATAACCTAAGACGAAATTTGC	
pQE31_6xHis-ΔNt100aaNHL25	TN97_D100NHL25pQE_BamHI	CGTACG<u>GGATCC</u>ACTAACCCGGTTTCAACTAAACC	pQE31_6xHis
	TN98_NHL25_PstI	AGCCAATGCATTGGTT<u>CTGCAG</u>TTATAGTCTAAACCTGTATTTGCAG	
pMAL-c2x_MBP-Xa-ΔNt100NHL25	TN96_D100NHL25_BamHI	CGTACG<u>GGATCC</u>CTAACCCGGTTTCAACTAAACC	pMAL-c2x_MBP
	TN98_NHL25_PstI	AGCCAATGCATTGGTT<u>CTGCAG</u>TTATAGTCTAAACCTGTATTTGCAG	
Plant expression vectors			
pSAT6_CaMV 35S:mVen-C	TN81_Venus-A206K_F	ACCTGAGCTACCAGTCC**AAG**CTGAGCAAAGACCCCAAC	pSAT6_CaMV 35S:Ven-C
	TN82_Venus-A206K_R	GTTGGGGTCTTTGCTCAG**CTT**GGACTGGTAGCTCAGGT	
pBA002_CaMV 35S:EYFP-NHL4	TN10_NHL4pBA_PacI	CC<u>TTAATTAA</u>GATGGGAGATCAACAAAAA	pBA002_CaMV 35S:EYFP
	TN11_NHL4pBA_SpeI	GG<u>ACTAGT</u>TCAGAGTTTGGCCTTAAAACT	
pBA002_CaMV 35S:EYFP-NHL6	TN12_NHL6pBA_PacI	CC<u>TTAATTAA</u>GATGTCTCAACACCAAAAA	pBA002_CaMV 35S:EYFP
	TN13_NHL6pBA_SpeI	GG<u>ACTAGT</u>CTATAACCTAAGACGAAATTT	

pBA002_CaMV 35S:EYFP-NHL25	TN14_NHL25pBA_PacI	CCTTAATTAAGATGTCCGATCACCAGAAA	pBA002_CaMV 35S:EYFP
	TN15_NHL25pBA_SpeI	GGACTAGTTTATAGTCTAAACCTGTATTT	
pBA002_CaMV 35S:NHL25	TN14_NHL25pBA_PacI	CCTTAATTAAGATGTCCGATCACCAGAAA	pBA002_CaMV 35S
	TN15_NHL25pBA_SpeI	GGACTAGTTTATAGTCTAAACCTGTATTT	
pBA002_CaMV 35S:mVenus-IAN12	TN72_mVe/Ce_MluI	CGACGCGTATGGTGAGCAAGGGCGAGGAG	pBA002_CaMV 35S:IAN12
	TN73_mVe/Ce_PacI	CCTTAATTAACTTGTACAGCTCGTCCATGCCG	
pBA002_CaMV 35S:mCherry-MCS-stop	TN69_mVe/Ce_XhoI	CCGCTCGAGATGGTGAGCAAGGGCGAGGA	pBA002_CaMV 35S
	TN111_mCheMCSstoSacI	CGAGCTCGTTACCGGACTAGTCCCGACGCGTCGTCCCCCGGGGGA TTAATTAACTTGTACAGCTCGTCCATGC	
pBA002_CaMV 35S:mCherry-NHL4	TN10_NHL4pBA_PacI	CCTTAATTAAGATGGGAGATCAACAAAAA	pBA002_CaMV 35S:mCherry-MCS-stop
	TN11_NHL4pBA_SpeI	GGACTAGTTCAGAGTTTGGCCTTAAAACT	
pBA002_CaMV 35S:mCherry-NHL25	TN14_NHL25pBA_PacI	CCTTAATTAAGATGTCCGATCACCAGAAA	pBA002_CaMV 35S:mCherry-MCS-stop
	TN15_NHL25pBA_SpeI	GGACTAGTTTATAGTCTAAACCTGTATTT	
pBA002_CaMV 35S:EYFP-NHL4(Ct10aa)	TN69_mVe/Ce_XhoI	CCGCTCGAGATGGTGAGCAAGGGCGAGGA	pBA002_CaMV 35S
	TN108_EYFPct10NHL4_ SpeI	GGACTAGTTCAGAGTTTGGCCTTAAAACTGCAATCACTAGCCTTGT ACAGCTCGTCCATGC	
pBA002_CaMV 35S:EYFP-NHL6(Ct10aa)	TN69_mVe/Ce_XhoI	CCGCTCGAGATGGTGAGCAAGGGCGAGGA	pBA002_CaMV 35S
	TN109_EYFPct10NHL6_SpeI	GGACTAGTTCATAACCTAAGACGAAATTTGCAACTACTACTCTTGTA CAGCTCGTCCATGC	
pBA002_CaMV 35S:EYFP-NHL25(Ct10aa)	TN69_mVe/Ce_XhoI	CCGCTCGAGATGGTGAGCAAGGGCGAGGA	pBA002_CaMV 35S
	TN110_EYFPct10NHL25_ SpeI	GGACTAGTTCATAGTCTAAACCTGTATTTGCAGTTACTACTCTTGTA CAGCTCGTCCATGC	
pBA002_CaMV 35S:EYFP-NHL25ΔPTS1	TN14_NHL25pBA_PacI	CCTTAATTAAGATGTCCGATCACCAGAAA	pBA002_CaMV 35S:EYFP
	TN107_NHL25DPTS1_SpeI	GGACTAGTTTACCTGTATTTGCAGTTAC	
pBA002_CaMV 35S:EYFP-NHL25(SRL>)	TN14_NHL25pBA_PacI	CCTTAATTAAGATGTCCGATCACCAGAAA	pBA002_CaMV 35S:EYFP

	TN115_NHL25SRL_SpeI	GG<u>ACTAGT</u>TTATAGTCTACTCCTGTATTTGC	
pBA002_CaMV 35S:TMD(NHL25)	TN113_TMDNHL25_PacI	CC<u>TTAATTAA</u>TGATCCTCCGAGGGAGAAGAAAG	pBA002_CaMV 35S:EYFP
	TN114_TMDNHL25_SpeI	CC<u>ACTAGT</u>TTATAGTTGAAACCGGGTTAGC	
pMDC123_NHL4pro:NHL4	TN122_CompNHL4attB1F	ggggacaagtttgtacaaaaaagcaggctGTCTCATTGACCTATTCGGTACCCT	pDONR223 and pMDC123
	TN123_CompNHL4attB2R	ggggaccactttgtacaagaaagctgggtTTGAGATGACGACATTTGGTTCCCTTG	
pMDC123_NHL6pro:NHL6	TN124_CompNHL6attB1F	ggggacaagtttgtacaaaaaagcaggctACCAAAATTTTATAGATATTCAAATTG	pDONR223 and pMDC123
	TN125_CompNHL6attB2R	ggggaccactttgtacaagaaagctgggtTATATCTATGTCTCTTTATTATCTCTTTC	
pMDC99_NHL25pro:NHL25	TN126_CompNHL25attB1F	ggggacaagtttgtacaaaaaagcaggctAAGGACTAGTATATAATCTAAGAAATATA	pDONR223 and pMDC99
	TN127_CompNHL25attB2R	ggggaccactttgtacaagaaagctgggtGCAATTCAATCAATCACTAACCAAAT	
pMDC162_NHL4pro:GUSA	TN101_attB1pNHL4F	ggggacaagtttgtacaaaaaagcaggctGTCTCATTGACCTATTCGGTAC	pMDC162_GUSA
	TN102_attB2pNHL4R	ggggaccactttgtacaagaaagctgggtGGATCTACAACTTTGTATTTAGTAATAC	
pMDC162_NHL6pro:GUSA	TN103_attB1pNHL6F	ggggacaagtttgtacaaaaaagcaggctACCAAAATTTTATAGATATTCAAATTG	pMDC162_GUSA
	TN104_attB2pNHL6R	ggggaccactttgtacaagaaagctgggtTTTTGGAAAATCTTGATGACACC	
pMDC162_NHL25pro:GUSA	TN105_attB1pNHL25F	ggggacaagtttgtacaaaaaagcaggctAAGGACTAGTATATAATCTAAGAAATAT	pMDC162_GUSA
	TN106_attB2pNHL25R	ggggaccactttgtacaagaaagctgggtGTTCTTGATTCGGCTTTAAG	

Yeast expression vectors

pGBKT7_BD-myc-AtPex5	TN63_PEX5_NcoI	CATG<u>CCATGG</u>CGATGAGAGACCTTGTTAAC	pGBKT7_BD-myc
	TN64_PEX5_BamHI	CG<u>GGATCC</u>TCACAGCGGGAATTCTTT	

pGBKT7_BD-myc-AtPex5(TPR)	TN65_TPR(PEX5)_NcoI	CATG<u>CCATGG</u>CTATGAATCCTTATGTGGGTC	pGBKT7_BD-myc
	TN64_PEX5_BamHI	CG<u>GGATCC</u>TCACAGCGGGAATTCTTT	
pACT2_AD-HA-ΔNt80aaNHL4	TN40_DN80NHL4_NcoI	CATG<u>CCATGG</u>CTCCTAAACTCCCGAGTTAC	pACT2_AD-HA
	TN41_NHL4_BamHI	CG<u>GGATCC</u>TCAGAGTTTGGCCTTAAA	
pACT2_AD-HA-ΔNt100aaNHL6	TN44_DN100NHL6_NcoI	CATG<u>CCATGG</u>CTGACCGGTTACAGCTCACC	pACT2_AD-HA
	TN45_NHL6_BamHI	CG<u>GGATCC</u>TATAACCTAAGACGAAATTTGC	
pACT2_AD-HA-ΔNt100aaNHL25	TN48_DN100NHL25_NcoI	CATG<u>CCATGG</u>CTCTAACCCGGTTTCAACTAAACC	pACT2_AD-HA
	TN49_NHL25_BamHI	CG<u>GGATCC</u>TTATAGTCTAAACCTGTATTTGC	
pACT2_AD-HA-NHL4(Ct30aa)	TN42_Ct30(NHL4)_NcoI	CATG<u>CCATGG</u>CTTTGGGGAGTTGTAAGCTT	pACT2_AD-HA
	TN41_NHL4_BamHI	CG<u>GGATCC</u>TCAGAGTTTGGCCTTAAA	
pACT2_AD-HA-NHL6(Ct30aa)	TN46_Ct30(NHL6)_NcoI	CATG<u>CCATGG</u>CTTTGGTCAGATGTGGTGTA	pACT2_AD-HA
	TN45_NHL6_BamHI	CG<u>GGATCC</u>TATAACCTAAGACGAAATTTGC	
pACT2_AD-HA-NHL25(Ct30aa)	TN50_Ct30(NHL25)_NcoI	CATG<u>CCATGG</u>CTTTGGTTAGGTGTGGTGTATC	pACT2_AD-HA
	TN49_NHL25_BamHI	CG<u>GGATCC</u>TTATAGTCTAAACCTGTATTTGC	
pACT2_AD-HA-MIF1	TN57_MIF1_NcoI	CATG<u>CCATGG</u>CTATGCCTTGTCTTTACATTAC	pACT2_AD-HA
	TN58_MIF1_BamHI	CG<u>GGATCC</u>CTAAAGTTTAGAAGGAAGAGGC	
pACT2_AD-HA-MIF1(Ct10aa)	TN52_pA_MluI	CG<u>ACGCGT</u>TTGGAATCACTACAGG	pACT2_AD-HA
	TN59_C10(MIF1)_BamHI	CG<u>GGATCC</u>CTAAAGTTTAGAAGGAAGAGGCAAAGAATTAATAG<u>CCATGG</u>CCATATGACCACCCAAG	
pACT2_AD-HA-Hs19	TN52_pA_MluI	CG<u>ACGCGT</u>TTGGAATCACTACAGG	pACT2_AD-HA
	TN53_C10(Hs19)_BamHI	CG<u>GGATCC</u>CTACAGGCGGCTCGCGGTGCAGCCAATGTTGTTAGCCATGGCCATATGACCACCCAAG	
pACT2_AD-HA-Hs27	TN52_pA_MluI	CG<u>ACGCGT</u>TTGGAATCACTACAGG	pACT2_AD-HA
	TN54_C10(Hs27)_BamHI	CG<u>GGATCC</u>CTACAGGCGCGCCCATTTTTTGCCCTGTTCAATAGCCATGGCCATATGACCACCCAAG	
pACT2_AD-HA-Nk02	TN52_pA_MluI	CG<u>ACGCGT</u>TTGGAATCACTACAGG	pACT2_AD-HA
	TN55_C10(Nk02)_BamHI	CG<u>GGATCC</u>CTACGCATCGCCTTTCGGCAGCCAGCCCAGGCGAGCCATGGCCATATGACCACCCAAG	

154

| pACT2_AD-HA-Nk03 | TN52_pA_MluI | CGACGCGTTTGGAATCACTACAGG | pACT2_AD-HA |
| | TN56_C10(Nk03)_BamHI | CGGGATCCCTACAGCATATCAATGCGGCCGCGGGTCCAGCCAGCC ATGGCCATATGACCACCCAAG | |

Supplementary Table 3: SOC medium

Ingredient	Final concentration (g·L^{-1})
Tryptone	20
Yeast extract	5
NaCl	0.6
KCl	0.2

After autoclaving, the medium was supplemented with following solutions (sterile-filtered): 10 mL·L^{-1} of 2 M Mg^{2+} stock solution (1 M MgCl$_2$·6 H$_2$O and 1 M MgSO$_4$·7 H$_2$O) and 20 mL·L^{-1} of 1 M glucose.

Supplementary Table 4: Components of YPDA medium

Ingredient	Final concentration (%)
Peptone (w/v)	2
Yeast extract (w/v)	1
Bacto Agar (w/v) for solid medium	2

After autoclaving at 121°C and approx. 2 atm for 15 min, sterile-filtered 40% glucose (w/v) and 2 g·L^{-1} adenine hemi-sulfate (w/v) were added to 2% and 0.04 mg·L^{-1} as a final conc., respectively.

Supplementary Table 5: Components of SD medium lacking leucine and tryptophan

Ingredient	Final concentration (g·L^{-1})
Complete Supplement Mixture (CSM)	0.625
L-His	0.02
Bacto Agar (for solid medium)	20

The medium was autoclaved at 121°C and 1 atm for 15 min (to avoid agar breakdown). After cooling down to 55°C, the medium was supplemented with the sterile-filtered components as follows: 40% glucose (w/v, C$_{final}$: 2%), 20x yeast nitrogen base (YNB) (134 g·L^{-1} stock of the YNB form with ammonium sulphate, C$_{final}$: 6.7 g·L^{-1}), and 50x adenine hemi sulfate (w/v, C$_{final}$: 40 mg·L^{-1} plus 20 mg·L^{-1} from CSM = 60 mg·L^{-1}).

Note: CSM is a combination of amino acids and purine (adenine) and pyrimidine bases (uracil) to support vigorous cells growth.

Supplementary Table 6: Components of 2x MSB solution

Ingredient	Final concentration (mM)
PIPES (Sigma P-6757)	100
EGTA (Sigma E-4378)	10
MgSO$_4$·7 H$_2$O	5

The pH buffer of 6.8 was adjusted with 1 M KOH. The 2x MSB solution was used to prepare a fixation solution which contained 1x MSB, 2% (v/v) paraformaldehyde, 0.1% (v/v) glutaraldehyde, and water. Paraformaldehyde (Merck Cat. 1.04005.1000) was dissolved in H_2O at 70°C under the fume hood to prepare a stock concentration of 16% (w/v). The pH was adjusted by adding 2 – 3 drops of warmed 1 M KOH until all powder of paraformaldehyde was dissolved. For the same fixation solution, 25% glutaraldehyde was used as stock.

Supplementary Table 7: Primers used for genotyping of T-DNA insertion lines

Gene-specific primers were used to detect the absence of the WT alleles in the T-DNA insertion lines. To verify the presence of the T-DNA in the mutant lines, the gene-specific reverse primer was used in combination with the corresponding T-DNA left border primer, e.g. LB1_SAIL (5' GCCTTTTCAGAAATGGATAAATAGCCTTGCTTCC 3') for SAIL lines and LBb1.3 (5' ATTTTGCCGATTTCGGAAC 3') for SALK lines. The same approach was performed for genotyping the double (*nhl6-1 x nhl25-1*) and triple (*nhl4-1 x nhl6-1 x nhl25-1*) mutant lines.

T-DNA insertion line	Gene-specific primer	Primer sequence (5' → 3')
nhl4-1 (SAIL_681_E12)	TN18_NHL4_SAIL_AK_F	TGGCCTTAAAACTGCAATCAC
	TN19_NHL4_SAIL_AK_R	ACGGGTTGTTGCTGAACATAG
nhl6-1 (SALK_148523)	TN36_NHL6_SALK_AK_F	TGGTAAAATTTTGGCAACGAC
	TN37_NHL6_SALK_AK_R	AATCTATCCGGTCCAAGATCC
nhl25-1 (SALK_113216)	TN38_NHL25_SALK_AK_F	GGCAAAAACATACGGATTGTG
	TN39_NHL25_SALK_AK_R	GGTTACAGCTAACCCGGTTTC

Supplementary Table 8: Primers used for gene expression analyses by qRT-PCR

Most primers used for amplification of *NHL25* transcript were designed in this study, and others were taken from the study of Mwaanga (2011).

Target gene	Primer name	Primer sequence (5' → 3')
NHL4	TN34_NHL4_qP_CM_F	TGCAGCAGCAACAACAAACAGG
	TN35_NHL4_qP_CM_R	TTCCGAGTTTGATGGCGACAGG
NHL6	TN36_NHL6_SALK_AK_F	TGGTAAAATTTTGGCAACGAC
	TN37_NHL6_SALK_AK_R	AATCTATCCGGTCCAAGATCC
NHL25	TN136_qPCR_NHL25_F	CAGTAATGGGTCGTTGCC
	TN137_qPCR_NHL25_R	TCAACGGATACACCACACCT
ACT2	TN20_ACT2_qPCR_asCM	TGC CAA TCT ACG AGG GTT TC
	TN21_ACT2_qPCR_asCM	CAG TAA GGT CAC GTC CAG CA

Supplementary Table 9: Components of Z buffer used for the colony-lift filter assay

Ingredient	Final concentration (g·L^{-1})
Na$_2$HPO$_4$·2 H$_2$O	10.7
NaH$_2$PO$_4$·2 H$_2$O	5.5
KCl	0.75
MgSO$_4$·7 H$_2$O	0.24
H$_2$O	ad 1 L

The pH was adjusted to 7.0 and autoclaved for long-term storage at RT.

Supplementary Table 10: Primers annealing to vector backbone and constructs

Vector	Primer name	Primer sequence (5' → 3')
pQE31	TN100_pQE31_SeqF	CAATTGTGAGCGGATAACAATTTC
pMAL-c2x	TN99_pMAL-c2x_SeqF	AGACGCGCAGACTAATTCGAGC
pSAT6_mVenus-C	SR320R	CCTTATCTGGGAACTACTCAC
pBA002	TN16_pBA_AK_F	CGT CTT CAA AGC AAG TGG ATT GAT G
	TN17_pBA_AK_R	TGCTTAACGTAATTCAACAACAGAAATT ATA
pENTR223_NHLX$_{pro}$	M13F	TGTAAAACGACGGCCAG
	M13R	CAGGAAACAGCTATGAC
pENTR223_NHL4$_{pro}$:NHL4	M13F	TGTAAAACGACGGCCAG
	M13R	CAGGAAACAGCTATGAC
	TN128_comNHL4se988	CCGAATGATTTATTGTTTTTGTTTT
pENTR223_NHL6$_{pro}$:NHL6	M13F	TGTAAAACGACGGCCAG
	M13R	CAGGAAACAGCTATGAC
	TN129_comNHL6se987	GCAAGTAATTTGATACCTACTAATG
pENTR223_NHL25$_{pro}$:NHL25	M13F	TGTAAAACGACGGCCAG
	M13R	CAGGAAACAGCTATGAC
	TN131_comNHL25se998	TTTTTCAAAAAATCTAGCACAAGGC
	TN132_comNHL25se1903	CAGCAAGCAGCACCGTTGGATCCTC
	TN117_comNHL25se1531	AGTAGGGGAAAATTGTGAGACCCAAG
pGBKT7-BD-myc-ProtX	SP49F	GTTGACTGTATCGCCGGAATTTGTAATA CG
	SP50R	GAAATTCGCCCGGAATTAGCTTGGCTGC
	TN64_PEX5_BamR (ProtX = AtPex5)	CGGGATCCTCACAGCGGGAATTCTTT
pACT2_AD-HA-ProtX	UP10	CTATTCGATGATGAAGATACCCCACCAA ACCC
	UP11	GTGAACTTGCGGGGTTTTTCAGTATCTA CGA
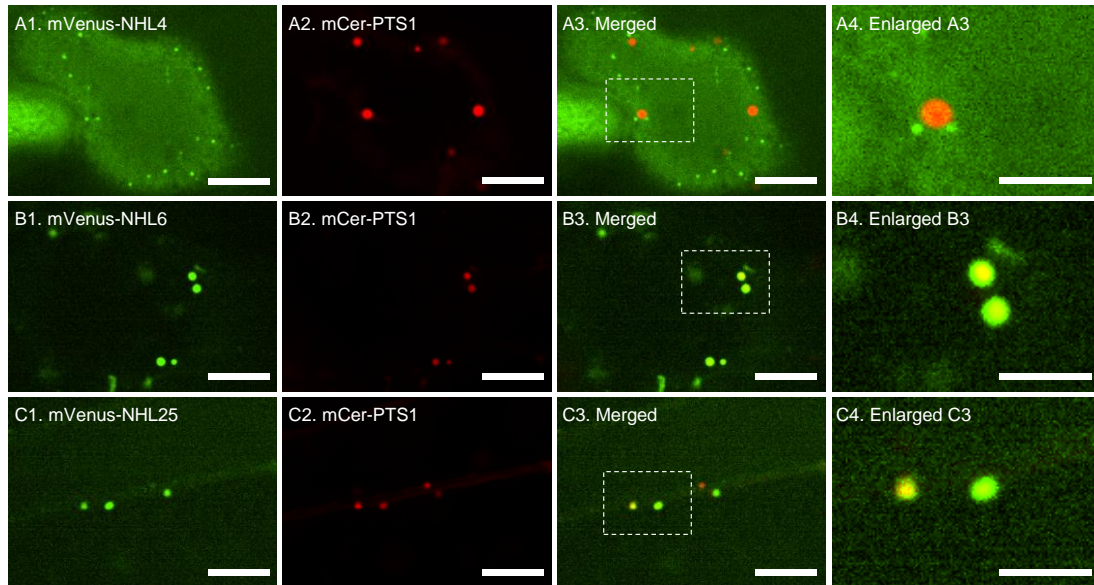
Supplementary Figure 1: *In vivo* **subcellular targeting analyses of mVenus tagged NHLs in transiently transformed Arabidopsis seedlings**

Four-day-old Arabidopsis seedlings were transformed by co-cultivation with *Agrobacterium*. Confocal images of epidermal cotyledon cells co-expressing *mVenus-NHLs* individually with *mCer-PTS1* (peroxisome marker) 3 dpc showed that (A) NHL4 targeted mVenus to non-peroxisomal vesicle-like structures and (B) NHL6 and (C) NHL25 targeted mVenus to peroxisomes. The blue fluorophore marker mCer-PTS1 labeled peroxisomes, and its blue fluorescence was converted to red. Scale bar = 10 μm (5 μm for enlarged regions).
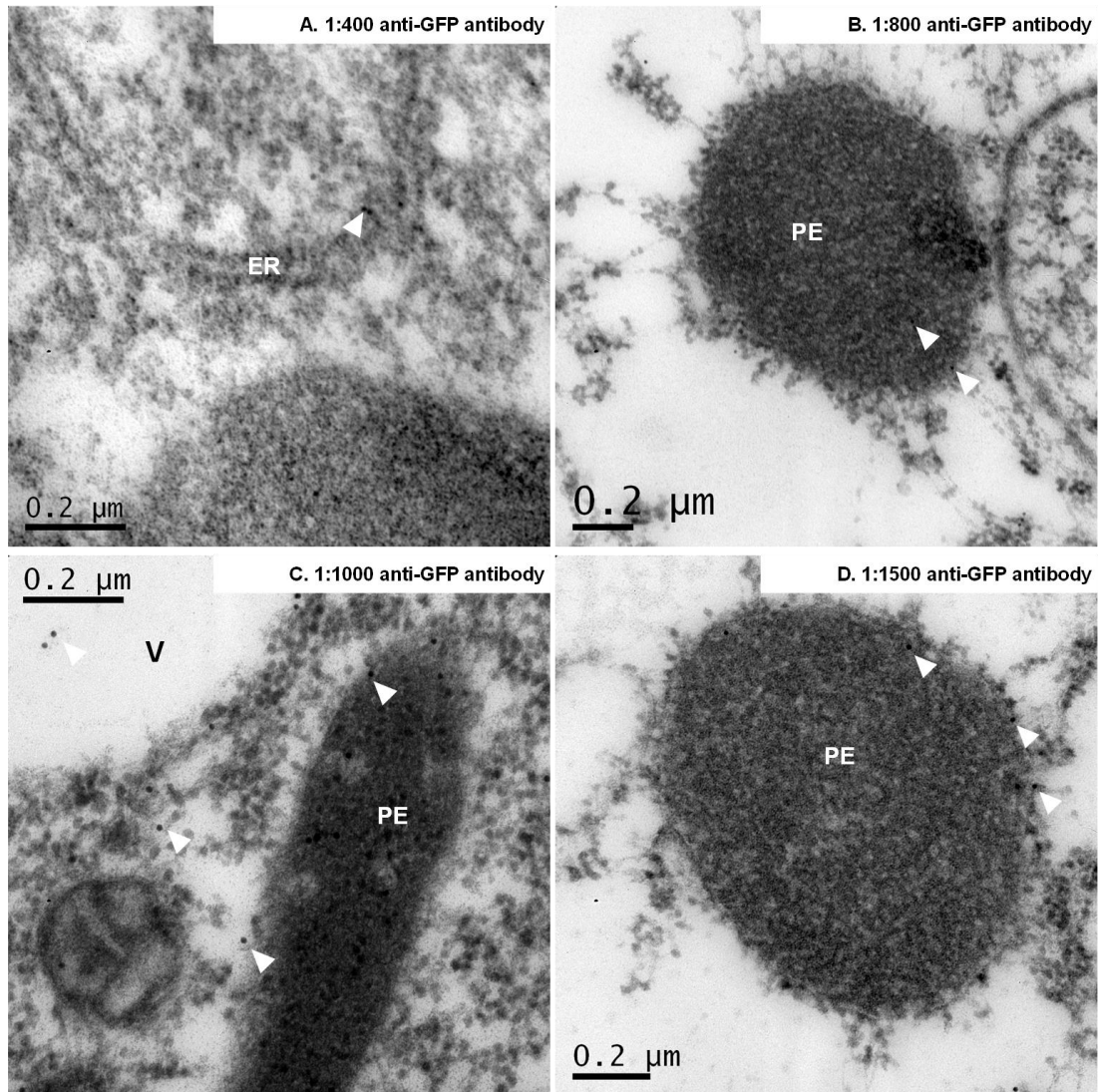
Supplementary Figure 2: TEM images of unspecific binding of anti-GFP antibody in WT Arabidopsis seedlings

Four-day-old seedlings were co-cultivated either with *Agrobacterium* carrying *EYFP-NHLx* or empty vector (negative or WT control). Cotyledons of Arabidopsis seedlings incubated in 0.25x MS liquid medium were harvested 5 dpc and were subjected to chemical fixation, embedding, and subsequently to TEM analyses. The control was used to investigate unspecific binding of the anti-GFP antibody, which also bound to EYFP. The unspecific binding of the primary antibody to the ER, peroxisomes (PE), vacuole (V), and cytosol (indicated by arrows) at different concentrations (A – D) is shown by TEM. The sample fixation, embedding, and sectioning were performed with technical assistance by Ms. Elke Woelken (University of Hamburg, Hamburg, Germany).
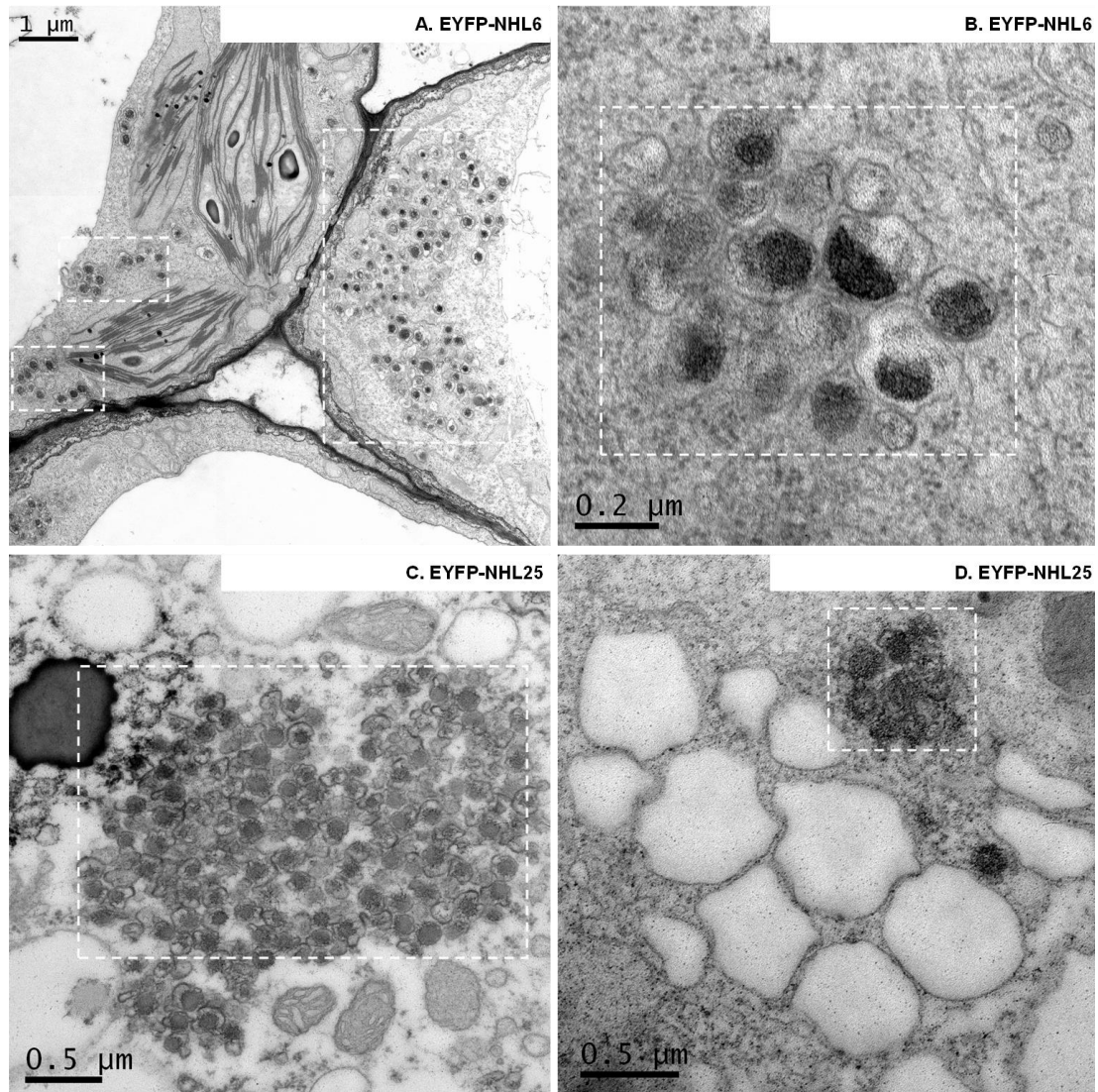
Supplementary Figure 3: TEM images of vesicles observed in transiently transformed Arabidopsis seedlings overexpressing *EYFP-NHL6* or *EYFP-NHL25*

Four-day-old seedlings were transiently transformed by co-cultivation with *Agrobacterium*. Cotyledons of Arabidopsis seedlings co-cultivated for 5 days with *Agrobacterium* were subjected to chemical fixation, embedding, and subsequently to the TEM analyses without immunogold labeling. Clusters of vesicles (dashed boxes) are shown (A, B) in epidermal and mesophyll cells of transiently transformed Arabidopsis seedlings expressing *EYFP-NHL6*. (C, D) Similar vesicle clusters were observed in mesophyll cells expressing *EYFP-NHL25,* as marked by the dashed boxes*.* The sample fixation, embedding, sectioning, and TEM were performed with technical assistance by Ms. Elke Woelken (University of Hamburg, Hamburg, Germany).
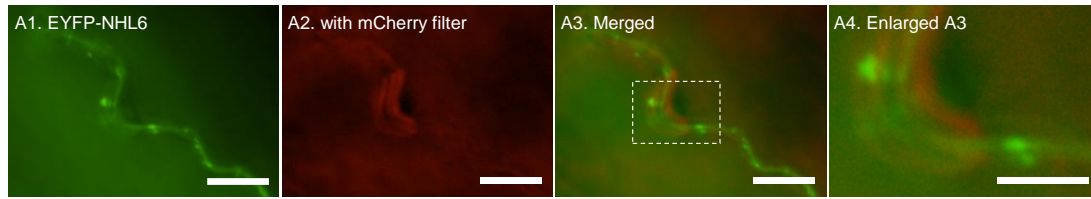
Supplementary Figure 4: Bleed-through analysis of EYFP fluorescence with the mCherry filter by epifluorescence microscopy

Four-day-old Arabidopsis seedlings were transformed by co-cultivation with *Agrobacterium* carrying the *EYFP-NHL6* construct 3 dpc. Epifluorescence images of epidermal cotyledon cells expressing *EYFP-NHL6* alone showed that NHL6 targeted EYFP to vesicle-like structures. The EYFP fluorescence was not detected with the mCherry filter even with longer exposure time of 5 sec. Scale bar = 10 μm (5 μm for enlarged regions).
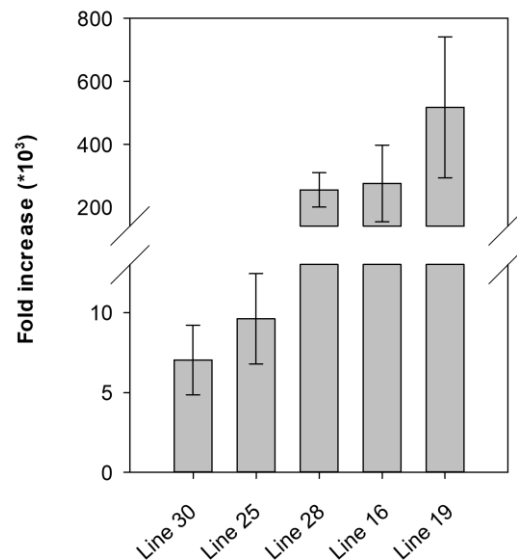
Supplementary Figure 5: Fold increase of *NHL4* expression in independent *EYFP-NHL4* overexpressor lines

Four-week-old plants of five independent $EYFP-NHL4_{OE}$ lines (T$_3$) were used to analyze *NHL4* expression levels by qRT-PCR. *ACT2* was the reference gene. The primer pairs amplifying *NHL4* and *ACT2* showed a similar amplification efficiency so that the relative quantification method ($2^{-\Delta Ct}$) could be applied (2.13.10). Since *NHL4* is a single exon gene, 1 μg of isolated RNA samples were treated with 2 U of DNase I instead of 1 U as recommended. Additionally, only 200 ng of DNase I-treated RNA was used to synthesize the first-strand cDNA that was later used as the template in qRT-PCR. Every cDNA sample was run with two technical replicates. Data show the increase of *NHL4* expression in different overexpressor lines in comparison with WT in which the relative *NHL4* expression (vs. *ACT2*) was set to 1. Error bars represent standard deviation from at least two biological samples.

A

BS Name	BS Genome Start	BS Genome End	Binding Site Sequence	Binding Site Family/TF
Bellringer/replumless/pennywise BS2 IN AG	20372400	20372407	aaattagt	Homeobox
Bellringer/replumless/pennywise BS3 IN AG	20372399	20372406	actaattt	Homeobox
MYB4 binding site motif	20372631	20372637	aacaacc	MYB
MYB4 binding site motif	20372473	20372479	aacaacc	MYB
RAV1-A binding site motif	20372767	20372771	caaca	ABI3VP1
RAV1-A binding site motif	20372693	20372697	caaca	ABI3VP1
RAV1-A binding site motif	20372625	20372629	caaca	ABI3VP1
RAV1-A binding site motif	20372530	20372534	caaca	ABI3VP1
RAV1-A binding site motif	20372513	20372517	caaca	ABI3VP1
RAV1-A binding site motif	20372476	20372480	caaca	ABI3VP1
LFY consensus binding site motif	20372522	20372527	ccaatg	LFY

B

BS Name	BS Genome Start	BS Genome End	Binding Site Sequence	Binding Site Family/TF
W-box promoter motif	24498559	24498564	ttgact	WRKY
W-box promoter motif	24499347	24499352	ttgact	WRKY
ARF1 binding site motif	24499222	24499227	tgtctc	ARF
DPBF1&2 binding site motif	24498715	24498721	acaccgg	bZIP
DPBF1&2 binding site motif	24498486	24498492	acacaag	bZIP
MYB4 binding site motif	24498518	24498524	accaaac	MYB
MYB4 binding site motif	24499196	24499202	aacaacc	MYB
MYB4 binding site motif	24498808	24498814	aactacc	MYB
RAV1-A binding site motif	24499256	24499260	caaca	ABI3VP1
RAV1-A binding site motif	24499675	24499679	caaca	ABI3VP1
RAV1-A binding site motif	24499128	24499132	caaca	ABI3VP1
RAV1-A binding site motif	24498490	24498494	caaca	ABI3VP1
LFY consensus binding site motif	24499192	24499197	ccagtg	LFY
LFY consensus binding site motif	24499477	24499482	ccaatg	LFY
LFY consensus binding site motif	24499477	24499482	ccattg	LFY
LFY consensus binding site motif	24499192	24499197	ccactg	LFY
LFY consensus binding site motif	24498969	24498974	ccactg	LFY
LFY consensus binding site motif	24498804	24498809	ccattg	LFY

163

C

BS Name	BS Genome Start	BS Genome End	Binding Site Sequence	Binding Site Family/TF
CCA1 motif1 BS in CAB1	14622543	14622552	aaacaatcta	...
CArG promoter motif	14623012	14623021	ccaaaaaagg	MADS
CArG promoter motif	14623011	14623020	cctttttttgg	MADS
CCA1 binding site motif	14622472	14622479	aaaaatct	MYB-related
CCA1 binding site motif	14622544	14622551	aacaatct	MYB-related
DPBF1&2 binding site motif	14623195	14623201	acacttg	bZIP
DPBF1&2 binding site motif	14622689	14622695	acacctg	bZIP
MYB binding site promoter	14623134	14623141	caccaaac	MYB
MYB4 binding site motif	14623135	14623141	accaaac	MYB
MYB4 binding site motif	14623042	14623048	accaaac	MYB
RAV1-A binding site motif	14622933	14622937	caaca	ABI3VP1
RAV1-A binding site motif	14623131	14623135	caaca	ABI3VP1
RAV1-A binding site motif	14622830	14622834	caaca	ABI3VP1
RAV1-A binding site motif	14622802	14622806	caaca	ABI3VP1
RAV1-B binding site motif	14622689	14622694	cacctg	ABI3VP1
LFY consensus binding site motif	14622870	14622875	ccattg	LFY

Supplementary Figure 6: Computational search for *cis*-regulatory elements in the promoter regions of *NHL4*, *NHL6*, and *NHL25*

The prediction of binding site motifs and their respective binding transcription factors in the promoters of (A) *NHL4*, (B) *NHL6*, and (C) *NHL25* are shown. The search was performed using the gene annotations of *NHL4* (At1g54540), *NHL6* (At1g65690), and *NHL25* (At5g36970) as an input query for the Arabidopsis *cis*-regulatory element database (https://agris-knowledgebase.org/AtcisDB/).
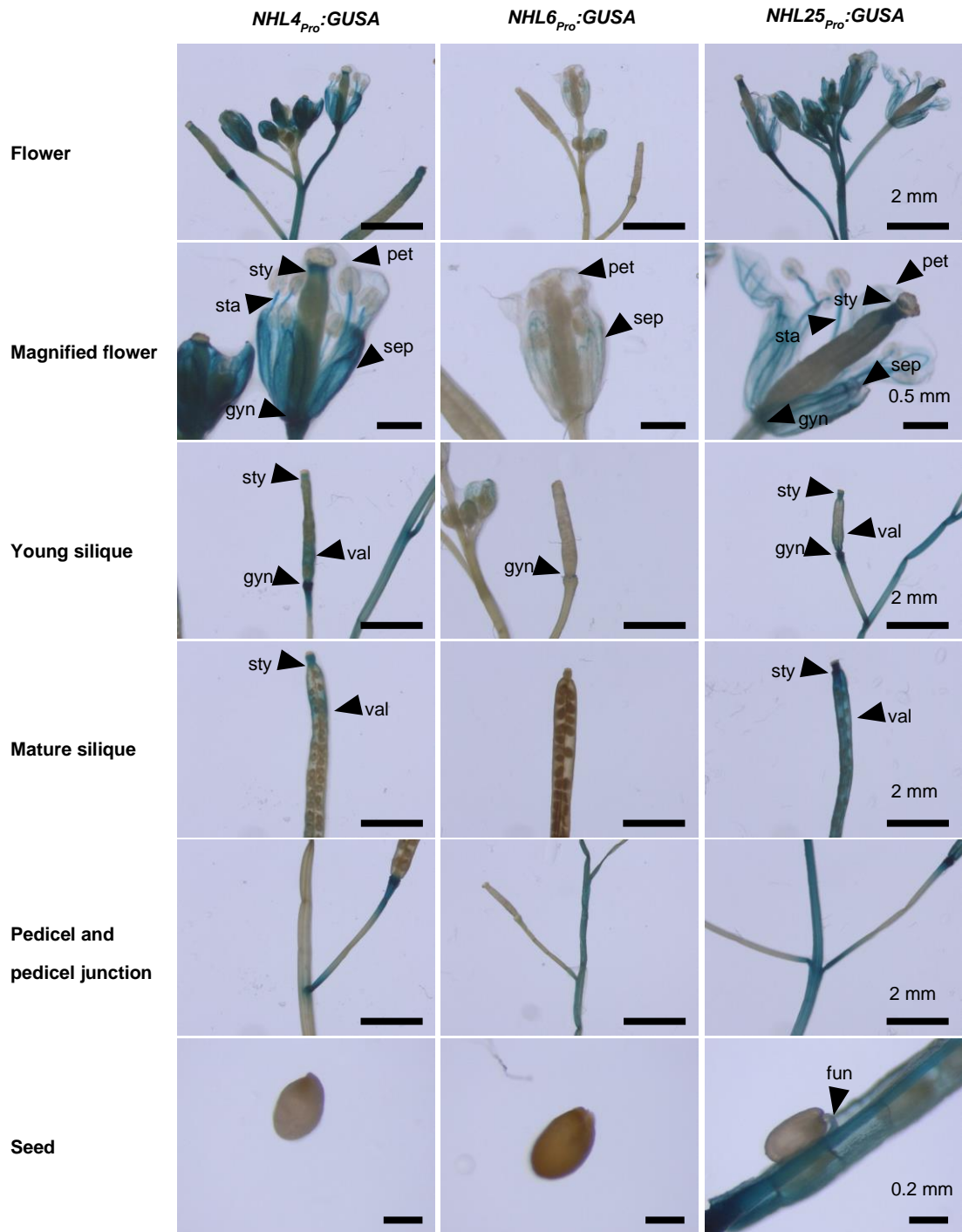
Supplementary Figure 7: *GUSA* expression analyses from the native *NHL* promoters in reproductive tissues of stable transgenic Arabidopsis lines

The experimental design is explained in Figure 3.17.

Abbreviations: fun, funiculus; gyn, gynophore; pet, petal; sep, sepal; sta, stamen; sty, style; val, valve.
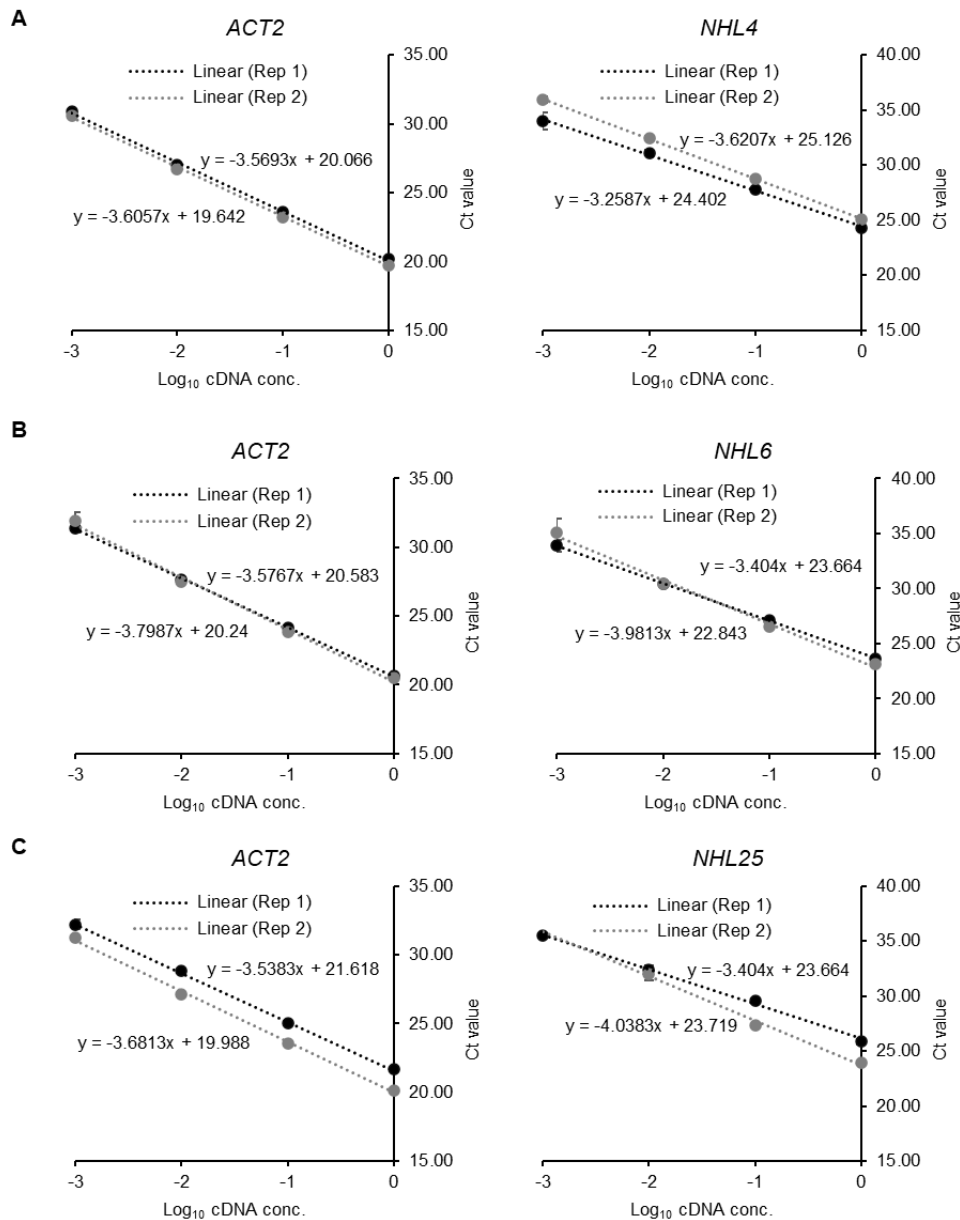
Supplementary Figure 8: Analyses of amplification efficiency of the primer pairs of *ACT2* and *NHL* genes in ABA and *Pseudomonas*-treated samples

The Ct values correspond to the analyses of (A) *NHL4*, (B) *NHL6*, and (C) *NHL25* at different cDNA dilutions, and in the same samples the reference gene *ACT2* were also detected. To determine the amplification efficiency (E) of each primer pair, the slope values of each linear regression were used to calculate E, i.e. $E = 10^{(-1/slope)}$. The transcript of *NHLs* must be sufficiently abundant to generate a serial 10-fold cDNA dilution and subsequently result in reliable Ct values (2.13.10). Thus, ABA-treated samples at 12 h (*NHL4*) and 6 h (*NHL6*) and *Pst*(*avrRpt2*) treated samples at 24 h (*NHL25*) were chosen (2.1.1 and 2.1.2). Likewise, the E values of *ACT2* was evaluated in all the samples. Data show mean and standard deviation from three technical replicates. The linear regressions were generated from two biological samples (referred to as Rep 1 and 2).
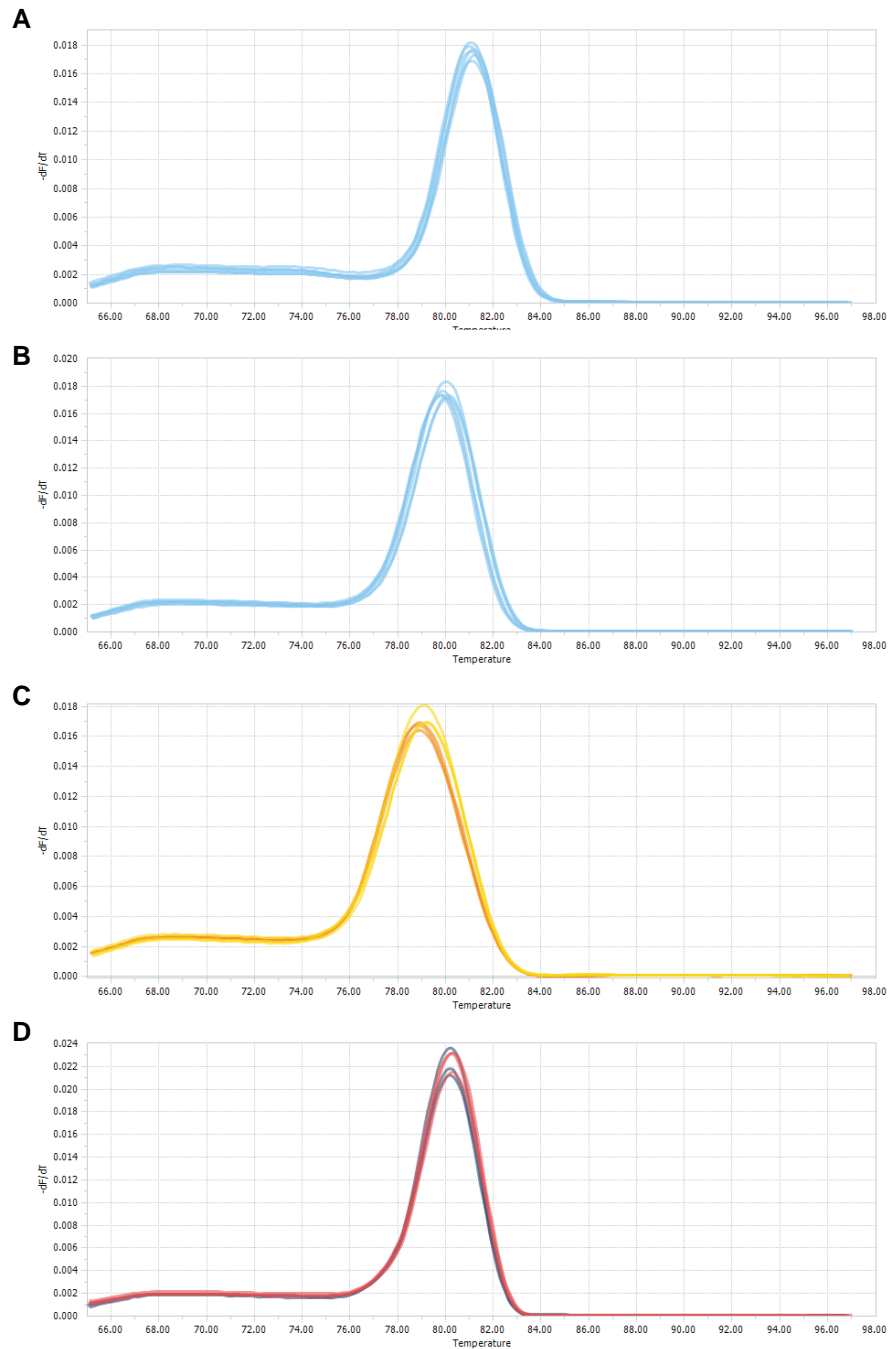
Supplementary Figure 9: Analyses of melting peaks of qRT-PCR products amplified by *ACT2* and *NHL* primer pairs

The graphs show the melting curves of qRT-PCR products amplified by the primer pairs of (A) *ACT2*, (B) *NHL4*, (C) *NHL6*, and (D) *NHL25*. The appearance of one melting peak indicates the presence of only amplicon. Data show the melting peak analyses from three technical replicates and two biological samples upon the same treatment.
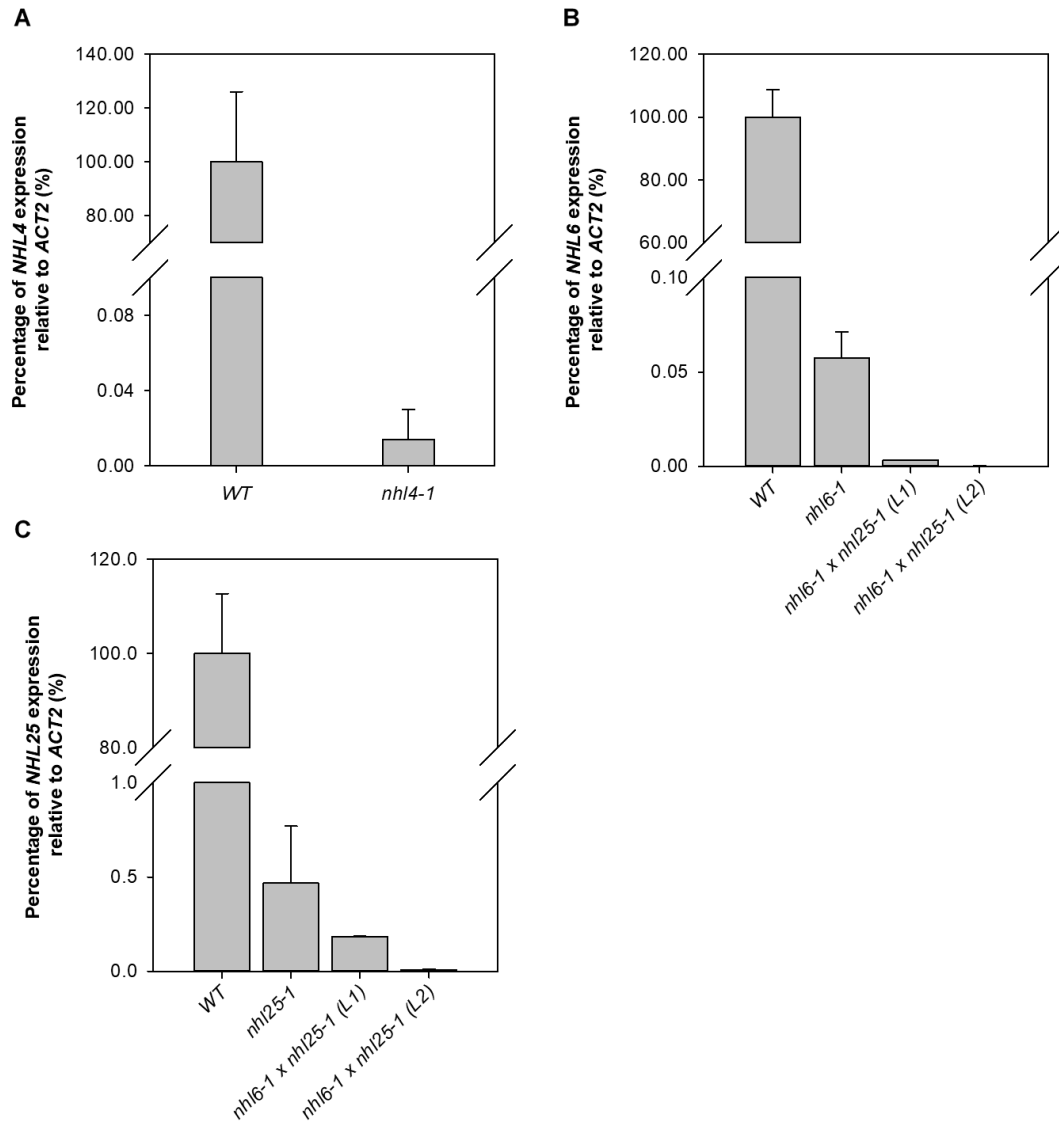
Supplementary Figure 10: Expression analyses of the putative gene knockout of *NHLs* in single and double mutants used in this study

Percentage of relative gene expression of (A) *NHL4*, (B) *NHL6*, and (C) *NHL25* is shown for the WT and the indicated mutants. Four-week-old plants were used for the analysis. The reference gene, *ACT2* was used for normalization by the $2^{-\Delta Ct}$ method. The relative gene expression of *NHLs* (vs. *ACT2*) in WT was set to 100%, and that of the corresponding genes in the mutants was calculated accordingly. Data represent mean values and standard errors from three technical replicates and from at least two biological samples.

7 REFERENCES

Aarts, N., Metz, M., Holub, E., Staskawicz, B.J., Daniels, M.J., and Parker, J.E. (1998). Different requirements for *EDS1* and *NDR1* by disease resistance genes define at least two *R* gene-mediated signaling pathways in *Arabidopsis*. Proceedings of the National Academy of Sciences of the United States of America *95*, 10306-10311.

Albertini, M., Rehling, P., Erdmann, R., Girzalsky, W., Kiel, J.A., Veenhuis, M., and Kunau, W.-H. (1997). Pex14p, a peroxisomal membrane protein binding both receptors of the two PTS-dependent import pathways. Cell *89*, 83-92.

Amara, I., Odena, A., Oliveira, E., Moreno, A., Masmoudi, K., Pages, M., and Goday, A. (2012). Insights into maize LEA proteins: from proteomics to functional approaches. Plant and Cell Physiology *53*, 312-329.

Amery, L., Brees, C., Baes, M., Setoyama, C., Miura, R., Mannaerts, G.P., and Veldhoven, P.P.V. (1998). C-terminal tripeptide Ser-Asn-Leu (SNL) of human D-aspartate oxidase is a functional peroxisome-targeting signal. Biochemical Journal *336*, 367-371.

Apel, K., and Hirt, H. (2004). Reactive oxygen species: metabolism, oxidative stress, and signal transduction. Annual Review of Plant Biology *55*, 373-399.

Arai, Y., Hayashi, M., and Nishimura, M. (2008). Proteomic identification and characterization of a novel peroxisomal adenine nucleotide transporter supplying ATP for fatty acid β-oxidation in soybean and Arabidopsis. The Plant Cell *20*, 3227-3240.

Artur, M.A.S., Zhao, T., Ligterink, W., Schranz, E., and Hilhorst, H.W. (2019). Dissecting the genomic diversification of *late embryogenesis abundant* (*LEA*) protein gene families in plants. Genome Biology and Evolution *11*, 459-471.

Aung, K., Zhang, X., and Hu, J. (2010). Peroxisome division and proliferation in plants. Biochemical Society Transactions *38*, 817-822.

Bao, Y., Song, W.-M., Pan, J., Jiang, C.-M., Srivastava, R., Li, B., Zhu, L.-Y., Su, H.-Y., Gao, X.-S., and Liu, H. (2016). Overexpression of the *NDR1/HIN1-like* gene *NHL6* modifies seed germination in response to abscisic acid and abiotic stresses in Arabidopsis. PLoS ONE *11*, e0148572.

Battaglia, M., Olvera-Carrillo, Y., Garciarrubio, A., Campos, F., and Covarrubias, A.A. (2008). The enigmatic LEA proteins and other hydrophilins. Plant Physiology *148*, 6-24.

Battista, J.R., Park, M.-J., and McLemore, A.E. (2001). Inactivation of two homologues of proteins presumed to be involved in the desiccation tolerance of plants sensitizes *Deinococcus radiodurans* R1 to desiccation. Cryobiology *43*, 133-139.

Baune, M.-C., Lansing, H., Fischer, K., Meyer, T., Charton, L., Linka, N., and von Schaewen, A. (2020). The Arabidopsis plastidial glucose-6-phosphate transporter GPT1 is dually targeted to peroxisomes via the endoplasmic reticulum. The Plant Cell *32*, 1703-1726.

Beck, M., Wyrsch, I., Strutt, J., Wimalasekera, R., Webb, A., Boller, T., and Robatzek, S. (2014). Expression patterns of *flagellin sensing 2* map to bacterial entry sites in plant shoots and roots. Journal of Experimental Botany *65*, 6487-6498.

Bednarek, P., Piślewska-Bednarek, M., Svatoš, A., Schneider, B., Doubský, J., Mansurova, M., Humphry, M., Consonni, C., Panstruga, R., and Sanchez-Vallet, A. (2009). A glucosinolate metabolism pathway in living plant cells mediates broad-spectrum antifungal defense. Science *323*, 101-106.

Bies-Etheve, N., Gaubier-Comella, P., Debures, A., Lasserre, E., Jobet, E., Raynal, M., Cooke, R., and Delseny, M. (2008). Inventory, evolution and expression profiling diversity of the LEA (late embryogenesis abundant) protein gene family in *Arabidopsis thaliana*. Plant Molecular Biology *67*, 107-124.

Bigeard, J., Colcombet, J., and Hirt, H. (2015). Signaling mechanisms in pattern-triggered immunity (PTI). Molecular Plant *8*, 521-539.

Bonsegna, S., Slocombe, S.P., De Bellis, L., and Baker, A. (2005). AtLACS7 interacts with the TPR domains of the PTS1 receptor PEX5. Archives of Biochemistry and Biophysics *443*, 74-81.

Bradford, M.M. (1976). A rapid and sensitive method for the quantitation of microgram quantities of protein utilizing the principle of protein-dye binding. Analytical Biochemistry *72*, 248-254.

Bradley, D.J., Kjellbom, P., and Lamb, C.J. (1992). Elicitor-and wound-induced oxidative cross-linking of a proline-rich plant cell wall protein: a novel, rapid defense response. Cell *70*, 21-30.

Brandizzi, F., and Barlowe, C. (2013). Organization of the ER–Golgi interface for membrane traffic control. Nature reviews Molecular cell biology *14*, 382-392.

Bray, E.A. (1993). Molecular responses to water deficit. Plant Physiology *103*, 1035.

Bretschneider, K.E., Gonella, M.P., and Robeson, D.J. (1989). A comparative light and electron microscopical study of compatible and incompatible interactions between *Xanthomonas campestris* pv. *campestris* and cabbage (Brassica oleracea). Physiological and Molecular Plant Pathology *34*, 285-297.

Brini, F., Hanin, M., Lumbreras, V., Amara, I., Khoudi, H., Hassairi, A., Pages, M., and Masmoudi, K. (2007). Overexpression of wheat dehydrin DHN-5 enhances tolerance to salt and osmotic stress in *Arabidopsis thaliana*. Plant Cell Reports *26*, 2017-2026.

Brocard, C., and Hartig, A. (2006). Peroxisome targeting signal 1: is it really a simple tripeptide? Biochimica et Biophysica Acta (BBA)-Molecular Cell Research *1763*, 1565-1573.

Brown, F.I., Mcadams, A., Cummins, J., Konkol, R., Inderjit, S., Moser, A., and Moser, H. (1982). Cerebro-hepato-renal (Zellweger) syndrome and neonatal adrenoleukodystrophy: similarities in phenotype and accumulation of very long chain fatty acids. Johns Hopkins Medical Journal *151*, 344-351.

Burkhart, S.E., Kao, Y.-T., and Bartel, B. (2014). Peroxisomal ubiquitin-protein ligases peroxin2 and peroxin10 have distinct but synergistic roles in matrix protein import and peroxin5 retrotranslocation in *Arabidopsis*. Plant Physiology *166*, 1329-1344.

Büttner, D., and Bonas, U. (2010). Regulation and secretion of Xanthomonas virulence factors. FEMS microbiology reviews *34*, 107-133.

Century, K.S., Holub, E.B., and Staskawicz, B.J. (1995). *NDR1*, a locus of Arabidopsis thaliana that is required for disease resistance to both a bacterial and a fungal pathogen. Proceedings of the National Academy of Sciences of the United States of America *92*, 6597-6601.

Century, K.S., Shapiro, A.D., Repetti, P.P., Dahlbeck, D., Holub, E., and Staskawicz, B.J. (1997). NDR1, a pathogen-induced component required for Arabidopsis disease resistance. Science *278*, 1963-1965.

Cerutti, A., Jauneau, A., Auriac, M.-C., Lauber, E., Martinez, Y., Chiarenza, S., Leonhardt, N., Berthomé, R., and Noël, L.D. (2017). Immunity at cauliflower hydathodes controls systemic infection by *Xanthomonas campestris* pv *campestris*. Plant Physiology *174*, 700-716.

Chardin, P., and McCormick, F. (1999). Brefeldin A: the advantage of being uncompetitive. Cell *97*, 153-155.

Charlton, W.L., Matsui, K., Johnson, B., Graham, I.A., Ohme-Takagi, M., and Baker, A. (2005). Salt-induced expression of peroxisome-associated genes requires components of the ethylene, jasmonate and abscisic acid signalling pathways. Plant, Cell & Environment *28*, 513-524.

Chen, Q., Tian, Z., Jiang, R., Zheng, X., Xie, C., and Liu, J. (2018). *StPOTHR1*, a *NDR1/HIN1-like* gene in *Solanum tuberosum*, enhances resistance against *Phytophthora* infestans. Biochemical and Biophysical Research Communications *496*, 1155-1161.

Chen, Y., Pieuchot, L., Loh, R.A., Yang, J., Kari, T.M.A., Wong, J.Y., and Jedd, G. (2014). Hydrophobic handoff for direct delivery of peroxisome tail-anchored proteins. Nature Communications *5*, 1-12.

Chong, J., Le Henanff, G., Bertsch, C., and Walter, B. (2008). Identification, expression analysis and characterization of defense and signaling genes in *Vitis vinifera*. Plant Physiology and Biochemistry *46*, 469-481.

Chowdhary, G., Kataya, A.R., Lingner, T., and Reumann, S. (2012). Non-canonical peroxisome targeting signals: identification of novel PTS1 tripeptides and characterization of enhancer elements by computational permutation analysis. BMC Plant Biology *12*, 1-14.

Ciccarelli, F.D., and Bork, P. (2005). The WHy domain mediates the response to desiccation in plants and bacteria. Bioinformatics *21*, 1304-1307.

Close, T.J., and Lammers, P.J. (1993). An osmotic stress protein of cyanobacteria is immunologically related to plant dehydrins. Plant Physiology *101*, 773-779.

Clough, S.J., and Bent, A.F. (1998). Floral dip: a simplified method forAgrobacterium-mediated transformation ofArabidopsis thaliana. The plant journal *16*, 735-743.

Coll, N., Epple, P., and Dangl, J. (2011). Programmed cell death in the plant immune system. Cell Death & Differentiation *18*, 1247-1256.

Coppinger, P., Repetti, P.P., Day, B., Dahlbeck, D., Mehlert, A., and Staskawicz, B.J. (2004). Overexpression of the plasma membrane-localized NDR1 protein results in enhanced bacterial disease resistance in *Arabidopsis thaliana*. Plant Journal *40*, 225-237.

Corpas, F.J., Leterrier, M., Valderrama, R., Airaki, M., Chaki, M., Palma, J.M., and Barroso, J.B. (2011). Nitric oxide imbalance provokes a nitrosative response in plants under abiotic stress. Plant Science *181*, 604-611.

Crappe, D. (2016). Protein targeting and functional analyses of peroxisome-targeted defense proteins in Arabidopsis (Stavanger), pp. 223.

Cross, L.L., Ebeed, H.T., and Baker, A. (2016). Peroxisome biogenesis, protein targeting mechanisms and PEX gene functions in plants. Biochimica et Biophysica Acta (BBA)-Molecular Cell Research *1863*, 850-862.

Curry, J., Morris, C.F., and Walker-Simmons, M. (1991). Sequence analysis of a cDNA encoding a group 3 LEA mRNA inducible by ABA or dehydration stress in wheat. Plant Molecular Biology *16*, 1073-1076.

Curtis, M.D., and Grossniklaus, U. (2003). A Gateway cloning vector set for high-throughput functional analysis of genes in planta. Plant Physiology *133*, 462-469.

Dangl, J.L., and Jones, J.D. (2001). Plant pathogens and integrated defence responses to infection. Nature *411*, 826-833.

Day, B., Dahlbeck, D., and Staskawicz, B.J. (2006). NDR1 interaction with RIN4 mediates the differential activation of multiple disease resistance pathways in *Arabidopsis*. The Plant Cell *18*, 2782-2791.

De Duve, C., and Baudhuin, P. (1966). Peroxisomes (microbodies and related particles). Physiological Reviews *46*, 323-357.

De Hoop, M., and Ab, G. (1992). Import of proteins into peroxisomes and other microbodies. Biochemical Journal *286*, 657-669.

Del Río, L.A., Corpas, F.J., Sandalio, L.M., Palma, J.M., and Barroso, J.B. (2003). Plant peroxisomes, reactive oxygen metabolism and nitric oxide. IUBMB life *55*, 71-81.

Del Río, L.A., and López-Huertas, E. (2016). ROS generation in peroxisomes and its role in cell signaling. Plant and Cell Physiology *57*, 1364-1376.

Díaz, E.M. (2020). Molecular analyses to elucidate the role of NDR1/HIN1-like protein 4 in abiotic stress tolerance in *Arabidopsis thaliana* (University of Hamburg).

Dong, X., Mindrinos, M., Davis, K.R., and Ausubel, F.M. (1991). Induction of Arabidopsis defense genes by virulent and avirulent *Pseudomonas syringae* strains and by a cloned avirulence gene. The Plant Cell *3*, 61-72.

Dörmann, P., Gopalan, S., He, S.Y., and Benning, C. (2000). A gene family in *Arabidopsis thaliana* with sequence similarity to *NDR1* and *HIN1*. Plant Physiology and Biochemistry *38*, 789-796.

Dure III, L. (1993). A repeating 11-mer amino acid motif and plant desiccation. The Plant Journal *3*, 363-369.

Dure III, L., Greenway, S.C., and Galau, G.A. (1981). Developmental biochemistry of cottonseed embryogenesis and germination: changing messenger ribonucleic acid populations as shown by *in vitro* and *in vivo* protein synthesis. Biochemistry *20*, 4162-4168.

Dure, L., Crouch, M., Harada, J., Ho, T.-H.D., Mundy, J., Quatrano, R., Thomas, T., and Sung, Z. (1989). Common amino acid sequence domains among the LEA proteins of higher plants. Plant Molecular Biology *12*, 475-486.

Edelheit, O., Hanukoglu, A., and Hanukoglu, I. (2009). Simple and efficient site-directed mutagenesis using two single-primer reactions in parallel to generate mutants for protein structure-function studies. BMC Biotechnology *9*, 1-8.

Eder, J., and Cosio, E.G. (1994). Elicitors of plant defense responses. International Review of Cytology *148*, 1-36.

Edward Purdue, P., Yang, X., and Lazarow, P.B. (1998). Pex18p and Pex21p, a novel pair of related peroxins essential for peroxisomal targeting by the PTS2 pathway. The Journal of Cell Biology *143*, 1859-1869.

Effelsberg, D., Cruz-Zaragoza, L.D., Schliebs, W., and Erdmann, R. (2016). Pex9p is a new yeast peroxisomal import receptor for PTS1-containing proteins. Journal of Cell Science *129*, 4057-4066.

Elgersma, Y., Kwast, L., Klein, A., Voorn-Brouwer, T., Van Den Berg, M., Metzig, B., America, T., Tabak, H.F., and Distel, B. (1996a). The SH3 domain of the *Saccharomyces cerevisiae*

peroxisomal membrane protein Pex13p functions as a docking site for Pex5p, a mobile receptor for the import PTS1-containing proteins. The Journal of Cell Biology *135*, 97-109.

Elgersma, Y., Vos, A., van den Berg, M., van Roermund, C.W., van der Sluijs, P., Distel, B., and Tabak, H.F. (1996b). Analysis of the carboxyl-terminal peroxisomal targeting signal 1 in a homologous context in Saccharomyces cerevisiae. Journal of Biological Chemistry *271*, 26375-26382.

Emanuelsson, O., Elofsson, A., Von Heijne, G., and Cristobal, S. (2003). *In silico* prediction of the peroxisomal proteome in fungi, plants and animals. Journal of Molecular Biology *330*, 443-456.

Endo, A., Sawada, Y., Takahashi, H., Okamoto, M., Ikegami, K., Koiwai, H., Seo, M., Toyomasu, T., Mitsuhashi, W., and Shinozaki, K. (2008). Drought induction of Arabidopsis 9-cis-epoxycarotenoid dioxygenase occurs in vascular parenchyma cells. Plant Physiology *147*, 1984-1993.

Erdmann, R., and Blobel, G. (1995). Giant peroxisomes in oleic acid-induced *Saccharomyces cerevisiae* lacking the peroxisomal membrane protein Pmp27p. The Journal of Cell Biology *128*, 509-523.

Eubel, H., Meyer, E.H., Taylor, N.L., Bussell, J.D., O'Toole, N., Heazlewood, J.L., Castleden, I., Small, I.D., Smith, S.M., and Millar, A.H. (2008). Novel proteins, putative membrane transporters, and an integrated metabolic network are revealed by quantitative proteomic analysis of Arabidopsis cell culture peroxisomes. Plant Physiology *148*, 1809-1829.

Eulgem, T., Rushton, P.J., Robatzek, S., and Somssich, I.E. (2000). The WRKY superfamily of plant transcription factors. Trends in Plant Science *5*, 199-206.

Faber, K.N., van Dijk, R., Keizer-Gunnink, I., Koek, A., van der Klei, I.J., and Veenhuis, M. (2002). Import of assembled PTS1 proteins into peroxisomes of the yeast *Hansenula polymorpha*: yes and no! Biochimica et Biophysica Acta-Molecular Cell Research *1591*, 157-162.

Fakieh, M.H., Drake, P.J., Lacey, J., Munck, J.M., Motley, A.M., and Hettema, E.H. (2013). Intra-ER sorting of the peroxisomal membrane protein Pex3 relies on its luminal domain. Biology Open *2*, 829-837.

Falter, C., Thu, N.B.A., Pokhrel, S., and Reumann, S. (2019). New guidelines for fluorophore application in peroxisome targeting analyses in transient plant expression systems. Journal of Integrative Plant Biology *61*, 884-899.

Fang, Y., Morrell, J.C., Jones, J.M., and Gould, S.J. (2004). PEX3 functions as a PEX19 docking factor in the import of class I peroxisomal membrane proteins. The Journal of Cell Biology *164*, 863-875.

Fargier, E., and Manceau, C. (2007). Pathogenicity assays restrict the species *Xanthomonas campestris* into three pathovars and reveal nine races within *X. campestris* pv. *campestris*. Plant Pathology *56*, 805-818.

Faso, C., Chen, Y.-N., Tamura, K., Held, M., Zemelis, S., Marti, L., Saravanan, R., Hummel, E., Kung, L., and Miller, E. (2009). A missense mutation in the Arabidopsis COPII coat protein Sec24A induces the formation of clusters of the endoplasmic reticulum and Golgi apparatus. The Plant Cell *21*, 3655-3671.

Fernandes, L.D., Moura, A.P.S.d., and Ciandrini, L. (2017). Gene length as a regulator for ribosome recruitment and protein synthesis: theoretical insights. Scientific Reports *7*, 17409.

Finkelstein, R. (2013). Abscisic acid synthesis and response. The Arabidopsis Book/American Society of Plant Biologists *11*.

Flynn, C.R., Mullen, R.T., and Trelease, R.N. (1998). Mutational analyses of a type 2 peroxisomal targeting signal that is capable of directing oligomeric protein import into tobacco BY-2 glyoxysomes. The Plant Journal *16*, 709-720.

Fujii, H., and Zhu, J.-K. (2009). Arabidopsis mutant deficient in 3 abscisic acid-activated protein kinases reveals critical roles in growth, reproduction, and stress. Proceedings of the National Academy of Sciences *106*, 8380-8385.

Fujimoto, M., Arimura, S.i., Mano, S., Kondo, M., Saito, C., Ueda, T., Nakazono, M., Nakano, A., Nishimura, M., and Tsutsumi, N. (2009). Arabidopsis dynamin-related proteins DRP3A and DRP3B are functionally redundant in mitochondrial fission, but have distinct roles in peroxisomal fission. The Plant Journal *58*, 388-400.

Fulda, M., Shockey, J., Werber, M., Wolter, F.P., and Heinz, E. (2002). Two long-chain acyl-CoA synthetases from Arabidopsis thaliana involved in peroxisomal fatty acid β-oxidation. The Plant Journal *32*, 93-103.

Funke, S., Knechten, T., Ollesch, J., and Schünemann, D. (2005). A unique sequence motif in the 54-kDa subunit of the chloroplast signal recognition particle mediates binding to the 43-kDa subunit. Journal of Biological Chemistry *280*, 8912-8917.

Gao, H., Kadirjan-Kalbach, D., Froehlich, J.E., and Osteryoung, K.W. (2003). ARC5, a cytosolic dynamin-like protein from plants, is part of the chloroplast division machinery. Proceedings of the National Academy of Sciences *100*, 4328-4333.

Gatto, G.J., Geisbrecht, B.V., Gould, S.J., and Berg, J.M. (2000). Peroxisomal targeting signal-1 recognition by the TPR domains of human PEX5. Nature Structural Biology *7*, 1091-1095.

Girzalsky, W., Rehling, P., Stein, K., Kipper, J., Blank, L., Kunau, W.-H., and Erdmann, R. (1999). Involvement of Pex13p in Pex14p localization and peroxisomal targeting signal 2–dependent protein import into peroxisomes. The Journal of Cell Biology *144*, 1151-1162.

Glazebrook, J. (2001). Genes controlling expression of defense responses in *Arabidopsis*—2001 status. Current Opinion in Plant Biology *4*, 301-308.

Glover, J.R., Andrews, D.W., and Rachubinski, R.A. (1994). i peroxisomal thiolase is imported as a dimer. Proceedings of the National Academy of Sciences *91*, 10541-10545.

Goda, H., Sasaki, E., Akiyama, K., Maruyama-Nakashita, A., Nakabayashi, K., Li, W., Ogawa, M., Yamauchi, Y., Preston, J., Aoki, K.*, et al.* (2008). The AtGenExpress hormone and chemical treatment data set: experimental design, data evaluation, model data analysis and data access. The Plant Journal *55*, 526-542.

Goldfischer, S., Moore, C.L., Johnson, A.B., Spiro, A.J., Valsamis, M.P., Wisniewski, H.K., Ritch, R.H., Norton, W.T., Rapin, I., and Gartner, L.M. (1973). Peroxisomal and mitochondrial defects in the cerebro-hepato-renal syndrome. Science *182*, 62-64.

Gómez-Gómez, L., and Boller, T. (2000). FLS2: An LRR receptor–like kinase involved in the perception of the bacterial elicitor flagellin in Arabidopsis. Molecular cell *5*, 1003-1011.

Gómez-Gómez, L., Felix, G., and Boller, T. (1999). A single locus determines sensitivity to bacterial flagellin in *Arabidopsis thaliana*. The Plant Journal *18*, 277-284.

Gopalan, S., Wei, W., and He, S. (1996). *hrp* gene-dependent induction of *hin1*: a plant gene activated rapidly by both harpins and the *avrPto* gene-mediated signal. Plant Journal *10*, 591-600.

Gosti, F., Beaudoin, N., Serizet, C., Webb, A.A., Vartanian, N., and Giraudat, J. (1999). ABI1 protein phosphatase 2C is a negative regulator of abscisic acid signaling. The Plant Cell *11*, 1897-1909.

Götte, K., Girzalsky, W., Linkert, M., Baumgart, E., Kammerer, S., Kunau, W.-H., and Erdmann, R. (1998). Pex19p, a farnesylated protein essential for peroxisome biogenesis. Molecular and Cellular Biology *18*, 616-628.

Gould, S., Keller, G.-A., and Subramani, S. (1987). Identification of a peroxisomal targeting signal at the carboxy terminus of firefly luciferase. The Journal of cell biology *105*, 2923-2931.

Gould, S.J., Kalish, J.E., Morrell, J.C., Bjorkman, J., Urquhart, A.J., and Crane, D.I. (1996). Pex13p is an SH3 protein of the peroxisome membrane and a docking factor for the predominantly cytoplasmic PTs1 receptor. The Journal of Cell Biology *135*, 85-95.

Gould, S.J., Keller, G.-A., Hosken, N., Wilkinson, J., and Subramani, S. (1989). A conserved tripeptide sorts proteins to peroxisomes. The Journal of Cell Biology *108*, 1657-1664.

Goyal, K., Walton, L.J., and Tunnacliffe, A. (2005). LEA proteins prevent protein aggregation due to water stress. Biochemical Journal *388*, 151-157.

Gray, J., Close, P.S., Briggs, S.P., and Johal, G.S. (1997). A novel suppressor of cell death in plants encoded by the *Lls1* gene of maize. Cell *89*, 25-31.

Grelet, J., Benamar, A., Teyssier, E., Avelange-Macherel, M.-H., Grunwald, D., and Macherel, D. (2005). Identification in pea seed mitochondria of a late-embryogenesis abundant protein able to protect enzymes from drying. Plant Physiology *137*, 157-167.

Guo, Z., Ou, W., Lu, S.-y., and Zhong, Q. (2006). Differential responses of antioxidative system to chilling and drought in four rice cultivars differing in sensitivity. Plant Physiology and Biochemistry *44*, 828-836.

Gurvitz, A., and Rottensteiner, H. (2006). The biochemistry of oleate induction: transcriptional upregulation and peroxisome proliferation. Biochimica et Biophysica Acta-Molecular Cell Research *1763*, 1392-1402.

Hadden, D.A., Phillipson, B.A., Johnston, K.A., Brown, L.-A., Manfield, I.W., El-Shami, M., Sparkes, I.A., and Baker, A. (2006). Arabidopsis PEX19 is a dimeric protein that binds the peroxin PEX10. Molecular Membrane Biology *23*, 325-336.

Hagen, S., Drepper, F., Fischer, S., Fodor, K., Passon, D., Platta, H.W., Zenn, M., Schliebs, W., Girzalsky, W., and Wilmanns, M. (2015). Structural insights into cargo recognition by the yeast PTS1 receptor. Journal of Biological Chemistry *290*, 26610-26626.

Hammond-Kosack, K.E., and Jones, J.D. (1997). Plant disease resistance genes. Annual Review of Plant Biology *48*, 575-607.

Hand, S.C., Menze, M.A., Toner, M., Boswell, L., and Moore, D. (2011). LEA proteins during water stress: not just for plants anymore. Annual Review of Physiology *73*, 115-134.

Hanton, S.L., Chatre, L., Renna, L., Matheson, L.A., and Brandizzi, F. (2007). De novo formation of plant endoplasmic reticulum export sites is membrane cargo induced and signal mediated. Plant Physiology *143*, 1640-1650.

Hanton, S.L., Matheson, L.A., Chatre, L., and Brandizzi, F. (2009). Dynamic organization of COPII coat proteins at endoplasmic reticulum export sites in plant cells. The Plant Journal *57*, 963-974.

Hara, M., Terashima, S., and Kuboi, T. (2001). Characterization and cryoprotective activity of cold-responsive dehydrin from *Citrus unshiu*. Journal of Plant Physiology *158*, 1333-1339.

Hawkins, J., Mahony, D., Maetschke, S., Wakabayashi, M., Teasdale, R.D., and Bodén, M. (2007). Identifying novel peroxisomal proteins. Proteins: Structure, Function, and Bioinformatics *69*, 606-616.

Hayashi, M., Aoki, M., Kondo, M., and Nishimura, M. (1997). Changes in targeting efficiencies of proteins to plant microbodies caused by amino acid substitutions in the carboxy-terminal tripeptide. Plant and Cell Physiology *38*, 759-768.

Hayashi, M., Nito, K., Toriyama-Kato, K., Kondo, M., Yamaya, T., and Nishimura, M. (2000). AtPex14p maintains peroxisomal functions by determining protein targeting to three kinds of plant peroxisomes. The EMBO Journal *19*, 5701-5710.

He, S., Tan, L., Hu, Z., Chen, G., Wang, G., and Hu, T. (2012). Molecular characterization and functional analysis by heterologous expression in *E. coli* under diverse abiotic stresses for OsLEA5, the atypical hydrophobic LEA protein from *Oryza sativa* L. Molecular Genetics and Genomics *287*, 39-54.

He, Z.-H., Cheeseman, I., He, D., and Kohorn, B.D. (1999). A cluster of five cell wall-associated receptor kinase genes, Wak1–5, are expressed in specific organs of *Arabidopsis*. Plant Molecular Biology *39*, 1189-1196.

Helm, M., Lück, C., Prestele, J., Hierl, G., Huesgen, P.F., Fröhlich, T., Arnold, G.J., Adamska, I., Görg, A., and Lottspeich, F. (2007). Dual specificities of the glyoxysomal/peroxisomal processing protease Deg15 in higher plants. Proceedings of the National Academy of Sciences *104*, 11501-11506.

Hettema, E.H., Girzalsky, W., van den Berg, M., Erdmann, R., and Distel, B. (2000). *Saccharomyces cerevisiae* Pex3p and Pex19p are required for proper localization and stability of peroxisomal membrane proteins. The EMBO Journal *19*, 223-233.

Hilhorst, H.W. (1995). A critical update on seed dormancy. I. Primary dormancy. Seed Science Research *5*, 61-73.

Hoagland, D.R., and Arnon, D.I. (1950). The water-culture method for growing plants without soil. Circular California Agricultural Experiment Station *347*.

Hoepfner, D., Schildknegt, D., Braakman, I., Philippsen, P., and Tabak, H.F. (2005). Contribution of the endoplasmic reticulum to peroxisome formation. Cell *122*, 85-95.

Hoepfner, D., Van Den Berg, M., Philippsen, P., Tabak, H.F., and Hettema, E.H. (2001). A role for Vps1p, actin, and the Myo2p motor in peroxisome abundance and inheritance in *Saccharomyces cerevisiae*. The Journal of Cell Biology *155*, 979-990.

Hofius, D., Schultz-Larsen, T., Joensen, J., Tsitsigiannis, D.I., Petersen, N.H., Mattsson, O., Jørgensen, L.B., Jones, J.D., Mundy, J., and Petersen, M. (2009). Autophagic components contribute to hypersensitive cell death in *Arabidopsis*. Cell *137*, 773-783.

Höhfeld, J., Veenhuis, M., and Kunau, W.-H. (1991). PAS3, a *Saccharomyces cerevisiae* gene encoding a peroxisomal integral membrane protein essential for peroxisome biogenesis. The Journal of Cell Biology *114*, 1167-1178.

Honsho, M., and Fujiki, Y. (2001). Topogenesis of peroxisomal membrane protein requires a short, positively charged intervening-loop sequence and flanking hydrophobic segments: study using human membrane protein PMP34. Journal of Biological Chemistry *276*, 9375-9382.

Honsho, M., Tamura, S., Shimozawa, N., Suzuki, Y., Kondo, N., and Fujiki, Y. (1998). Mutation in PEX16 is causal in the peroxisome-deficient Zellweger syndrome of complementation group D. The American Journal of Human Genetics *63*, 1622-1630.

Hruz, T., Laule, O., Szabo, G., Wessendorp, F., Bleuler, S., Oertle, L., Widmayer, P., Gruissem, W., and Zimmermann, P. (2008). Genevestigator V3: A reference expression database for the meta-analysis of transcriptomes. Advances in Bioinformatics *2008*, 420747.

Hu, J., Baker, A., Bartel, B., Linka, N., Mullen, R.T., Reumann, S., and Zolman, B.K. (2012). Plant peroxisomes: biogenesis and function. The Plant Cell *24*, 2279-2303.

Hua, R., Gidda, S.K., Aranovich, A., Mullen, R.T., and Kim, P.K. (2015). Multiple domains in PEX16 mediate its trafficking and recruitment of peroxisomal proteins to the ER. Traffic *16*, 832-852.

Hugouvieux, V., Barber, C.E., and Daniels, M.J. (1998). Entry of *Xanthomonas campestris* pv. *campestris* into hydathodes of *Arabidopsis thaliana* leaves: a system for studying early infection events in bacterial pathogenesis. Molecular Plant-Microbe Interactions *11*, 537-543.

Huhse, B., Rehling, P., Albertini, M., Blank, L., Meller, K., and Kunau, W.-H. (1998). Pex17p of *Saccharomyces cerevisiae* is a novel peroxin and component of the peroxisomal protein translocation machinery. The Journal of Cell Biology *140*, 49-60.

Hundertmark, M., and Hincha, D.K. (2008). LEA (late embryogenesis abundant) proteins and their encoding genes in *Arabidopsis thaliana*. BMC Genomics *9*, 118.

Hunt, J.E., and Trelease, R.N. (2004). Sorting pathway and molecular targeting signals for the *Arabidopsis* peroxin 3. Biochemical and Biophysical Research Communications *314*, 586-596.

Hwang, I., and Robinson, D.G. (2009). Transport vesicle formation in plant cells. Current Opinion in Plant Biology *12*, 660-669.

Islinger, M., Li, K.W., Seitz, J., Völkl, A., and Lüers, G.H. (2009). Hitchhiking of Cu/Zn superoxide dismutase to peroxisomes–evidence for a natural piggyback import mechanism in mammals. Traffic *10*, 1711-1721.

Jakoby, M., Weisshaar, B., Dröge-Laser, W., Vicente-Carbajosa, J., Tiedemann, J., Kroj, T., and Parcy, F. (2002). bZIP transcription factors in Arabidopsis. Trends in Plant Science *7*, 106-111.

Jeworutzki, E., Roelfsema, M.R.G., Anschütz, U., Krol, E., Elzenga, J.T.M., Felix, G., Boller, T., Hedrich, R., and Becker, D. (2010). Early signaling through the *Arabidopsis* pattern recognition receptors FLS2 and EFR involves Ca^{2+}-associated opening of plasma membrane anion channels. The Plant Journal *62*, 367-378.

Jia, F., Qi, S., Li, H., Liu, P., Li, P., Wu, C., Zheng, C., and Huang, J. (2014). Overexpression of *Late Embryogenesis Abundant 14* enhances *Arabidopsis* salt stress tolerance. Biochemical and Biophysical Research Communications *454*, 505-511.

Jin, H., and Martin, C. (1999). Multifunctionality and diversity within the plant *MYB*-gene family. Plant Molecular Biology *41*, 577-585.

Johansson, O.N., Nilsson, A.K., Gustavsson, M.B., Backhaus, T., Andersson, M.X., and Ellerström, M. (2015). A quick and robust method for quantification of the hypersensitive response in plants. Peer-Reviewed Journal *3*, e1469.

Jones, J.D., and Dangl, J.L. (2006). The plant immune system. Nature *444*, 323.

Jones, J.M., Morrell, J.C., and Gould, S.J. (2004). PEX19 is a predominantly cytosolic chaperone and import receptor for class 1 peroxisomal membrane proteins. Journal of Cell Biology *164*, 57-67.

Karnik, S.K., and Trelease, R.N. (2007). *Arabidopsis* peroxin 16 trafficks through the ER and an intermediate compartment to pre-existing peroxisomes via overlapping molecular targeting signals. Journal Of Experimental Botany *58*, 1677-1693.

Katagiri, F., Thilmony, R., and He, S.Y. (2002). The *Arabidopsis thaliana-Pseudomonas syringae* interaction. The Arabidopsis Book/American Society of Plant Biologists *1*.

Kataya, A.R., Heidari, B., Hagen, L., Kommedal, R., Slupphaug, G., and Lillo, C. (2015). Protein phosphatase 2A holoenzyme is targeted to peroxisomes by piggybacking and positively affects peroxisomal β-oxidation. Plant Physiology *167*, 493-506.

Kataya, A.R., and Reumann, S. (2010). *Arabidopsis* glutathione reductase 1 is dually targeted to peroxisomes and the cytosol. Plant Signaling & Behavior *5*, 171-175.

Kataya, A.R.A. (2011). Identification of peroxisome-targeted proteins implicated in plant innate immunity in *Arabidopsis thaliana* (University of Stavanger), pp. 147.

Kato, A., Hayashi, M., Kondo, M., and Nishimura, M. (1996). Targeting and processing of a chimeric protein with the N-terminal presequence of the precursor to glyoxysomal citrate synthase. The Plant Cell *8*, 1601-1611.

Kermode, A.R. (2005). Role of abscisic acid in seed dormancy. Journal of Plant Growth Regulation *24*, 319-344.

Khan, B.R., and Zolman, B.K. (2010). *pex5* Mutants that differentially disrupt PTS1 and PTS2 peroxisomal matrix protein import in *Arabidopsis*. Plant Physiology *154*, 1602-1615.

Kiel, J.A., Veenhuis, M., and van der Klei, I.J. (2006). *PEX* genes in fungal genomes: common, rare or redundant. Traffic *7*, 1291-1303.

Kim, P., and Hettema, E. (2015). Multiple pathways for protein transport to peroxisomes. Journal of Molecular Biology *427*, 1176-1190.

Kim, P.K., Mullen, R.T., Schumann, U., and Lippincott-Schwartz, J. (2006). The origin and maintenance of mammalian peroxisomes involves a de novo PEX16-dependent pathway from the ER. The Journal of Cell Biology *173*, 521-532.

Kimura, M., Yamamoto, Y.Y., Seki, M., Sakurai, T., Sato, M., Abe, T., Yoshida, S., Manabe, K., Shinozaki, K., and Matsui, M. (2003). Identification of arabidopsis genes regulated by high light–stress using cDNA microarray¶. Photochemistry and Photobiology *77*, 226-233.

Knepper, C., Savory, E.A., and Day, B. (2011a). *Arabidopsis* NDR1 is an integrin-like protein with a role in fluid loss and plasma membrane-cell wall adhesion. Plant Physiology *156*, 286-300.

Knepper, C., Savory, E.A., and Day, B. (2011b). The role of NDR1 in pathogen perception and plant defense signaling. Plant Signaling & Behavior *6*, 1114-1116.

Kobayashi, S., Tanaka, A., and Fujiki, Y. (2007). Fis1, DLP1, and Pex11p coordinately regulate peroxisome morphogenesis. Experimental Cell Research *313*, 1675-1686.

Koch, A., Thiemann, M., Grabenbauer, M., Yoon, Y., McNiven, M.A., and Schrader, M. (2003). Dynamin-like protein 1 is involved in peroxisomal fission. Journal of Biological Chemistry *278*, 8597-8605.

Koch, A., Yoon, Y., Bonekamp, N.A., McNiven, M.A., and Schrader, M. (2005). A role for Fis1 in both mitochondrial and peroxisomal fission in mammalian cells. Molecular Biology of The Cell *16*, 5077-5086.

Koiwai, H., Nakaminami, K., Seo, M., Mitsuhashi, W., Toyomasu, T., and Koshiba, T. (2004). Tissue-specific localization of an abscisic acid biosynthetic enzyme, AAO3, in *Arabidopsis*. Plant Physiology *134*, 1697-1707.

Koller, A., Snyder, W.B., Faber, K.N., Wenzel, T.J., Rangell, L., Keller, G.A., and Subramani, S. (1999). Pex22p of Pichia pastoris, essential for peroxisomal matrix protein import, anchors the ubiquitin-conjugating enzyme, Pex4p, on the peroxisomal membrane. The Journal of Cell Biology *146*, 99-112.

Komori, M., Rasmussen, S., Kiel, J., Baerends, R., Cregg, J., Van der Klei, I., and Veenhuis, M. (1996). The *Hansenula polymorpha* PEX14 gene encodes a novel peroxisomal membrane protein involved in matrix protein import. The EMBO Journal *16*, 44-53.

Koornneef, M., Jorna, M., Brinkhorst-Van der Swan, D., and Karssen, C. (1982). The isolation of abscisic acid (ABA) deficient mutants by selection of induced revertants in non-germinating gibberellin sensitive lines of *Arabidopsis thaliana* (L.) Heynh. Theoretical and Applied Genetics *61*, 385-393.

Koornneef, M., Reuling, G., and Karssen, C. (1984). The isolation and characterization of abscisic acid-insensitive mutants of *Arabidopsis thaliana*. Physiologia Plantarum *61*, 377-383.

Kosová, K., Holková, L., Prášil, I.T., Prášilová, P., Bradáčová, M., Vítámvás, P., and Čapková, V. (2008). Expression of dehydrin 5 during the development of frost tolerance in barley (*Hordeum vulgare*). Journal of Plant Physiology *165*, 1142-1151.

Kragler, F., Lametschwandtner, G., Christmann, J., Hartig, A., and Harada, J.J. (1998). Identification and analysis of the plant peroxisomal targeting signal 1 receptor NtPEX5. Proceedings of the National Academy of Sciences *95*, 13336-13341.

Kragt, A., Voorn-Brouwer, T., van den Berg, M., and Distel, B. (2005). Endoplasmic reticulum-directed Pex3p routes to peroxisomes and restores peroxisome formation in a *Saccharomyces cerevisiae pex3Δ* strain. Journal of Biological Chemistry *280*, 34350-34357.

Kumar, S., Singh, R., Williams, C.P., and van der Klei, I.J. (2016). Stress exposure results in increased peroxisomal levels of yeast Pnc1 and Gpd1, which are imported via a piggy-backing mechanism. Biochimica et Biophysica Acta-Molecular Cell Research *1863*, 148-156.

Kurochkin, I.V., Mizuno, Y., Konagaya, A., Sakaki, Y., Schönbach, C., and Okazaki, Y. (2007). Novel peroxisomal protease Tysnd1 processes PTS1-and PTS2-containing enzymes involved in β-oxidation of fatty acids. The EMBO Journal *26*, 835-845.

Kuromori, T., Sugimoto, E., and Shinozaki, K. (2014). Intertissue signal transfer of abscisic acid from vascular cells to guard cells. Plant Physiology *164*, 1587-1592.

Laemmli, U.K. (1970). Cleavage of structural proteins during the assembly of the head of bacteriophage T4. Nature *227*, 680-685.

Lee, S.-B., Ham, B.-K., Park, J.M., Kim, Y.J., and Paek, K.-H. (2006). BnNHL18A shows a localization change by stress-inducing chemical treatments. Biochemical and Biophysical Research Communications *339*, 399-406.

Leng, P., Yuan, B., and Guo, Y. (2013). The role of abscisic acid in fruit ripening and responses to abiotic stress. Journal of Experimental Botany *65*, 4577-4588.

León, J. (2013). Role of plant peroxisomes in the production of jasmonic acid-based signals. Peroxisomes and their Key Role in Cellular Signaling and Metabolism, 299-313.

Li, B., Meng, X., Shan, L., and He, P. (2016). Transcriptional regulation of pattern-triggered immunity in plants. Cell Host & Microbe *19*, 641-650.

Li, J.-F., Park, E., von Arnim, A.G., and Nebenführ, A. (2009). The FAST technique: a simplified *Agrobacterium*-based transformation method for transient gene expression analysis in seedlings of *Arabidopsis* and other plant species. Plant Methods *5*, 1.

Lingard, M.J., and Trelease, R.N. (2006). Five *Arabidopsis* peroxin 11 homologs individually promote peroxisome elongation, duplication or aggregation. Journal of Cell Science *119*, 1961-1972.

Lingner, T., Kataya, A.R., Antonicelli, G.E., Benichou, A., Nilssen, K., Chen, X.-Y., Siemsen, T., Morgenstern, B., Meinicke, P., and Reumann, S. (2011). Identification of novel plant peroxisomal targeting signals by a combination of machine learning methods and *in vivo* subcellular targeting analyses. The Plant Cell *23*, 1556-1572.

Lipka, V., Dittgen, J., Bednarek, P., Bhat, R., Wiermer, M., Stein, M., Landtag, J., Brandt, W., Rosahl, S., and Scheel, D. (2005). Pre-and postinvasion defenses both contribute to nonhost resistance in *Arabidopsis*. Science *310*, 1180-1183.

Lisenbee, C.S., Heinze, M., and Trelease, R.N. (2003). Peroxisomal ascorbate peroxidase resides within a subdomain of rough endoplasmic reticulum in wild-type *Arabidopsis* cells. Plant Physiology *132*, 870-882.

Liu, C., Peang, H., Li, X., Liu, C., Lv, X., Wei, X., Zou, A., Zhang, J., Fan, G., and Ma, G. (2020). Genome-wide analysis of *NDR1/HIN1-like* genes in pepper (*Capsicum annuum* L.) and functional characterization of *CaNHL4* under biotic and abiotic stresses. Horticulture Research *7*, 1-15.

Liu, Y., and Zheng, Y. (2005). PM2, a group 3 LEA protein from soybean, and its 22-mer repeating region confer salt tolerance in *Escherichia coli*. Biochemical and Biophysical Research Communications *331*, 325-332.

Livak, K.J., and Schmittgen, T.D. (2001). Analysis of relative gene expression data using real-time quantitative PCR and the $2^{-\Delta\Delta CT}$ method. Methods *25*, 402-408.

Lopez-Huertas, E., Charlton, W.L., Johnson, B., Graham, I.A., and Baker, A. (2000). Stress induces peroxisome biogenesis genes. The EMBO Journal *19*, 6770-6777.

Ma, C., Haslbeck, M., Babujee, L., Jahn, O., and Reumann, S. (2006). Identification and characterization of a stress-inducible and a constitutive small heat-shock protein targeted to the matrix of plant peroxisomes. Plant Physiology *141*, 47-60.

Ma, C., and Reumann, S. (2008). Improved prediction of peroxisomal PTS1 proteins from genome sequences based on experimental subcellular targeting analyses as exemplified for protein kinases from *Arabidopsis*. Journal of Experimental Botany *59*, 3767-3779.

Ma, C., Schumann, U., Rayapuram, N., and Subramani, S. (2009). The peroxisomal matrix import of Pex8p requires only PTS receptors and Pex14p. Molecular Biology of The Cell *20*, 3680-3689.

Ma, Y., Walker, R.K., Zhao, Y., and Berkowitz, G.A. (2012). Linking ligand perception by PEPR pattern recognition receptors to cytosolic Ca^{2+} elevation and downstream immune signaling in plants. Proceedings of the National Academy of Sciences *109*, 19852-19857.

Maldonado, A., Youssef, R., McDonald, M., Brewer, E., Beard, H., and Matthews, B. (2014). Overexpression of four *Arabidopsis thaliana NHL* genes in soybean (*Glycine max*) roots and their effect on resistance to the soybean cyst nematode (*Heterodera glycines*). Physiological and Molecular Plant Pathology *86*, 1-10.

Mano, S., Nakamori, C., Kondo, M., Hayashi, M., and Nishimura, M. (2004). An *Arabidopsis* dynamin-related protein, DRP3A, controls both peroxisomal and mitochondrial division. The Plant Journal *38*, 487-498.

Mano, S., Nakamori, C., Nito, K., Kondo, M., and Nishimura, M. (2006). The *Arabidopsis pex12* and *pex13* mutants are defective in both PTS1-and PTS2-dependent protein transport to peroxisomes. The Plant Journal *47*, 604-618.

Marshall, P.A., Krimkevich, Y.I., Lark, R.H., Dyer, J.M., Veenhuis, M., and Goodman, J.M. (1995). Pmp27 promotes peroxisomal proliferation. The Journal of Cell Biology *129*, 345-355.

Maruyama, Y., Yamoto, N., Suzuki, Y., Chiba, Y., Yamazaki, K.-i., Sato, T., and Yamaguchi, J. (2013). The Arabidopsis transcriptional repressor ERF9 participates in resistance against necrotrophic fungi. Plant Science *213*, 79-87.

Marzioch, M., Erdmann, R., Veenhuis, M., and Kunau, W.-H. (1994). PAS7 encodes a novel yeast member of the WD-40 protein family essential for import of 3-oxoacyl-CoA thiolase, a PTS2-containing protein, into peroxisomes. The EMBO Journal *13*, 4908-4918.

Matsushima, R., Hayashi, Y., Yamada, K., Shimada, T., Nishimura, M., and Hara-Nishimura, I. (2003). The ER body, a novel endoplasmic reticulum-derived structure in *Arabidopsis*. Plant and Cell Physiology *44*, 661-666.

Matsuzaki, T., and Fujiki, Y. (2008). The peroxisomal membrane protein import receptor Pex3p is directly transported to peroxisomes by a novel Pex19p-and Pex16p-dependent pathway. The Journal of Cell Biology *183*, 1275-1286.

Matsuzono, Y., and Fujiki, Y. (2006). In vitro transport of membrane proteins to peroxisomes by shuttling receptor Pex19p. Journal of Biological Chemistry *281*, 36-42.

Mayerhofer, P.U. (2016). Targeting and insertion of peroxisomal membrane proteins: ER trafficking versus direct delivery to peroxisomes. Biochimica et Biophysica Acta-Molecular Cell Research *1863*, 870-880.

McDonnell, M.M., Burkhart, S.E., Stoddard, J.M., Wright, Z.J., Strader, L.C., and Bartel, B. (2016). The early-acting peroxin PEX19 is redundantly encoded, farnesylated, and essential for viability in *Arabidopsis thaliana*. PloS ONE *11*, e0148335.

McDowell, J.M., Cuzick, A., Can, C., Beynon, J., Dangl, J.L., and Holub, E.B. (2000). Downy mildew (*Peronospora parasitica*) resistance genes in *Arabidopsis* vary in functional requirements for NDR1, EDS1, NPR1 and salicylic acid accumulation. The Plant Journal *22*, 523-529.

McNew, J.A., and Goodman, J.M. (1994). An oligomeric protein is imported into peroxisomes *in vivo*. The Journal of Cell Biology *127*, 1245-1257.

Meteignier, L.-V., El Oirdi, M., Cohen, M., Barff, T., Matteau, D., Lucier, J.-F., Rodrigue, S., Jacques, P.-E., Yoshioka, K., and Moffett, P. (2017). Translatome analysis of an NB-LRR immune response identifies important contributors to plant immunity in *Arabidopsis*. Journal of Experimental Botany *68*, 2333-2344.

Mitsuya, S., El-Shami, M., Sparkes, I.A., Charlton, W.L., Lousa, C.D.M., Johnson, B., and Baker, A. (2010). Salt stress causes peroxisome proliferation, but inducing peroxisome proliferation does not improve NaCl tolerance in *Arabidopsis thaliana*. PloS ONE *5*, e9408.

Mittova, V., Guy, M., Tal, M., and Volokita, M. (2004). Salinity up-regulates the antioxidative system in root mitochondria and peroxisomes of the wild salt-tolerant tomato species *Lycopersicon pennellii*. Journal of Experimental Botany *55*, 1105-1113.

Møller, S.G., Kim, Y.-S., Kunkel, T., and Chua, N.-H. (2003). PP7 is a positive regulator of blue light signaling in *Arabidopsis*. The Plant Cell *15*, 1111-1119.

Moreau, M., Tian, M., and Klessig, D.F. (2012). Salicylic acid binds NPR3 and NPR4 to regulate NPR1-dependent defense responses. Cell Research *22*, 1631-1633.

Morel, J.-B., and Dangl, J.L. (1997). The hypersensitive response and the induction of cell death in plants. Cell Death & Differentiation *4*, 671-683.

Morré, D., Selldén, G., Ojanperä, K., Sandelius, A.S., Egger, A., Morré, D.M., Chalko, C.M., and Chalko, R. (1990). Peroxisome proliferation in Norway spruce induced by ozone. Protoplasma *155*, 58-65.

Mullen, R.T., Lee, M.S., Flynn, C.R., and Trelease, R.N. (1997). Diverse amino acid residues function within the type 1 peroxisomal targeting signal (implications for the role of accessory residues upstream of the type 1 peroxisomal targeting signal). Plant Physiology *115*, 881-889.

Mullen, R.T., Lisenbee, C.S., Miernyk, J.A., and Trelease, R.N. (1999). Peroxisomal membrane ascorbate peroxidase is sorted to a membranous network that resembles a subdomain of the endoplasmic reticulum. The Plant Cell *11*, 2167-2185.

Mullen, R.T., and Trelease, R.N. (2000). The sorting signals for peroxisomal membrane-bound ascorbate peroxidase are within its C-terminal tail. Journal of Biological Chemistry *275*, 16337-16344.

Munder, F. (2017). Heterologous expression and characterization of a peroxisomal *Arabidopsis thaliana* homolog of human macrophage migration inhibitory factor (University of Hamburg), pp. 62.

Munder, F. (2020). Elucidating the Mechanism of Protein Translocation into Peroxisomes: Biophysical, Structural and in vivo Characterization of two Peroxisomal Biogenesis Proteins from *Arabidopsis thaliana* (University of Hamburg), pp. 108.

Murphy, M.A., Phillipson, B.A., Baker, A., and Mullen, R.T. (2003). Characterization of the targeting signal of the Arabidopsis 22-kD integral peroxisomal membrane protein. Plant Physiology *133*, 813-828.

Mwaanga, C. (2011). Identification and expression analysis of peroxisome-targeted defence proteins mediating innate immunity in the model plant *Arabidopsis thaliana* (University of Stavanger), pp. 97.

Nagai, T., Ibata, K., Park, E.S., Kubota, M., Mikoshiba, K., and Miyawaki, A. (2002). A variant of yellow fluorescent protein with fast and efficient maturation for cell-biological applications. Nature Biotechnology *20*, 87.

Nagaraju, M., Kumar, S.A., Reddy, P.S., Kumar, A., Rao, D.M., and Kavi Kishor, P. (2019). Genome-scale identification, classification, and tissue specific expression analysis of *late embryogenesis abundant* (*LEA*) genes under abiotic stress conditions in *Sorghum bicolor* L. PLoS ONE *14*, e0209980.

Naito, K., Taguchi, F., Suzuki, T., Inagaki, Y., Toyoda, K., Shiraishi, T., and Ichinose, Y. (2008). Amino acid sequence of bacterial microbe-associated molecular pattern flg22 is required for virulence. Molecular Plant-Microbe Interactions *21*, 1165-1174.

Nakashima, K., Fujita, Y., Kanamori, N., Katagiri, T., Umezawa, T., Kidokoro, S., Maruyama, K., Yoshida, T., Ishiyama, K., and Kobayashi, M. (2009). Three Arabidopsis SnRK2 protein kinases, SRK2D/SnRK2. 2, SRK2E/SnRK2. 6/OST1 and SRK2I/SnRK2. 3, involved in ABA signaling are essential for the control of seed development and dormancy. Plant and Cell Physiology *50*, 1345-1363.

Nakashima, K., Kiyosue, T., Yamaguchi-Shinozaki, K., and Shinozaki, K. (1997). A nuclear gene, *erd1*, encoding a chloroplast-targeted Clp protease regulatory subunit homolog is not only induced by water stress but also developmentally up-regulated during senescence in Arabidopsis thaliana. The Plant Journal *12*, 851-861.

Nakayama, K., Okawa, K., Kakizaki, T., Honma, T., Itoh, H., and Inaba, T. (2007). *Arabidopsis* Cor15am is a chloroplast stromal protein that has cryoprotective activity and forms oligomers. Plant Physiology *144*, 513-523.

Nambara, E., Okamoto, M., Tatematsu, K., Yano, R., Seo, M., and Kamiya, Y. (2010). Abscisic acid and the control of seed dormancy and germination. Seed Science Research *20*, 55.

NDong, C., Danyluk, J., Wilson, K.E., Pocock, T., Huner, N.P., and Sarhan, F. (2002). Cold-regulated cereal chloroplast late embryogenesis abundant-like proteins. Molecular characterization and functional analyses. Plant Physiology *129*, 1368-1381.

Nelson, B.K., Cai, X., and Nebenführ, A. (2007). A multicolored set of in vivo organelle markers for co-localization studies in *Arabidopsis* and other plants. The Plant Journal *51*, 1126-1136.

Neuberger, G., Maurer-Stroh, S., Eisenhaber, B., Hartig, A., and Eisenhaber, F. (2003a). Motif refinement of the peroxisomal targeting signal 1 and evaluation of taxon-specific differences. Journal of Molecular Biology *328*, 567-579.

Neuberger, G., Maurer-Stroh, S., Eisenhaber, B., Hartig, A., and Eisenhaber, F. (2003b). Prediction of peroxisomal targeting signal 1 containing proteins from amino acid sequence. Journal of Molecular Biology *328*, 581-592.

Nito, K., Hayashi, M., and Nishimura, M. (2002). Direct interaction and determination of binding domains among peroxisomal import factors in *Arabidopsis thaliana*. Plant and Cell Physiology *43*, 355-366.

Nito, K., Kamigaki, A., Kondo, M., Hayashi, M., and Nishimura, M. (2007). Functional classification of *Arabidopsis* peroxisome biogenesis factors proposed from analyses of knockdown mutants. Plant and Cell Physiology *48*, 763-774.

Nito, K., Yamaguchi, K., Kondo, M., Hayashi, M., and Nishimura, M. (2001). Pumpkin peroxisomal ascorbate peroxidase is localized on peroxisomal membranes and unknown membranous structures. Plant and Cell Physiology *42*, 20-27.

Nyathi, Y., Zhang, X., Baldwin, J.M., Bernhardt, K., Johnson, B., Baldwin, S.A., Theodoulou, F.L., and Baker, A. (2012). Pseudo half-molecules of the ABC transporter, COMATOSE, bind Pex19 and target to peroxisomes independently but are both required for activity. FEBS letters *586*, 2280-2286.

Nylander, M., Svensson, J., Palva, E.T., and Welin, B.V. (2001). Stress-induced accumulation and tissue-specific localization of dehydrins in *Arabidopsis thaliana*. Plant Molecular Biology *45*, 263-279.

Oh, S.K., Baek, K.H., Park, J.M., Yi, S.Y., Yu, S.H., Kamoun, S., and Choi, D. (2008). *Capsicum annuum* WRKY protein CaWRKY1 is a negative regulator of pathogen defense. New Phytologist *177*, 977-989.

Ono, A., Izawa, T., Chua, N.-H., and Shimamoto, K. (1996). The rab16B promoter of rice contains two distinct abscisic acid-responsive elements. Plant Physiology *112*, 483-491.

Onsando, J. (1992). Black rot of crucifers. Black Rot of Crucifers, 243-252.

Ortega-Galisteo, A.P., Rodríguez-Serrano, M., Pazmiño, D.M., Gupta, D.K., Sandalio, L.M., and Romero-Puertas, M.C. (2012). S-Nitrosylated proteins in pea (*Pisum sativum* L.) leaf peroxisomes: changes under abiotic stress. Journal of Experimental Botany *63*, 2089-2103.

Orth, T., Reumann, S., Zhang, X., Fan, J., Wenzel, D., Quan, S., and Hu, J. (2007). The PEROXIN11 protein family controls peroxisome proliferation in *Arabidopsis*. The Plant Cell *19*, 333-350.

Osumi, T., Tsukamoto, T., Hata, S., Yokota, S., Miura, S., Fujiki, Y., Hijikata, M., Miyazawa, S., and Hashimoto, T. (1991). Amino-terminal presequence of the precursor of peroxisomal 3-ketoacyl-CoA thiolase is a cleavable signal peptide for peroxisomal targeting. Biochemical and Biophysical Research Communications *181*, 947-954.

Otera, H., Setoguchi, K., Hamasaki, M., Kumashiro, T., Shimizu, N., and Fujiki, Y. (2002). Peroxisomal targeting signal receptor Pex5p interacts with cargoes and import machinery components in a spatiotemporally differentiated manner: conserved Pex5p WXXXF/Y motifs are critical for matrix protein import. Molecular and Cellular Biology *22*, 1639-1655.

Otzen, M., Wang, D., Lunenborg, M.G., and van der Klei, I.J. (2005). *Hansenula polymorpha* Pex20p is an oligomer that binds the peroxisomal targeting signal 2 (PTS2). Journal of Cell Science *118*, 3409-3418.

Palma, J., Garrido, M., Rodriguez-Garcia, M.I., and Luis, A. (1991). Peroxisome proliferation and oxidative stress mediated by activated oxygen species in plant peroxisomes. Archives of Biochemistry and Biophysics *287*, 68-74.

Pan, R., Reumann, S., Lisik, P., Tietz, S., Olsen, L.J., and Hu, J. (2018). Proteome analysis of peroxisomes from dark-treated senescent Arabidopsis leaves. Journal of integrative plant biology *60*, 1028-1050.

Paul, A., Singh, S., Sharma, S., and Kumar, S. (2014). A stress-responsive *late embryogenesis abundant protein 7* (*CsLEA7*) of tea [*Camellia sinensis* (L.) O. Kuntze] encodes for a chaperone that imparts tolerance to *Escherichia coli* against stresses. Molecular Biology Reports *41*, 7191-7200.

Pimpl, P., Movafeghi, A., Coughlan, S., Denecke, J., Hillmer, S., and Robinson, D.G. (2000). *In situ* localization and *in vitro* induction of plant COPI-coated vesicles. The Plant Cell *12*, 2219-2235.

Platta, H.W., Grunau, S., Rosenkranz, K., Girzalsky, W., and Erdmann, R. (2005). Functional role of the AAA peroxins in dislocation of the cycling PTS1 receptor back to the cytosol. Nature Cell Biology *7*, 817-822.

Platta, H.W., Magraoui, F.E., Schlee, D., Grunau, S., Girzalsky, W., and Erdmann, R. (2007). Ubiquitination of the peroxisomal import receptor Pex5p is required for its recycling. The Journal of Cell Biology *177*, 197-204.

Punta, M., Coggill, P.C., Eberhardt, R.Y., Mistry, J., Tate, J., Boursnell, C., Pang, N., Forslund, K., Ceric, G., Clements, J.*, et al.* (2011). The Pfam protein families database. Nucleic Acids Research *40*, D290-D301.

Rehling, P., Skaletz-Rorowski, A., Girzalsky, W., Voorn-Brouwer, T., Franse, M.M., Distel, B., Veenhuis, M., Kunau, W.-H., and Erdmann, R. (2000). Pex8p, an intraperoxisomal peroxin of *Saccharomyces cerevisiae* required for protein transport into peroxisomes binds the PTS1 receptor Pex5p. Journal of Biological Chemistry *275*, 3593-3602.

Reuber, T.L., and Ausubel, F.M. (1996). Isolation of Arabidopsis genes that differentiate between resistance responses mediated by the RPS2 and RPM1 disease resistance genes. The Plant Cell *8*, 241-249.

Reumann, S. (2004). Specification of the peroxisome targeting signals type 1 and type 2 of plant peroxisomes by bioinformatics analyses. Plant Physiology *135*, 783-800.

Reumann, S., Babujee, L., Ma, C., Wienkoop, S., Siemsen, T., Antonicelli, G.E., Rasche, N., Lüder, F., Weckwerth, W., and Jahn, O. (2007). Proteome analysis of *Arabidopsis* leaf peroxisomes reveals novel targeting peptides, metabolic pathways, and defense mechanisms. The Plant Cell *19*, 3170-3193.

Reumann, S., and Bartel, B. (2016). Plant peroxisomes: recent discoveries in functional complexity, organelle homeostasis, and morphological dynamics. Current Opinion in Plant Biology *34*, 17-26.

Reumann, S., Buchwald, D., and Lingner, T. (2012). PredPlantPTS1: a web server for the prediction of plant peroxisomal proteins. Frontiers in Plant Science *3*, 194.

Reumann, S., and Chowdhary, G. (2018). Prediction of peroxisomal matrix proteins in plants. Proteomics of Peroxisomes, 125-138.

Reumann, S., Chowdhary, G., and Lingner, T. (2016). Characterization, prediction and evolution of plant peroxisomal targeting signals type 1 (PTS1s). Biochimica et Biophysica Acta-Molecular Cell Research *1863*, 790-803.

Reumann, S., Ma, C., Lemke, S., and Babujee, L. (2004). AraPerox. A database of putative Arabidopsis proteins from plant peroxisomes. Plant Physiology *136*, 2587-2608.

Reumann, S., Quan, S., Aung, K., Yang, P., Manandhar-Shrestha, K., Holbrook, D., Linka, N., Switzenberg, R., Wilkerson, C.G., and Weber, A.P. (2009). In-depth proteome analysis of *Arabidopsis* leaf peroxisomes combined with in vivo subcellular targeting verification indicates novel metabolic and regulatory functions of peroxisomes. Plant Physiology *150*, 125-143.

Reynolds, E.S. (1963). The use of lead citrate at high pH as an electron-opaque stain in electron microscopy. The Journal of Cell Biology *17*, 208.

Rhodin, J. (1954). Correlation of ultrastructural organization and function in normal and experimentally changed proximal convoluted tubule cells of the mouse kidney. Doctoral Thesis, Karolinska Institutet, Stockholm, Aktiebolaget Godvil *1*.

Rodríguez-Serrano, M., Romero-Puertas, M.C., Sanz-Fernández, M., Hu, J., and Sandalio, L.M. (2016). Peroxisomes extend peroxules in a fast response to stress via a reactive oxygen species-mediated induction of the peroxin PEX11a. Plant Physiology *171*, 1665-1674.

Romo, S., Labrador, E., and Dopico, B. (2001). Water stress-regulated gene expression in *Cicer arietinum* seedlings and plants. Plant Physiology and Biochemistry *39*, 1017-1026.

Rottensteiner, H., Kramer, A., Lorenzen, S., Stein, K., Landgraf, C., Volkmer-Engert, R., and Erdmann, R. (2004). Peroxisomal membrane proteins contain common Pex19p-binding sites that are an integral part of their targeting signals. Molecular Biology of The Cell *15*, 3406-3417.

Rottensteiner, H., Stein, K., Sonnenhol, E., and Erdmann, R. (2003). Conserved function of pex11p and the novel pex25p and pex27p in peroxisome biogenesis. Molecular Biology of the Cell *14*, 4316-4328.

Ruohonen, L., Aalto, M.K., and Keränen, S. (1995). Modifications to the *ADH1* promoter of *Saccharomyces cerevisiae* for efficient production of heterologous proteins. Journal of Biotechnology *39*, 193-203.

Sacksteder, K.A., Jones, J.M., South, S.T., Li, X., Liu, Y., and Gould, S.J. (2000). PEX19 binds multiple peroxisomal membrane proteins, is predominantly cytoplasmic, and is required for peroxisome membrane synthesis. The Journal of Cell Biology *148*, 931-944.

Salmeron, J.M., Oldroyd, G.E., Rommens, C.M., Scofield, S.R., Kim, H.-S., Lavelle, D.T., Dahlbeck, D., and Staskawicz, B.J. (1996). Tomato Prf is a member of the leucine-rich repeat class of plant disease resistance genes and lies embedded within the Pto kinase gene cluster. Cell *86*, 123-133.

Sanchez-Ballesta, M.T., Rodrigo, M.J., Lafuente, M.T., Granell, A., and Zacarias, L. (2004). Dehydrin from citrus, which confers in vitro dehydration and freezing protection activity, is constitutive and highly expressed in the flavedo of fruit but responsive to cold and water stress in leaves. Journal of Agricultural and Food Chemistry *52*, 1950-1957.

Schenk, P.M., Kazan, K., Wilson, I., Anderson, J.P., Richmond, T., Somerville, S.C., and Manners, J.M. (2000). Coordinated plant defense responses in *Arabidopsis* revealed by microarray analysis. Proceedings of the National Academy of Sciences *97*, 11655-11660.

Schmittgen, T.D., and Livak, K.J. (2008). Analyzing real-time PCR data by the comparative C T method. Nature Protocols *3*, 1101.

Schrader, M., Baumgart, E., Völkl, A., and Fahimi, H. (1994). Heterogeneity of peroxisomes in human hepatoblastoma cell line HepG2. Evidence of distinct subpopulations. European Journal of Cell Biology *64*, 281-294.

Schrader, M., Costello, J.L., Godinho, L.F., Azadi, A.S., and Islinger, M. (2016). Proliferation and fission of peroxisomes—an update. Biochimica Et Biophysica Acta-Molecular Cell Research *1863*, 971-983.

Schrader, M., and Fahimi, H.D. (2008). The peroxisome: still a mysterious organelle. Histochemistry and Cell Biology *129*, 421-440.

Schrader, M., King, S.J., Stroh, T.A., and Schroer, T.A. (2000). Real time imaging reveals a peroxisomal reticulum in living cells. Journal of Cell Science *113*, 3663-3671.

Schuhmann, H., Huesgen, P.F., Gietl, C., and Adamska, I. (2008). The DEG15 serine protease cleaves peroxisomal targeting signal 2-containing proteins in *Arabidopsis*. Plant Physiology *148*, 1847-1856.

Schuldiner, M., Metz, J., Schmid, V., Denic, V., Rakwalska, M., Schmitt, H.D., Schwappach, B., and Weissman, J.S. (2008). The GET complex mediates insertion of tail-anchored proteins into the ER membrane. Cell *134*, 634-645.

Scott, I., Tobin, A.K., and Logan, D.C. (2006). BIGYIN, an orthologue of human and yeast FIS1 genes functions in the control of mitochondrial size and number in *Arabidopsis thaliana*. Journal of Experimental Botany *57*, 1275-1280.

Shai, N., Schuldiner, M., and Zalckvar, E. (2016). No peroxisome is an island—peroxisome contact sites. Biochimica et Biophysica Acta-Molecular Cell Research *1863*, 1061-1069.

Shapiro, A.D., and Zhang, C. (2001). The role of NDR1 in avirulence gene-directed signaling and control of programmed cell death in *Arabidopsis*. Plant Physiology *127*, 1089-1101.

Sharma, A., Kumar, D., Kumar, S., Rampuria, S., Reddy, A.R., and Kirti, P.B. (2016). Ectopic expression of an atypical hydrophobic group 5 LEA protein from wild peanut, *Arachis diogoi* confers abiotic stress tolerance in tobacco. PLoS ONE *11*, e0150609.

Singh, S., Cornilescu, C.C., Tyler, R.C., Cornilescu, G., Tonelli, M., Lee, M.S., and Markley, J.L. (2005). Solution structure of a late embryogenesis abundant protein (LEA14) from *Arabidopsis thaliana*, a cellular stress-related protein. Protein Science *14*, 2601-2609.

Skoulding, N.S., Chowdhary, G., Deus, M.J., Baker, A., Reumann, S., and Warriner, S.L. (2015). Experimental validation of plant peroxisomal targeting prediction algorithms by systematic comparison of in vivo import efficiency and in vitro PTS1 binding affinity. Journal of Molecular Biology *427*, 1085-1101.

Smith, J.J., Marelli, M., Christmas, R.H., Vizeacoumar, F.J., Dilworth, D.J., Ideker, T., Galitski, T., Dimitrov, K., Rachubinski, R.A., and Aitchison, J.D. (2002). Transcriptome profiling to identify genes involved in peroxisome assembly and function. The Journal of Cell Biology *158*, 259-271.

Soon, F.-F., Ng, L.-M., Zhou, X.E., West, G.M., Kovach, A., Tan, M.E., Suino-Powell, K.M., He, Y., Xu, Y., and Chalmers, M.J. (2012). Molecular mimicry regulates ABA signaling by SnRK2 kinases and PP2C phosphatases. Science *335*, 85-88.

Sørhagen, K., Laxa, M., Peterhänsel, C., and Reumann, S. (2013). The emerging role of photorespiration and non-photorespiratory peroxisomal metabolism in pathogen defence. Plant Biology *15*, 723-736.

Spurr, A.R. (1969). A low-viscosity epoxy resin embedding medium for electron microscopy. Journal of Ultrastructure Research *26*, 31-43.

Stacy, R.A., and Aalen, R.B. (1998). Identification of sequence homology between the internal hydrophilic repeated motifs of Group 1 late-embryogenesis-abundant proteinsin plants and hydrophilic repeats of the general stress protein GsiB of *Bacillus subtilis*. Planta *206*, 476-478.

Stanley, W.A., Filipp, F.V., Kursula, P., Schüller, N., Erdmann, R., Schliebs, W., Sattler, M., and Wilmanns, M. (2006). Recognition of a functional peroxisome type 1 target by the dynamic import receptor pex5p. Molecular Cell *24*, 653-663.

Stefanovic, S., and Hegde, R.S. (2007). Identification of a targeting factor for posttranslational membrane protein insertion into the ER. Cell *128*, 1147-1159.

Stracke, R., Werber, M., and Weisshaar, B. (2001). The R2R3-MYB gene family in *Arabidopsis thaliana*. Current Opinion in Plant Biology *4*, 447-456.

Sugiura, A., Mattie, S., Prudent, J., and McBride, H.M. (2017). Newly born peroxisomes are a hybrid of mitochondrial and ER-derived pre-peroxisomes. Nature *542*, 251-254.

Sussmilch, F.C., Brodribb, T.J., and McAdam, S.A. (2017). What are the evolutionary origins of stomatal responses to abscisic acid in land plants? Journal of Integrative Plant Biology *59*, 240-260.

Suzuki, M., Kao, C.Y., and McCarty, D.R. (1997). The conserved B3 domain of VIVIPAROUS1 has a cooperative DNA binding activity. The Plant Cell *9*, 799-807.

Swinkels, B.W., Gould, S., Bodnar, A., Rachubinski, R., and Subramani, S. (1991). A novel, cleavable peroxisomal targeting signal at the amino-terminus of the rat 3-ketoacyl-CoA thiolase. The EMBO Journal *10*, 3255-3262.

Swire-Clark, G.A., and Marcotte, W.R. (1999). The wheat LEA protein Em functions as an osmoprotective molecule in *Saccharomyces cerevisiae*. Plant Molecular Biology *39*, 117-128.

Takagi, J., Kimori, Y., Shimada, T., and Hara-Nishimura, I. (2020). Dynamic capture and release of endoplasmic reticulum exit sites by golgi stacks in *Arabidopsis*. Iscience *23*, 101265.

Tam, Y.Y.C., Fagarasanu, A., Fagarasanu, M., and Rachubinski, R.A. (2005). Pex3p initiates the formation of a preperoxisomal compartment from a subdomain of the endoplasmic reticulum in *Saccharomyces cerevisiae*. Journal of Biological Chemistry *280*, 34933-34939.

Tam, Y.Y.C., Torres-Guzman, J.C., Vizeacoumar, F.J., Smith, J.J., Marelli, M., Aitchison, J.D., and Rachubinski, R.A. (2003). Pex11-related proteins in peroxisome dynamics: a role for the novel peroxin Pex27p in controlling peroxisome size and number in *Saccharomyces cerevisiae*. Molecular Biology of The Cell *14*, 4089-4102.

Tang, X., Frederick, R., Zhou, J., Halterman, D., Jia, Y., and Martin, G. (1996). Physical interaction of avrPto and the Pto kinase defines a recognition event involved in plant disease resistance. Science *274*, 2060-2063.

Tani, K., Tagaya, M., Yonekawa, S., and Baba, T. (2011). Dual function of Sec16B: Endoplasmic reticulum-derived protein secretion and peroxisome biogenesis in mammalian cells. Cellular Logistics *1*, 164-167.

Thoms, S., Harms, I., Kalies, K.U., and Gärtner, J. (2012). Peroxisome Formation Requires the Endoplasmic Reticulum Channel Protein S ec61. Traffic *13*, 599-609.

Tian, G.-W., Mohanty, A., Chary, S.N., Li, S., Paap, B., Drakakaki, G., Kopec, C.D., Li, J., Ehrhardt, D., and Jackson, D. (2004). High-throughput fluorescent tagging of full-length Arabidopsis gene products in planta. Plant Physiology *135*, 25-38.

Titorenko, V.I., Smith, J.J., Szilard, R.K., and Rachubinski, R.A. (1998). Pex20p of the yeast *Yarrowia lipolytica* is required for the oligomerization of thiolase in the cytosol and for its targeting to the peroxisome. The Journal of Cell Biology *142*, 403-420.

Tornow, J., and Santangelo, G.M. (1990). Efficient expression of the Saccharomyces cerevisiae glycolytic gene ADH1 is dependent upon a cis-acting regulatory element (UASRPG) found initially in genes encoding ribosomal proteins. Gene *90*, 79-85.

Tran, L.-S.P., Urao, T., Qin, F., Maruyama, K., Kakimoto, T., Shinozaki, K., and Yamaguchi-Shinozaki, K. (2007). Functional analysis of AHK1/ATHK1 and cytokinin receptor histidine kinases in response to abscisic acid, drought, and salt stress in *Arabidopsis*. Proceedings of the National Academy of Sciences *104*, 20623-20628.

Trapet, P., Kulik, A., Lamotte, O., Jeandroz, S., Bourque, S., Nicolas-Francès, V., Rosnoblet, C., Besson-Bard, A., and Wendehenne, D. (2015). NO signaling in plant immunity: a tale of messengers. Phytochemistry *112*, 72-79.

Tsien, R.Y. (1998). The green fluorescent protein. Annual Review of Biochemistry *67*, 509-544.

Van den Bosch, H., Schutgens, R., Wanders, R., and Tager, J. (1992). Biochemistry of peroxisomes. Annual Review of Biochemistry *61*, 157-197.

van der Zand, A., Braakman, I., and Tabak, H.F. (2010). Peroxisomal membrane proteins insert into the endoplasmic reticulum. Molecular Biology of The Cell *21*, 2057-2065.

Varet, A., Hause, B., Hause, G., Scheel, D., and Lee, J. (2003). The *Arabidopsis NHL3* gene encodes a plasma membrane protein and its overexpression correlates with increased resistance to *Pseudomonas syringae* pv. *tomato* DC3000. Plant Physiology *132*, 2023-2033.

Varet, A., Parker, J., Tornero, P., Nass, N., Nürnberger, T., Dangl, J.L., Scheel, D., and Lee, J. (2002). *NHL25* and *NHL3*, two *NDR1/HIN1-like* genes in *Arabidopsis thaliana* with potential role (s) in plant defense. Molecular Plant Microbe Interaction *15*, 608-616.

Veenhuis, M., Mateblowski, M., Kunau, W.H., and Harder, W. (1987). Proliferation of microbodies in *Saccharomyces cerevisiae*. Yeast *3*, 77-84.

Vilaine, F., Kerchev, P., Clément, G., Batailler, B., Cayla, T., Bill, L., Gissot, L., and Dinant, S. (2013). Increased expression of a phloem membrane protein encoded by *NHL26* alters phloem export and sugar partitioning in *Arabidopsis*. The Plant Cell *25*, 1689-1708.

Walton, P.A., Gould, S.J., Feramisco, J.R., and Subramani, S. (1992). Transport of microinjected proteins into peroxisomes of mammalian cells: inability of Zellweger cell lines to import proteins with the SKL tripeptide peroxisomal targeting signal. Molecular and Cellular Biology *12*, 531-541.

Wanders, R.J. (2014). Metabolic functions of peroxisomes in health and disease. Biochimie *98*, 36-44.

Wang, D., Amornsiripanitch, N., and Dong, X. (2006). A genomic approach to identify regulatory nodes in the transcriptional network of systemic acquired resistance in plants. PLoS Pathogens *2*, e123.

Wang, M., Li, P., Li, C., Pan, Y., Jiang, X., Zhu, D., Zhao, Q., and Yu, J. (2014). SiLEA14, a novel atypical LEA protein, confers abiotic stress resistance in foxtail millet. BMC Plant Biology *14*, 290.

Wang, X.-S., Zhu, H.-B., Jin, G.-L., Liu, H.-L., Wu, W.-R., and Zhu, J. (2007). Genome-scale identification and analysis of LEA genes in rice (Oryza sativa L.). Plant Science *172*, 414-420.

Williams, C., van den Berg, M., Geers, E., and Distel, B. (2008). Pex10p functions as an E3 ligase for the Ubc4p-dependent ubiquitination of Pex5p. Biochemical and Biophysical Research Communications *374*, 620-624.

Wise, M.J., and Tunnacliffe, A. (2004). POPP the question: what do LEA proteins do? Trends in plant science *9*, 13-17.

Woodward, A.W., and Bartel, B. (2005). The *Arabidopsis* peroxisomal targeting signal type 2 receptor PEX7 is necessary for peroxisome function and dependent on PEX5. Molecular Biology of The Cell *16*, 573-583.

Wu, Y., Xun, Q., Guo, Y., Zhang, J., Cheng, K., Shi, T., He, K., Hou, S., Gou, X., and Li, J. (2016). Genome-wide expression pattern analyses of the *Arabidopsis* leucine-rich repeat receptor-like kinases. Molecular Plant *9*, 289-300.

Xin, X.-F., Nomura, K., Ding, X., Chen, X., Wang, K., Aung, K., Uribe, F., Rosa, B., Yao, J., and Chen, J. (2015). *Pseudomonas syringae* effector avirulence protein E localizes to the host plasma membrane and down-regulates the expression of the *NONRACE-SPECIFIC DISEASE RESISTANCE1/HARPIN-INDUCED1-LIKE13* gene required for antibacterial immunity in *Arabidopsis*. Plant Physiology *169*, 793-802.

Xiong, L., and Zhu, J.-K. (2003). Regulation of abscisic acid biosynthesis. Plant Physiology *133*, 29-36.

Yagita, Y., Hiromasa, T., and Fujiki, Y. (2013). Tail-anchored PEX26 targets peroxisomes via a PEX19-dependent and TRC40-independent class I pathway. Journal of Cell Biology *200*, 651-666.

Yamamoto, K., and Fahimi, H.D. (1987). Three-dimensional reconstruction of a peroxisomal reticulum in regenerating rat liver: evidence of interconnections between heterogeneous segments. The Journal of Cell Biology *105*, 713-722.

Yang, F., Moss, L.G., and Phillips, G.N. (1996). The molecular structure of green fluorescent protein. Nature biotechnology *14*, 1246-1251.

Yang, Y.-d., Elamawi, R., Bubeck, J., Pepperkok, R., Ritzenthaler, C., and Robinson, D.G. (2005). Dynamics of COPII vesicles and the Golgi apparatus in cultured Nicotiana tabacum BY-2 cells provides evidence for transient association of Golgi stacks with endoplasmic reticulum exit sites. The Plant Cell *17*, 1513-1531.

Yasuda, M., Ishikawa, A., Jikumaru, Y., Seki, M., Umezawa, T., Asami, T., Maruyama-Nakashita, A., Kudo, T., Shinozaki, K., and Yoshida, S. (2008). Antagonistic interaction between systemic acquired resistance and the abscisic acid–mediated abiotic stress response in *Arabidopsis*. The Plant Cell *20*, 1678-1692.

Yonekawa, S., Furuno, A., Baba, T., Fujiki, Y., Ogasawara, Y., Yamamoto, A., Tagaya, M., and Tani, K. (2011). Sec16B is involved in the endoplasmic reticulum export of the peroxisomal membrane biogenesis factor peroxin 16 (Pex16) in mammalian cells. Proceedings of the National Academy of Sciences *108*, 12746-12751.

Yoshida, T., Christmann, A., Yamaguchi-Shinozaki, K., Grill, E., and Fernie, A.R. (2019). Revisiting the basal role of ABA–roles outside of stress. Trends in Plant Science *24*, 625-635.

Yoshida, T., Fujita, Y., Maruyama, K., Mogami, J., Todaka, D., Shinozaki, K., and Yamaguchi-Shinozaki, K. (2015). Four *Arabidopsis* AREB/ABF transcription factors function predominantly in gene expression downstream of SnRK2 kinases in abscisic acid signalling in response to osmotic stress. Plant, Cell & Environment *38*, 35-49.

Yuan, M., Jiang, Z., Bi, G., Nomura, K., Liu, M., Wang, Y., Cai, B., Zhou, J.-M., He, S.Y., and Xin, X.-F. (2021a). Pattern-recognition receptors are required for NLR-mediated plant immunity. Nature, 1-5.

Yuan, M., Ngou, B.P.M., Ding, P., and Xin, X.-F. (2021b). PTI-ETI crosstalk: an integrative view of plant immunity. Current Opinion in Plant Biology *62*, 102030.

Zacharias, D.A., Violin, J.D., Newton, A.C., and Tsien, R.Y. (2002). Partitioning of lipid-modified monomeric GFPs into membrane microdomains of live cells. Science *296*, 913-916.

Zeng, L.-R., Qu, S., Bordeos, A., Yang, C., Baraoidan, M., Yan, H., Xie, Q., Nahm, B.H., Leung, H., and Wang, G.-L. (2004). Spotted leaf11, a negative regulator of plant cell death and defense, encodes a U-box/armadillo repeat protein endowed with E3 ubiquitin ligase activity. The Plant Cell *16*, 2795-2808.

Zhang, J.W., and Lazarow, P.B. (1995). PEB1 (PAS7) in *Saccharomyces cerevisiae* encodes a hydrophilic, intra-peroxisomal protein that is a member of the WD repeat family and is essential for the import of thiolase into peroxisomes. The Journal of Cell Biology *129*, 65-80.

Zhang, X.-C., and Hu, J.-P. (2008). FISSION1A and FISSION1B proteins mediate the fission of peroxisomes and mitochondria in Arabidopsis. Molecular plant *1*, 1036-1047.

Zhang, X., and Hu, J. (2009). Two small protein families, DYNAMIN-RELATED PROTEIN3 and FISSION1, are required for peroxisome fission in *Arabidopsis*. The Plant Journal *57*, 146-159.

Zhang, X., and Hu, J. (2010). The *Arabidopsis* chloroplast division protein DYNAMIN-RELATED PROTEIN5B also mediates peroxisome division. The Plant Cell *22*, 431-442.

Zheng, M.S., Takahashi, H., Miyazaki, A., Hamamoto, H., Shah, J., Yamaguchi, I., and Kusano, T. (2004). Up-regulation of *Arabidopsis thaliana NHL10* in the hypersensitive response to Cucumber mosaic virus infection and in senescing leaves is controlled by signalling pathways that differ in salicylate involvement. Planta *218*, 740-750.

Zipfel, C., Kunze, G., Chinchilla, D., Caniard, A., Jones, J.D., Boller, T., and Felix, G. (2006). Perception of the bacterial PAMP EF-Tu by the receptor EFR restricts *Agrobacterium*-mediated transformation. Cell *125*, 749-760.

Zipfel, C., Robatzek, S., Navarro, L., Oakeley, E.J., Jones, J.D., Felix, G., and Boller, T. (2004). Bacterial disease resistance in *Arabidopsis* through flagellin perception. Nature *428*, 764-767.

Zolman, B.K., and Bartel, B. (2004). An *Arabidopsis* indole-3-butyric acid-response mutant defective in PEROXIN6, an apparent ATPase implicated in peroxisomal function. Proceedings of the National Academy of Sciences *101*, 1786-1791.

Zolman, B.K., Monroe-Augustus, M., Silva, I.D., and Bartel, B. (2005). Identification and functional characterization of *Arabidopsis* PEROXIN4 and the interacting protein PEROXIN22. The Plant Cell *17*, 3422-3435.

ACKNOWLEDGEMENT

First of all, I would like to give my special thanks to my supervisor, Prof. Dr. Sigrun Reumann. I would not have been able to reach this final phase of my Ph.D. study without her dedicated supervision and her care. In 2016 I joined her lab, and since then with her encouragement and academic support I improved myself a lot through my Ph.D. study. Her advice is very valuable for my future academic career.

I would also express my deeply thanks to my supervisor, Prof. Dr. Sigrun Reumann for her precious time and dedication on correcting my Ph.D. thesis. Many thanks should also go to Dr. Christian Falter, Dr. Thanh-Hao Nguyen, and Dr. Imke de Grahl for their critical reading of my Ph.D. dissertation.

I would also like to acknowledge the MIN faculty (Universität Hamburg) and the German Academic Exchange Service (DAAD) organization for their financial support so that I could successfully finalize my Ph.D. study in the last 9 months, from April to December 2020.

It was my pleasure to have Prof. Dr. Arp Schnittger as my second supervisor. I would like to express my appreciation for his examination of my Ph.D. dissertation.

I would also want to acknowledge Dr. Thanh Hao Nguyen for his great and dedicated work on the NHL project. I would also like to thank MOPS rotation and Master students, Eduardo Muñoz Díaz, Kashmery Khan, and Muzaffer Emre Gül, for their experimental work relevant to this project.

Many thanks should also go to Ms. Elke Woelken for her great TEM assistance.

I am grateful to all the lab members in the Reumann group, especially to Saugat, Christian, Ulrike, Pierre, Olga, Sweta, Ebenezer, and Imke and to our retired lab technician Martina for their unwavering support in the lab. I would like to thank Olga for her assistance on official formalities during the time I was there. I will never forget about the coffee time, skating, Hamburg exploration trips, and lab retreat with the lab members. Those would be beautiful memories of this unforgettable journey.

Again, to Thanh-Hao, as my colleague and husband, he has motivated me so much on both sides of work and life. This journey would not have been easy for me to go through until the end without his scientific advice and support. Finally, this thesis is dedicated to my parents and my grandparents, who care and believe in me unconditionally.

PUBLICATIONS AND PRESENTATIONS

Falter C*, **Thu NBA***, Pokhrel S, Reumann S (2019). New Guidelines for Fluorophore Application in Peroxisome Targeting Analyses in Transient Plant Expression Systems. Journal of Integrative and Plant Biology, 61(7), 884-899.

*as co-first author

Thu NBA, Reumann S (2019). Functional Characterization of Peroxisomal NDR1 Homologs in Biotic and Abiotic Stress Responses in Arabidopsis. Molecular Biology of Plants Conference, Dabringhausen, Germany (Poster).

Thu NBA, Reumann S (2018). Functional and Biogenesis Analyses of Peroxisome-Targeted Defense Proteins in Arabidopsis. Plant Biochemistry Conference, Wallenfels, Germany (Oral presentation).

Thu NBA, Falter C, Kataya ARA, Reumann S (2017). Subcellular Targeting and Expression Analyses of Peroxisomal NDR1 Homologs under Abiotic and Biotic Stress Conditions. Botanikertagung, Kiel, Germany (Poster).

DECLARATION ON OATH/EIDESSTATTLICHE VERSICHERUNG

Hiermit erkläre ich an Eides statt, dass ich die vorliegende Dissertationsschrift selbst verfasst und keine anderen als die angegebenen Quellen und Hilfsmittel benutzt habe.

I hereby declare, on oath, that I have written the present dissertation by my own and have not used other than the acknowledged resources and aids.

Hamburg, den 22.05.2021   Unterschrift

                                                                     Binh Anh Thu Nguyen

DECLARATION OF CONTRIBUTION

I hereby confirm that all results presented in this Ph.D. dissertation were conducted by myself except for those indicated in the respective figure legends. The contributions from colleagues are shown as follows:

Figure 3.9 - The sample fixation, embedding, sectioning, and TEM were performed with technical assistance by Ms. Elke Woelken (University of Hamburg, Hamburg, Germany).

Figure 3.17, Figure 3.18, and Supplementary Figure 7 - GUS assay optimization, experimental analyses of the reporter lines, and image documentation were kindly performed by Dr. Thanh-Hao Nguyen (University of Hamburg, Hamburg, Germany).

Figure 3.20 - Experiments were repeated and conducted with major assistance by Dr. Thanh Hao Nguyen (University of Hamburg, Hamburg, Germany), who also performed image documentation.

Figure 3.25 and Figure 3.27 - Method establishment and experiments were carried out with major contributions of Dr. Thanh-Hao Nguyen (University of Hamburg, Hamburg, Germany).

Supplementary Figure 2 - The sample fixation, embedding, and sectioning were performed with technical assistance by Ms. Elke Woelken (University of Hamburg, Hamburg, Germany).

Supplementary Figure 3 - The sample fixation, embedding, sectioning, and TEM were per-formed with technical assistance by Ms. Elke Woelken (University of Hamburg, Hamburg, Germany).

CONFIRMATION OF CORRECT ENGLISH

To whom it may concern -

I, Oren Rabinowitz, a native English speaker, have read and revised the dissertation by Binh Anh Thu Nguyen to make corrections in the English language. The English used in this dissertation was satisfactory and understandable; minor grammatical revisions were suggested.

Sincerely

Oren Rabinowitz, M.Sc.

Raskin Laboratory, Rutgers University

59 Dudley Road, New Brunswick, NJ, 08901

email: oren.rabinowitz7878@gmail.com

lab site: https://sites.rutgers.edu/ilya-raskin-lab/